ACI 228.2R-13

Report on Nondestructive Test Methods for Evaluation of Concrete in Structures

Reported by ACI Committee 228

American Concrete Institute®

First Printing
June 2013

American Concrete Institute®
Advancing concrete knowledge

Report on Nondestructive Test Methods for Evaluation of Concrete in Structures

The technical committees responsible for ACI committee reports and standards strive to avoid ambiguities, omissions, and errors in these documents. In spite of these efforts, the users of ACI documents occasionally find information or requirements that may be subject to more than one interpretation or may be incomplete or incorrect. Users who have suggestions for the improvement of ACI documents are requested to contact ACI via the errata website at www.concrete.org/committees/errata.asp. Proper use of this document includes periodically checking for errata for the most up-to-date revisions.

ACI committee documents are intended for the use of individuals who are competent to evaluate the significance and limitations of its content and recommendations and who will accept responsibility for the application of the material it contains. Individuals who use this publication in any way assume all risk and accept total responsibility for the application and use of this information.

All information in this publication is provided “as is” without warranty of any kind, either express or implied, including but not limited to, the implied warranties of merchantability, fitness for a particular purpose or non-infringement.

ACI and its members disclaim liability for damages of any kind, including any special, indirect, incidental, or consequential damages, including without limitation, lost revenues or lost profits, which may result from the use of this publication.

It is the responsibility of the user of this document to establish health and safety practices appropriate to the specific circumstances involved with its use. ACI does not make any representations with regard to health and safety issues and the use of this document. The user must determine the applicability of all regulatory limitations before applying the document and must comply with all applicable laws and regulations, including but not limited to, United States Occupational Safety and Health Administration (OSHA) health and safety standards.

Participation by governmental representatives in the work of the American Concrete Institute and in the development of Institute standards does not constitute governmental endorsement of ACI or the standards that it develops.

Order information: ACI documents are available in print, by download, on CD-ROM, through electronic subscription, or reprint and may be obtained by contacting ACI.

Most ACI standards and committee reports are gathered together in the annually revised *ACI Manual of Concrete Practice* (MCP).

American Concrete Institute
38800 Country Club Drive
Farmington Hills, MI 48331
U.S.A.
Phone: 248-848-3700
Fax: 248-848-3701

www.concrete.org

ISBN-13: 978-0-87031-820-7
ISBN: 0-87031-820-9

ACI 228.2R-13

Report on Nondestructive Test Methods for Evaluation of Concrete in Structures

Reported by ACI Committee 228

Michael C. Forde, Chair

Bernard H. Hertlein, Secretary

Muhammed P. A. Basheer
Jacob K. Bice
Andrew J. Boyd
Honggang Cao
Nicholas J. Carino
William Ciggelakis
Neil A. Cumming
Ethan. C. Dodge
Boris Dragunsky
Christopher C. Ferraro
Frederick D. Heidbrink
Kal R. Hindo
Robert S. Jenkins
Keith E. Kesner
H. S. Lew
Malcolm K. Lim
Kenneth M. Lozen
Larry D. Olson
Stephen Pessiki
John S. Popovics
Randall W. Poston
Paul L. Siwek
Patrick J. E. Sullivan

Consulting members
John H. Bungey
Hermenegildo Caratin
Gerardo G. Clemena
Al Ghorbanpoor
Alexander M. Leshchinsky
V. M. Malhotra
Claus G. Petersen
George V. Teodoro

Allen. G. Davis (deceased) made many contributions to this report.

A review is presented of nondestructive test (NDT) methods for evaluating the condition of concrete and steel reinforcement in structures. Methods discussed include visual inspection, stress-wave, nuclear, measurement of fluid transport properties, magnetic and electrical, infrared thermography, and ground-penetrating radar. The principle of each method is discussed and the typical instrumentation described. Testing procedures are summarized and the data analysis methods explained. The advantages and limitations of the methods are highlighted. This report concludes with a discussion of planning a NDT program. General information is provided for those faced with the task of evaluating the condition of a concrete structure and who are considering the applicability of NDT methods to aid in that evaluation.

Keywords: covermeter; deep foundations; half-cell potential; infrared thermography; nondestructive testing; polarization resistance; radar; radiography; radiometry; stress-wave methods; transport properties; visual inspection.

CONTENTS

ACI 228.2R-13 supersedes ACI 228.2R-98(04) and was adopted and published June 2013.

CHAPTER 1—INTRODUCTION

1.1—Scope

Nondestructive testing (NDT) methods are used to determine concrete properties and to evaluate the condition of concrete in deep foundations, bridges, buildings, pavements, dams, and other concrete construction. For this report, NDT is defined as generally noninvasive, with the exception of transport property tests, which may cause easily-repaired surface damage. While coring and load testing may be considered nondestructive, they are excluded from this report. Refer to ACI 437R for more information about strength evaluation of existing concrete buildings.

NDT methods are applied to concrete construction for four primary reasons:

1. Quality control of new construction
2. Troubleshooting problems with new and old construction
3. Condition evaluation of older concrete for rehabilitation purposes
4. Quality assurance of concrete repairs

NDT technologies are evolving and research continues to enhance existing methods and develop new methods. The report is intended to provide an overview of the principles of various NDT methods practiced and to summarize their applications and limitations. Emphasis is placed on methods that have been applied to measure physical properties other than the strength of concrete in structures, to detect flaws or discontinuities, and to provide data for condition evaluation. Methods to estimate in-place compressive strength are presented in ACI 228.1R.

1.2—Needs and applications

Nondestructive testing (NDT) methods are increasingly applied for the investigation of concrete structures. This increase in the application of NDT methods is due to a number of factors:

a) Technological improvements in hardware and software for data collection and analysis

b) The economic advantages in assessing large volumes of concrete compared with other methods

c) Ability to perform rapid, comprehensive assessments of existing construction

d) Specification of NDT methods for quality assurance of deep foundations and concrete repairs

An increased use of NDT methods is occurring despite the lack of testing standards for many of the methods. The development of testing standards is critical for proper application and expanded use of NDT methods for evaluation of concrete construction.

Traditionally, quality assurance of concrete construction has been performed largely by visual inspection of the construction process and by sampling the concrete to perform standard tests on fresh and hardened specimens. This approach does not provide data on the in-place properties of concrete. NDT methods offer the advantage of providing information on the in-place properties of hardened concrete, such as the elastic constants, density, resistivity, moisture content, and fluid transport characteristics.

Condition assessment of concrete for structural evaluation purposes has been performed mostly by visual examination, coring, and surface sounding, which refers to striking the object surface and listening to characteristics of the resulting sound. Condition assessments are used to examine internal concrete conditions and to obtain specimens for testing. This approach limits the areas of concrete that can be investigated effectively. Some coring may be necessary for calibration purposes, particularly if the concrete strength is required. Cores also cause local damage and limit the information to the core location. Condition assessments can be made with NDT methods to provide essential information for the structural performance of the concrete, such as:

a) Member dimensions

b) Location of cracking, delamination, and debonding

c) Degree of consolidation, presence of voids, and honeycomb

d) Steel reinforcement location and size

e) Corrosion activity of reinforcement

f) Extent of damage from freezing and thawing, fire, or chemical exposure

g) Strength of concrete

1.3—Objective

This report reviews the state of the practice for nondestructively determining nonstrength physical properties and conditions of hardened concrete. The overall objective is to provide the potential user with a guide to assist in planning, conducting, and interpreting the results of nondestructive tests (NDT) of concrete construction.

Chapter 3 discusses the principles, equipment, testing procedures, and data analysis of the various NDT methods. Typical applications and inherent limitations of the methods are discussed to assist the potential user in selecting the most appropriate method for a particular situation. Chapter 4 discusses the planning and performance of NDT investigations. Included in Chapter 4 are references to in-place tests covered in ACI 228.1R and other applicable methods for evaluating the characteristics of existing concrete.

CHAPTER 2—NOTATION AND DEFINITIONS

2.1—Notation

Because NDT crosses different science and engineering disciplines, the same symbols are used differently by different practitioners. The context of the symbol should be established and related to the body of text.

A = cross-sectional area (3.5.3, 3.6.2); wetted area (3.6.2)

A_c = shaft cross-sectional area (3.3.3, Appendix A)
B = magnetic induction (3.5.5)
B = constant in volts (3.5.4)
C = concentration (3.6.2); capacitance (3.5.4); electromagnetic wave speed (3.8)
C_b = bar wave speed (3.2, 3.3.1, 3.3.3); stress wave speed along the pile (Appendix A)
C_o = speed of light in air (3.8)
C_p = P-wave speed (3.2, 3.2.3)
$C_{R(f)}$ = surface wave speed of component with frequency f (3.2.4)
C_r = ratio of the R-wave speed to the S-wave speed (3.2)
C_s = S-wave speed (3.2, 3.2.2)
D = depth (3.2.3, 3.8); diffusion coefficient (3.5.3, 3.6.2); diameter (3.2.3)
D_p = diffusion coefficient of the ions through the pore fluid (3.5.3)
d = depth (3.2.1); diameter (3.3.1)
E = Young's modulus of elasticity (3.2); voltage (3.5.4); maximum acceptable error (4.2)
e = emissivity of the surface (3.7)
F = mass flux (3.6.2)
f = frequency (3.2.3)
G = shear modulus of elasticity (3.2)
H = magnetic field strength (3.5.5)
I = characteristic shaft impedance (3.3.3); amplitude of alternating current between outer electrodes (3.5.3); hydraulic gradient (3.6.2)
I_p = applied polarization current (3.5.4)
i = current (3.5.4)
i_{corr} = corrosion current density (3.5.4)
k = statistical factor (4.2); coefficient of permeability (3.6.2)
k_d = dynamic stiffness from mobility plot (3.2.5, 3.3.2; Appendix A)
L = length (3.3.1, 3.3.3, 3.5.3, Appendix A)
M_p = mass of pile (Appendix A)
m = mass (3.6.2)
N = average mobility (Appendix A)
n = sample size (4.2)
P = soil damping measure (Appendix A)
p_o = advance estimate of fraction defective (4.2)
Q = soil damping measure (Appendix A)
Q = flow rate (3.6.2); maximum amplitude in mobility plot of pile
R = rate of energy radiation per unit area of surface (3.7); reflection coefficient (3.2); electrical resistance in ohm (3.5.3, 3.5.4)
R_p = polarization resistance (3.5.4)
r = radius (Appendix A)
s = spacing between electrodes (3.5.3); sorptivity (3.6.2)
T = depth of reflecting interface (3.2.2); absolute temperature of surface (3.7)
t = travel time from transmitter to receiver (3.2.2); time (3.6.2, 3.8)
t_c = contact time (3.2.3)
V = volume of fluid absorbed (3.6.2); voltage (3.5.3)
V_d = wave speed in damaged concrete (3.2.1)
V_s = wave speed in sound concrete (3.2.1)
X = separation between transmitter and receiver (3.2.1, 3.2.2, 3.2.4)
X_o = distance at which the travel times for two wave paths are equal (3.2.1)
x = distance (3.6.2)
Z = specific acoustic impedance (3.2); depth (3.8)
α = signal attenuation (3.8)
β_s = the lateral soil shear wave velocity (Appendix A)
ε = dielectric constant (3.8)
ε_0 = dielectric constant of free space (air) (3.8)
ε_r = relative dielectric constant (3.8)
ϕ_f = phase angle of component with frequency f (3.2.4)
λ = wavelength (3.2.3)
λ_f = wavelength corresponding to component frequency (3.2.4)
μ = magnetic permeability (3.5.5)
ν = Poisson's ratio (3.2)
ρ = density (3.2); electrical resistivity of material (3.5.3)
$\rho_{1,2}$ = reflection coefficient (3.8)
ρ_c = density of shaft concrete (3.3.3, Appendix A)
ρ_s = soil density (Appendix A)
σ = conductivity (3.5.3, 3.8); the Stefan-Boltzmann constant (3.7); soil damping factor (Appendix A)
σ_p = conductivity of the pore fluid (3.5.3)

2.2—Definitions

ACI provides a comprehensive list of definitions through an online resource, "ACI Concrete Terminology," http://terminology.concrete.org.

CHAPTER 3—SUMMARY OF METHODS

Chapter 3 reviews the various nondestructive test (NDT) methods for evaluating concrete for characteristics other than strength. The underlying principles are discussed, the instrumentation is described, and the inherent advantages and limitations of each method are summarized. Where it is appropriate, examples of test data are provided. Table 3 summarizes the methods to be discussed. The first column lists the report section where the method is described, the second column provides a brief explanation of the underlying principles, and the third column gives typical applications.

Most NDT methods are indirect tests because the condition of the concrete is inferred from the measured response to some stimulus, such as impact or electromagnetic radiation. For favorable combinations of test method and site conditions, test results may be unambiguous and supplemental testing may be unnecessary. In other cases, the NDT results may be inconclusive and additional testing may be needed. Supplemental testing can be another NDT method, or often it may be an invasive method to allow direct observation of the internal condition. Invasive inspection can range from drilling small holes to removing test samples by coring or sawing. The combination of nondestructive and invasive inspection allows the reliability of the NDT method to be assessed for the specific project. Once the reliability of the

Table 3—Summary of nondestructive testing methods

Section no.	Method and principle	Applications
3.1	**Visual inspection**—Observe, classify, and document the appearance of distress on exposed surfaces of the structure.	Map patterns of distress such as cracking, spalling, scaling, erosion, or construction defects.
3.2.1	**Ultrasonic through transmission (pulse velocity)**—Measure the travel time of a pulse of ultrasonic waves over a known path length.	Determine the relative condition or uniformity of concrete based on measured pulse velocity.
3.2.2	**Ultrasonic-echo—**Transducer emits short pulse of ultrasonic waves, which is reflected by the opposite side of member or an internal defect; arrival of reflected pulse is recorded by an adjacent receiver (pitch-catch method), and round-trip travel time is determined.	Locate within concrete elements a variety of defects such as delaminations, voids, honeycombing, or measure element thickness.
3.2.3	**Impact-echo**—Receiver adjacent to impact point monitors arrival of stress wave as it undergoes multiple reflections between surface and opposite side of plate-like member or from internal defects. Frequency analysis permits determination of distance to reflector if wave speed is known.	Locate a variety of defects within concrete elements such as delaminations, voids, honeycombing, or measure element thickness.
3.2.4	**Spectral analysis of surface waves**—Impact is used to generate a surface wave and two receivers monitor the surface motion; signal analysis allows determination of wave speed as a function of wavelength; inversion process determines elastic constants of layers.	Determine the stiffness profile of a pavement system. Also used to determine depth of deteriorated concrete.
3.2.5 3.3.2	**Impulse-response**—Surface of element is struck with instrumented hammer and adjacent transducers measure dynamic response; signal analysis allows determining characteristics of tested element.	Locate anomalous regions in plate-like structures. Locate voids below slabs-on-ground. Locate cracks or constrictions (neck-in) in deep foundations. Provides information on the low-strain dynamic stiffness of the shaft/soil system.
3.3.1	**Sonic-echo**—Hammer impact on surface and a receiver monitors reflected stress wave. Time-domain analysis used to determine travel time.	Determine the length of deep foundations (piles and piers); determine the location of cracks or constrictions (neck-in).
3.3.2	**Impulse-response (mobility) method**—Surface of element is struck with instrumented hammer and adjacent transducers measure dynamic response; frequency domain signal analysis allows determining characteristics of tested element.	Determine the length of deep foundations (piles and piers); determine the location of cracks or constrictions (neck-in).
3.3.3	**Impedance logging**—Test is similar to sonic-echo or impulse-response, but the use of more complex signal analyses (time and frequency domains) allows reconstructing the approximate shape of the deep foundation.	Determine the approximate two-dimensional (2-D) shape of the deep foundation.
3.3.4	**Crosshole sonic logging (CSL)**—Analogous to the ultrasonic pulse velocity (UPV) test, but transducers are positioned within water-filled tubes cast into the deep foundation or holes drilled after construction.	Determine the location of low-quality concrete and defects along the length of the shaft and between transducers. With drilled holes permits direct determination of shaft length.
3.3.5	**Parallel seismic**—Receiver is placed in hole adjacent to the foundation. Foundation is struck with a hammer and signal from receiver is recorded. Test is repeated with receiver at increasing depth.	Determine the foundation depth and determine whether it is of uniform quality.
3.4.2	**Direct transmission radiometry for density**—Measure the intensity of high-energy electromagnetic radiation after passing through concrete.	Determine in-place density of fresh or hardened concrete. Locate reinforcing steel or voids.
3.4.3	**Backscatter radiometry for density**—Measure the intensity of high-energy electromagnetic radiation that is backscattered (reflected) by the near-surface region of a concrete member.	Determine in-place density of fresh or hardened concrete.
3.4.4	**Radiography**—The intensity of high-energy electromagnetic radiation, which passes through a member, is recorded on photographic film.	Locate reinforcing and prestressing steel, conduits, pipes, voids, and honeycombing.
3.4.5	**Gamma-gamma logging of deep foundations**—See direct transmission and backscatter radiometry. Radioactive source and detector are lowered into separate access tubes cast into deep foundation.	Locate regions of low density along length of foundation.
3.5.1	**Covermeters—**Sometimes known as a reinforcing bar locator, is a low-frequency alternating magnetic field applied on the surface of the structure; the presence of embedded reinforcement alters this field, and measurement of this change provides information on the reinforcement.	Locate embedded steel reinforcement, measure depth of cover, estimate diameter, and determine direction of reinforcement.
3.5.2	**Half-cell potential**—Measure the potential difference (voltage) between the steel reinforcement and a standard reference electrode; the measured voltage provides an indication of the likelihood that corrosion is occurring in the reinforcement.	Identify region or regions in a reinforced concrete structure where there is a high probability that corrosion is occurring at the time of the measurement.
3.5.3	**Concrete resistivity**—In four-electrode method, often called Wenner Array, measures the electric potential between two inner electrodes due to current between two outer electrodes. Calculate resistivity based on assumed model.	Used to supplement half-cell potential survey; regions of low resistivity may be associated with high corrosion rate of reinforcement if there is active corrosion. In the laboratory, method can be used to assess resistance to fluid transport of saturated specimens.

Table 3—Summary of nondestructive testing methods (cont.)

3.5.4	**Linear polarization resistance**—Apply small current and measure change in the potential difference between the reinforcement and a standard reference electrode; the measured current and voltage changes allow determination of the polarization resistance, which is related to the rate of corrosion.	Determine the instantaneous corrosion rate of the reinforcement located below the test point. By taking readings at key times during an annual cycle, one can approximate service life.
3.5.5	**Magnetic-flux leakage**—Strong magnetic field is applied to a reinforced concrete member. The field induces a magnetic flux in the reinforcement. If there is a fractured bar or wire, flux is disrupted and magnetic lines flow out of the concrete, which are detected by a magnetic field sensor. Presence of flux leakage is used as indicator of wire break.	Commonly used for pipeline inspection of welds. Has been adapted for detecting wire breaks in prestressed concrete members.
3.6	**Methods for measuring transport properties**—Measure the flow of a fluid (air or water) into concrete under prescribed test conditions; the flow rate depends on the transport properties of the concrete. Transport may be by permeation, absorption, diffusion, or their combination.	Compare alternative concrete mixtures. Primarily research tools, but have the potential to be used for assessing adequacy of curing process.
3.7	**Infrared thermography**—The presence of flaws within the concrete affects the heat conduction properties of the concrete and the presence of defects are indicated by differences in surface temperatures when the test object is exposed to correct ambient conditions. Under controlled, pulsed heating conditions, the evolution of the surface temperature distribution can be related to relative flaw depth.	Locate near-surface delaminations in pavements and bridge decks. Well-suited for detecting delaminations in fiber-reinforced polymer laminates used for strengthening concrete members. Also widely used for detecting moist insulation in buildings.
3.8	**Radar**—Analogous to the ultrasonic pitch-catch method except that electromagnetic waves are used instead of stress waves. Interface between materials with different dielectric properties results in reflection of a portion of incident electromagnetic pulse.	Locate metal embedments, voids beneath pavements, and regions of high moisture contents; determine thickness of members.

NDT method is established, a thorough inspection of the structure can be completed economically.

3.1—Visual inspection

3.1.1 *General*—Normally, a visual inspection is one of the first steps in the evaluation of a concrete structure (Perenchio 1989). Visual inspection performed by a qualified investigator can provide a wealth of information that may lead to positive identification of the cause of observed distress. Broad knowledge in structural engineering, concrete materials, deterioration mechanisms, and construction methods is needed to extract the most information from the visual inspection. ACI 201.1R, ACI 207.3R, ACI 224.1R, ACI 362.2R, and ACI 349.3R provide information for recognizing and classifying different types of damage and can help to identify the probable cause of the distress.

3.1.2 *Planning*—Before undertaking a detailed visual inspection, the investigator should develop and follow a preestablished plan to maximize the quality of the recorded data. A suitable approach typically involves the following activities:

a) Cursory walk-through inspection to become familiar with the structure

b) Gathering background documents and information on the design, construction, ambient conditions, and operation and maintenance of the structure

c) Planning the complete investigation

d) Selecting necessary tools and appropriate safety equipment; laying out a control grid on the structure to serve as a basis for recording observations

e) Undertaking the visual inspection

f) Performing necessary supplemental tests

ACI 207.3R, ACI 224.1R, ACI 349.3R, ACI 362.2R, and ACI 437R should be consulted for additional guidance on planning and carrying out the complete investigation.

3.1.3 *Supplemental tools*—Visual inspection is one of the most versatile and powerful of all the NDT methods; however, its effectiveness depends on the knowledge and experience of the investigator. It has the obvious limitation that only visible surfaces can be inspected. Internal defects go unnoticed and no quantitative information is obtained about the properties of the concrete. For these reasons, a visual inspection is usually supplemented by one or more of the other NDT methods discussed in this chapter. The inspector should consider other useful tools that can enhance the power of a visual inspection.

Optical magnification allows for a more detailed view of local areas of distress. Available instruments range from simple magnifying glasses to more expensive hand-held microscopes. Understanding the fundamental principles of optical magnification is helpful in selecting the correct tool. For example, the focal length decreases with increasing magnifying power, requiring the primary lens be placed closer to the surface being inspected. The field of view also decreases with increasing magnification, making it tedious to inspect a large area at high magnification. The depth of field is the maximum difference in elevation of points on a rough textured surface that are simultaneously in focus; this decreases with increasing magnification of the instrument. To assure that the hills and valleys are in focus simultaneously, the depth of field has to be greater than the elevation differences in the texture of the surface that is being viewed. The illumination required to see clearly increases with magnification level with artificial lighting necessary at high magnification.

A useful tool for crack inspection is a small hand-held magnifier with a built-in measuring scale on the lens closest to the surface being viewed (ACI 224.1R). With such a crack comparator, the width of surface cracks can be measured accurately.

A stereo microscope includes two viewing lenses that allow a three-dimensional observation of the surface. By calibrating the focus adjustment screw (change in height per screw revolution), the investigator can estimate the elevation

differences in surface features. This is done by first focusing on the lowest point within the field of view and determining how many turns of the screw it takes to bring the highest point into focus.

Fiberscopes and borescopes allow inspection of regions that are otherwise inaccessible to the naked eye. A fiberscope is composed of a bundle of optical fibers and a lens system; it allows viewing into cavities within a structure by means of small access holes. The fiberscope is designed so that some fibers transmit light to illuminate the cavity. The operator can rotate the viewing head to allow a wide viewing angle from a single access hole. A borescope, which is composed of a rigid tube with mirrors and lenses, is designed to view straight ahead or at right angles to the tube. The image is clearer using a borescope, whereas the fiberscope offers more flexibility in the field of view. The use of these scopes requires drilling small holes if other access channels are absent, and the holes should intercept the cavity to be inspected. Additional methods discussed in this chapter may be used to locate these cavities. Therefore, the fiberscope or borescope may be used to verify the results of other NDT methods without having to take cores. The locations of drilled access holes need to be chosen carefully to avoid drilling into utility conduits or reinforcing steel.

Flexibility of visual inspection was expanded by development of the small, inexpensive, digital video camera. These are used like borescopes with the added benefit of video output that can be displayed on a monitor and stored on the appropriate recording media. These cameras have various optical systems that come in a variety of sizes, resolutions, and focal lengths. Miniature versions attached to the ends of flexible shafts are available. These can be inserted into holes drilled into the structure for views of internal cavities. Alternatively, these small cameras can be mounted on robotic devices for inspections in pipes, or within areas that pose health or safety hazards.

3.1.4 *Reliability*—The Federal Highway Administration (FHWA) conducted a study to evaluate the reliability of visual inspection of bridges (Moore et al. 2001). Although there are differences in inspecting bridges compared with buildings, the study provides insight into the limitations of visual inspection. The study sought to evaluate the reliability of routine, in-depth bridge inspections; the influence of key factors on the results of visual inspections; and the differences in procedures and report formats for different states. The purpose of a bridge inspection is to assign a condition rating to the outcome, which numbers from 0 (failed condition) to 9 (excellent condition).

Routine inspections are regularly scheduled inspections consisting of observations, measurements, or both, that are required to determine the physical and functional condition of the bridge, to identify any changes from initial or previously recorded conditions, and to ensure that the structure continues to satisfy present service requirements (Moore et al. 2001). Results showed that 95 percent of ratings from routine inspections varied within two points of the average rating for a given bridge. Factors that appeared to correlate with the results included fear of traffic, visual acuity and color vision, formal inspection training, light intensity, and time constraints to complete the inspection. Interestingly, the following factors had minimal correlation to the bridge ratings assigned by the inspector: being a licensed engineer, general education level, and bridge inspection experience.

An in-depth inspection is a close-up, hands-on inspection of one or more members above or below the water level to identify any deficiency or deficiencies not readily detectable using routine inspection procedures (Moore et al. 2001). Results showed that in-depth inspections using visual inspection alone are not likely to detect the specific defects for which the inspection is prescribed, and they may not reveal deficiencies beyond those noted in routine inspections. Factors that appeared to relate to the results of an in-depth inspection include overall thoroughness with which the inspector completed the task, completion time, comfort with access equipment and heights, complexity of the structure and its accessibility, and flashlight use.

Based on the results of the study, authors of the FHWA report provided a set of recommendations that included the following (Moore et al. 2001):

a) Accuracy and reliability of in-depth inspections could be increased by increased training in the types of defects that should be identified and the best methods to use.

b) Factors that were found to correlate with inspection results should be considered in choosing and training inspectors.

c) Further study of the types of defects that could occur and are likely to be identified in concrete structures is warranted.

In summary, visual inspection is a powerful NDT method. Its effectiveness, however, is limited by the investigator's experience and knowledge. A broad knowledge of structural behavior, materials, and construction methods is desirable. Low-cost tools are available to extend the capabilities of visual inspection, which is typically only one aspect of the total evaluation plan. Visual inspections will often be supplemented by a series of other NDT methods or invasive procedures.

3.2—Stress-wave methods for structures

Several test methods based on stress-wave propagation can be used for nondestructive testing (NDT) of concrete structures. The ultrasonic through-transmission (pulse velocity) method can be used for locating abnormal regions in a member. The term "ultrasonic" refers to stress waves above the audible range, which is usually assumed to be above a frequency of 20 kHz.

The echo methods can be used for thickness measurements and flaw detection. The spectral analysis of surface waves (SASW) method can be used to determine the thickness and elastic moduli of layered pavement systems. The following subsections describe the principles and instrumentation for each method. Section 3.3 discusses stress-wave methods for integrity testing of deep foundations. Additional information is provided in Carino (2004a).

Stress waves occur when pressure or deformation is applied suddenly, such as by impact, to the surface of a solid. The disturbance propagates through the solid in a manner

analogous to how sound travels through air. The speed of stress-wave propagation in an elastic solid is a function of the Young's modulus of elasticity, Poisson's ratio, the density, and the geometry of the solid. This dependence between the properties of a solid and the resultant stress-wave propagation behavior permits inferences about the characteristics of the solid by monitoring the propagation of stress waves.

When pressure is applied suddenly at a point on the surface of a solid half-space, the disturbance propagates through the solid as three different waves: P-wave, S-wave, and R-wave. The P-wave and S-wave propagate into the solid along hemispherical wavefronts. The P-wave, also called the dilatational or compression (primary) wave, is associated with the propagation of normal stress and particle motion is parallel to the propagation direction. The S-wave, also called the shear or transverse wave, is associated with shear stress and particle motion is perpendicular to the propagation direction. In addition, an R-wave travels away from the disturbance along the surface. In an isotropic, elastic solid, the P-wave speed, C_p, is related to the Young's modulus of elasticity E; Poisson's ratio ν; and density ρ (Krautkrämer and Krautkrämer 1990)

$$C_p = \sqrt{\frac{E(1-\nu)}{\rho(1+\nu)(1-2\nu)}} \tag{3.2a}$$

The S-wave propagates at a slower speed, C_s, given by (Krautkrämer and Krautkrämer 1990)

$$C_s = \sqrt{\frac{G}{\rho}} \tag{3.2b}$$

where G is the shear modulus of elasticity.

A useful parameter is the ratio of S-wave speed to P-wave speed

$$\frac{C_s}{C_p} = \sqrt{\frac{1-2\nu}{2(1-\nu)}} \tag{3.2c}$$

For a Poisson's ratio ν of 0.2, which is typical of concrete, this ratio equals 0.61. The ratio of the R-wave speed, C_r, to the S-wave speed may be approximated by (Krautkrämer and Krautkrämer 1990)

$$\frac{C_r}{C_s} = \frac{0.87+1.12\nu}{1+\nu} \tag{3.2d}$$

For a Poisson's ratio ν between 0.15 and 0.25, the R-wave speed is from 90 to 92 percent of the S-wave speed.

Equation (3.2a) represents the P-wave speed in an infinite solid. In the case of bounded solids, wave speed is affected by the geometry of the solid. For wave propagation along the axis of slender bar, the wave speed of the dominant pulse is independent of Poisson's ratio and is given by

Table 3.2—*Z*-values for common materials

Material	Specific acoustic impedance, kg/(m²·s) (psi·s/ft)
Air	0.4 (1.7×10^{-5})
Water	1.5×10^6 (66)
Soil	0.3 to 4×10^6 (13 to 180)
Concrete	7 to 10×10^6 (310 to 440)
Limestone	7 to 19×10^6 (310 to 840)
Granite	15 to 17×10^6 (660 to 750)
Steel	47×10^6 (2100)

$$C_b = \sqrt{\frac{E}{\rho}} \tag{3.2e}$$

where C_b is the bar wave speed. For a Poisson's ratio between 0.15 and 0.25, the bar wave speed in a slender bar is 3 to 9 percent slower than the P-wave speed in a large solid.

When a stress wave traveling through Material 1 is incident on the interface between a dissimilar Material 2, a portion of the incident wave is reflected. The amplitude of the reflected wave is a function of the angle of incidence and is a maximum when this angle is 90 degrees (normal incidence). For normal incidence, the reflection coefficient R is given by

$$R = \frac{Z_2 - Z_1}{Z_2 + Z_1} \tag{3.2f}$$

where R is the ratio of sound pressure of the reflected wave to the sound pressure of the incident wave; Z_2 is the specific acoustic impedance of Material 2; and Z_1 is the specific acoustic impedance of Material 1.

The specific acoustic impedance is the product of the wave speed and density of the material. Table 3.2 shows approximate Z-values for some materials (Carino 2004a).

Thus, for a stress wave that encounters an air interface as it travels through concrete, the absolute value of the reflection coefficient is nearly 1.0, and there is almost total reflection at the interface. This is why NDT methods based on stress-wave propagation have proven to be successful for locating defects within concrete.

3.2.1 *Ultrasonic through transmission (pulse velocity) method*—One of the oldest NDT methods for concrete is based on measuring the travel time over a known path length of a pulse of ultrasonic compressional waves. The technique is known as ultrasonic through transmission or, more commonly, as the ultrasonic pulse velocity (UPV) method. Naik et al. (2004) provide a summary of this test method, and Tomsett (1980) reviewed the various applications of the technique.

The development of field instruments to measure the pulse velocity occurred nearly simultaneously in the late 1940s in Canada and England (Whitehurst 1967). In Canada, there was a need for an instrument that could measure the extent of cracking in dams (Leslie and Cheesman 1949). In the UK,

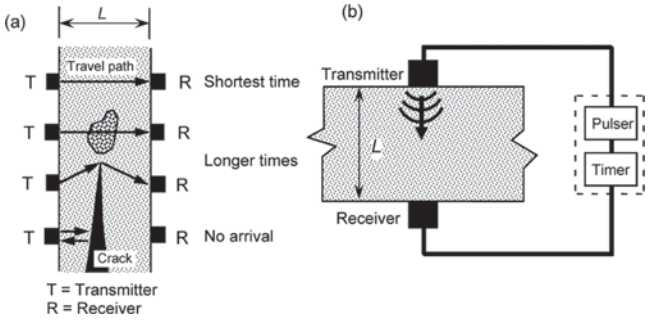

Fig. 3.2.1.1a—(a) Effects of defects on travel time of ultrasonic pulse; and (b) schematic of through-transmission test system.

the emphasis was on the development of an instrument to assess the quality of concrete pavements (Jones 1949).

3.2.1.1 *Principle*—The speed of propagation of stress waves depends on the density and the elastic constants of the solid. In a concrete member, variations in density can arise from non-uniform consolidation, and variations in elastic properties can occur due to variations in materials, mixture proportions, or curing. Thus, by determining the wave speed at different locations in a structure, it is possible to make inferences about the uniformity of the concrete. The compressional wave speed is determined by measuring the travel time of the stress pulse over a known distance.

The testing principle is illustrated in Fig. 3.2.1.1a(a), which depicts the paths of ultrasonic pulses as they travel from one side of a concrete member to the other. The top case represents the shortest direct path through sound concrete, which would result in the shortest travel time or the fastest apparent wave speed. The second case represents a path that passes through a portion of inferior concrete, and the third case shows a diffracted path around the edge of a large void or crack. In these latter cases, the travel time would be greater than the first case. The last case indicates a travel path that is interrupted by a void. This air interface results in total reflection of the stress waves with no arrival at the opposite side. The apparent wave speeds are determined by dividing the member thickness by the measured travel time. A comparison of the wave speeds at the different test points would indicate the areas of anomalies within the member. It might also be possible to use signal attenuation as an indicator of relative quality of concrete. This, however, requires special care to ensure consistent coupling of the transducers at all test points (Teodoru 1994).

An apparatus for through-transmission measurements has also been used on the same surface, as shown in Fig. 3.2.1.1b(a). This approach has been suggested for measuring the depth of a fire-damaged surface layer having a lower wave speed than the underlying sound concrete (Chung and Law 1985) and for measuring the depth of concrete damaged by freezing (Teodoru and Herf 1996). The test is carried out by measuring the travel time as a function of the separation, X, between transmitter and receiver. The method assumes that stress-wave arrival at the receiver occurs along two paths: Path 1, which is directly through the damaged concrete, and

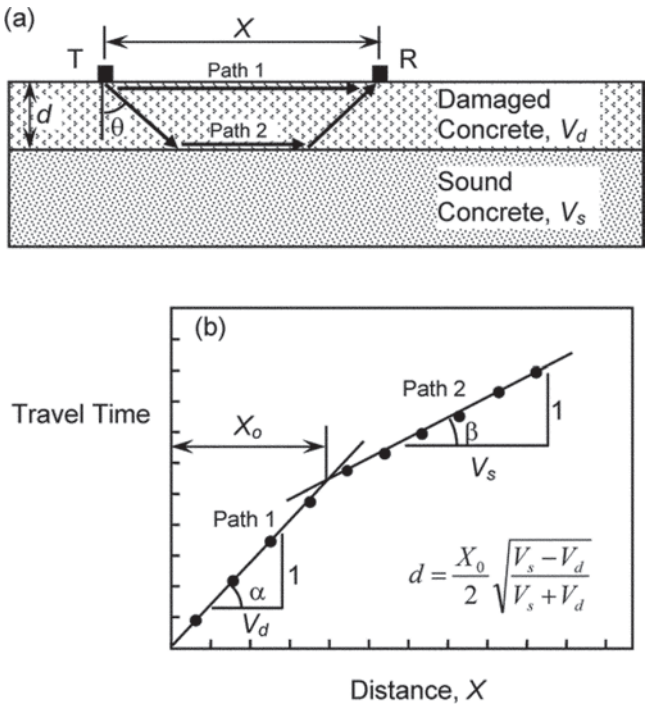

Fig. 3.2.1.1b—(a) Wave paths for ultrasonic testing on surface of concrete having damaged surface layer; and (b) travel time as a function of distance between transmitter and receiver.

Path 2, which is through the damaged and sound concrete. For small separation, the travel time is shorter for Path 1, and for large separation, the travel time is shorter for Path 2. By plotting the travel time as a function of the distance X, the presence of a damaged surface layer is indicated by a change in the slope of the data. The distance X_o, at which the travel times for the two paths are equal, is found from the intersection of the straight lines, as shown in Fig. 3.2.1.1b(b). The slopes of the two lines are reciprocals of the wave speeds in the damaged (V_d) and sound (V_s) concrete. The depth of the damaged layer is found using Eq. (3.2.1.1) (Chung and Law 1985).

$$d = \frac{X_o}{2}\sqrt{\frac{V_s - V_d}{V_s + V_d}} \qquad (3.2.1.1)$$

For the surface method, which relies on measuring the arrival time of low-amplitude waves, the user should understand the capabilities of the instrument to measure the correct arrival times. The user should also be familiar with the underlying theory of seismic refraction (Richart et al. 1970) that forms the basis of Eq. (3.2.1.1). The method is only applicable if the upper layer has a slower wave speed than the lower layer.

It is also possible to use multiple pulse velocity data to construct a two-dimensional (2-D) tomographic image of the interior of the concrete. This requires the ability to make multiple through-transmission measurements so that a chosen cross section is traversed by many direct ray paths. The cross section is modeled as a grid of elements whose

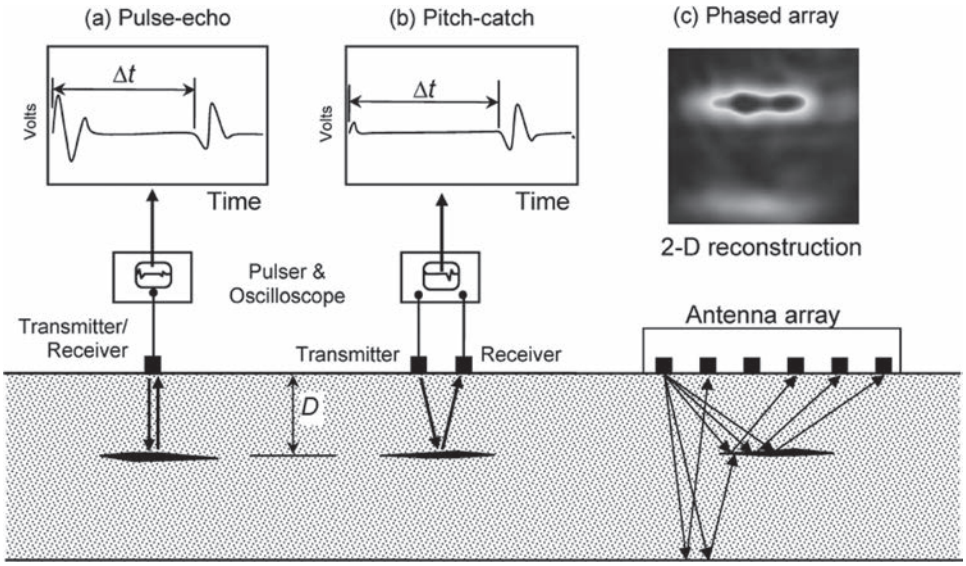

Fig. 3.2.2.1—Schematic of ultrasonic-echo methods: (a) pulse-echo method; (b) pitch-catch method; and (c) multiple pitch-catch using transducer array.

size depends on the number of measurements that are made. Based on the many calculated pulse velocities, computer software can be used to back-calculate a characteristic pulse velocity for each element. The result will be a 2-D image of the distribution of pulse velocity within the element cross section. Regions with abnormally low pulse velocity can then be identified as defects (Martin et al. 2001).

3.2.1.2 *Instrumentation*—The main components of modern devices for measuring the UPV are shown schematically in Fig. 3.2.1.1a(b). A transmitting transducer is positioned on one face of the member and a receiving transducer is positioned on the opposite face. The transducers contain piezoelectric ceramic elements. Piezoelectric materials change dimension when a voltage is applied to them, or they produce a voltage change when they are deformed. A pulser is used to apply a high voltage to the transmitting transducer (source), and the suddenly-applied voltage causes the transducer to vibrate at its natural frequency. The vibration of the transmitter produces the stress pulse that propagates into the member. At the same time that the voltage pulse is generated, an accurate electronic timer is turned on. When the pulse arrives at the receiver, the vibration is changed to a voltage signal that turns off the timer and the travel time is displayed. Requirements for a suitable pulse-velocity device are given in ASTM C597.

The transducers are coupled to the test surfaces using a viscous material, such as grease, or a nonstaining ultrasonic gel couplant if staining of the concrete is a problem. Transducers of various resonant frequencies have been used, with 50 kHz transducers being the most common. Generally, lower-frequency transducers are used for mass concrete (20 kHz) and higher-frequency transducers (>100 kHz) are used for thinner members, where accurate travel times have to be measured. In most applications, 50 kHz transducers are suitable.

3.2.2 *Ultrasonic-echo method*—Drawbacks of the through-transmission method include the need for access to both sides of the member and lack of information on the location (depth) of a detected anomaly. These limitations can be overcome by using the echo method, where testing is performed on one face of the member and the arrival time of a stress wave reflected from a defect is determined. This approach, which has been developed for testing metals, is known as the pulse-echo method. Since the 1960s, a number of different experimental ultrasonic-echo systems based on P-waves have been developed for concrete (Bradfield and Gatfield 1964; Howkins 1968). Successful applications have been limited mainly to measuring the thickness of and detecting flaws in thin slabs, pavements, and walls (Mailer 1972; Alexander and Thornton 1989). In the late 1990s, an ultrasonic-echo system based on S-waves and using multiple sensors was developed (Kozlov et al. 1997).

3.2.2.1 *Principle*—In the pulse-echo method, a stress pulse is introduced into an object at an accessible surface by a transmitter. The pulse propagates into the test object and is reflected by flaws or interfaces. The surface response caused by the arrival of reflected waves, or echoes, is monitored by the same transducer acting as a receiver. This technique is illustrated in Fig. 3.2.2.1(a). Due to technical problems in developing a suitable pulse-echo transducer for testing concrete, successful ultrasonic-echo methods have, in the past, used a separate receiving transducer located close to the transmitting transducer. This system, which is known as pitch-catch, is illustrated in Fig. 3.2.2.1(b). In early instruments, the receiver output was displayed on an oscilloscope as a time-domain waveform. The round-trip travel time of the pulse can be obtained from the waveform by determining the time from the start of the transmitted pulse to the reception of the echo. If the wave speed in the material is known, this travel time can be used to determine the depth of the reflecting interface. Pitch-catch systems developed in the 1990s use an array of transducers so that multiple pitch-catch measurements are made sequentially. The resulting

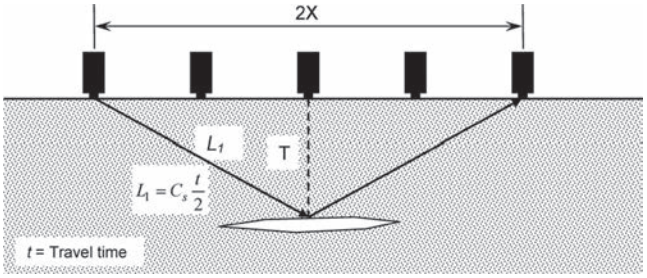

Fig. 3.2.2.2a—Principle of depth correction used in SAFT method.

travel time measurements are used to reconstruct an image of the reflecting interfaces. This type of system is illustrated in Fig. 3.2.2.1(c).

3.2.2.2 *Instrumentation*—The key components of a traditional pitch-catch ultrasonic-echo test system are the transmitting and receiving transducer(s), a pulser, and an oscilloscope or a computer for data acquisition and signal analysis. Transducers that transmit and receive short-duration, low-frequency (200 kHz) focused waves are needed for testing concrete. Note that a frequency of 200 kHz is considered low compared with the higher frequencies used in pulse-echo systems for testing metals, where frequencies in excess of 1 MHz are common.

In the early work, transmitting transducers were designed to have a focused P-wave field so that only the portion of the concrete directly below the transducers would be viewed. However, it was difficult to construct them and their dimensions often became large, making the transducers cumbersome and difficult to couple to the surface of the concrete (Mailer 1972). Although advances have resulted in improved transducers (Alexander and Thornton 1989), their penetration depths were limited to approximately 10 in. (250 mm).

A true pulse-echo system, where the source and receiver are one transducer, was developed and applied in the laboratory to concrete with small-sized aggregate (Hillger 1993). This system used a heavily damped 500 kHz transducer as both the source and receiver. A computer was used to process the data and display results using conventional techniques like ultrasonic testing of metals. One display method is the B-scan, where successive time-domain traces (obtained as the transducer is scanned over the test object) are oriented vertically and placed next to each other. The resulting plot is a cross-sectional view of the object showing the location of reflecting interfaces along the scan line. Because the system was cumbersome, requiring each transducer be cemented into place at each test point, a commercial system was never developed.

In the 1990s, dry point contact (DPC) transducers were developed that were capable of transmitting short pulses of low-frequency (less than 150 kHz) S-waves into concrete (Shevaldykin et al. 2003). The term "dry" means that no coupling fluid is necessary and the transducers are spring-loaded to ensure efficient coupling to irregular surfaces. These transducers are arranged in a 2-D array within a housing unit and operated on the pitch-catch principle as illustrated in Fig. 3.2.2.1(c). A computer software program is used to control the transducers so that they operate as transmitters and receivers in a predefined sequence. The result of a measurement is an array of round-trip travel times from transmitting to receiving transducers. Because of the inclined ray paths, as shown in Fig. 3.2.2.2a, the measured travel times between transducer pairs have to be corrected to obtain the correct depth of the reflecting interface. If the distance between the transmitter and receiver is 2*X*, the depth *T* of the reflecting interface is as follows

$$T = \sqrt{\left(C_s \frac{t}{2}\right)^2 - X^2} \qquad (3.2.2.2)$$

where C_s is the shear wave speed, and *t* is the travel time from transmitter to receiver.

A signal processing method known as the synthetic aperture focusing technique (SAFT) is used to reconstruct an internal image of the test object based on the corrected depths determined from Eq. (3.2.2.2) (Schickert et al. 2003; De La Haza et al. 2008). The reconstruction is done by representing the test object as a mesh of small elements, much like a finite-element mesh. From the known location of the transducer pairs and the corrected depths, the locations of reflectors are identified. The SAFT algorithm results in a constructed three-dimensional (3-D) image that can be viewed on any of three orthogonal image planes. The result is analogous to medical tomographic images that can be manipulated to look at different slices through the scanned object.

Figure 3.2.2.2b shows an example of a plain concrete block (Fig. 3.2.2.2b(a)) and an image (Fig. 3.2.2.2b(b)) that was obtained from a commercially available system. Figure 3.2.2.2b(a) shows a plain concrete masonry unit with a single 1.2 in. (30 mm) diameter hole at a depth of 5.1 in. (130 mm) and two 0.5 in. (13 mm) holes at depths of 2.2 in. (55 mm) and 6.3 in. (160 mm). In Fig. 3.2.2.2b(b), a 2-D image is shown that represents an end view of the block. The presence of the three holes is shown clearly. The back wall of the block is indicated as the light zone at the bottom of the image.

3.2.3 *Impact-echo method*—The idea of using an impact to generate a stress pulse is an old idea that has the advantage of eliminating the need for a bulky transmitting transducer and providing a stress pulse with greater penetration ability. However, the stress pulse generated by impact at a point is not focused like a pulse from an ultrasonic transducer. Instead, waves propagate into a test object in all directions, and reflections may arrive from many directions. Since the early 1970s, impact methods, usually called seismic-echo or sonic-echo methods, have been widely used for evaluation of concrete piles and drilled shaft foundations (Steinbach and Vey 1975). These foundation NDT methods are discussed in 3.3.1. Beginning in the mid-1980s, the impact-echo technique was developed for testing concrete structural members (Sansalone and Carino 1986; Sansalone 1997). Applications of the impact-echo technique include determining the thickness of and detecting flaws in plate-like structural members such as slabs and bridge decks with or without overlays;

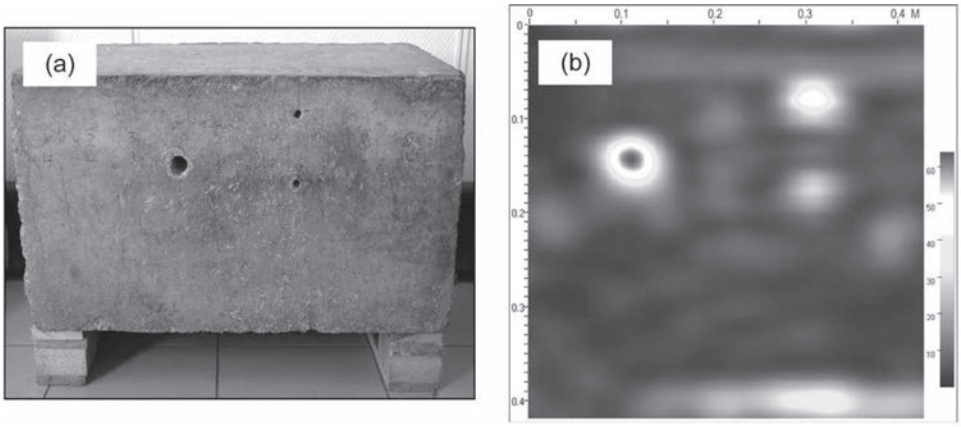

Fig. 3.2.2.2b—(a) Concrete block with three holes; (b) and elevation view based of SAFT reconstruction using multiple pitch-catch measurements (figure courtesy of Germann Instruments).

detecting flaws in beams, columns, and hollow cylindrical structural members; assessing the quality of bond in overlays; measuring crack depth; and voiding detection in grouted ducts of post tensioned bridge beams (Sansalone and Streett 1997; Sansalone and Carino 1988, 1989a,b; Lin and Sansalone 1992a,b,c; Cheng and Sansalone 1993; Lin and Sansalone 1993, 1994a,b, 1996; Lin and Su 1996; Abraham et al. 2002; Colla 2002; Muldoon et al. 2007). The use of the impact-echo method for determination of the thickness of concrete plate elements was standardized in ASTM C1383.

3.2.3.1 *Principle*—The principle of the impact-echo technique is illustrated in Fig. 3.2.3.1(a). A transient stress pulse is introduced into a test object by mechanical impact on the surface. The P- and S-waves produced by the stress pulse propagate into the object along hemispherical wavefronts. In addition, a surface wave travels along the surface away from the impact point. The waves are reflected by internal interfaces or external boundaries. The arrival of these reflected waves, or echoes, at the surface where the impact was generated produces displacements that are measured by a receiving transducer and recorded using a data-acquisition system. Interpretation of waveforms in the time domain has been successful in seismic-echo applications involving long, slender structural members such as piles and drilled shafts (Steinbach and Vey 1975; Olson and Wright 1990). In such cases, there is sufficient time between the generation of the stress pulse and the reception of the wave reflected from the bottom surface or from an inclusion or other flaw, so that the arrival time of the reflected wave is generally easy to determine, even if long-duration impacts produced by hammers are used.

Although for relatively thin structural members, such as slabs and walls, time-domain analysis is feasible if short-duration impacts are used, it is time consuming and can be difficult depending on the geometry of the structure (Sansalone and Carino 1986). The preferred approach, which is much quicker and simpler, is frequency analysis of displacement waveforms (Carino et al. 1986). The underlying principle of frequency analysis is that the waves generated by the impact undergo multiple reflections within the element and set up a resonant thickness mode vibration (Gibson and Popovics 2005). The frequency of this resonant vibration depends on the wave speed and the distance between the test surface and the reflecting interface or back wall of the element. For the case of reflections in a plate-like structure, this frequency is called thickness frequency. The frequency varies with the inverse of member thickness.

In frequency analysis, the time-domain signal is transformed into the frequency domain using the fast Fourier transform (FFT) technique. The result is an amplitude spectrum that indicates the amplitude of the various frequency components in the waveforms. The frequency corresponding to the setup resonance vibration—that is, the thickness frequency—is indicated by a peak in the amplitude spectrum. For a plate-like structure, the approximate relationship between the distance D to the reflecting interface, the P-wave speed C_p, and the thickness frequency f is

$$D = \frac{C_p}{2f} \tag{3.2.3.1}$$

For accurate assessment of plate thickness, the P-wave speed in Eq. (3.2.3.1) should be multiplied by a factor that ranges from 0.96 to 0.94, depending on material's Poisson's ratio (Gibson and Popovics 2005). In ASTM C1383, the P-wave speed is multiplied by 0.96.

As an example, Fig. 3.2.3.1(b) shows the amplitude spectrum obtained from an impact-echo test of a 20 in. (0.5 m) thick concrete slab. The peak at 3.42 kHz corresponds to the thickness frequency of the solid slab and a velocity of 11,200 ft/s (3420 m/s) is calculated. Figure 3.2.3.1(c) shows the amplitude spectrum for a test over a void within the same slab. The peak has shifted to a frequency of 7.32 kHz, indicating that the reflections are occurring from an interface within the slab. The ratio 3.42 kHz/7.32 kHz = 0.46 indicates that the interface is at approximately the middle of the slab with a calculated depth of 9 in. (0.23 m).

In using the impact-echo method to determine the locations of flaws within a slab or other plate-like structure,

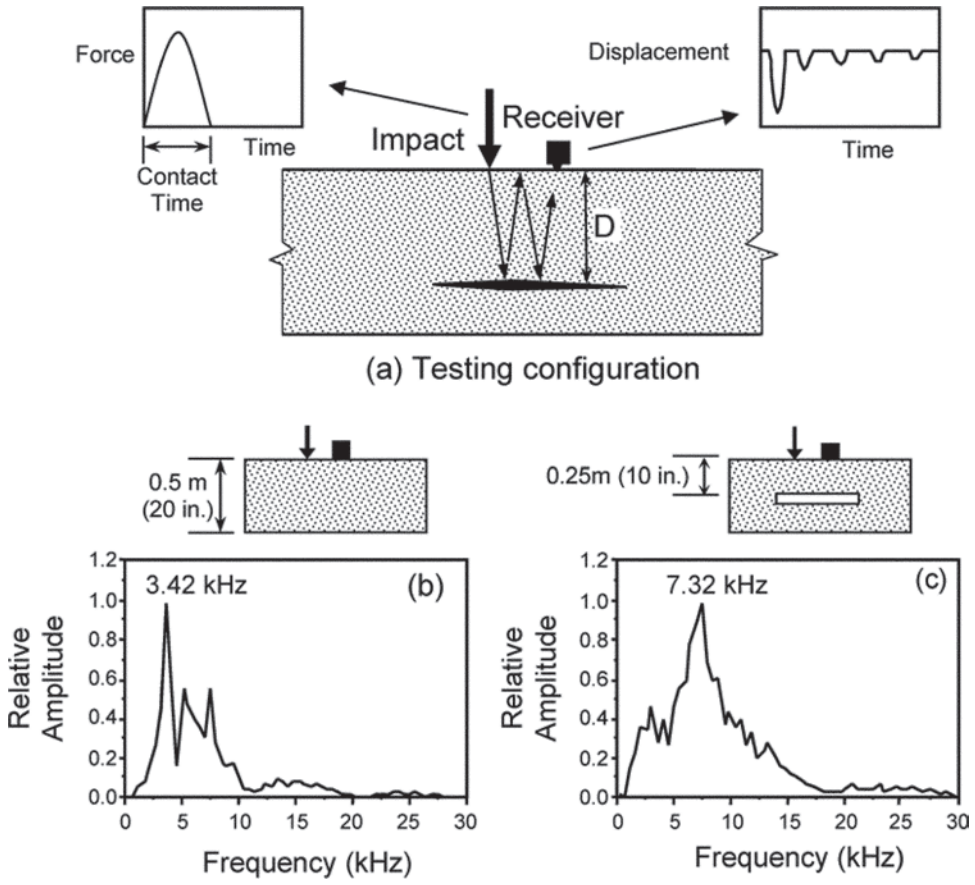

Fig. 3.2.3.1—(a) Schematic of impact-echo method; (b) amplitude spectrum for test of solid slab; and (c) amplitude spectrum for test over void in slab.

tests can be performed at regularly spaced points along lines marked on the surface. Spectra obtained from such a series of tests can be analyzed with the aid of computer software that can identify those test points corresponding to the presence of flaws and can plot a cross-sectional view along the test line (Pratt and Sansalone 1992).

Frequency analysis of signals obtained from impact-echo tests on bar-like structural elements, such as reinforced concrete beams and columns, bridge piers, and similar members, is more complicated than the case of slab-like structural members. The presence of the side boundaries gives rise to transverse modes of vibration of the cross section (Sansalone and Streett 1997). Thus, before attempting to interpret test results, the characteristic frequencies associated with the transverse modes of vibration of a solid structural member have to be determined. These frequencies depend on the shape and dimensions of the cross section. It has been shown that the presence of a flaw disrupts these modes, making it possible to determine that a flaw exists (Lin and Sansalone 1992a,b,c).

3.2.3.2 *Instrumentation*—An impact-echo test system, in accordance with ASTM C1383, is composed of three components: an impact source; a receiving transducer; and a data-acquisition system that is used to capture the output of the transducer, store the digitized waveforms, and perform signal analysis. A suitable impact-echo test system can be assembled from off-the-shelf components. Several field systems (hardware and analysis software) are commercially available.

The selection of the impact source is a critical aspect of a successful impact-echo test system. The impact duration determines the frequency content of the stress pulse generated by the impact and determines the minimum flaw depth that can be determined. As the impact duration is shortened, higher-frequency components are generated. In evaluation of piles, hammers are used that produce energetic impacts with long contact times (greater than 1 ms) suitable for testing long, slender structural members. Impact sources with shorter-duration impacts (20 to 80 μs), such as a spherical impactors, have been used for detecting flaws within structural members less than 40 in. (1 m) thick.

The impact duration, called the contact time, can be estimated from the width of the surface wave signal on the time-domain plot. The contact time of the impact used in the test influences several additional factors that determine the minimum depth and lateral dimension of the flaw that can be detected. These factors are as follows:

a) When spherical impactors are used, the contact time t_c for an elastic impact, assuming no local crushing of the concrete, is approximately a linear function of the ball diameter $t_c \approx 4.3D$ (μs units), where D is the impactor diameter, in millimeters.

b) The maximum useable frequency contained in the impact is approximately the inverse of the contact time ($f_{max} \approx 1/t_c$).

Table 3.2.3.2—Minimum depth and lateral dimension of flaw for detection by impact-echo using impactors of various diameters (C_p = 15,750 ft/s [4000 m/s])

Sphere diameter, in. (mm)	Contact time t_c, μs	Maximum useful frequency = $1/t_c$, kHz	Minimum depth of flaw that can be detected, in. (mm)	Minimum lateral dimension of flaw that can be detected, in. (mm)
0.20 (5)	22	47	1.69 (43)	3.39 (86)
0.25 (6.5)	28	36	2.20 (56)	4.41 (112)
0.31 (8)	34	29	2.72 (69)	5.43 (138)
0.37 (9.5)	41	24	3.22 (82)	6.42 (163)
0.43 (11)	47	21	3.74 (95)	7.44 (189)
0.5 (12.5)	54	19	4.25 (108)	8.46 (215)

c) Using Eq. (3.2.3.1), by replacing f with $1/t_c$, $D_{min} = C_p t_c/2$, which gives the smallest flaw depth, or plate thickness, that can be measured for a given wave speed and impact duration. This equates to half the wavelength (λ/2) associated with the resonant thickness frequency (Sansalone and Streett 1997; Martin and Forde 1995; Martin et al. 1998).

d) The minimum lateral dimension of a flaw that can be detected, regardless of depth, equals the wavelength associated with the maximum useable frequency ($\lambda = C_p/f = C_p t_c$) (Sansalone and Streett 1997).

e) The minimum lateral dimension of a flaw that can be detected is approximately 1/4 of its depth (Sansalone and Streett 1997).

Thus, the minimum lateral dimension of flaw that can be detected is affected both by the contact time and flaw depth (Sansalone and Streett 1997).

Assuming a P-wave speed through concrete of 15,750 ft/s (4000 m/s), Table 3.2.3.2 gives the minimum depth and lateral dimension of a flaw that can be detected for typical sizes of spherical impactors. The least lateral dimension assumes that this is greater than one-quarter of the flaw depth. The values in Table 3.2.3.2 are based on a maximum useful frequency equal to the inverse of the contact time. Sansalone and Streett (1997), however, suggest a maximum useable frequency of 1.25 times this value. The lower maximum frequency recommended herein is believed to be appropriate to provide a more conservative estimate of detectable flaw depth or size, which may account for some inelastic behavior during impact.

New methods of analysis for evaluating the condition of grouted tendon ducts that increase the usefulness of the impact-echo method have been developed:

a) It has been found that if the contact time is too long and does not contain useable frequencies greater than the resonant frequency corresponding to the depth of the void, the presence of the void results in a lower thickness frequency for the solid plate. The presence of an internal duct defect lowers the apparent stiffness of the material through the thickness, giving rise to a lower thickness resonance frequency, which would manifest itself as an apparent increase in the depth of the back wall of the structure. This frequency shift can often be used as an indication of a void and the test should be repeated using a smaller contact time (smaller impactor) (Sansalone and Streett 1997).

b) Presentation of impact-echo amplitude spectra in the form of B-scans (or frequency profiles), which makes it easier to identify changes in the frequency response corresponding to the back wall of the element due to the presence of voids in ducts (Abraham et al. 2002; Colla 2002).

c) Application of the stack imaging technique based on the impact-echo (SIBIE) (Ohtsu and Watanabe 2002; Muldoon et al. 2007). The SIBIE technique enhances the identification of internal reflectors, such as voided tendon ducts, using an impact-echo time signal obtained from a single test location. The impact duration should be relatively short to generate the needed resolution within the time signal; the impact from an aluminum bullet is used as the source of wave energy (Ohtsu and Watanabe 2002). In the analysis, the known cross section of a tested member is divided into square elements, and the travel distance from the impactor to the receiver through the center of each element is calculated. Spectral amplitudes corresponding to virtual resonant frequencies (Eq. (3.2.2.2)) are summarized at each element.

Thus, reflection intensity is estimated as a stack image at each element, which results in a contour map of the reflection intensity across the cross section of the tested member.

In evaluation of piles, geophones (velocity transducers) or accelerometers have been used as the receiving transducer. For impact-echo testing of slabs, walls, beams, and columns, a broad-band conically-tipped piezoelectric transducer (Proctor 1982) that responds to surface displacement has been used as the receiver (Sansalone and Carino 1986). Small accelerometers have also been used as the receiver. In this case, additional signal processing is carried out in the frequency domain to obtain the appropriate amplitude spectrum (Olson and Wright 1990). Such accelerometers should have resonant frequencies well above the anticipated thickness frequencies to be measured.

ASTM adopted the C1383 test method on the use of the impact-echo method to measure the thickness of plate-like concrete members. ASTM C1383 defines a plate as a structure or portion of a structure in which the lateral dimensions are at least six times the thickness. The test method includes two procedures. Procedure A measures the P-wave speed in the concrete, and Procedure B determines the thickness frequency using the impact-echo method. Thickness is calculated from the wave speed and thickness frequency. P-wave speed may be determined by measuring the P-wave speed at the surface using two transducers (Sansalone et al. 1997). Alternately, the P-wave speed may be determined by measuring the thickness frequency at a point and then drilling a hole to measure the actual thickness. Limited comparisons with the length of drilled cores demonstrated

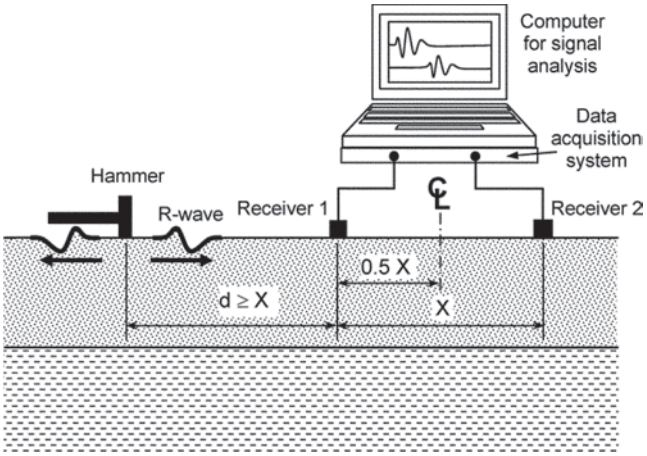

Fig. 3.2.4.1a—Schematic of spectral analysis of surface wave (SASW) method.

that the impact-echo results were within 3 percent of the core lengths (Sansalone and Streett 1997).

3.2.4 *Spectral analysis of surface waves (SASW) method*—In the late 1950s and early 1960s, Jones reported on the use of surface waves to determine the thickness and elastic stiffness of pavement slabs and of the underlying layers (Jones 1955, 1962). The method involved determining the relationship between the wavelength and velocity of surface vibrations as the vibration frequency was varied. Apart from the studies reported by Jones and work in France during the 1960s and 1970s, there seems to have been little additional use of this technique for testing concrete pavements. In the early 1980s, however, researchers at The University of Texas at Austin began studies of a surface wave technique that involved an impactor or vibrator that excited a range of frequencies. Digital signal processing, SASW, was used to develop the relationship between wavelength and velocity (Heisey et al. 1982; Nazarian et al. 1983). The SASW method has been used successfully to determine the elastic modulus profiles of soil sites, asphalt and concrete pavement systems, and concrete structural members. The method has been extended to the measurement of changes in the elastic properties of concrete slabs during curing and assessment of damage (Bay and Stokoe 1990; Kalinski 1997).

3.2.4.1 *Principle*—The general test configuration is illustrated in Fig. 3.2.4.1a (Nazarian and Stokoe 1986a). An impact is used to generate a surface or R-wave. Two receivers are used to monitor the motion as the R-wave propagates along the surface. The received signals are processed and a subsequent calculation scheme is used to infer the stiffness of the underlying layers.

Just as the stress pulse from impact contains a range of frequency components, the R-wave also contains a range of components of different frequencies or wavelengths. The product of frequency and wavelength equals wave speed. This range depends on the contact time of the impact; a shorter contact time results in a broader range. The longer-wavelength or lower-frequency components penetrate more deeply, which is the key to using the R-wave to gain information about the properties of the underlying layers (Rix and Stokoe 1989). In a layered system, the propagation speed of these different components is affected by the wave speed in those layers through which the components propagate. A layered system is a dispersive medium for R-waves, which means that different frequency components of the R-wave propagate with different speeds, which are called phase velocities.

Phase velocities are calculated by determining the time it takes for each frequency (or wavelength) component to travel between the two receivers. These travel times are determined from the phase difference of the frequency components arriving at the receivers (Nazarian and Stokoe 1986b). The phase differences are obtained by computing the cross-power spectrum of the signals recorded by the two receivers. The phase portion of the cross-power spectrum gives phase differences in degrees as a function of frequency. The phase velocities are determined as

$$C_{R(f)} = X\frac{360}{\phi_f}f \qquad (3.2.4.1a)$$

where $C_{R(f)}$ is the surface wave speed of component with frequency f; X is the distance between receivers (refer to Fig. 3.2.4.1a); and ϕ_f is the phase angle of component with frequency f.

The wavelength λ_f corresponding to a component frequency is calculated using the equation

$$\lambda_f = X\frac{360}{\phi_f} \qquad (3.2.4.1b)$$

By repeating the calculations in Eq. (3.2.4.1a) and (3.2.4.1b) for each component frequency, a plot of phase velocity versus wavelength is obtained. Such a plot is called a dispersion curve. Figure 3.2.4.1b(a) shows an example of a dispersion curve obtained by Nazarian and Stokoe (1986a) from tests on a concrete pavement. The short-wavelength components have higher speeds because they correspond to components traveling through the concrete slab.

A process called inversion is used to obtain the approximate stiffness profile at the test site from the experimental dispersion curve (Nazarian and Stokoe 1986b; Nazarian and Desai 1993; Yuan and Nazarian 1993). Although this process is called inversion, the technique actually uses forward modeling, with trial and error, until there is agreement between the measured and computed dispersion curves. The test site is modeled as layers of varying thickness. Each layer is assigned a density and elastic constants. Using this information, the solution for surface wave propagation in a layered system is obtained and a theoretical dispersion curve is calculated for the assumed layered system. The theoretical curve is compared with the experimental dispersion curve. If the curves match, the problem is solved and the assumed stiffness profile is correct. If there are significant discrepancies, the assumed layered system is changed or refined and a new theoretical curve is calculated. This process continues

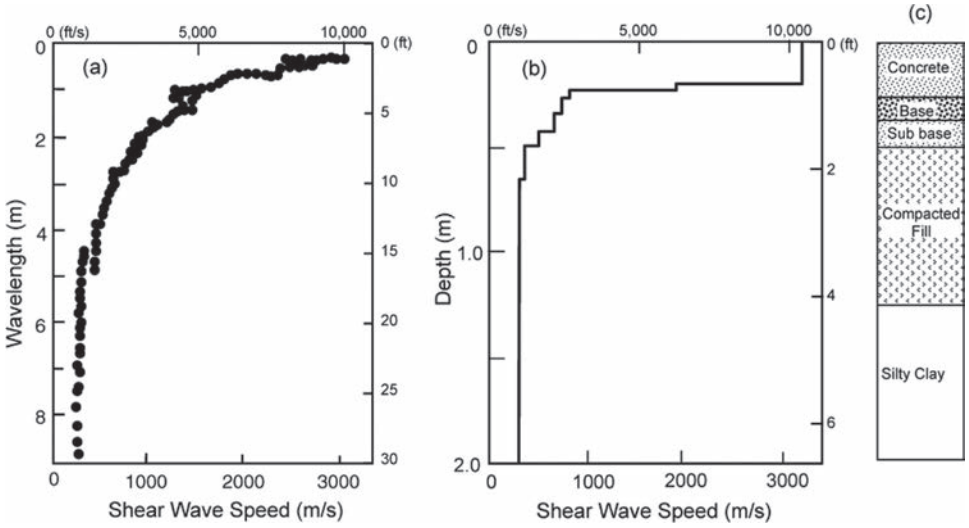

Fig. 3.2.4.1b—(a) Dispersion curve obtained from SASW testing of concrete pavement; (b) S-wave speed obtained from inversion of experimental dispersion curve; and (c) soil profile based on boring (adapted from Nazarian and Stokoe [1986a]).

until there is a satisfactory agreement between the theoretical and experimental curves. Figure 3.2.4.1b(b) shows the wave speed versus depth profile that corresponds to the dispersion curve, whereas the soil profile described in Fig. 3.2.4.1b(c) shows the actual conditions.

3.2.4.2 *Instrumentation*—There are three components to an SASW test system (Fig. 3.2.4.1a)

1. Although the energy source is usually a hammer, it could also be a vibrator with variable frequency excitation
2. Two receivers that are geophones (velocity transducers) or accelerometers
3. A two-channel data acquisition system and a computer for recording and processing the waveforms

The required characteristics of the impact source depend on the elastic modulus of the layers, the distances between the two receivers, and the depth to be investigated (Nazarian et al. 1983). When investigating concrete pavements and structural members, the receivers are located relatively close together. In this case, a small hammer, or even smaller impactor or vibrator, is required so that a short-duration pulse is produced with sufficient energy at frequencies up to approximately 50 to 100 kHz. As the depth to be investigated increases, the distance between receivers is increased, and an impact that generates a pulse with greater energy at lower frequencies is required. Thus, heavier hammers, such as a sledge hammer, are used.

The two receiving transducers measure vertical surface velocity or acceleration. The selection of transducer type depends in part on the test site (Nazarian and Stokoe 1986a). For tests where deep layers are to be investigated and a larger receiver spacing is required, geophones are generally used because of their superior low-frequency sensitivity. For tests of concrete pavements, the receivers should provide accurate measurements at higher frequencies. Thus, for pavements, a combination of geophones and accelerometers is often used. For concrete structural members, small accelerometers and small impactors or high-frequency vibrators are typically used (Bay and Stokoe 1990).

The receivers are first located close together and the spacing is increased by a factor of two for subsequent tests. As a check on the measured phase information for each receiver spacing, a second series of tests is carried out by reversing the position of the source. Typically, five receiver spacings are used at each test site. For tests of concrete pavements, the closest spacing is usually approximately 6 in. (0.15 m) (Nazarian and Stokoe 1986b).

3.2.5 *Impulse response method*—This method was initially developed in the 1970s for testing deep foundations (refer to 3.3). Its application to general concrete structures occurred in the 1990s. The impulse response method uses a low-strain impact to send a stress wave through the tested element. The time history of impact force is measured by an instrumented hammer. The maximum compressive stress at the impact point in concrete is related directly to the elastic properties of the impactor tip. Typically a 3 lb (1.5 kg) hammer with a plastic tip is used. The impact duration is much longer than in the impact-echo method. The long-duration impact in the impulse-response method means that the structural element responds to the impact in a bending vibration mode over a much lower frequency range (0 to 1 kHz for plate structures), as opposed to a higher frequency thickness mode of the impact-echo test. Response may be measured with an appropriate geophone with a linear response from a very low frequency (approximately 20 Hz) up to 1 kHz. Research for the impulse response method applied to structural concrete began in the mid-1980s (Pederson and Senkowski 1986; Davis and Hertlein 1987). In 2010, ASTM adopted a standard practice on using impulse response to evaluate the condition of concrete plates (ASTM C1740). Applications of the impulse response method include:

a) Voiding beneath concrete pavements, as well as spillway and floor slabs (Davis and Hertlein 1987)

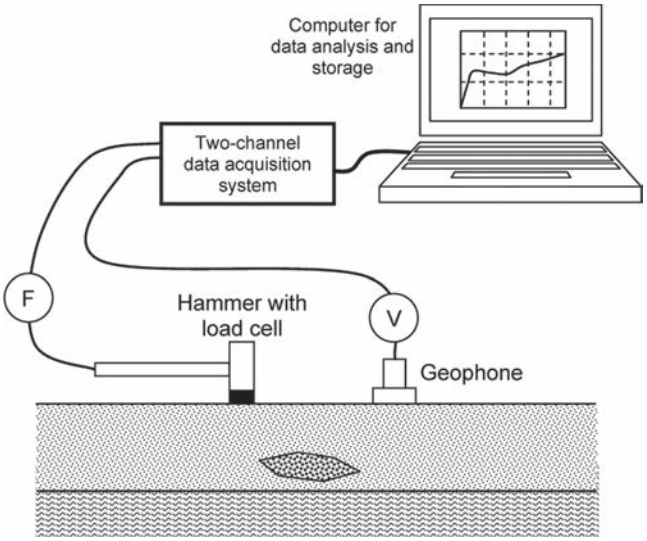

Fig. 3.2.5.1a—Schematic of impulse response method applied to plate-like structures.

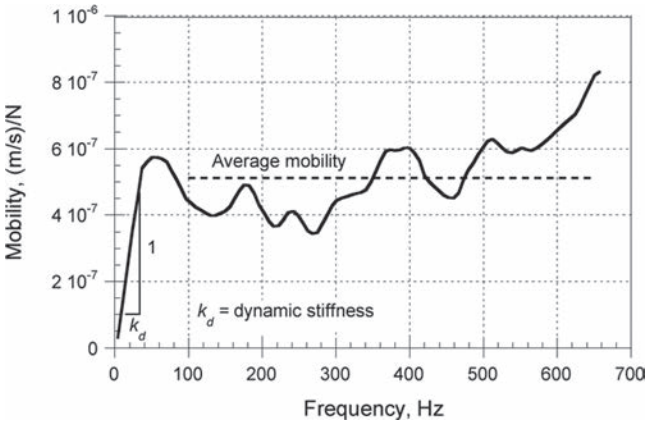

Fig. 3.2.5.1b—Impulse response mobility-frequency plot for a sound response.

b) Delamination of concrete around steel reinforcement in slabs

c) Walls and large structures such as dams, chimney stacks, and silos (Davis and Hertlein 1995)

d) Location of low-density concrete (honeycombing) and cracking in concrete elements (Davis and Hertlein 1995; Davis et al. 1997)

e) Depth of alkali-silica reaction attack in drilled shafts used as pylon foundations (Davis and Kennedy 1998)

f) Debonding of asphalt and concrete overlays to concrete substrates (Davis et al. 1996)

g) The degree of stress transfer through load-transfer systems across joints in concrete slabs (Davis and Hertlein 1987)

Davis (2002) presents a review of these applications.

3.2.5.1 *Principle*—The general test configuration is illustrated in Fig. 3.2.5.1a. A transient stress pulse is introduced into the test element by mechanical impact on the surface. The resultant bending behavior of the element is analyzed to characterize the integrity of the element. Both the time records for the hammer force and the geophone velocity response are processed in the field computer using the fast Fourier transform (FFT) algorithm. The resulting velocity spectrum is divided by the force spectrum to obtain a transfer function called the mobility of the element under test. The plot of mobility (vertical axis) versus frequency (horizontal axis) over the range of 0 to 1 kHz is called the mobility plot. Figure 3.2.5.1b is an example of a mobility plot, where the vertical axis is in units of speed per unit of force.

The mobility plot contains information on the condition and the integrity of the concrete in the tested elements, obtained from the following measured parameters.

3.2.5.1.1 *Dynamic stiffness*—The slope of the portion of the mobility plot below 0.1 kHz defines the compliance or flexibility of the area around the test point for a normalized force input. The inverse of the compliance is the dynamic stiffness of the structural element at the test point. The dynamic stiffness of a plate-like element depends on the thickness of the plate, the density and elastic modulus of the material, and the support conditions.

3.2.5.1.2 *Mobility and damping*—The test element's response to the impact-generated elastic wave will be damped by the element's intrinsic rigidity (body damping). For example, the mean mobility value over 0.1 to 1 kHz is directly related to the density and the thickness of a plate element. A reduction in plate thickness corresponds to an increase in mean mobility. As an example, when total debonding of an upper layer is present, a higher mean mobility reflects the thickness of the upper debonded layer (the slab becomes more mobile). Also, any cracking or honeycombing in the concrete will reduce the body damping and stability of the mobility plots over the tested frequency range. As a result, the mobility plot will display an increasing mobility with frequency above approximately 0.1 kHz.

3.2.5.1.3 *Peak/mean mobility ratio*—When debonding or delamination is present within a structural element, or when there is loss of support beneath a concrete slab-on-ground, the response behavior of the uppermost layer controls the impulse response test result. In addition to the increase in mean mobility between 0.1 and 1 kHz, the dynamic stiffness decreases greatly. The peak mobility below 0.1 kHz becomes appreciably higher than the mean mobility from 0.1 to 1 kHz. The result is a mobility plot with a high amplitude peak at low frequency. The ratio of this peak-to-mean mobility is an indicator of the presence and degree of either debonding within the element or voiding or loss of support beneath a slab-on-ground.

Test points are usually laid out on the test element surface in a grid pattern spacing (20 to 40 in. [0.5 to 1 m]), and the parameters of average mobility, stiffness, mobility slope, and peak-to-mean mobility ratio for each test point are measured. The results for each parameter are presented in the form of a contour plot representing a plan of the area tested. From this contour plot, comparative results enable overall assessments to be made. Figure 3.2.5.1.3 shows an example of a contour plot of average mobility obtained by testing a floor (slab-on-ground). The darker shading represents higher mobility. It is seen that higher mobility was obtained at the corners of the slab. This could be an indication that the slab has lifted off

the ground at the corners. There also appears to be a location of high mobility at grid point C7-R9 that would merit further investigation.

The results from impulse response tests, such as the dynamic stiffness or average mobility, cannot be readily predicted from engineering mechanics theory due to the potential variation in support and subgrade conditions. Therefore, the evaluation of impulse-response tests is typically performed in a comparative manner, with the change or variation in results between test points used to identify anomalous conditions.

3.2.5.2 *Instrumentation*—An impulse response test system is composed of three main components:

1. An impact source

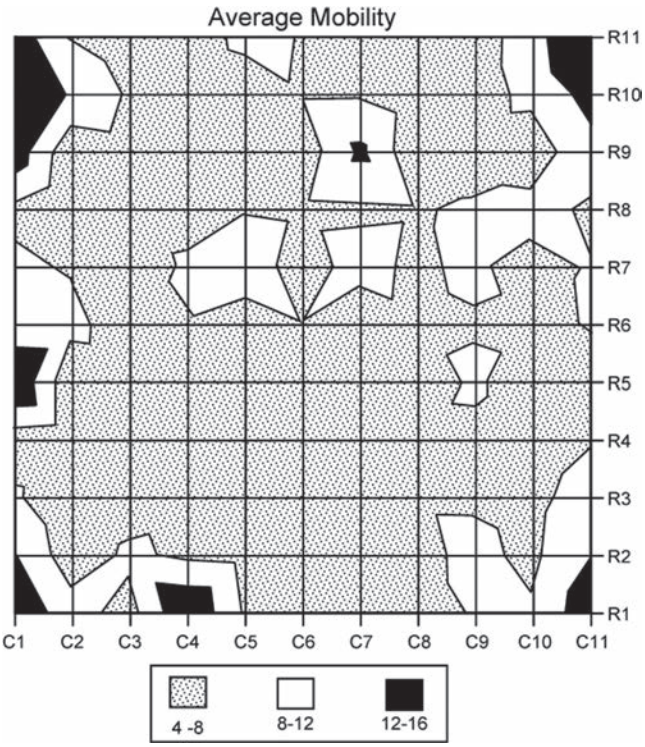

Fig. 3.2.5.1.3—Contour plot of average mobility values from a concrete floor slab.

2. A receiving transducer and twin-channel data acquisition system that are used to capture the output signals from the impactor and the receiving transducer, store the digitized waveforms, and perform signal analysis
3. An impulse response system that can be assembled from off-the-shelf components

In 2002, a complete field system for structure testing, including hardware and analysis software, became commercially available.

The impactor is normally a 3 lb (1.5 kg) sledgehammer equipped with a load cell to measure the force-time trace for each hammer blow. The 2 in. (51 mm) diameter hammer tip is composed of hard neoprene to obtain a useful force spectrum over a minimum range of 0 to 1.5 kHz. Larger or smaller hammers may produce clearer results, depending on slab thickness and support conditions, but the useful frequency range changes as a function of hammer mass. The receiving transducer is usually a velocity transducer or geophone mounted in a ruggedized plastic case. The response from a typical geophone is direction sensitive. Therefore, different geophone types are used to monitor displacement in different directions (that is, horizontal geophone, vertical geophone). Curved surfaces, such as tunnel linings, can be tested using triaxial geophones. The advantages of geophones over accelerometers are the direct measurement of velocity and their stability at low frequencies to 5 Hz.

3.2.6 *Advantages and limitations*—Each of the stress-wave propagation methods has distinct advantages and limitations summarized in Table 3.2.6. The UPV and impact echo methods have been standardized by ASTM with a variety of commercial devices available. The SASW method suffers from the complexity of the signal processing, but there have been efforts to automate this signal processing (Nazarian and Desai 1993).

3.3—Low strain stress-wave methods for deep foundations

During the 1930s, viable stress-wave methods for evaluation of deep foundations originated in the pile-driving industry. They were initially developed as a means of predicting pile capacity from the measured resistance of the pile to each driving hammer impact. When electronic

Table 3.2.6—Advantages and limitations of stress-wave methods for structures

Method	Advantages	Limitations
Ultrasonic through or direct transmission (pulse velocity) (ASTM C597)	Portable equipment is available; relatively easy to use.	Requires access to two sides of members; does not provide information on depth of defect.
Ultrasonic-echo	Access to only one face is needed; provides information on depth of defect. Method based on S-wave point transducers and SAFT permit construction of 3-D tomographic images.	Applicable to limited member thickness; experienced operator is required.
Impact-echo (ASTM C1383 for plate thickness)	Access to only one face is needed; equipment is commercially available; capable of locating a variety of defects; does not require coupling materials.	Experienced operator is required; current instrumentation limited to testing members 40 in. (1 m) thick.
Spectral analysis of surface waves	Capable of determining the elastic properties of layered systems, such as pavements, interlayered good and poor-quality concrete.	Experienced operator is required; involves complex signal processing.
Impulse response (ASTM C1740)	Access to only one face is needed; equipment is commercially available; does not require coupling materials; large areas tested in short time.	Experienced operator is required; Thickness limitation of 40 in. (1 m). Comparative results.

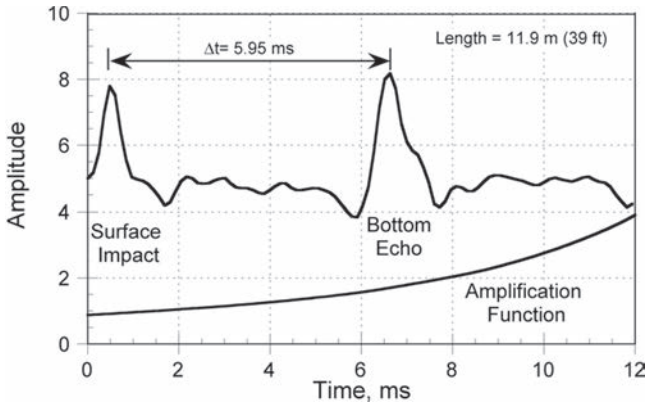

Fig. 3.3.1.1—Example of sonic-echo test result (signal is amplified by function at bottom of graph).

measurements of strain and acceleration became possible, however, it was soon realized that the test results included valuable information about shaft integrity. When integrity methods using hand-held impactors were developed, they become known as low-strain tests to differentiate them from the methods that measured the high-strain stresses caused by the pile driving hammers. Because the high-strain tests are still primarily used as load test methods, they are considered beyond the scope of this committee report. Additional information on high-strain testing can be found in the Deep Foundations Institute Manual on Nondestructive Testing and Evaluation (DFI 2006), Hertlein and Davis (2006), or Davis and Hertlein (1997).

Since the 1960s, test methods based on low-strain stress-wave propagation have been commercially available for the NDT of concrete deep foundations and mass concrete. First developed in France and Holland and closely followed by the United States, they are now routinely specified as quality assurance tools for new pile construction in Western Europe, Northern Africa, and parts of East Asia. In the United States, federally-funded and many state-funded highway projects require quality assurance testing. The use of these methods for evaluation of deep foundations is becoming more common. Continuing advances in electronic hardware and portable computers have resulted in more reliable and faster testing systems that are becoming progressively less influenced by the operator in terms of both testing procedure and analysis of test results.

There are two types of low-strain stress wave methods for evaluation of deep foundations:

1. Reflection techniques (sonic-echo and impulse response)
2. Direct transmission through the concrete (crosshole sonic logging)

3.3.1 *Sonic-echo method*—This method is the earliest of all NDT methods to become commercially available (Paquet 1968; Steinbach and Vey 1975; Van Koten and Middendorp 1981) for deep-foundation integrity or length evaluation. This method is known variously as the seismic-echo, sonic-echo or pile integrity test (PIT) (Rausche and Seitz 1983). Procedures for conducting this type of test are given in ASTM D5882, also called the pulse-echo method (PEM).

3.3.1.1 *Principle*—The sonic-echo method uses a small impact delivered at the head of the deep foundation (pile or shaft), and measures the time taken for the stress wave generated by the impact to travel down the pile and to be reflected back to a transducer, usually an accelerometer, coupled to the pile head. The impact is typically from a small sledge-hammer, having a mass of approximately 2.2 lb (1 kg). The accelerometer captures the motion generated by the impact of the hammer and subsequent wave reflections from within the shaft. The vertical movement of the shaft head due to the impact and the subsequent arrival of the reflected stress wave is captured by a digital data acquisition system that stores the data as a function of time, which is also known as time domain. Figure 3.3.1.1 illustrates the results of a sonic-echo test on a concrete shaft. The time for the stress wave to travel down the shaft and back to the surface is called transit time, and can be determined as shown in Fig. 3.3.1.1.

If the length of the foundation shaft is known and the transit time for the stress wave to return to the transducer is measured, then the wave velocity can be calculated. Conversely, if the velocity is known, then the length can be deduced. Because the velocity of the stress wave is primarily a function of the dynamic elastic modulus and density of the concrete, the calculated velocity can provide information on concrete quality. Where the stress wave has traveled the full length of the shaft, these calculations are based on the formula

$$C_b = \frac{2L}{\Delta t} \qquad (3.3.1.1)$$

where C_b is the bar wave speed in concrete; L is the shaft length; and Δt is the transit time of stress wave.

Bar waves are propagating pulse resonances that are set up in long elements when the wavelength of the propagating wave is significantly larger than the bar's cross section dimension. Bar waves propagate at a velocity that is slightly lower than that of P-waves.

Empirical data have shown that a typical range of values for C_b can be assumed, where 15,000 to 15,750 ft/s (3800 to 4000 m/s) would indicate good-quality concrete. The actual strength will vary according to aggregate type and mixture proportions. A project-specific correlation is required to estimate in-place strength from the wave speed (refer to ACI 228.1R).

Where the length of the shaft is known, an earlier-than-expected arrival of the reflected wave means that it has encountered a reflector, which is a change in stiffness or density other than in the toe of the shaft. This may be a break or defect in the shaft, a significant change in shaft cross section, or the point at which the shaft is restrained by a stiffer soil layer. In certain cases, the polarity of the reflected wave, whether positive or negative with respect to the initial impact, can indicate whether the anomaly is due to an increase or decrease of stiffness at the reflective point.

The energy imparted to the shaft by the impact is small, and the damping effect of the soils around the shaft will progressively dissipate that energy as the stress wave travels

down and up the shaft. To increase information from the test, the response signal can be progressively amplified with time. However, caution should be used with this approach because background geo-noise will also be amplified, causing results that can be misleading. Geo-noise is ground-borne noise caused by ocean waves, human activity, storms, seismic events, and similar phenomena.

Depending on the stiffness of the lateral soils, a limiting length-to-diameter ratio (L/d) exists beyond which all the wave energy is dissipated and no response is detected at the shaft head. In this situation, the only information that can be derived is that there are no significant irregularities in the upper portion of the shaft, because any irregularity closer to the head than the critical L/d would reflect part of the wave. This limiting L/d value will vary according to the properties of the adjacent soils, with a typical value of approximately 30:1 for medium stiff clays.

3.3.2 *Impulse-response (mobility) method*—This method was originally developed as a steady-state vibration test in France (Davis and Dunn 1974), where a controlled force was applied to the shaft head by a swept-frequency generator. The vertical shaft response was recorded by geophone velocity transducers, and the input force from the vibrator was continuously monitored. The resulting response curve plotted the shaft mobility (geophone particle velocity divided by vibrator force, v/F) against frequency. The useful frequency range was typically approximately 0 to 2000 Hz.

The evolution of data-processing equipment during the 1980s and 1990s allowed the use of computers on site to transform the shaft response due to a hammer impact (similar to that used in the sonic-echo method) into the frequency domain (Stain 1982; Olson et al. 1990). This reduced the effort required to obtain the mobility as a function of frequency. The impulse response method is also covered by ASTM D5882, where it is called the transient response method (TRM).

Further studies demonstrated that the impulse-response method could be applied to integrity testing of structures other than deep foundations (Davis and Hertlein 1990). The application of impulse response to integrity evaluation of plate-like structures is discussed in 3.2.5.

3.3.2.1 *Principle*—An impact on the shaft head by a small sledge hammer equipped with a force transducer generates a stress wave with a wide frequency content, which can vary from 0 to 1000 Hz for soft rubber-tipped hammers, and from 0 to 3000 Hz or higher for metal-tipped hammers. The load cell measures the force input and the vertical response of the shaft head is monitored by a geophone.

The force and velocity time-domain signals are recorded by a digital acquisition device, and then processed by computer using a fast Fourier transform (FFT) algorithm to convert the data to the frequency domain. At each frequency value, velocity is divided by force to provide the normalized response, transfer function, or frequency response function (FRF), which is displayed as a graph of shaft mobility versus frequency (mobility plot). Appendix A discusses the theoretical aspects of the mobility plot for a deep foundation shaft.

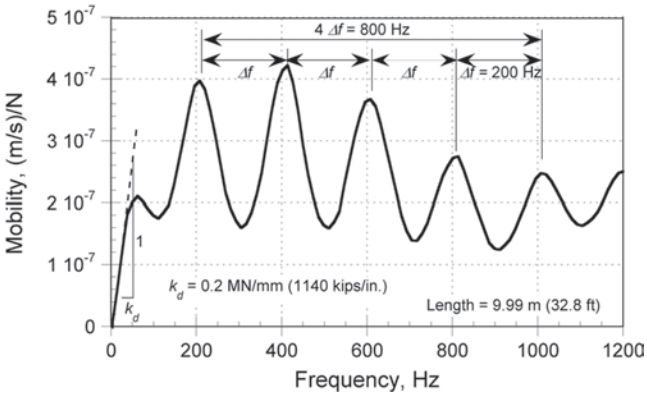

Fig. 3.3.2.1a—Example of impulse-response (mobility) plot for test of pile.

An example of a mobility plot for a foundation shaft is given in Fig. 3.3.2.1a. This response curve consists of two major portions, which contain the following information:

a) At low frequencies (less than 100 Hz), lack of inertial effects cause the shaft-soil composite system to behave as a spring, which is shown as a linear increase in amplitude with increasing frequency. The slope of this portion of the mobility plot is known as the compliance or flexibility, and the inverse of flexibility is the dynamic stiffness. The dynamic stiffness, which is a property of the shaft-soil system, can be used to assess shafts on a comparative basis, either to assess uniformity or as an aid to selecting a representative shaft for full-scale load testing by either static or dynamic means.

b) The peaks in the higher-frequency portion of the mobility plot are due to longitudinal resonances of the shaft. The resonant frequencies are a function of the shaft length and the degree of shaft toe anchorage and their relative amplitude is a function of the lateral soil damping. The frequency difference between adjacent peaks is constant and is related to the length of the shaft and the wave speed of the concrete according to Eq. (A.1) in Appendix A. The mean amplitude of the resonance portion of the curve is a function of the impedance of the shaft, which depends in turn on the shaft cross-sectional area, the concrete density, and the bar wave propagation velocity C_b (refer to Appendix A).

As with the sonic-echo test, when the shaft length is known, a shorter apparent length measurement indicates the presence of an anomaly. Appendix A describes how additional information can be derived from the mobility-frequency plot, such as the shaft cross section and dynamic stiffness, which can help in differentiating between an increase and reduction in cross section.

Figure 3.3.2.1b shows a mobility plot of a 30.5 ft (9.3 m) long shaft with similar soil conditions to the shaft in Fig. 3.3.2.1a, except for a necked section at 10.2 ft (3.1 m). The reflection from the shaft base at 30.5 ft (9.3 m) depth is clearly visible on the plot, indicated by resonance peaks at the constant frequency spacing of 215 Hz. The frequency spacing of 645 Hz between the two more prominent peaks corresponds to the reflection from the necked section at a depth of 10.2 ft (3.1 m).

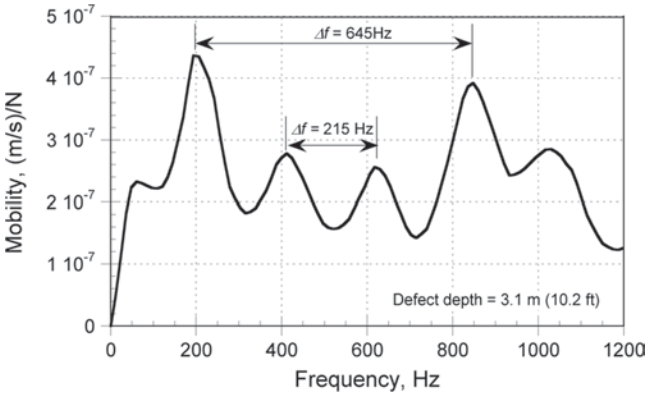

Fig. 3.3.2.1b—Impulse-response (mobility) plot of pile with necked section 10.2 ft (3.1 m) below top.

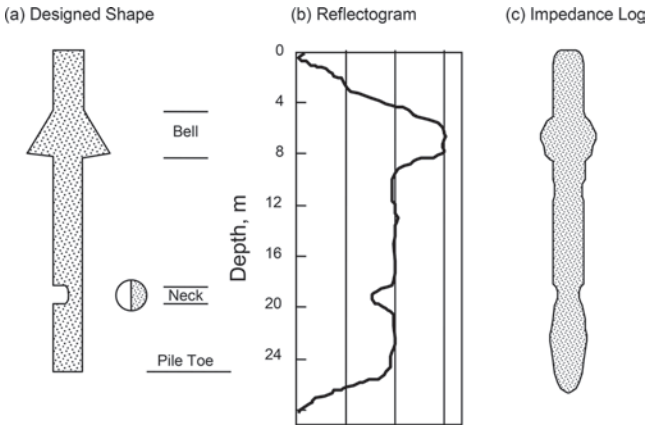

Fig. 3.3.3.1—(a) Planned defects in experimental pile; (b) reflectogram obtained by signal processing of sonic-echo data; and (c) impedance log obtained by combining information from reflectogram and characteristic impedance obtained from impulse-response analysis.

In common with the sonic-echo test, a relatively small amount of energy is generated by the hammer impact, and soil damping effects limit the depth from which useful information may be obtained. However, even where no measurable shaft base response is present, the dynamic stiffness is still a useful parameter for comparative shaft assessment.

3.3.3 *Impedance logging*—Another approach to interpreting the responses from a combination of both sonic-echo and impulse-response methods is impedance logging (Paquet 1991). In this technique, the information from the amplified time-domain response of the sonic echo is combined with the characteristic impedance of the shaft measured with the mobility test to create an image of the variation in shaft impedance with depth.

3.3.3.1 *Principle*—The force applied to the head of the shaft by the surface reflection method is a brief transient event—1 to 3 milliseconds—that generates an elastic wave that propagates down the shaft. This wave collects information about changes in shaft impedance as it proceeds downward, and is then reflected back to the shaft head. The only useful reflections in the analysis process are those that arrive after the initial surface disturbances from the impact (Rayleigh waves) have dissipated.

The reflectogram obtained from the sonic-echo test does not indicate the relative size of the irregularity that caused the reflection. However, it is possible with modern recording equipment to combine the information from wave reflection with the impedance properties of the shaft. Measurements of force and velocity response are stored as time-based data, with a very wide band-pass filter and rapid sampling. In the reflectogram, a defect extending across the entire shaft cross section (zero impedance) is equivalent to 100 percent reflection, whereas an infinitely long shaft with no defects would give zero reflection.

If either a defect or the shaft tip is at a considerable distance from the shaft head, the reflected amplitude is reduced by damping within the shaft. With uniform lateral soil conditions, this damping function has the form $e^{-}\sigma^{L}$, where L is the shaft length and σ is the damping factor (refer to Appendix A). The reflectogram can be corrected for the effects of damping by using an amplification function that yields a high-amplitude response over the total shaft length, similar to the treatment of sonic-echo data. Figure 3.3.3.1 shows an example of a reflectogram that has been corrected in this way.

The analysis of the mobility plot from the impulse-response test confirms shaft length, gives the shaft-soil system dynamic stiffness, and gives the characteristic shaft impedance I as

$$I = \rho_c A_c C_b \qquad (3.3.3.1)$$

In addition, Davis and Dunn (1974) showed that finite element simulation of the tested shaft and its surrounding soil can be carried out most efficiently in the frequency domain. The reflectogram and the characteristic impedance can then be combined to produce a trace called the impedance log (Fig. 3.3.3.1(c)). The output of this analysis is in the form of a vertical section through the shaft, giving a calculated visual representation of the effective pile shape. The final result can be adjusted to eliminate varying soil reflections using the simulation technique.

Field testing equipment should meet the following:

a) Hammer load cell and the velocity transducer or accelerometer should be correctly calibrated, generally within 6 months before testing.

b) Digital data acquisition and storage equipment should be used to allow subsequent analysis.

c) Both time and frequency-domain test responses should be stored.

3.3.4 *Crosshole sonic logging*—The crosshole sonic logging (CSL) method overcomes the depth limitation of the sonic-echo and mobility methods, and is appropriate for use on deep drilled shafts and mass concrete foundations such as slurry trench walls, dams, and machinery bases (Levy 1970; Davis and Robertson 1975; Baker and Khan 1971). This method is based on the principle of ultrasonic through transmission, as discussed in 3.2.1, and its use for deep foundations is covered by ASTM D6760.

3.3.4.1 *Principle*—This is a method that requires a number of parallel metal or plastic tubes to be placed in the structure before concrete placement, or core holes to be drilled after the concrete has gained sufficient strength to permit drilling. Typically, a transmitting transducer initially placed at the bottom of one tube emits an ultrasonic pulse that is detected by a receiving transducer at the bottom of a second tube. A recording unit measures the time taken for the ultrasonic pulse to pass through the concrete between the tubes. The transducers are watertight sealed units, and the tubes are filled with water to provide coupling between the transducers and the concrete. For the pulse to be transmitted between the concrete and transducers, mechanical bond is required between the concrete and the outer walls of the tubes.

The transducer cables are withdrawn over an instrumented wheel that measures the cable length and, thus, transducer depth. Alternatively, the cables can be marked along their lengths so that the transducer depths are known. Continuous pulse measurements are made during withdrawal at height increments ranging from 0.5 to 2 in. (10 to 50 mm), providing a series of measurements that can be printed out to create a vertical profile of the material between the tubes. A typical test result for a specific commercial system is shown in Fig. 3.3.4.1. The presence of an anomaly is indicated by an increase in the time of flight of the signal or the complete absence of a received signal.

As discussed in 3.2, the ultrasonic pulse velocity (UPV) is a function of the density and dynamic elastic constants of the concrete. If the signal path length is known and the transit time is recorded, the apparent UPV can be calculated to provide a guide to the quality of the concrete. A reduction in elastic modulus results in a lower UPV. If the path length is not known, but the tubes are reasonably parallel, the continuous measurement profile will clearly show any sudden changes in transit time caused by a lower pulse velocity due to poor-quality material, such as contaminated concrete or inclusions. Voids will have a similar effect by forcing the pulse to detour around them by diffraction, thus increasing the path length and the transit time.

Although the amplitude of the received pulse is also likely to be affected by anomalies within the concrete, it can also be affected by other factors, such as the transducers location within the tubes, the quality of the bond between the tubes and the concrete, the distribution and orientation of the coarse aggregate within the concrete, and the amplitude of the pulse emitted by the transmitter. Reliance solely on variations in signal amplitude as an indication of concrete anomalies is therefore prone to error.

By varying the geometric arrangement of the transducers, the method can resolve the vertical and horizontal extent of such irregularities and locate cracks or discontinuities. This additional information can help the engineer decide whether the irregularity is merely an insignificant flaw that will not impact the performance or durability of the foundation or a defect that could have a significant adverse effect on shaft capacity or durability.

This method, which provides a direct measurement of foundation depth, can be used to assess the quality of the interface between the shaft base and the bedrock if the access holes are extended below the base. A major limitation of this method is the requirement to install access tubes either before concrete placement or by core drilling afterward. One major advantage is that the method has no practical depth limitation, unlike the surface reflection methods.

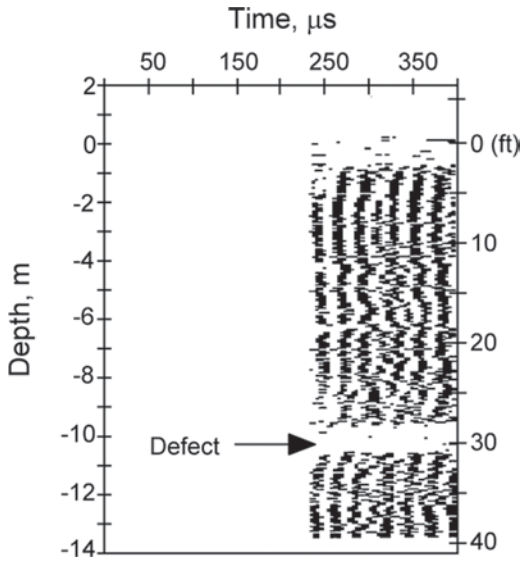

Fig. 3.3.4.1—Example of crosshole sonic log. Absence of signal arrival at depth of approximately 33 ft (10 m) indicates presence of potential defect.

The information obtained is limited to the material immediately between pairs of tubes. Therefore, in piles or drilled shafts, the access tubes should be arranged as close to the shaft periphery as possible in a pattern that allows the maximum coverage of the concrete between them. Very little useful information will be obtained about increases or decreases in shaft cross section in regions outside the direct paths between all possible pair combinations of the access tubes.

3.3.5 *Parallel-seismic method*—All of the aforementioned methods depend on clear access to the head of the foundation shaft, making them the easiest and most practical to perform during the construction phase, as foundation heads may later be inaccessible. The parallel-seismic method was developed specifically for situations arising after the foundation has been built upon, as in the evaluation of older, existing structures where direct access to the shaft head is no longer possible without some demolition or material removal (Davis 1995).

3.3.5.1 *Principle*—A small-diameter (typically 6 to 8 in. [150 to 200 mm] in size) access borehole is drilled into the soil parallel and close to the foundation to be tested. The borehole should extend beyond the known or estimated depth of the foundation. The borehole is lined normally with a plastic tube to retain water, which serves as an acoustic couplant, and allows the transducer unrestricted access to the bottom of the borehole. The inside diameter of the tube is typically 2 to 3 in. (50 to 75 mm), and the tube is fully grouted into the borehole with bentonite or material with a modulus similar to that of the surrounding soil.

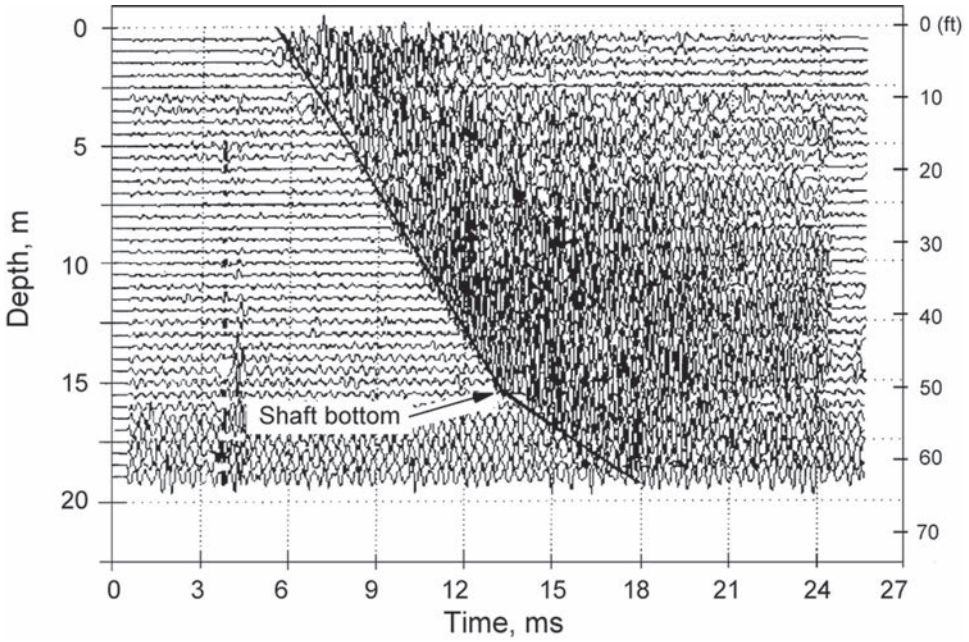

Fig. 3.3.5.1—Example of results from parallel-seismic test. Depth of pile shaft is indicated by change in slope of line representing arrival time of stress pulse as a function of depth.

An acoustic receiving transducer, or hydrophone, is placed in the top or the bottom of the tube, and the structure is struck as close to the head of the foundation as possible using a hammer equipped with an electronic trigger. A portion of the energy traveling down the foundation element is refracted into the soil and the hydrophone will respond to the arrival of the refracted portion of the stress pulse. The signal from the hammer impact triggers the data acquisition system, which records the time domain signal from the hydrophone. The received signal allows determination of the time taken for the stress wave to travel through the foundation and the adjacent soil to the hydrophone. The hydrophone is then lowered or raised in uniform increments and the process repeated at each stage, with the impact at the same point each time. The recorded time domain waveforms are stacked vertically in a single plot of depth versus time (waterfall plot), with each waveform plotted at the corresponding depth of the hydrophone, as shown in Fig. 3.3.5.1. A best-fit straight line is drawn through the times corresponding to pulse arrival for each hydrophone position.

The velocity of the wave will be lower through soil than the foundation. If the access tube is reasonably parallel to the foundation, the effect of the soil between the tube and the pile shaft will be constant. Transit time, however, will increase proportionally as the depth of the hydrophone increases. When the receiver has passed beyond the foundation base, the transit time of the signal will increase due to the lower velocity of the additional intervening soil, and the lines linking signal arrival points on the graph show a distinct change in slope at the level of the foundation base. Similarly, any significant discontinuity or inclusion in the foundation will force the signal to detour around it, increasing the path length and transit time, which results in a deviation of the transit time from the best-fit straight line.

3.3.5.2 *Interpretation*—The results of low-strain stress wave methods are affected by the size and location of the irregularity within the foundation. A small inclusion or reduction in cross section near the top of a shaft being tested with one of the impulse methods or close to one of the access tubes in the crosshole sonic logging (CSL) test can appear as a more significant anomaly in the data than a similar-sized feature further away. Often, a small irregularity will have no significant effect on foundation capacity or durability, making it uneconomical and unnecessary to repair. Using the word "defect" to describe all irregularities is therefore misleading, and creates an unnecessarily negative impression for evaluation. The Test and Evaluation Committee of the DFI therefore recommends that interpretation of integrity test data be subjected to a three-level classification (DFI 2006):

1. Anomaly—Any irregular feature identified in the NDT graphic results that could be caused by testing instrumentation, like noise, or from any other means used to perform the test, for example access tube debonding in CSL, or to the shaft itself. The NDT practitioner is responsible for gathering and analyzing all the relevant data and attempting to resolve every anomaly before it is declared a flaw or defect.
2. Flaw—Any deviation from any combination of the planned shape, size, or material of the shaft.
3. Defect—A flaw caused by either the size or location that might detract from the shaft's intended performance or durability. The geotechnical engineer and the structural engineer are jointly responsible for deciding which flaw constitutes a defect.

3.3.6 *Advantages and limitations*—Table 3.3.6 summarizes the advantages and limitations of stress-wave methods for deep foundations.

Table 3.3.6—Advantages and limitations of stress-wave methods for deep foundations

Method	Advantages	Limitations
Surface reflection methods		
Sonic-echo	No preplaced tubes. Portable equipment. Rapid.	Can confuse necking and bulging. Does not measure diameter. May be unable to measure length or detect irregularities in lower portions of shafts with L/d greater than approximately 30:1.
Impulse-response (mobility)	No preplaced tubes. Stiffness measurement. Portable equipment. Rapid.	Results interpretation is complex. Similar limitations on geometry of shafts tested as sonic-echo.
Impedance logging	Same as for mobility test, plus effective shape of shaft derived from analysis.	Requires very good test data for accurate analysis. Full analysis requires experience, and cannot yet be completed on-site at time of test.
Direct transmission methods		
Sonic logging	Relatively fast. Detection of irregularities between tubes is more accurate than in surface reflection tests. Performance is not limited by depth.	Preplaced tubes or coring required. May not detect irregularities at edge of shaft.
Parallel-seismic	Relatively fast. Foundations under existing structures can be tested. Not affected by soil damping as much as surface reflection methods.	Requires testing hole to be bored adjacent to the foundation that is to be inspected. May not detect defects that are not complete discontinuities.

3.4—Nuclear methods

3.4.1 *Introduction*—Nuclear methods for nondestructive evaluation of concrete is subdivided into two groups, depending on the type of radiation used, which is either gamma rays or neutrons. The gamma-ray-based techniques include radiometric methods and radiographic methods. All involve gaining information about a test object due to interactions between the incident radiation and the material in the test object. A review of the early developments in the use of nuclear methods was presented by Malhotra (1976). Their developments up to the 1990s were reviewed by Mitchell (2004). Examples of further developments in the 2000s, given by Mariscotti et al. (2009), use radioactive materials and require test personnel to have specialized safety training and licensing.

3.4.1.1 *Radiometry*—Radiometry is used to assess the density of fresh or hardened concrete by measuring the intensity of electromagnetic radiation (gamma rays) that passes through the concrete. The radiation is emitted by a radioactive isotope, and the radiation passing through the concrete is sensed by a detector. The detector converts the received radiation into electrical pulses, which can be counted or analyzed by means of electronic devices (Mitchell 2004). Radiometry can be further subdivided into two procedures. One is based on measurement of gamma rays after transmission directly through concrete, and the second is based on measurement of gamma rays reflected, or backscattered, from within the concrete. These procedures are analogous to the ultrasonic through-transmission method and the pitch-catch method using stress waves.

3.4.1.2 *Radiography*—Radiography involves the use of the radiation passing through the test object to produce a photograph of the internal structure of the concrete. Typically, a radioactive source is placed on one side of the object and special photographic film or a reusable image plate is placed on the opposite side to record the intensity of radiation passing through the object. The higher the intensity of the radiation, the greater the exposure of the film or the stimulation of phosphors in an image plate. This method is identical to that used to produce medical X-ray images.

3.4.1.3 *Neutron*—Neutron sources can be used to measure the amount of moisture in concrete and to determine the elemental composition of concrete. The assessment of moisture is based on the knowledge that neutrons are strongly scattered by hydrogen atoms that are part of water molecules. In the usual arrangement, a neutron source and one or more neutron detectors are placed on a concrete surface with the latter being well-shielded from the source. Neutrons scattered back from within the concrete are registered by the detector(s) (refer to 3.4.3). In the second application, the elemental composition of concrete is determined by measuring the characteristic wavelength of the gamma rays emitted by the atoms in the concrete when these are hit by neutrons. In this case, gamma-ray spectrometers, which are detectors sensitive to the difference in wavelengths, are used in conjunction with a neutron source (Collico Savio et al. 1995; Saleh and Livingston 2000). A less practical alternative, which involves irradiating concrete samples in a nuclear reactor, is termed neutron activation analysis as described by Malhotra (1976).

3.4.2 *Direct transmission radiometry for density*—Direct transmission techniques can be used to detect reinforcement. The more common use of the technique, however, is to measure the in-place density both in fresh and hardened concrete (ASTM C1040/C1040M). Structures made with high-density (heavyweight) concrete or roller-compacted concrete are cases where this method is of particular value.

3.4.2.1 *Principle*—The direct transmission radiometric method is, as stated, analogous to the ultrasonic through-transmission technique discussed in 3.2. The radiation source is placed on one side of the concrete element to be tested and the detector is placed on the opposite side. For testing fresh concrete, the source is typically embedded to the concrete and the detector is located on the surface or embedded at a fixed distance from the source. As the radiation passes through the concrete, a portion is scattered by free electrons (Compton scattering) and another portion is absorbed by atoms. The amount of Compton scattering depends on the density of the concrete and the amount of absorption depends on chemical composition (Mitchell 2004). If the source-detector spacing and the concrete thickness are held

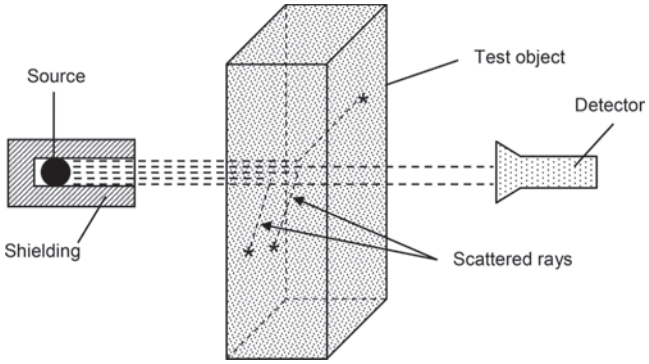

Fig. 3.4.2.2a—Direct transmission radiometry with source and detector external to test object.

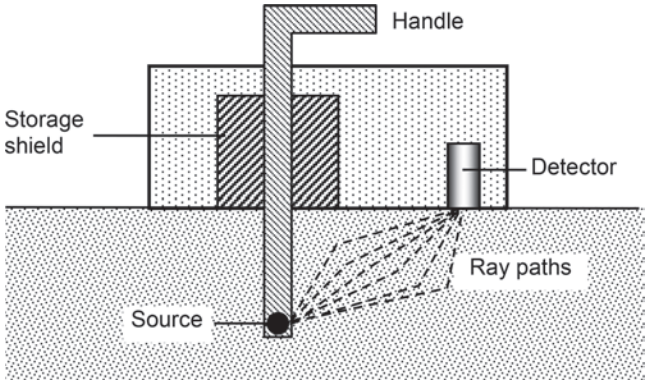

Fig 3.4.2.2b—Schematic of direct transmission nuclear gauge.

constant, a decrease (or increase) in concrete density leads to a change in the intensity of the detected radiation.

3.4.2.2 *Instrumentation*—Figure 3.4.2.2a shows the arrangement of source and detector for direct measurement through a hardened concrete member. This arrangement could also be used for testing fresh concrete with allowance made for the effects of the formwork material. The most widely used source is the radioactive isotope cesium-137 (^{137}Cs). The common detector is a Geiger-Müller tube, which produces electrical pulses when radiation enters the tube. Other detectors can be scintillation crystals that convert incident radiation into light pulses.

Figure 3.4.2.2b is a schematic of a commercially available nuclear transmission gauge that is used to test fresh concrete by pushing the source assembly into the concrete. It can also be used in hardened concrete by drilling a hole and inserting the source assembly. The equipment is portable and provides an immediate readout of the results. Most of the available units were developed for monitoring soil compaction and measuring the in-place density of asphalt concrete.

The VUT density meter was developed specifically for measuring the density of fresh concrete (Hönig 1984). Figure 3.4.2.2c is a schematic of this device. The source can be lowered up to a depth of 8 in. (200 mm) into a hollow steel needle that is pushed into the fresh concrete. A spherical lead shield suppresses the radiation when the source is in its retracted position. Detectors are located beneath the treads

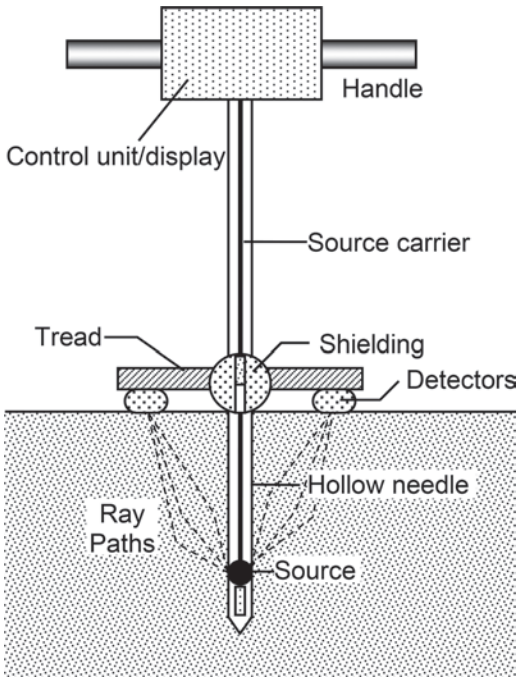

Fig. 3.4.2.2c—Schematic of nuclear gauge for measuring density of fresh concrete (based on Hönig [1984]).

used to push the needle into the concrete. The unit is claimed to have a resolution of 0.6 lb/ft^3 (10 kg/m^3) (Hönig 1984).

The direct transmission gauges mentioned previously provide a measurement of the average density between the source and detector. Figure 3.4.2.2d is a schematic of a two probe source/detector system for measuring the density of fresh concrete as a function of depth (Iddings and Melancon 1986). The source and detector are moved up and down within metal tubes that are pushed into the fresh concrete, making it possible to measure density as a function of depth.

ASTM C1040/C1040M provides procedures for using nuclear methods to measure the in-place density of fresh or hardened concrete. A key element in the procedure is determining a calibration curve for the instrument by making test specimens of different densities and determining the gauge output for each specimen. The gauge output is plotted as a function of the density and a best-fit curve determined. The procedure for using the direct transmission method to measure density of fresh concrete is given in ASTM C1040/C1040M (Procedure A).

3.4.3 *Backscatter radiometry for density*—Backscatter techniques are particularly suitable for applications where a large number of in-place measurements are required. Because backscatter measurements are affected by the top 1.6 to 4 in. (40 to 100 mm), the method is best suited for measurement of the surface zone of a concrete element. A good example of this method is monitoring the density of bridge deck overlays. Noncontacting equipment is available to use for continuously monitoring concrete pavement density during slipforming operations.

3.4.3.1 *Principle*—When measuring density by backscatter, the radiation source and the detector are placed on the same side of the sample (analogous to pitch-catch method for

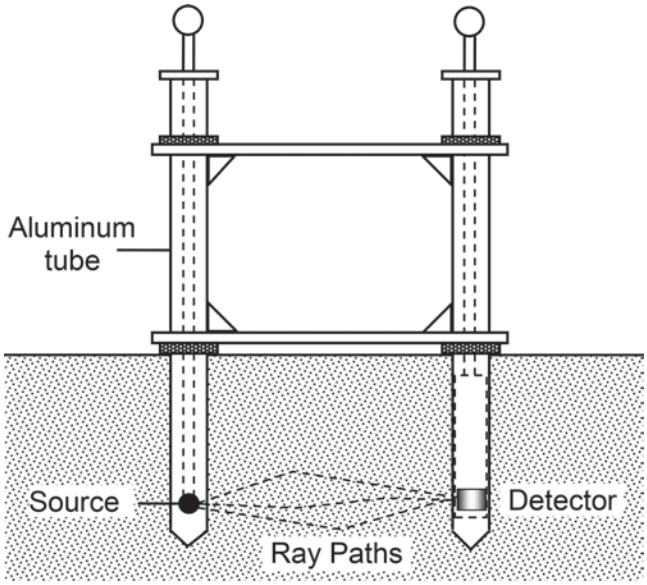

Fig. 3.4.2.2d—Schematic of direct transmission nuclear gauge for measuring density of fresh concrete at different depth (adapted from Iddings and Melancon [1986]).

stress waves discussed in 3.2). The difference between backscatter radiometry and direct transmission radiometry is that, in the former case, the detector only receives gamma rays that are scattered within the concrete rather than registering both scattered and direct radiation. Scattered rays have lower energy than the direct (primary) rays and are produced when a gamma-ray photon collides with an electron in an atom. Part of the photon energy is imparted to the electron and a new photon emerges, traveling in a different direction with lower energy, which is a process known as Compton scattering (Mitchell 2004).

The procedure for using the backscatter method to measure density of fresh or hardened concrete is given in ASTM C1040/C1040M (Procedure B). Like direct transmission measurements, it is necessary to establish a calibration curve before using a nuclear backscatter gauge to measure in-place density.

3.4.3.2 *Instrumentation*—Figure 3.4.3.2 is a schematic of a backscatter nuclear gauge for density measurement. Many commercial gauges are designed so that they can be used in either direct transmission or backscatter mode. To operate the gauge in backscatter mode, the source is positioned so that it is located on the surface of the concrete. Shielding is provided to prevent radiation traveling directly from the source to reach the detector.

Specialized versions of backscatter equipment have been developed. Two of particular interest are described in 3.4.3.1.1 and 3.4.3.1.2.

3.4.3.1.1 *ETG probe*—The electronic thickness gauge (ETG) probe was developed in Denmark to use backscatter measurements for estimating density variation at different depths in a medium. The technique involves determination of the intensity of backscattered gamma radiation as a function of energy level. A beam of parallel (collimated) gamma rays is used and multiple measurements are made

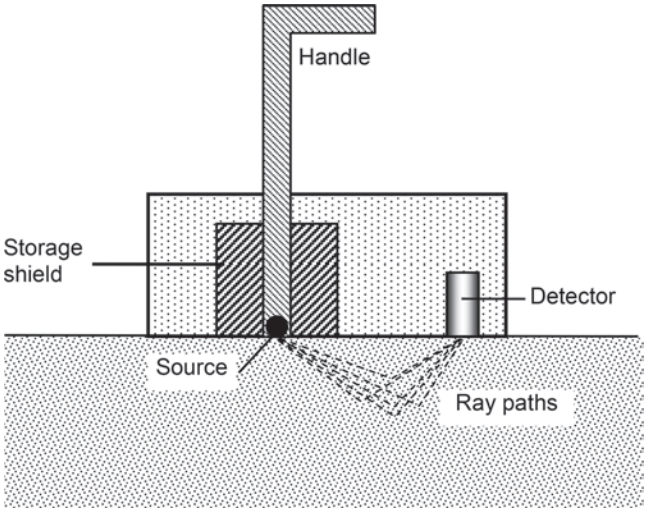

Fig. 3.4.3.2—Schematic of backscatter nuclear density gauge.

with the beam at slightly different angles of penetration. By comparing the radiation spectra for the multiple measurements, information can be obtained about the density in a specific layer of the concrete. In addition to permitting measurement of density at discrete layers, the ETG probe also permits density measurements at greater depths of up to 6 in. (150 mm) than are possible by ordinary backscatter gauges (Berg et al. 1989).

3.4.3.1.2 *Consolidation monitoring device*—This equipment was developed for continuous monitoring of pavement consolidation during slipform construction (Mitchell et al. 1979). The device is mounted on the rear of a highway paving machine and traverses across the finished pavement at a height of approximately 1 in. (25 mm) above the pavement surface. An air gap compensating device allows for air gap variations of up to 0.4 in. (10 mm). The device measures the average density within the top 4 in. (100 mm) of the pavement.

3.4.4 *Radiography*—Radiography provides a means of obtaining a radiation-based photograph of the interior of concrete because denser materials block more of the radiation. From this photograph, the location of reinforcement, voids in concrete, or voids in grouting of post-tensioning ducts can be identified. When the radiation source produces gamma rays, the method is called gammagraphy, but in this report, the term “radiography” is used both for X-ray and gamma ray sources.

3.4.4.1 *Principle*—A radiation source is placed on one side of the test object and a beam of radiation is emitted. Alternatively, the radiation source can be placed in a hole drilled into the concrete (Mariscotti et al. 2009). As the radiation passes through the member, it is attenuated by differing amounts, depending on the density and thickness of the material that is traversed. The radiation that emerges from the opposite side of the object strikes a special photographic film (Fig. 3.4.4.1). The film is exposed in proportion to the intensity of the incident radiation. When the film is developed, a two-dimensional (2-D) visualization (a photograph) of the interior structure of the object is obtained. The

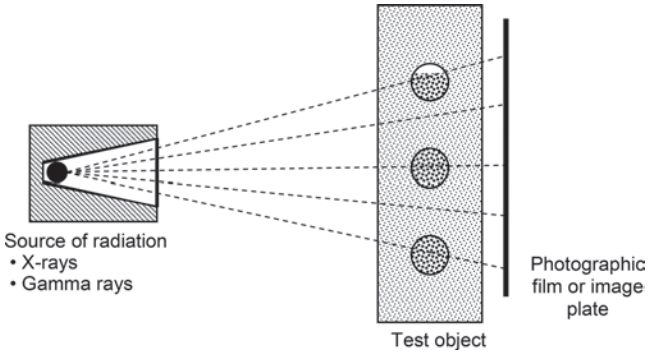

Fig. 3.4.4.1—Schematic of radiographic method.

presence of a high-density material, such as reinforcement, is shown on the developed film as a light area, and a region of low density, such as a void, is shown as a dark area.

An image plate instead of photographic film can also be used. An image plate is composed of a phosphor screen that captures the energy of the radiation passing through the test object. A laser beam is then used to convert the stored energy to a luminescent signal that is captured and stored as a 2-D digital array. The digital information can be subjected to signal processing to obtain quantitative estimates of, among other things, loss of cross section of reinforcement due to corrosion (Mariscotti et al. 2009). If images are obtained with the source in different positions, accurate three dimensional (3-D) reconstructions of the reinforcement can be generated through triangulation by projecting an array of calibrated reference marks onto the plates (Mariscotti et al. 2009; Thieberger et al. 2009).

The British Standards Institute (BSI) has adopted a standard for radiographic testing of concrete based on BS 1881-205. The standard provides recommendations for investigators considering radiographic examinations of concrete (Mitchell 2004).

3.4.4.2 *Instrumentation*—In X-radiography, the radiation is produced by an X-ray tube (Mitchell 2004). The penetrating ability of the X-rays depends on the operating voltage of the X-ray tube. In gammagraphy, a radioactive isotope is used as the radiation source. The selection of a source depends on the density and thickness of the test object and on the exposure time that can be tolerated. The most energetic source is cobalt-60 (Co), which can be used to penetrate up to 20 in. (500 mm) of concrete. For members with thickness of 10 in. (250 mm) or less, iridium-192 (Ir) or cesium-137(Cs) can be used based on BS 1881-205. The film type will depend on the thickness and density of the member being tested. The source Ir is the least energetic of these three sources and can be used to image a concrete thickness up to 12 in. (300 mm) using approximately 15 to 30 minutes of exposure time (Mariscotti et al. 2009). Despite these limitations, Ir is preferred because it requires the least amount of shielding material and can be effectively used in most applications by inserting the source inside a hole drilled in the concrete (Mariscotti et al. 2009).

Most field applications have used radioactive sources because of their greater penetrating ability (higher energy radiation) compared with X-rays. A system developed in France uses an electron linear accelerator to produce very-high-energy X-rays that can penetrate up to 40 in. (1 m) of concrete. This system was developed for the inspection of prestressed members to establish the condition and location of prestressing strands and to determine the quality of grouting in tendon ducts (Mitchell 2004). Note that the technique is difficult to apply in the field and beam hardening effects may hide voids (Im et al. 2010). Beam hardening refers to the process whereby the average energy level of an X-ray beam increases with penetration as the lower energy photons are filtered out.

3.4.5 *Gamma-gamma logging of deep foundations*—This technique is used to evaluate the integrity of drilled shaft and slurry wall foundations by measuring the density of the concrete surrounding access tubes or holes in the deep foundations. Gamma-gamma logging uses a radioactive source and a radiation detector that may be either in separate units (direct transmission) or housed in the same unit (backscatter) (Preiss and Caiserman 1975; Davis and Hertlein 1994).

3.4.5.1 *Principle*—The most common method is by backscatter, with the source-detector unit (probe) lowered down a single dry plastic access tube, and raised at a uniform rate to the surface. Low-density zones, such as soil inclusions, within 2 to 4 in. (50 to 100 mm) from the probe will decrease the radiation count because less radiation is backscattered than in a zone of intact concrete. A limitation of the method is the need for stronger radiation sources to increase the zone of influence of the probe around the tube.

The effect of different access tube materials on relative gamma-ray count is demonstrated in Fig. 3.4.5.1, which shows plots of radiation counts from an experimental drilled shaft with four access tubes: two of plastic and two of steel (Baker et al. 1993). The response from the shaft constriction at 36 to 39 ft (11 to 12 m) is attenuated by the steel tubes. The figure also shows that a small elliptical inclusion at 13 ft (4 m) is not detected in any of the traces, demonstrating the limitation of the method to locate small flaws, unless they are located close to the access tubes.

When gamma-gamma logging is used in the direct transmission mode in parallel tubes (Preiss 1971), the data can be analyzed in a similar manner to that from crosshole sonic logging (3.3). This technique requires a strong source and dedicated equipment; for these latter reasons, it is difficult to use in North America.

3.4.6 *Advantages and limitations*—Table 3.4.6 summarizes the advantages and limitations of the nuclear methods. Direct transmission radiometry, which requires a drilled hole in hardened concrete, provides rapid determination of the in-place density of concrete. The equipment is reasonably portable, making it suitable for use in the field. Minimal operator skills are required to make the measurements. For the commercially available equipment, the source/detector separation is limited to a maximum of approximately 12 in. (300 mm). The most commonly available equipment, which measures an average density between the immersed source

and the surface detector, is incapable of identifying areas of low compaction at specific depths. All immersed-probe techniques for fresh concrete have another drawback in that the immersion of the probe may have a localized influence on the concrete being measured. Test results may be affected by the presence of reinforcing steel located near the source-detector path.

Backscatter tests can be used on finished surfaces where direct transmission measurements would be impractical or disruptive. The equipment is portable and tests can be conducted rapidly. The precision of backscatter gauges, however, is less than that of direct transmission devices. ASTM C1040/C1040M requires that a suitable backscatter gauge for density measurement should result in a single-operator standard deviation of less than 1 lb/ft^3 (16 kg/m^3); for a suitable direct-transmission gauge, the single-operator standard deviation should be less than 0.5 lb/ft^3 (8 kg/m^3). According to ASTM C1040/C1040M, backscatter gauges are typically influenced by the top 3 to 5 in. (75 to 125 mm) of material. The top 1 in. (25 mm) determines 50 to 70 percent of the count rate and the top 2 in. (50 mm) determines 80 to 95 percent of the count rate. When the material being tested is homogenous, this inherent characteristic of the method is not significant. When a thin overlay, however, is placed on existing concrete, this effect has to be considered in interpreting the results. Also, the presence of reinforcing steel within the influence zone will affect the count rate.

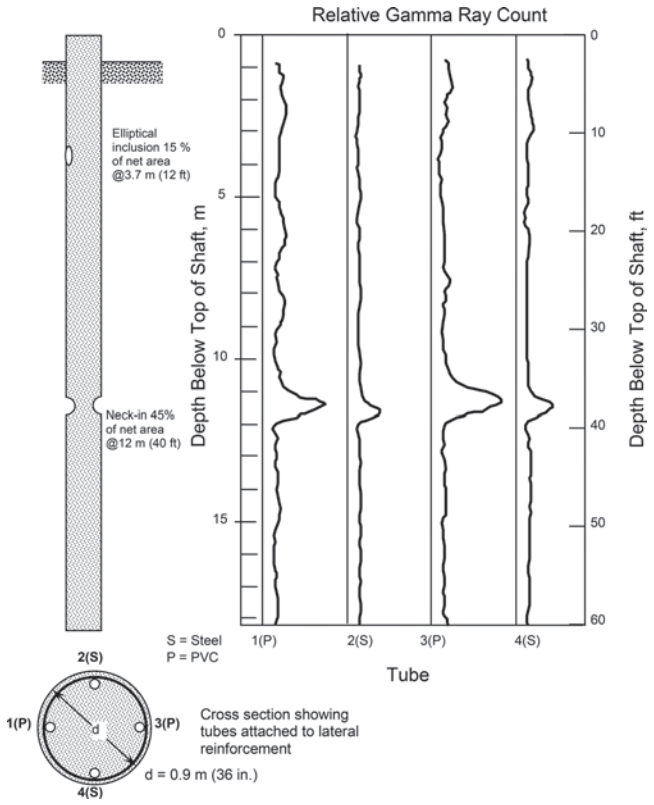

Fig. 3.4.5.1—Gamma-gamma backscatter log on experimental shaft with planned defects (Baker et al. 1993).

Radiographic methods allow the possibility of seeing some of the internal structure of a concrete member where density variations exist. Although both gamma ray and X-ray sources can be used for radiography, X-ray equipment is comparatively expensive and cumbersome for field application. Because of this, less costly and more portable gamma-ray equipment is generally chosen for field use. X-ray equipment, however, has the advantage that it can be turned off when not in use. In contrast, gamma rays are emitted continuously from a radioactive source requiring heavy shielding to protect personnel. In addition, special X-ray equipment, such as electron linear accelerators, can produce more energetic radiation than radioactive sources, which permits the inspection of thicker members or the use of shorter exposure times. When image plates are used instead of film, digital signal processing can be used to extract quantitative information about the internal conditions. By taking multiple images with difference source-detector orientations, tomographic images of the interior structure can be created.

The main concern in the use of all nuclear methods is safety. In general, personnel who perform nuclear tests should obtain a license from the appropriate governmental agency (Mitchell 2004). Testing across the full thickness of a concrete element is particularly hazardous and requires extensive precautions, skilled personnel, and highly specialized equipment. Radiographic procedures require evacuation of the site where measurements are carried out by persons not involved in the actual testing. The use of X-ray equipment poses an additional danger due to the high voltages used. There are limits on the thicknesses of the members that can be tested by radiographic methods. For gamma-ray radiography, the maximum thickness is approximately 20

Table 3.4.6—Advantages and limitations of nuclear methods

Method	Advantages	Limitations
Direct transmission radiometry	Portable equipment available for determination of in-place density. Minimal operator skill is required.	Operators must be licensed. Available equipment limited to path lengths less than 12 in. (300 mm). Requires access to inside of member or opposite faces.
Backscatter radiometry	Requires access only to surface of test object and is suitable for fresh or hardened concrete. Equipment is portable and testing is rapid.	Operators must be licensed. Precision of density measurements is lower than direct transmission. Measurement is affected by near-surface material and is sensitive to chemical composition.
Radiography	Provides view of the internal structure of the test object. Use of image plates allows for digital signal processing to extract more information about the internal structure. Tomography of reinforcement in large columns and beams can be achieved introducing portable ^{192}Ir sources in holes drilled in the concrete.	Operators must be licensed and highly skilled. X-ray equipment is bulky and expensive. Difficult to identify cracks perpendicular to radiation beam. Gamma-ray penetration limited to 20 in. (500 mm) of concrete. Access to opposing faces is required.

in. (500 mm) because thicker members require unacceptably long exposure times. Tomography of reinforcement in large columns and beams can be achieved in most cases by introducing 192 Ir sources in holes drilled in the concrete. Radiography is not very useful for locating crack planes perpendicular to the radiation beam.

3.5—Magnetic and electrical methods

Knowledge about the quantity and location of reinforcement is needed to evaluate the strength of reinforced concrete members. Knowing whether there is active corrosion of reinforcement is necessary to assess the need for remedial actions before structural safety or serviceability is jeopardized. This section discusses some of the magnetic and electrical methods used to gain information about the layout and condition of embedded steel reinforcement (Bungey et al. 2006; Lauer 2004; Carino 2004b). Devices to locate reinforcing bars and estimate the depth of cover are known as covermeters, reinforcing bar locators, or pachometers. In this report they will be called covermeters.

Electrical methods are used to evaluate corrosion activity of steel reinforcement. As is the case with other nondestructive test (NDT) methods, an understanding of the underlying principles of these electrical methods is needed to obtain meaningful results. In addition, an understanding of the factors involved in the corrosion mechanism is essential for reliable interpretation of data from this type of testing. The likelihood of corrosion activity can be monitored using the half-cell potential technique, where the potential for high corrosion rate can be inferred from the concrete resistivity and information on the rate of corrosion can be obtained from linear-polarization methods. Sections 3.5.2 through 3.5.4 provide basic information about these methods. Actual testing and interpretation of test results should, however, be completed by experienced personnel.

The magnetic flux leakage method may be able to detect fractures in prestressing steel.

3.5.1 *Covermeters*—As is common with other NDT methods used to infer conditions within concrete, covermeters measure the depth of cover by monitoring the interaction of the reinforcing bars with some other process. For most covermeters, the interaction is between the bars and a low-frequency electromagnetic field. The basic relationships between electricity and magnetism are key to understanding the operation of covermeters. One important principle is electromagnetic induction, which is an alternating magnetic field intersecting an electrical circuit that induces an electrical potential in that circuit. According to Faraday's law, the induced electrical potential is proportional to the rate of change of the magnetic flux through the area bounded by the circuit (Serway 1983).

Commercial covermeters can be divided into two classes: those based on the principle of magnetic reluctance and those based on eddy currents. Their differences are summarized in 3.5.1.1 and 3.5.1.2 (Carino 1992).

3.5.1.1 *Magnetic reluctance meters*—When electrical charge flows through an electrical coil, a magnetic field is created and a magnetic flux composed of magnetic lines is set up between the magnetic poles of the coil. This leads to a magnetic circuit, in which the magnetic flux between poles is analogous to the current in an electrical circuit (Fitzgerald et al. 1967). The resistance to creation of magnetic flux is called reluctance, which is analogous to the resistance to flow of charge (current) in an electrical circuit.

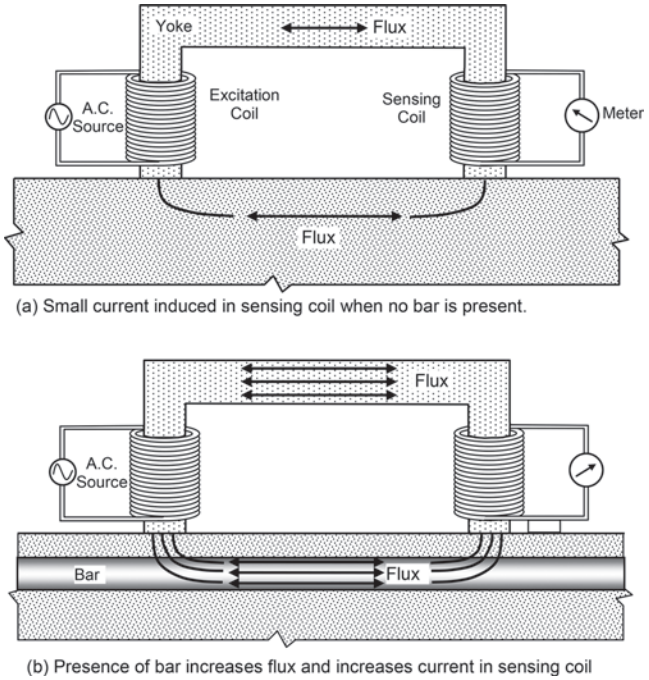

Fig. 3.5.1.1—Covermeter based on principle of magnetic reluctance (adapted from Carino [1992]): (a) small current induced in sensing coil when no bar is present; and (b) presence of bar increase current in sensing coil.

Figure 3.5.1.1 is a simplified schematic of a covermeter based on changes in the reluctance of a magnetic circuit caused by the presence or absence of a bar within the vicinity of the search head. The search head is composed of a ferromagnetic U-shaped core (yoke), an excitation coil, and a sensing coil. Note that while modern covermeters may not use exactly the type of core shown in Fig. 3.5.1.1, the basic principle of operation is the same. When alternating current (less than 100 Hz) is applied to the excitation coil, an alternating magnetic field is created and there is a magnetic flux between the poles of the yoke. In the absence of a bar (Fig. 3.5.1.1(a)), the magnetic circuit, composed of the yoke and the concrete between ends of the yoke, has a high reluctance and the amplitude of alternating magnetic flux between the poles is small. The alternating flux induces a small, secondary current in the sensing coil. If a ferromagnetic bar is present (Fig. 3.5.1.1(b)), the reluctance decreases, the magnetic flux amplitude increases, and the sensing coil current increases. Thus, the presence of the bar is indicated by a change in the output from the sensing coil. For a given reinforcing bar, the reluctance of the magnetic circuit depends strongly on the distance between the bar and the poles of the yoke. An increase in concrete cover increases the reluctance and reduces the current in the sensing coil. If the meter output was plotted as a function of the cover, a calibration relation-

ship would be established that could be used to measure the cover. Because the size of the bar affects the reluctance of the magnetic circuit, there would be a separate relationship for each bar size. These aspects are discussed in-depth later in this section.

3.5.1.2 *Eddy-current meters*—If a coil carrying an alternating current is brought near an electrical conductor, the changing magnetic field induces circulating currents, known as eddy currents, in the conductor. Because any current gives rise to a magnetic field, eddy currents produce a secondary magnetic field that interacts with the field of the coil. The second class of covermeters is based on monitoring the effects of the eddy currents induced in a reinforcing bar. There are two categories of eddy-current meters: one is based on the continuous excitation of the coil by an alternating current (usually at approximately 1 kHz), and the other is based on pulsed excitation.

Figure 3.5.1.2a is a schematic of a continuous eddy-current covermeter. In the absence of a reinforcing bar, the magnitude of the alternating current in the coil depends on the coil impedance. Note that when direct current is applied to a circuit, the amount of current equals the voltage divided by the electrical resistance of the circuit. When alternating current is applied to the coil, the amount of current is governed by the value of the applied voltage, the resistance, and another quantity called inductance. The vector sum of resistance and inductance defines the impedance of the coil.

If the coil is brought near a reinforcing bar, alternating eddy currents are established within the surface skin of the bar. The eddy currents give rise to an alternating secondary magnetic field that induces a secondary current in the coil. In accordance with Lenz's law (Serway 1983), the secondary current opposes the primary current. As a result, the net current through the coil is reduced and the apparent impedance of the coil increases (Hagemaier 1990). The presence of the bar is inferred by monitoring the change in current through the coil.

Figure 3.5.1.2b is a schematic of a cover meter based on pulsed excitation of coils within the search head. A repetitive current pulse is applied to the coils. There is a period of dead time between the end of the pulse and the start of the next pulse. During each pulse, current increases gradually but is turned off rapidly. The sudden end of the pulse causes a sudden collapse in the magnetic field of the coils, which induces eddy currents in a bar located within the coils' influence zone. As the eddy currents decay, a decaying magnetic field induces a secondary current in the coils. The amplitude of the induced current depends on the depth and size of the bar. By measuring the amplitude of the induced current, information about the bar can be inferred. Note that in this case the search head includes two coils, which make the search head directional, that is, the output is largest when the coils are aligned with the bar (Carino 1992).

In summary, magnetic reluctance covermeters are based on monitoring changes in the magnetic flux that is set up in the magnetic circuit composed of the path through the yoke, concrete, and the reinforcing bar. For a given cover, the meter output depends on the cross-sectional area of the

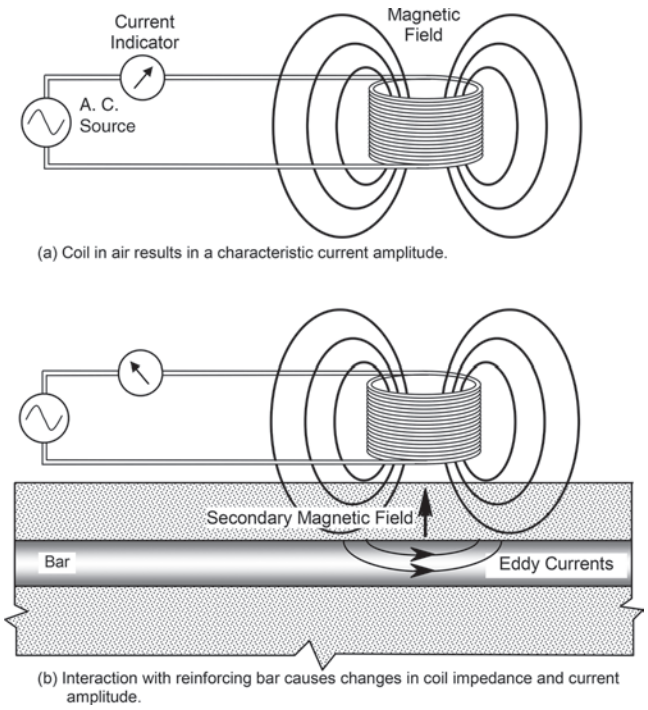

Fig. 3.5.1.2a—Covermeter based on eddy current principle (adapted from Carino [1992]): (a) coil in air results in characteristic current amplitude; and (b) interaction with reinforcing bar causes changes in coil impedance and current amplitude.

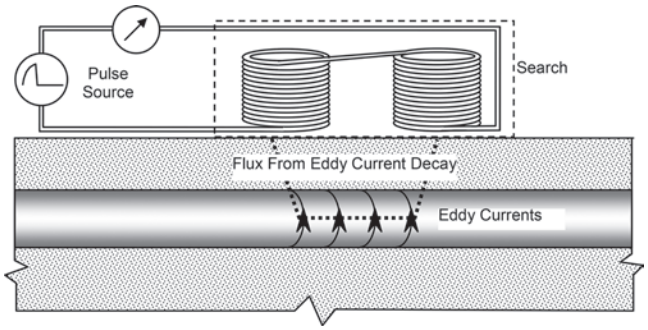

Fig. 3.5.1.2.b—Covermeter based on pulse induction eddy current technique (adapted from Carino [1992]).

reinforcing bar and its magnetic properties, which is affected by alloy composition and type of mechanical processing. Alternately, eddy-current covermeters depend mostly on the electrical conductivity of the bar, detecting magnetic as well nonmagnetic metallic objects. A ferromagnetic material will produce a stronger signal because of the enhanced strength of the secondary magnetic field created by the eddy currents. The response of magnetic reluctance covermeters is affected by the presence of iron-bearing aggregates in the concrete, whereas eddy-current meters are not.

3.5.1.2.1 *Limitations*—A reinforcing bar is detected by a covermeter when the bar lays within the zone of influence of the search head (yoke or coil). Figure 3.5.1.2.1a(a) illustrates that influence zone of the search head. The response is maximum when the search head lies directly above the rein-

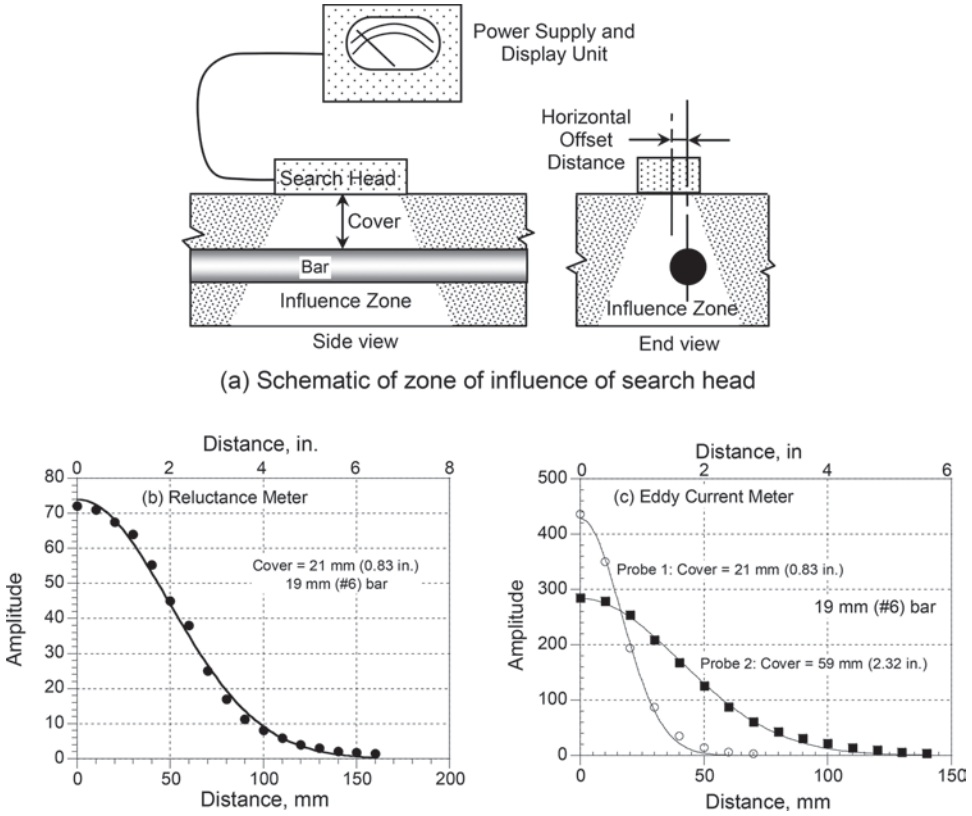

Fig. 3.5.1.2.1a—(a) Zone of influence of covermeter search head; variation of amplitude with horizontal offset for: (b) magnetic reluctance covermeter; and (c) eddy current covermeter (adapted from Carino [1992]).

forcing bar. An important characteristic of a covermeter is the relationship between meter amplitude and the horizontal distance from the center of the bar to the center of the search head, that is, the horizontal offset. Figure 3.5.1.2.1a(b) shows the variation in amplitude with horizontal offset for a magnetic reluctance covermeter when the search head is moved away from a No. 6 (19 mm) bar with a cover depth of 0.83 in. (21 mm). The variation is approximately a bell-shaped curve. The width of the curve in Fig. 3.5.1.2.1a(b) defines the zone of influence of the search head. Figure 3.5.1.2.1a(c) shows the relationships between amplitude and horizontal offset for two different search heads (probes) of an eddy-current meter. One search head has a smaller zone of influence than the other, making it a more focused search head. A covermeter with a focused search head can discern individual bars when they are closely spaced and the response is affected less by bars perpendicular to the bars being measured. Focused search heads, however, generally have less penetrating ability and are unable to locate bars with deep cover. This is a direct engineering trade-off that occurs in the design of eddy-current meters. Designs that feature multiple search heads have become common to broaden the useful range of an individual meter. Search heads with multiple electronically selectable coils are also available. The influence zone of the search head also affects the accuracy with which the end of a reinforcing bar can be detected (Carino 1992).

An important distinction among covermeters is the directionality characteristics of the search heads. Due to the shape of the yoke, a magnetic reluctance meter is directional compared with a continuous eddy-current meter with a symmetrical coil. Maximum response occurs when the yoke is aligned with the axis of the bar. This directionality can be used to an advantage when testing a structure with an orthogonal grid of reinforcing bars (Tam et al. 1977).

As mentioned previously, each covermeter has a unique relationship between meter amplitude and depth of cover. Figure 3.5.1.2.1b(a) shows a technique that can be used to develop these relationships for different bar diameters. A single bar is placed on a nonmagnetic and nonconducting surface and the meter amplitude is determined as a function of the distance between the search head and the top of the bar. Figure 3.5.1.2.1b(b) and 3.5.1.2.1b(c) show these relationships for a magnetic reluctance and for an eddy-current meter, respectively. These relationships illustrate a basic limitation of covermeters. Because the amplitude is a function of bar diameter and depth of cover, one cannot determine both parameters from a single measurement. As a result, a dual measurement is needed to estimate both depth of cover and diameter (BS 1881-204; Das Gupta and Tam 1983). This may be done by recording the meter amplitude first with the search head in contact with the concrete and then when the search head is located a known distance above the concrete. Alternatively, other methods can be used to change the field strength, such as using different search heads or rotating a

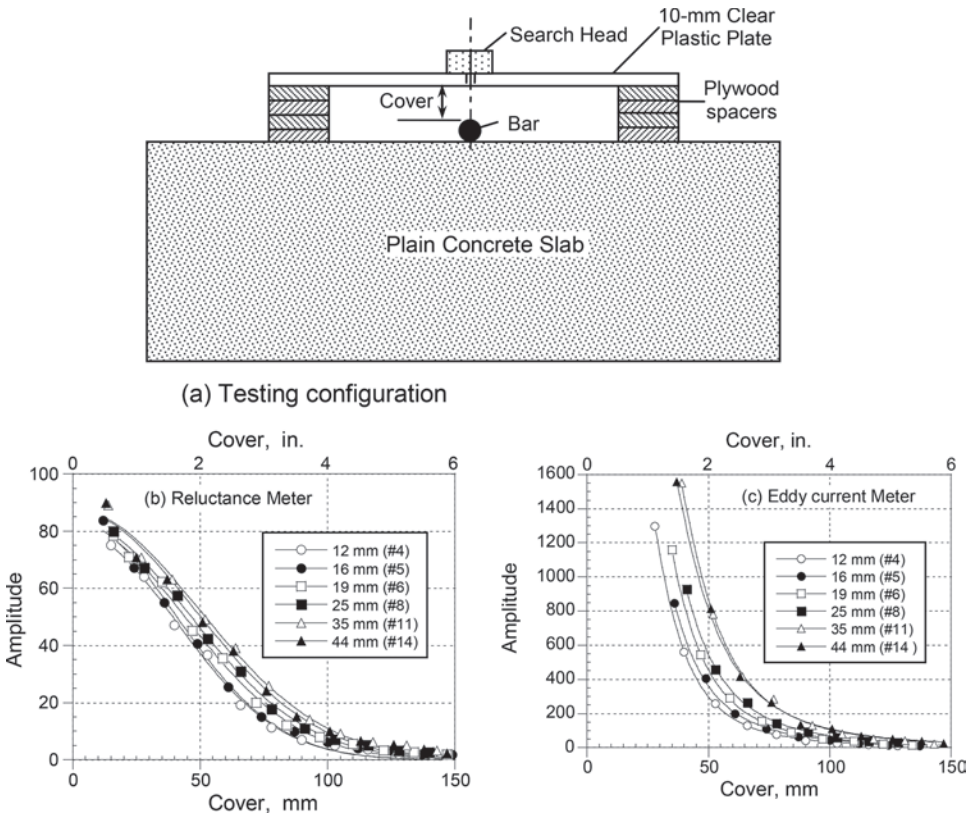

Fig. 3.5.1.2.1b—Covermeter amplitude versus cover: (a) testing configuration; (b) results for magnetic reluctance meter; and (c) results for eddy current meter (adapted from Carino [1992]).

search head. The difference in amplitudes and the amplitude-cover relationships are used to estimate the cover and bar diameter. The accuracy of this dual-measurement technique depends on how distinct the amplitude-cover relationships are for the different bar sizes. Because these relationships are generally similar for adjacent bar sizes, it is generally only possible to estimate bar diameter within two adjacent sizes (Bungey et al. 2006).

The single-bar, amplitude-cover relationships are only valid when the bars are sufficiently far apart so that there is little interference by adjacent bars. Figure 3.5.1.2.1c(a) shows a technique used to investigate the effect of bar spacing on covermeter response (Carino 1992). For multiple closely-spaced bars, the amplitude may exceed the amplitude for a single bar at the same cover depth. If they are closer than a critical amount, the individual bars cannot be discerned. The critical spacing depends on the type of covermeter and the cover depth. In general, as cover increases, the critical spacing also increases. Figure 3.5.1.2.1c(b) and 3.5.1.2.1c(c) show the response for multiple bars at different spacing using a magnetic reluctance meter. The horizontal line is the single-bar amplitude for the same bar size and cover depth. For the 3 in. (75 mm) center-to-center spacing, the meter is just barely able to discern the locations of the individual bars, and the amplitude is not too much higher than the single response. Figures 3.5.1.2.1c(d) and 3.5.1.2.1c(e) show the responses for an eddy-current meter. Locations of the individual bars are easily identified for the 2.8 in. (70 mm) spacing, but the amplitude is greater than the single-bar amplitude. Thus, the cover would be underestimated if the single-bar, amplitude-cover relationship were used. The response of a covermeter to the presence of multiple closely-spaced bars depends on its design. Teodoru (1996) reports that problems may be encountered when bar spacings are less than approximately the lateral dimensions of the search head. For eddy-current meters, the coil dimensions have a direct effect on the depth of penetration and the response to closely spaced bars.

The presence of two layers of reinforcement within the zone of influence cannot generally be identified with ordinary covermeters (Bungey et al. 2006; Carino 1992). The upper layer produces a much stronger signal than the deeper, second layer, so that the presence of the second layer cannot be discerned. It has been shown, however, that it may be possible to determine lap length when bars are in contact (Carino 1992).

Commercial systems have been developed that will store covermeter readings at the intersections of an orthogonal grid laid out over the test surface. The stored data are then used to construct a two-dimensional (2-D) visualization of signal amplitude, or cover. Other scanning devices include multiple search heads to speed up testing. Such devices have been found effective in determining the depth and alignment of dowel bars in concrete pavements (FHWA 2005).

Table 3.5.1.2.1 summarizes the advantages and limitations of covermeters. These devices are effective in locating

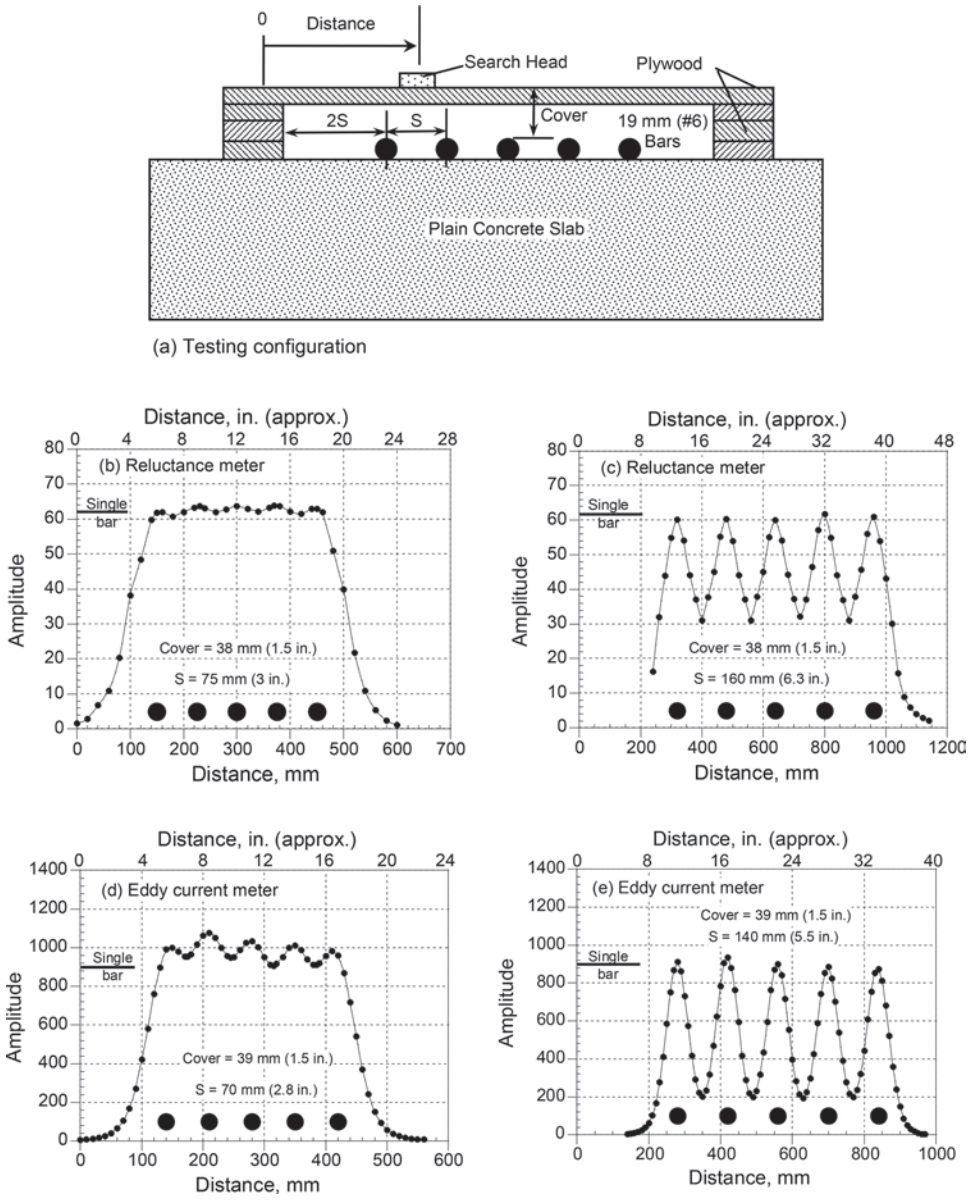

Fig. 3.5.1.2.1c—Covermeter response with multiple parallel bars at different spacing: (a) testing configuration; (b) response of magnetic reluctance meter, S *= 3 in. (75 mm); (c) response of magnetic reluctance meter,* S *= 6.3 in. (160 mm); (d) response of eddy current meter,* S *= 2.8 in. (70 mm); and (e) response of eddy current meter,* S *= 5.5 in. (140 mm) (adapted from Carino [1992]).*

individual bars, provided that the spacing exceeds a critical value that depends on the meter design and the cover depth. By using multiple measurement methods, bar diameter can generally be estimated to within two adjacent bar sizes if the spacing exceeds certain limits that are also dependent on the particular meter. Meters are available that can estimate bar diameter without using spacers to make multiple measurements. Again, the accuracy of these estimates decreases as bar spacing decreases. To obtain reliable measurements, it is advisable to prepare mockups of the expected reinforcement configuration to establish whether the desired accuracy is feasible. The mockups can be made without using concrete, provided the in-place concrete does not contain significant amounts of iron-bearing aggregates.

3.5.2 *Half-cell potential method*—The half-cell potential method is used to delineate those portions of the structure where there is a high likelihood of corrosion activity. Before describing the test procedure, a brief discussion of the basic principles of corrosion testing is provided. Readers should consult ACI 222R for additional information on the factors affecting corrosion of steel in concrete.

3.5.2.1 *Principle*—Corrosion is an electrochemical process involving the flow of charges (electrons and ions). Figure 3.5.2.1 shows a corroding steel bar embedded in concrete. At active sites on the bar, called anodes, iron atoms lose electrons and move into the surrounding concrete as ferrous

Table 3.5.1.2.1—Advantages and limitations of magnetic and electrical methods

Method	Advantages	Limitations
Covermeter	Able to locate reinforcing bars and other embedded metal objects. Equipment is lightweight, portable, and easy to use. Cover depth can be estimated.	Accuracy of estimated cover depth affected by bar size and bar spacing. Bar diameters difficult to estimate with precision. Cannot identify presence of second layer of reinforcement. Ability to discern individual bars is affected by the meter design, cover depth, and bar spacing. Meters based on magnetic reluctance can detect only ferromagnetic objects. Maximum penetration is limited and depends on meter design.
Half-cell potential (ASTM C876)	Lightweight, portable equipment. Provides indication of likelihood of corrosion activity at time of testing.	Requires a connection to embedded reinforcement, and reinforcement should be electrically connected. Not applicable to epoxy-coated bars. Concrete has to be moist. No indication of corrosion rate. Testing and interpretation should be done by experienced personnel.
Concrete resistivity	Lightweight portable equipment. Provides qualitative indication of relative corrosion rate when active corrosion is present. Surface resistivity test of cylinder specimens can be related to resistance to fluid penetration.	No standard test method for concrete. Lack of agreement between different test systems. Measured values based on assumed models. Some systems require electrical connection to embedded reinforcement. Testing and interpretation should be done by experienced personnel. For evaluating resistance to fluid penetration, specimen should be in saturated condition.
Linear polarization	Lightweight portable equipment. Provides indication of corrosion rate at time of testing.	Requires a connection to embedded reinforcement, and reinforcement should be electrically connected. Not applicable to epoxy-coated or galvanized bars. No standards for interpreting test results. Inherent uncertainty in converting polarization resistance to corrosion current density. Different devices give different values of corrosion rate. Cover depth has to be less than 4 in. (100 mm). Concrete surface has to be smooth, uncracked, free of impermeable coating, and free of visible moisture. Testing and interpretation should be done by experienced personnel.
Magnetic flux leakage	Locate fractures in prestressing steel.	Commercial test system for reinforced concrete is not available. Data interpretation is complex. Signals due to embedded ferromagnetic objects can be misinterpreted as wire fractures.

ions. This process is called a half-cell oxidation reaction, or the anodic reaction, and is represented as

$$Fe \rightarrow Fe^{2+} + 2e^{-} \qquad (3.5.2.1a)$$

The electrons remain in the bar and flow to sites called cathodes, where they combine with water and oxygen present in the concrete. The reaction at the cathode is called a reduction reaction and the most dominant and likely reaction is represented as

$$2H_2O + O_2 + 4e^{-} \rightarrow 4OH^{-} \qquad (3.5.2.1b)$$

To maintain electrical neutrality, the ferrous ions migrate through the concrete to these cathodic sites where they combine to form hydrated iron oxide, or rust. Thus, when the bar is corroding, electrons flow through the bar and ions flow through the concrete.

If the steel is corroding, the potential at the anode is more negative. The half-cell potential method is used to detect this negative charge and thereby provide an indication of corrosion activity.

3.5.2.2 *Instrumentation*—The standard test method is given in ASTM C876 and is illustrated in Fig. 3.5.2.2. The apparatus includes a copper-copper sulfate electrode (CSE),

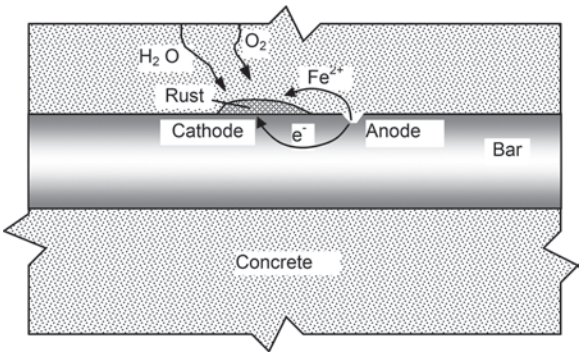

Fig 3.5.2.1—Corrosion of steel bar embedded in concrete. Iron is dissolved at anode and precipitates as rust at the cathode.

or other half-cell; connecting wires; and a high-impedance voltmeter. Note that the half-cell is composed of a copper bar immersed in a saturated copper sulfate solution, one of many half-cells that can be used as a reference to measure the electrical potential of embedded bars. Note that all subsequent potential values will be with respect to CSE. The measured voltage depends on the type of half-cell, and conversion factors are available to convert readings obtained with other references cells to the copper-copper sulfate half-cell

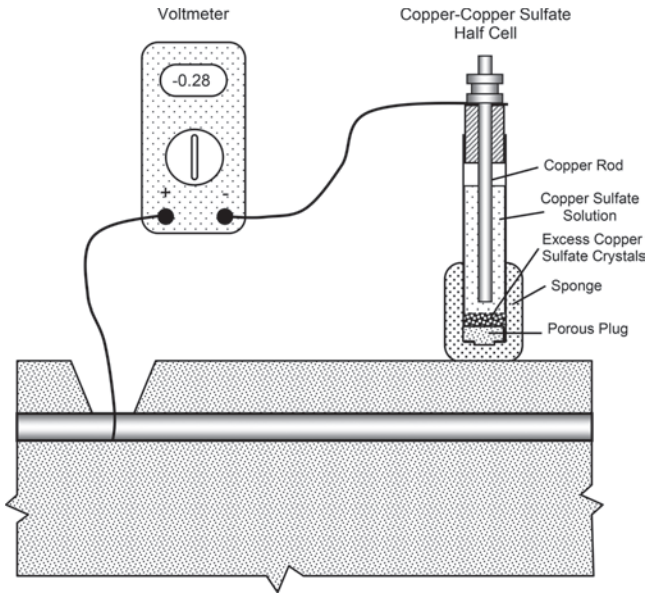

Fig. 3.5.2.2—Apparatus for half-cell potential method described in ASTM C876.

(Roberge 2008). For example, when a silver/silver chloride electrode in saturated potassium chloride is used as a reference half-cell, the potential reading will be more positive by 119 mV compared with a copper-copper sulfate half-cell.

The positive terminal of the voltmeter is attached to the reinforcement and the negative terminal is attached to the copper-copper sulfate half-cell. A high-impedance voltmeter is used so that there is only a small current in the measuring circuit. As shown in Fig. 3.5.2.2, the half-cell makes electrical contact with the concrete by means of a porous plug and a sponge that is moistened with a wetting solution such as liquid detergent.

The positive terminal of the voltmeter is attached to the reinforcement and the negative terminal is attached to the CSE. A high-impedance voltmeter is used so that there is only a small negligible current in the measuring circuit. The measured half-cell potential, which is also called the corrosion potential, is an open-circuit potential because it is measured under the condition of no current in the measuring circuit (ASTM G15). As shown in Fig. 3.5.2.2 the half-cell CSE makes electrical contact with the concrete by means of a porous plug and a sponge that is moistened with a wetting solution such as liquid detergent. Because the positive terminal of the voltmeter is connected to the bar, it indicates a negative potential. If the negative terminal of the voltmeter was to be connected to the bar, the sign of the voltage would be reversed. In general, the more negative the voltage reading, the higher the likelihood that the bar is corroding. Exceptions exist that are described in a subsequent section.

The half-cell potential readings are indicative of the probability of corrosion activity of reinforcement located beneath the reference cell. This is true, however, only if all of the reinforcement is electrically connected. To ensure that this condition exists, electrical resistance measurements between widely separated reinforcing bars should be carried out (ASTM C876). Access to the reinforcement has to be provided. The method cannot be applied to concrete with epoxy-coated reinforcement.

Testing is usually performed at points arranged in a grid. The required spacing between test points depends on the particular structure. Excessive spacings can miss points of activity or provide insufficient data for proper evaluation, whereas closer spacings increase the complexity and price of the survey. In surveying bridge decks, ASTM C876 recommends a spacing of 48 in. (1.2 m). If the differences in voltages between adjacent points exceed 150 mV, a closer spacing is suggested. Others have suggested that spacing should be approximately half this value to obtain a reliable assessment of the extent of the corrosion (Clemeña et al. 1992a). Test apparatus is available that includes multiple cells to speed up data collection at close spacings.

A key aspect of the test is assuring that the concrete is sufficiently moist. If the measured potential at a test point does not change by more than ±20 mV within a 5-minute period (ASTM C876), the concrete is sufficiently moist. If this condition is not satisfied, the concrete surface should be wetted and two approaches given in ASTM C876 should be applied. When prewetting is necessary, there should be no free surface water between test points. If stability cannot be achieved by prewetting, it may be due to stray electrical currents and the half-cell potential method should not be used. When testing is performed outside of the range of 62 to 82°F (17 to 28°C), a correction factor is applied to the measured voltages.

3.5.2.3 *Data analysis*—According to ASTM C876, to formulate conclusions about corrosion activity, half-cell potential readings should be used in conjunction with other data, such as chloride content, depth of carbonation, findings of delamination surveys, and the exposure conditions. Data from a half-cell potential survey can be presented in two ways: an equipotential contour map, or a cumulative frequency diagram.

The equipotential contour map is used most often to summarize survey results. First, test locations are drawn on a scaled plan view of the test area. The half-cell voltage readings at each test point are marked on the plan and contours of equal voltage values are sketched. Figure 3.5.2.3 is an example of an equipotential contour map created from test points on a 300 in. (0.76 m) spacing (Clemeña et al. 1992a).

The cumulative frequency diagram is obtained by plotting the data on normal probability paper and drawing a best-fit straight line to the data, according to the procedure in ASTM C876. The cumulative frequency diagram is used to determine the percentage of half-cell potential readings that are more negative than a certain value.

According to ASTM C876, two techniques can be used to evaluate the results: the numeric technique or the potential difference technique. In the numeric technique, the value of the potential is used as an indicator of the likelihood of corrosion activity. If the potential is more positive than –200 mV, there is a high likelihood that no corrosion is occurring at the time of measurement. If the potential is more negative than –350 mV, there is a high likelihood of active corrosion. Corrosion activity is uncertain when the voltage ranges

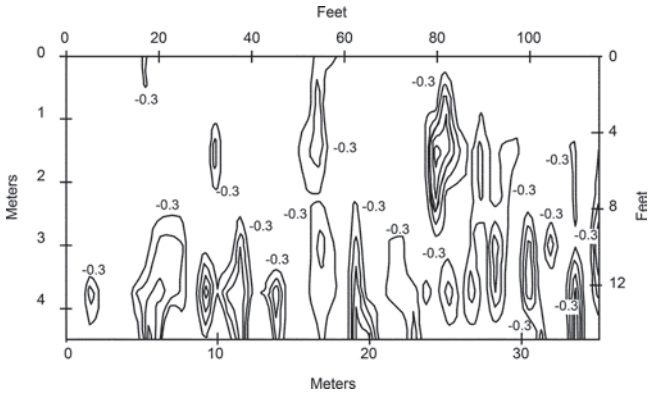

Fig. 3.5.2.3—Equipotential contours from survey data of bridge deck at grid spacing of 30 in. (0.76 m) (only contours less than –0.30 V are shown and contour interval is –0.05 V; adapted from Clemeña et al. [1992a]).

from –200 to –350 mV. ASTM C876 states that, unless there is positive evidence to suggest their applicability, these numeric criteria should not be used:

a) If carbonation extends to the level of the reinforcement

b) To evaluate indoor concrete that has not been subjected to frequent wetting

c) To compare corrosion activity in outdoor concrete with highly variable moisture or oxygen content

d) To formulate conclusions about changes in corrosion activity due to repairs that changed the moisture or oxygen content at the level of the steel

In the potential difference technique, the areas of active corrosion are identified on the basis of the corrosion gradients. In the equipotential contour plot, regions of high gradients are indicated by the close spacing of the voltage contours. In Fig. 3.5.2.3, areas of corrosion activity are indicated by the closely spaced contours.

3.5.2.4 *Limitations*—The advantages and limitations of the half-cell potential method are summarized in Table 3.5.1.2.1. As has been stated, valid potential readings can be obtained only if the concrete is sufficiently moist. Therefore, the user should understand how to recognize when there is insufficient moisture. Because of the factors that affect corrosion testing results, a corrosion specialist is recommended to properly interpret half-cell potential surveys under the following conditions (ASTM C876):

a) Concrete is saturated with water

b) Concrete is carbonated to the depth of the reinforcement

c) Steel is coated (galvanized)

In addition, potential surveys should be supplemented with tests for carbonation and water-soluble chloride content. A major limitation of the half-cell potential method is that it does not measure the rate of corrosion of the reinforcement. It only provides an indication of the likelihood of corrosion activity at the time the measurement is made. The corrosion rate of the reinforcement depends on the availability of oxygen needed for the cathodic reaction. It also depends on the electrical resistance of the concrete, as discussed in 3.5.3.

3.5.3 *Concrete resistivity method*—As was mentioned in 3.5.2, to sustain corrosion, ferrous ions should travel from

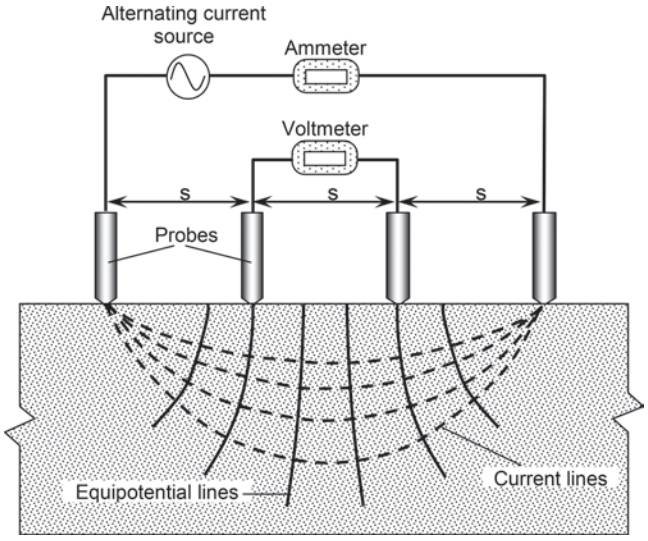

Fig. 3.5.3.1—Four-probe method for measuring concrete resistivity (adapted from Bungey et al. [2006]).

anodic sites on a steel bar through the concrete to cathodic sites. The electrical resistance of concrete controls the ease with which ions migrate through concrete between anodic and cathodic sites. Electrical resistance of concrete, in turn, depends on the microstructure and volume fraction of the paste, the conductivity of the pore solution, and the degree of saturation of the concrete. When both concretes are fully saturated, a concrete with a less porous microstructure, as obtained by using a low water-cementitious materials ratio (*w*/*cm*) and good curing, has a higher electrical resistance than a concrete with a more porous microstructure. A useful test, in conjunction with a half-cell potential survey, is to measure the resistivity of the concrete. The resistivity of a material and the electrical resistance of a conductor made of that material are related as (Tipler 1991)

$$R = \rho \frac{L}{A} \tag{3.5.3}$$

where R is the electrical resistance, in ohm; L is the length of conductor, in cm; A is the cross-sectional area of conductor, in cm^2; and ρ is the resistivity of material, in ohm·cm.

Note that the SI unit for resistivity is ohm·meter, but ohm·cm is used often in the literature. The conversion is 1 ohm·cm = 0.01 ohm·m. The in.-lb equivalent is rarely used.

3.5.3.1 *Four-electrode method*—There is no ASTM test method for measuring the in-place resistivity of concrete. One technique that has been used successfully is shown in Fig. 3.5.3.1 (Millard et al. 1989, 1990; Bungey et al. 2006). This method is based on the classical four-electrode system described by Wenner (1916), which has been incorporated into a standard test method for measuring soil resistivity (ASTM G57). The four equally-spaced electrodes are electrically connected to the concrete surface by using, for example, a conducting cream (Millard et al. 1990). The outer electrodes are connected to a source of alternating current and the inner electrodes are connected to a voltmeter. Morris

Table 3.5.3.4—Relationships between concrete resistivity and corrosion rate

Reference	Resistivity, kΩ·cm	Corrosion condition
Feliú et al. (1996)	> 100	Negligible corrosion; concrete too dry.
	50 to 100	Low corrosion rate.
	10 to 50	Moderate to high corrosion rate.
	< 10	Resistivity does not control corrosion rate.
Bungey et al. (2006)	> 20	Low likelihood of significant corrosion.
	10 to 20	Low to moderate likelihood of significant corrosion.
	5 to 10	High likelihood of significant corrosion.
	< 5	Very high likelihood of significant corrosion.

et al. (1996) compared the readings obtained by two devices operating at approximately 13 Hz and 97 Hz and reported that the measured resistivities were essentially the same.

The apparent resistivity is given by (Millard et al. 1990; Wenner 1916)

$$\rho = \frac{2\pi sV}{I} \qquad (3.5.3.1)$$

where ρ is the resistivity of material, in ohm·cm; s is the spacing between electrodes, in cm; I is the amplitude of alternating current between outer electrodes, in ampere; and V is the measured voltage between inner electrodes, in volt.

The word "apparent" is used because Wenner derived Eq. (3.5.3.1) under the assumption that the material is semi-infinite and homogeneous. Thus, the relationship gives the correct measure of resistivity when these assumptions are satisfied. Any deviations from Wenner's assumptions lead to differences between the calculated apparent resistivity and the true resistivity of the material (Millard et al. 1990).

3.5.3.2 *Limitations*—Millard et al. (1990) have carried out experimental and analytical studies to establish the magnitudes of the errors between the apparent and true resistivities when Eq. (3.5.3.1) is applied to a finite-sized concrete member. One important variable is the electrode spacing. Because concrete is made of paste and aggregates, which have different resistivities, the spacing should be large enough so that a representative average resistivity of concrete is measured. The minimum spacing depends on the maximum size of coarse aggregate. The larger the aggregate, the greater is the required minimum spacing. The electrode spacing also determines the depth of the material that affects the measurement. The greater the spacing, the greater is the depth of concrete that contributes to the measurements. If the member is too shallow, relative to the electrode spacing, there are boundary effects and the Wenner relationship is not a good approximation. Based on their studies, Millard et al. (1990) recommend an electrode spacing of 2 in. (50 mm) as sufficient for typical concrete mixtures with a width and depth at least four times the electrode spacing. In addition, the edge distance should not be less than twice the electrode spacing. When these minimum dimensions are not satisfied, the apparent resistivity calculated by Eq. (3.5.3.1) will exceed the true resistivity.

Other factors that affect the measured resistivity are the presence of a thin surface layer of resistivity different than the bulk resistivity and the presence of reinforcing bars. Both of these conditions will result in an apparent resistivity that is lower than the true value. The effect of reinforcing bars is related strongly to the depth of cover and less so to the bar diameter. If possible, resistivity measurements should be conducted midway between two bars. When depth of cover is low and bar spacing is small, it may be possible to apply a correction factor when the diameter and location of the reinforcement is known (Millard et al. 1990).

3.5.3.3 *Two-electrode method*—Another technique for measuring resistivity is incorporated into devices used for corrosion rate measurements, which are described in 3.5.4 (Broomfield 1996; Tang 2002). In this case, the resistance of the concrete is measured between the reinforcing bar and the point on the surface where the probe is located. To determine resistivity from the measured resistance, the depth of the bar is needed. Published comparisons of concrete resistivities measured in-place by the four-electrode device and the two-electrode method are unavailable.

3.5.3.4 *Relationship to corrosion rate*—As mentioned previously, concrete resistivity affects corrosion rate by affecting the flow of ions through the concrete. Table 3.5.3.4 summarizes published relationships between concrete resistivity. Note the lack of consistency between the resistivity and corrosion rate values and the qualitative descriptors of likely corrosion rate, a discrepancy that could be attributed to the varying systems that have been used to measure resistivity. Feliú et al. (1996) used the single-probe system whereas Bungey et al. (2006) used the four-electrode system. There is, however, a direct relationship between corrosion rate and concrete resistivity when the steel has lost its passivity and is actively corroding.

Figure 3.5.3.4 shows the results of hundreds of field measurements of concrete resistivity and corrosion current measured using the linear polarization method described in the following section. Feliú et al. (1996) suggested that a corrosion of current density of less than 0.1 μA/cm^2 corresponds to negligible corrosion risk. As shown in Fig. 3.5.3.4, if the concrete resistivity is above 100 kΩ·cm, there is a 90 percent likelihood that the corrosion rate is negligible, and if the resistivity is less than 10 kΩ·cm, the likelihood of significant corrosion activity is almost certain. The resistivity values in Fig. 3.5.3.4 are based on using the single-probe system to measure resistivity.

3.5.3.5 *Relationship to chloride ion penetrability*—The inverse of electrical resistivity is electrical conductivity, a property that has a fundamental relationship to diffusivity (refer to 3.6). Note that if resistivity is given in units of ohm·meter, conductivity is in units of siemens/meter (S/m). For a saturated porous material, such as hardened concrete, the diffusion coefficient of a particular ion can be related to electrical conductivity through the Nernst-Einstein equation

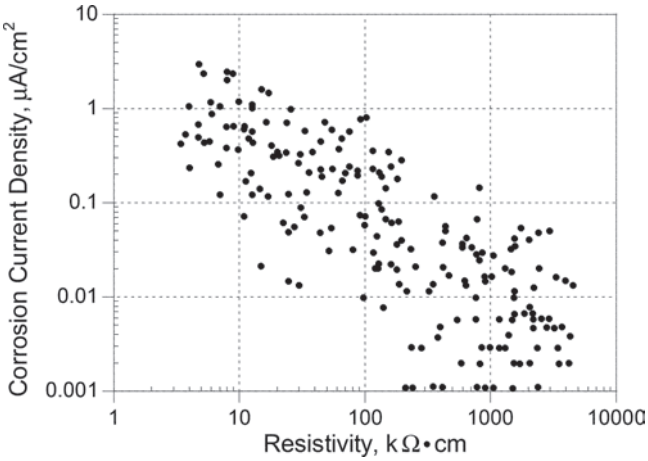

Fig. 3.5.3.4—Relationship between corrosion current density and concrete resistivity from field measurements (adapted from Feliú et al. [1996]).

as follows (Garboczi 1990; Snyder et al. 2000; Nokken and Hooton 2006)

$$\frac{\sigma}{\sigma_p} = \frac{D}{D_p} \qquad (3.5.3.5)$$

where σ is the bulk electrical conductivity of the saturated porous material; σ_p is the conductivity of the pore fluid; D is the bulk diffusion coefficient of the ions through the porous material; and D_p is the diffusion coefficient of the ions through the pore fluid.

Studies were conducted in the 1990s and 2000s on evaluating the measurement of resistivity on laboratory specimens as an alternative to more time-consuming methods of measuring resistance to chloride ion penetration (Berke and Hicks 1992; Liu and Beaudoin 2000; Snyder et al. 2000). Morris et al. (1996) evaluated the use of the four-electrode array on cylindrical concrete specimens and made recommendations for electrode spacing and testing location. In these tests, the array is centered longitudinally along the side of the cylinder. Because of the cylinder geometry, Eq. (3.5.3.1) should be modified by an adjustment factor that depends on the electrode spacing and size of the cylinder (Morris et al. 1996). The Florida Department of Transportation (FDOT) performed research using this array configuration and developed a procedure for testing that is given in Florida Sampling and Test Method (FSTM) 5-578 (FDOT 2004). According to FSTM 5-578, a 4 x 8 in. (100 x 200 mm) cylinder is used with an electrode spacing of 1.5 in. (38 mm) to avoid edge effects. This spacing is slightly lower than that recommended by Millard et al. (1990) for resistivity measurements on concrete structures. The specimens are to be cured in a moist room in accordance with ASTM C192/C192M. According to FSTM 5-578, the single-operator coefficient of variation for measured electrical resistivity is 8.2 percent.

Kessler et al. (2005) performed comparative studies of surface resistivity measurements and rapid chloride penetrability (RCP) measurements in accordance with ASTM C1202/AASHTO T277. Figure 3.5.3.5a shows the results of many such measurements. In Fig. 3.5.3.5a(a), surface resistivity is plotted as a function of charge passed. In Fig. 3.5.3.5b(b), the inverse of surface resistivity, or surface conductivity in mS/m, is plotted versus the charge passed. Except for several cases of high conductivity, which likely have questionably high RCP values due to specimen heating during testing (Berke and Hicks 1992), there is an obvious linear relationship between surface conductivity and charge passed. This is to be expected because the RCP test is actually a conductivity test. Berke and Hicks (1992) obtained similar results to those of Kessler et al. (2005).

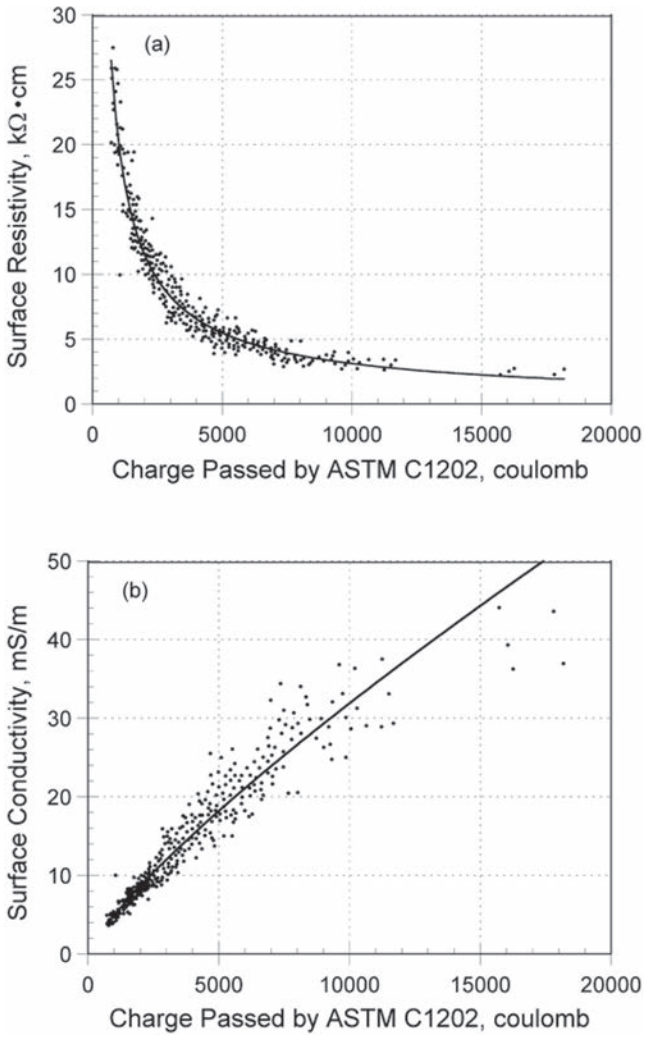

Fig. 3.5.3.5a—(a) Relationship between concrete surface resistivity by FSTM 5-578 and charge passed according to ASTM C1202; (b) same data presented as conductivity versus charge passed (adapted from Kessler et al. [2005]).

As a result of the testing by Kessler et al. (2005), FSTM 5-578 (FDOT 2004) contains a table similar to Table 3.5.3.5 that provides equivalent surface resistivity values for the different classes of chloride penetrability defined in ASTM C1202/AASHTO T277.

Kessler et al. (2008) and Berke and Hicks (1992) performed studies comparing concrete resistivity measure-

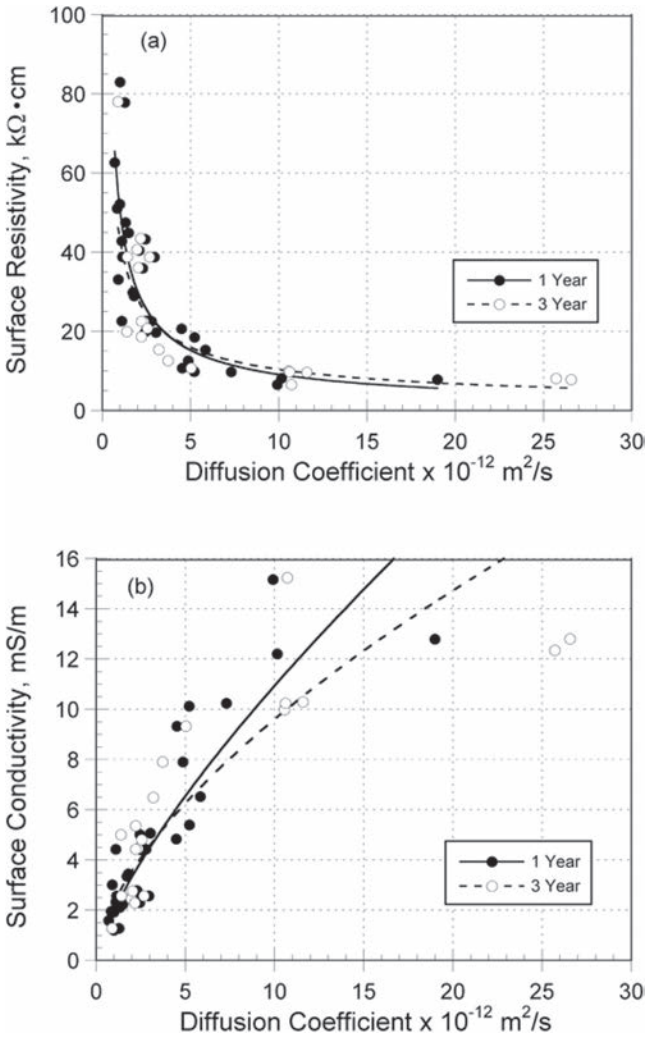

Fig. 3.5.3.5b—(a) Relationship between concrete surface resistivity at 91 days by FSTM 5-578 and apparent chloride diffusion coefficient at 1 and 3 years; and (b) same data presented as conductivity versus diffusion coefficient (adapted from Kessler et al. [2008]).

ments at 91 days with chloride bulk diffusion measurements at 1 and 3 years. Figure 3.5.3.5b(a) compares surface resistivity measured at 91 days with the apparent chloride diffusion coefficients measured in accordance with NordTest Build 443 (1995), which is similar to ASTM C1556. Figure 3.5.3.5b(b) shows the same data, except the vertical axis is conductivity. As was the case with the RCP test, except for a few outliers, there are linear relationships between conductivity and apparent diffusion coefficient. These studies indicate that electrical resistivity, or its inverse electrical conductivity, provides a good indicator of concrete's resistance to chloride penetration. Note, however, that electrical measurements should be performed on saturated specimens to obtain resistivities or conductivities that are indicative of the pore structure in concrete.

3.5.3.6 *Summary*—Measurement of concrete resistivity provides additional information for assessing the likelihood of different levels of corrosion activity, a useful supplement to a half-cell potential survey. A high resistivity indicates

Table 3.5.3.5—Relationships between concrete resistivity and chloride ion penetration (Adapted from FSTM 5-578 [FDOT 2004])

Chloride ion penetrability	Charge passed per ASTM C1202/AASHTO T277, coulombs	Surface resistivity* at 28 days per FSTM 5-578, kΩ·cm
High	> 4000	< 12
Moderate	2000 to 4000	12 to 21
Low	1000 to 2000	21 to 37
Very Low	100 to 1000	37 to 254
Negligible	< 100	> 254

*Using 4 x 8 in. (100 x 200 mm) cylinders.

that even though the steel is actively corroding as determined from the potential survey, the corrosion rate may be low. As mentioned, the resistivity of concrete is related to the ease with which ions can migrate through the concrete under the action of the potential field surrounding anodes and cathodes. Resistivity increases as the capillary pore space in the paste is reduced. This explains why high-quality concrete is crucial for long service life under corrosion-inducing conditions. In the laboratory, resistivity testing can be used as an alternative to other time-consuming tests to evaluate relative resistance of concrete to chloride penetration. Table 3.5.1.2.1 summarizes the advantages and limitations of concrete resistivity measurement.

3.5.4 *Linear-polarization method*—Several techniques to measure the rate of corrosion have been investigated (Rodríguez et al. 1994). The linear-polarization method is used most frequently (Flis et al. 1992) and prestandards have been proposed (Cady and Gannon 1992; Andrade and Alonso 2004). Testing and interpretation of test results should be conducted by experienced personnel.

3.5.4.1 *Principle*—In the field of corrosion science, the term "polarization" refers to a change in the open-circuit potential in response to the passage of current (ASTM G15). In the polarization resistance test, the current used to cause a small change in the value of the half-cell potential of the corroding bar is measured. For a small perturbation about the open-circuit potential, a linear relationship exists between the change in voltage, ΔE, and the change in current per unit surface area of bar surface that is polarized, Δi. This ratio is called the polarization resistance, R_p

$$R_p = \frac{\Delta E}{\Delta i} \qquad (3.5.4.1a)$$

Because the corrosion current density i is used, the units of R_p are resistance times area, such as $\Omega \cdot cm^2$. The quantity R_p is not a resistance in the usual sense of the term (Stern and Roth 1957), although the term is widely used (ASTM G15). The underlying relationships between the corrosion rate of the bar and polarization resistance were established by Stern and Geary (1957), with no attempt made to explain these relationships. Simply stated, the corrosion rate is related directly to the corrosion current density of the bar (corrosion current per unit surface area of bar), and is determined by

$$i_{corr} = \frac{B}{R_p} \qquad (3.5.4.1b)$$

where i_{corr} is the corrosion current density, in ampere/cm^2; B is a constant, in volt; and R_p is the polarization resistance, in ohm·cm^2.

The constant B is a characteristic of the corrosion system and a value of 0.026 V is commonly used for corrosion of steel in concrete (Feliú et al. 1989). This value, however, is appropriate for actively corroding bars and a value of 0.050 V is more accurate under less active conditions (Broomfield 1996; Feliú et al. 1996). There is an inherent uncertainty of a factor of 2 in corrosion rate measurements based on Eq. (3.5.4.1b), when a fixed value of B is used.

It is possible to convert the corrosion rate into the section loss of the steel bar per unit of time. Based on Faraday's second law of electrolysis, a corrosion current density of 1 μA/cm^2 corresponds to a loss of approximately 0.0005 in./year (0.012 mm/year) of steel (Andrade and Alonso 2004). Although this assumes that corrosion occurs uniformly over the bar, pitting rates can be up to 10 times greater than the uniform rate (Andrade and Alonso 2004).

3.5.4.2 *Instrumentation*—The basic apparatus for measuring the polarization resistance is the three-electrode system shown in Fig. 3.5.4.2a (Escalante 1989; Clear 1989), which is often called a 3LP device. One electrode is composed of a reference half-cell, and the reinforcement is a second electrode called the working electrode. The third electrode, which is called the counter electrode, supplies the polarization current to the bar. Supplementary instrumentation measures the voltages and currents during different stages of the test. Such a device can be operated in the potentiostatic mode, where the current is varied to maintain constant potential of the working electrode or it can be operated in the galvanostatic mode, where the potential is varied to maintain constant current from the counter electrode to the working electrode.

In simple terms, the procedure for using the 3LP device in the potentiostatic mode is as follows (Cady and Gannon 1992):

a) Locate the reinforcing steel grid with a covermeter and mark it on the concrete surface.

b) Record the cover depth and bar diameters in area of interest.

c) Make an electrical connection to the reinforcement (the working electrode).

d) Locate the bar whose corrosion rate is to be measured, wet the surface, and locate the counter electrode over the center of the bar.

e) Measure the corrosion potential of the reinforcement relative to the reference electrode, that is, measure the open circuit half-cell potential (Fig. 3.5.4.2a(a)).

f) Measure the current from the counter electrode to the working electrode that is necessary to produce a –4 mV change in the potential of the working electrode (Fig. 3.5.4.2a(b)).

g) Repeat the previous step for different values of potential, namely, –8 and –12 mV beyond the corrosion potential.

h) Determine the area of bar affected by the measurement by taking the circumference of bar and multiplying by the length below the counter electrode.

i) Plot the potential versus the current per unit area of the bar and determine the slope of the best-fit straight line. This is the polarization resistance (refer to Eq. (3.5.4.1a)).

A major uncertainty in obtaining the polarization resistance is the area of the steel bar that is affected by the current from the counter electrode to the bar. In the application of the 3LP device, it is assumed that current follows straight line paths perpendicular to the bar (working electrode) and the counter electrode. Thus, the bar area affected during the tests is the bar circumference multiplied by the length of the bar below the counter electrode. Numerical simulations, however, show that the assumption is incorrect and the current lines are not confined to the region directly below the counter electrode (Feliú et al. 1989; Flis et al. 1992). To better control the current path from the counter electrode to the bar, a device has been developed that includes a fourth electrode, a guard or auxiliary electrode, that surrounds the counter electrode (Feliú et al. 1990a,b). Figure 3.5.4.2b is a schematic of this type of corrosion meter. The guard electrode is maintained at the same potential as the counter electrode and, as a result, the current to the working electrode is confined to the region below the counter electrode.

Commercial devices using the guard electrode method while operating in a galvanostatic mode apply a constant current for a period of time and measure the resulting voltage. The voltage change and applied current are used to determine the polarization resistance. The duration of current application required to obtain a valid measurement may vary from 30 to 100 seconds depending on whether there is active or less active corrosion, respectively (Andrade and Alonso 2004). Typically, the current is applied for 100 seconds and it takes from 3 to 5 minutes to complete a measurement at each test point (Tang 2002).

Another approach is to determine polarization resistance from measuring the response during the application of a short duration current pulse. This is called the galvanostatic pulse method (Frølund et al. 2002). Instrumentation is similar to that shown in Fig. 3.5.4.2b, except the voltage response to the applied current is measured over a short period of time, such as 10 seconds. The polarization resistance is obtained from the assumption that the polarization of the bar can be modeled by a simple electrical circuit, known as Randles circuit, as shown in Fig. 3.5.4.2c(a) (Andrade and Alonso 2004). When current is applied to this circuit, the voltage-time history across the circuit is described by

$$\Delta E = I_p \left[R + R_p \left(1 - e^{\frac{-t}{R_p C}} \right) \right] \qquad (3.5.4.2)$$

where ΔE is the voltage change, in volt; I_p is the applied polarization current, in ampere; R is the electrical resistance of concrete between counter electrode and bar, in ohm; R_p is

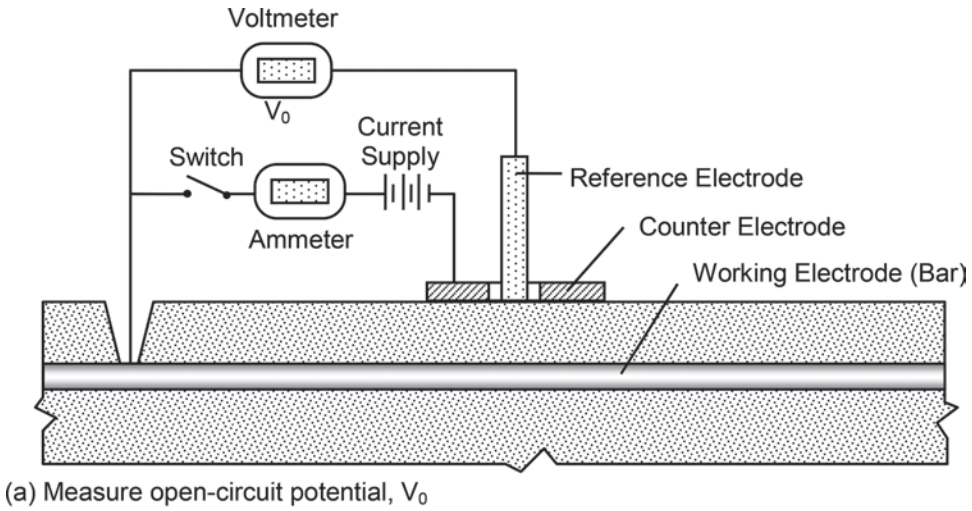

Fig. 3.5.4.2a—Three-electrode, linear-polarization method to measure corrosion current: (a) measurement of open-circuit potential; and (b) measurement of current to produce small change in potential of working electrode (bar).

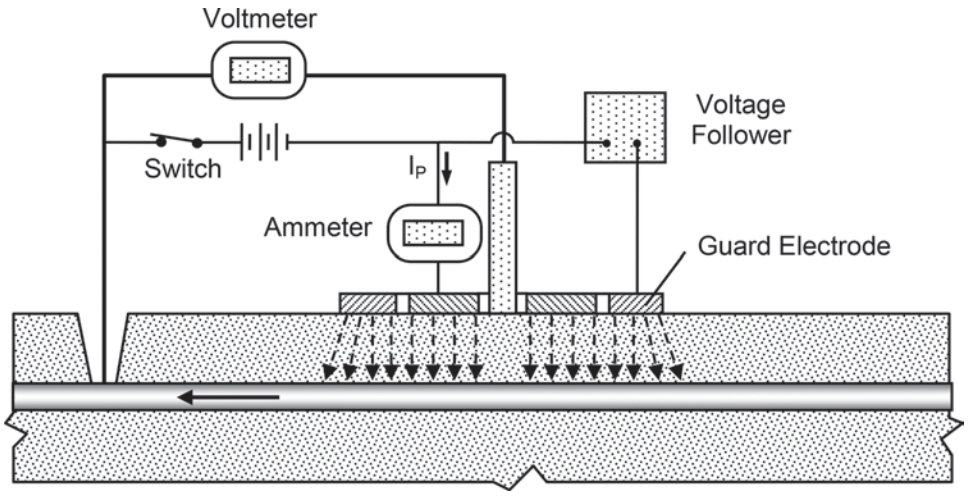

Fig. 3.5.4.2b—Linear-polarization technique using guard electrode to confine flow from counter electrode to reinforcement (adapted from Feliú et al. [1990a]).

the polarization resistance, in ohm; and C is the capacitance of double layer and concrete-bar interface, in farad.

Figure 3.5.4.2c(b) shows an example of a measured voltage history for an applied current pulse (Frølund et al. 2002). By means of regression analysis, Eq. (3.5.4.2) is fitted to the measured voltage-time data and the best-fit values of the three components of the equivalent Randles circuit are obtained. Thus, the polarization resistance is determined. After multiplying by the polarized area of the bar, Eq. (3.5.4.1a) is used to determine the corrosion rate.

The pulse technique has the advantage of reducing the measurement time; however, the value of the calculated polarization resistance increases as the pulse duration and duration of data acquisition increases (Tang 2002). This means that corrosion rate will be overestimated for short pulses. Because it has also been found that there is a well-defined relationship between polarization duration and polarization resistance, procedures have been developed for converting measurements made at short durations to measurements made at a longer duration (Tang 2002).

A comparative study was conducted in the early 1990s using the laboratory and field tests of three commercially available corrosion-rate devices (Flis et al. 1992). Field test sites were chosen in three different environments representing the range of conditions that might be encountered in practice. Measurements were made on bridge structures at identical locations using all three devices. One device was of the 3LP type (Clear 1989) while the other two used guard electrodes. The 3LP device gave higher values of corrosion current at the same test sites. The device, which was developed in Spain (Feliú et al. 1990a), gave corrosion rates closest to the true corrosion currents. Each device was, however, capable of distinguishing between passive and active sites, and there were well-defined relationships between the corrosion currents measured by the different devices. It was concluded that all three devices could be used to locate active corrosion in a structure.

Another study (Tang 2002) compared the average corrosion rates measured over a period of 1 year with actual mass loss measurements by destructive examination. The study involved three organizations and four devices:

a) Two similar devices based on galvanostatic measurements with a guard electrode (GS-1 and GS-2)

b) A device based on the galvanostatic pulse method with circular electrodes (GP-1)

c) A device based on the galvanostatic pulse method with rectangular electrodes (GP-2)

Results of the comparative measurements are shown in Fig. 3.5.4.2d. The measured mass losses were converted to a uniform loss of bar radius, and then converted to an equivalent current density using Faraday's law. For the pulse device GP-2 (rectangular electrodes), a measurement time of 5 seconds was used, but the measurements were extrapolated to a measurement time of 100 seconds, which is the duration used with the galvanostatic devices. The results show that the corrosion rates based on the pulse devices tend to overestimate the actual values. For the pulse device GP-2, the use of a correction factor to convert to a 100-second measurement time improved the agreement with corrosion rates based on mass loss.

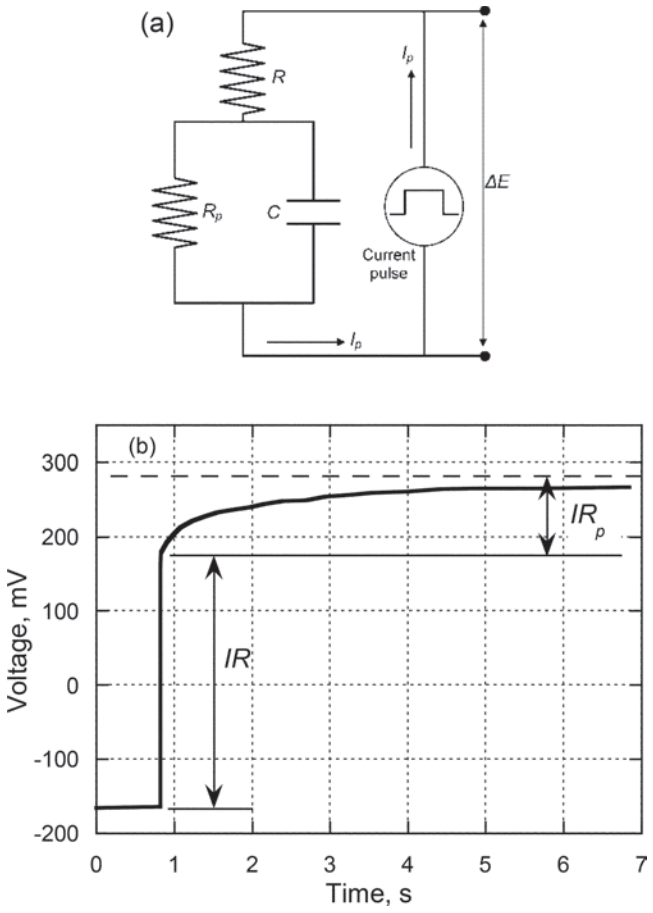

Fig. 3.5.4.2c—(a) Randles circuit model of the polarization of steel bar in concrete; and (b) voltage-time curve for polarization resistance measurement using galvanostatic-pulse technique (Andrade and Alonso 2004; Frølund et al. 2002).

3.5.4.3 *Limitation*—Advantages and limitations of the linear-polarization method are summarized in Table 3.5.1.2.1. The corrosion rate at a particular point in a structure is expected to depend on several factors, such as moisture content of the concrete, availability of oxygen, and temperature. The corrosion rate at any point in an exposed structure would be expected to have seasonal variations. Such variations were observed during multiple measurements that extended over a period of more than 1 year (Clemeña et al. 1992b). To project the amount of corrosion that would occur after an extended period, it is necessary to repeat the corrosion-rate measurements at different times of the year. As suggested by Clemeña et al. (1992b), alternatives to predict the future condition of the reinforcement include using the maximum measured corrosion rates to obtain a conservative estimate of remaining life; yearly average corrosion rate at a typical or worst location in the structure; or minimum and maximum corrosion rates to estimate the range of remaining life.

Because there are no standard procedures for interpreting corrosion-rate measurements obtained with different devices at this time, a qualified corrosion specialist should be

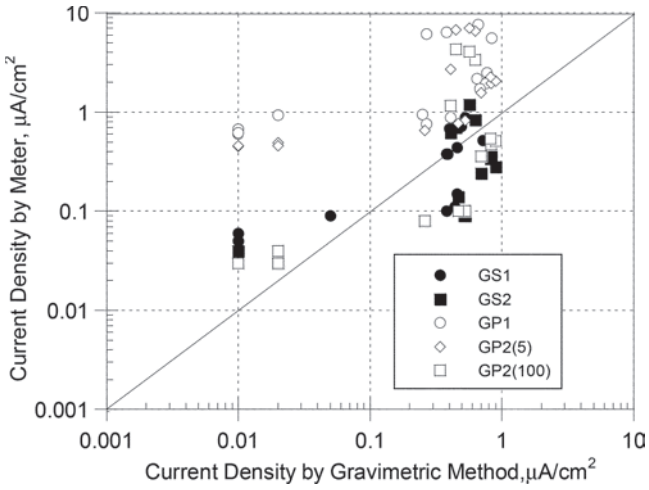

Fig. 3.5.4.2d—Comparison of average corrosion current density after 1 year based on gravimetric mass loss and current measurements by different instruments (Tang 2002).

consulted. For example, based on years of experience from laboratory and field testing, Clear (1989) developed guidelines for interpreting corrosion-rate measurements using a specific 3LP device. Note that the guidelines were given in mA/ft^2. These have been converted to μA/cm^2 by using the approximate conversion 1 mA/ft^2 ≈ 1 μA/cm^2, the metric units commonly used in the corrosion literature:

a) If i_{corr} is less than 0.2 μA/cm^2, no corrosion damage is expected

b) If i_{corr} is between 0.2 and 1.0 μA/cm^2, corrosion damage is possible within 10 to 15 years

c) If i_{corr} is between 1.0 and 10.0 μA/cm^2, corrosion damage is expected within 2 to 10 years

These guidelines assume that the corrosion rate is constant with time.

Andrade and Alonso (2004) have proposed the levels shown in Table 3.5.4.3 for interpreting corrosion rate measurements. These values are based on the assumption of uniform surface corrosion. Due to concentrated pitting corrosion, pit depth can be up to 10 times the uniform rates calculated using Eq. (3.5.4.1b) (Andrade and Alonso 2004).

Other limitations should be considered when planning corrosion-rate testing. Some of these have been outlined in a proposed test method (Cady and Gannon 1992) and are:

a) The concrete surface has to be smooth (not cracked, scarred, or uneven)

b) The concrete surface has to be free of water impermeable coatings or overlays

c) The cover depth has to be less than 4 in. (100 mm)

d) The reinforcing steel cannot be epoxy-coated or galvanized

e) The steel to be monitored has to be in direct contact with the concrete

f) The reinforcement is not cathodically protected

g) The reinforced concrete is not near areas of stray electric currents or strong magnetic fields

h) The ambient temperature is between 41 and 104°F (5 and 40°C)

Table 3.5.4.3—Levels of corrosion activity from corrosion rate measurements (Andrade and Alonso 2004)

Current density, μA/cm^2	Thickness loss, mm/y*	Corrosion level
< 0.1	< 0.001	Negligible
0.1 to 0.5	0.001 to 0.005	Low
0.5 to 1	0.005 to 0.01	Moderate
> 1	> 0.01	High

*0.01 mm/y ≈ 0.0004 in./y.

i) The concrete surface at the test location should be free of visible moisture

j) Test locations should not be closer than 12 in. (300 mm) to discontinuities, such as edges and joints

3.5.5 *Magnetic-flux leakage method*—The magnetic-flux leakage method (MFL) has been adapted for use to detect breaks and fractures in steel strands in tendons of prestressed and post-tensioned concrete elements (Ghorbanpoor et al. 2000). A local magnetic field is applied to the member and fractures in the steel bars disrupt the magnetic lines of the induced flux in the bars. This disruption can be detected by a magnetometer at the surface of the concrete element. The method has the advantage of having contactless application through concrete and ducts, allowing relatively rapid noninvasive inspection. The method, which is used widely for inspecting steel pipelines, is able to detect embedded wire or bar breaks in concrete (Ghorbanpoor et al. 2000). A similar technique is called the remanent-magnetism method (RM), in which flux leakage is measured after the applied magnetic field is removed (Scheel and Hillemeier 2003). As discussed in the following section, magnetic flux remains in a ferrous material after the applied magnetic field is removed.

3.5.5.1 *Principle*—Magnetic fields penetrate into all materials. The effect of a magnetic field on a material depends on the material's magnetic permeability μ. Materials with high values of permeability tend to develop high levels of magnetic induction B for a given magnitude of applied magnetic field H. For low values of applied field, the relationship is

$$B = \mu H \qquad (3.5.5.1)$$

where B is the magnetic induction, in tesla; μ is the magnetic permeability, in henry/meter; and H is the magnetic field strength, in ampere/meter.

The magnitude of B, which is known as the magnetic-flux density (MFD), represents the number of magnetic lines per unit cross-sectional area that are set up within the material. The concept is similar to what was discussed in 3.5.1 for magnetic reluctance covermeters. Ferromagnetic materials, such as iron and steel, have high values of magnetic permeability, whereas paramagnetic and diamagnetic materials, such as aluminum and copper, respectively, have low values of μ, which can be assumed to be the same as that for a free space or μ_0. Thus, high levels of MFD can be induced in a steel bar if it is exposed to a magnetic field; the flux is aligned with the direction of the applied magnetic field.

As the amplitude of the magnetic field applied to a ferromagnetic material increases, the response departs from linear behavior as given by Eq. (3.5.5.1) and eventually the material becomes magnetically saturated. This behavior is illustrated in Fig. 3.5.5.1a; as the applied field is increased, the MFD levels off, and when the applied field is removed, a remanent flux remains (remanence). This principle is used to create magnetized tools, such as screwdrivers, by exposure to a magnetic field.

If a solid steel bar is exposed to a magnetic field, magnetic flux is induced in the bar between the poles of the magnet along lines that coincide with the inducing magnetic field, as shown in the left side of Fig. 3.5.5.1b. The presence of a crack in the bar disrupts the magnetic flux, extending magnetic lines beyond the material boundary, as shown in the right side of Fig. 3.5.5.1b. This behavior is called magnetic-flux leakage. If a magnetometer is scanned across the surface of the bar, it will respond to the flux leakage with a characteristic up-down pattern as shown in Fig. 3.5.5.1b.

3.5.5.2 *Data analysis*—To apply the MFL method, the steel in the concrete is saturated magnetically by an externally applied magnetic field, usually generated by an electromagnet. Using a magnetometer, the component of the flux density perpendicular to the longitudinal axis of the bar is monitored along the length of the bar. Fractures in the steel give rise to a characteristic shape of the measured leakage flux signal because the sensed flux leakage is directed toward and away from the sensor as the scanner is moved along the surface. The location of the fracture along the length of the steel tendon is identified by the midpoint between the positive and negative peaks. The peak-to-peak amplitude of the signal is affected by several factors as discussed in the following.

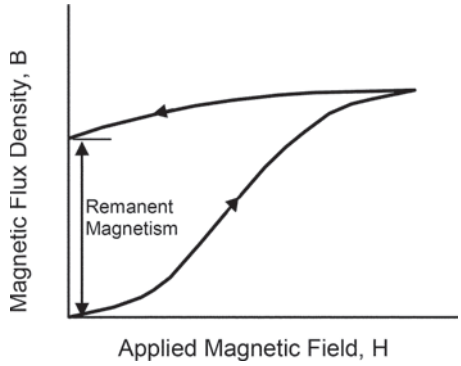

Fig. 3.5.5.1a—Relationship between applied magnetic field and flux density for a ferromagnetic material.

3.5.5.3 *Limitations*—Whereas the principle of MFL is straightforward, there are several factors that complicate signal analysis and interpretation of test results (Scheel and Hillemeier 2003):

a) The peak-to-peak leakage flux amplitude can be affected by many factors: cover depth to steel, number of strand fractures, the width of fractures, the type of steel, and the amount of stress in the steel.

b) The method, which is less sensitive to deeper tendons, may not be able to detect individual single-strand fractures in a multi-strand tendon.

c) Noise from nearby mild steel reinforcing bars or other ferromagnetic elements may disrupt the interpretation.

d) It is sensitive to surface condition in external post-tensioning tendons (Im et al. 2010).

Application of the MFL method to reinforced concrete is relatively new. Successful demonstrations have been reported; however, the method has not been widely applied and accepted in the civil engineering community. A high level of expertise is needed to interpret test results. The method does not yet have a standard procedure for application to concrete structures.

3.5.6 *Advantages and limitations*—Table 3.5.1.2.1 summarizes the advantages and limitations of the magnetic and electrical methods that can be used to gain information about the location and condition of steel reinforcement in concrete members. Covermeters are effective in locating bars, but there are difficulties when the steel is congested or the concrete cover is thick. Half-cell potential (ASTM C876) provides an indication of the likelihood of active corrosion, but data interpretation is not simple. Concrete resistivity affects the rate of corrosion when passivity is lost due to carbonation or high levels of chloride ions. Resistivity of saturated concrete specimens can be used as an indicator of resistance to chloride ion penetration. Although the linear-polarization methods provide information about corrosion

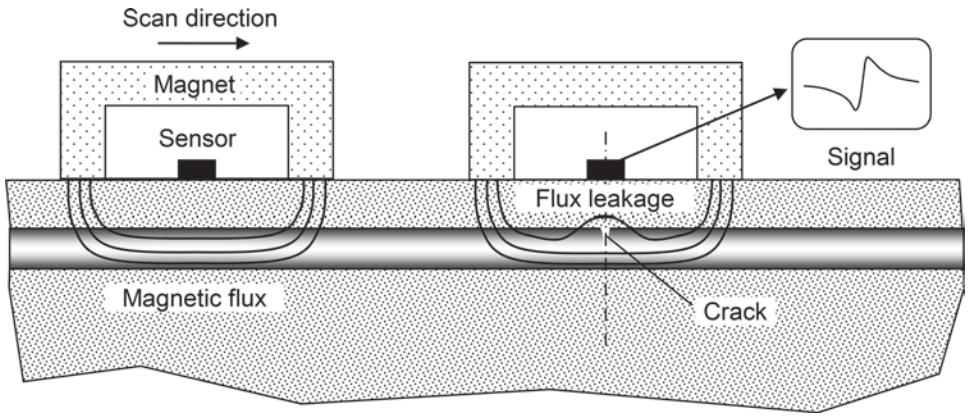

Fig. 3.5.5.1b—Schematic of MFL method; when sensor is scanned over fracture in bar, it responds to the flux leakage.

rate at the time of testing, data interpretation is complicated. The magnetic-flux leakage method may be able to locate fracture of prestressing steel (Scheel and Hillemeier 2003).

3.6—Methods for measuring transport properties

3.6.1 *Introduction*—Many of the degradation mechanisms in concrete involve the ingress of aggressive materials such as sulfates, carbon dioxide, and chloride ions. In most cases, water is also required to sustain the degradation mechanisms. As a result, concrete that has a surface zone highly resistant to the ingress of water will generally be durable.

The ability of concrete to withstand environmental deterioration depends on the materials that were used to make the concrete, the mixture proportions, type of formwork, the degree of consolidation, the curing conditions, and treatments applied on the hardened concrete. The quality of the surface zone is acknowledged increasingly as the major factor affecting the rate of degradation of a concrete structure (Kropp and Hilsdorf 1995). To assess the potential durability of in-place concrete, one needs to assess the ability of the surface zone to restrict the passage of external agents that may lead to direct deterioration of the concrete or to depassivation and corrosion of embedded reinforcement. The surface zone tests described in this section provide useful information for evaluation of the potential durability of concrete. Section 3.5 discusses the use of electrical conductivity of saturated specimens as an indicator of resistance to the ingress of dissolved ions.

3.6.2 *Ingress mechanisms*—There are three principal mechanisms by which external agents can penetrate into concrete.

3.6.2.1 *Absorption*—This term refers to the ingress of liquids due to capillary forces. Contaminants, such as chloride ions and sulfates, are transported within the liquid. The term "sorptivity" is used to describe the tendency of a material to absorb a fluid. For one-dimensional (1-D) water absorption into an initially dry porous solid, the volume of absorbed fluid can be related to time by the following empirical equation (Hall 1989)

$$V = As\sqrt{t} \qquad (3.6.2.1)$$

where V is the volume of fluid absorbed, m^3 (ft^3); A is the wetted area, m^2 (ft^2); s is the sorptivity, $m/\sqrt{s}$ ($ft/\sqrt{s}$); and t is the time, in seconds.

3.6.2.2 *Permeation*—This term refers to the flow of a fluid under the action of a pressure head. For steady-state, unidirectional flow of a liquid through a saturated porous material, the flow rate is described by Darcy's law, as follows

$$Q = kAI \qquad (3.6.2.2)$$

where Q is the flow rate, m^3/s (ft^3/s); k is the the coefficient of permeability, m/s (ft/s); A is the cross-sectional area of flow, m^2 (ft^2); and I is the hydraulic gradient, m/m (ft/ft).

The coefficient of permeability depends on the structure of the material and the properties of the fluid. In the case of concrete, the coefficient of permeability depends primarily on the mixture proportions; the water-cement ratio (w/c); the size of coarse aggregate; and the maturity, which is the extent of hydration and pozzolanic reaction, if applicable. If the fluid is a gas, an equation analogous to Eq. (3.6.2.2) can be used to describe the unidirectional flow rate in terms of the differential pressure.

3.6.2.3 *Diffusion*—This term refers to the movement of molecular or ionic substances from regions of higher concentration to regions of lower concentration of the substances. The rate of movement of the substance is proportional to the concentration gradient along the direction of movement and the diffusion coefficient, and is given mathematically by Fick's first law of diffusion (Kropp and Hilsdorf 1995)

$$F = \frac{\partial m}{\partial t}\frac{1}{A} = -D\frac{\partial C}{\partial t} \qquad (3.6.2.3)$$

where F is the mass flux, lb/ft^2s (kg/m^2s); m is the mass of flowing substance, lb (kg); t is the time, in seconds; A is the area, ft^2 (m^2); D is the diffusion coefficient, ft^2/s (m^2/s); C is the concentration, lb/ft^3 (kg/m^3); and x is the distance, ft (m).

3.6.3 *Methods of measuring transport properties*—Various test methods have been devised for assessing the durability potential of a concrete surface. Most of the techniques attempt to model one of the aforementioned transport mechanisms, which can be grouped into the following four categories:

1. Water absorption
2. Water permeation
3. Air permeation
4. Diffusion

Section 3.6.4 describes the instrumentation and procedures for some of the commonly used or promising new test procedures.

3.6.4 *Description of test methods*

3.6.4.1 *Absorption tests*—Absorption tests measure the rate at which water is absorbed into the concrete under a relatively low pressure head. The absorption rate is a function of the capillary porosity, which is, in turn, dependent on the w/c, type of cementitious material used, and the curing history. Of the tests to be described, two are surface-absorption techniques and the others measure absorption within a hole drilled into the concrete.

3.6.4.1.1 *Initial surface-absorption test (ISAT)*—The rate of absorption of water into concrete per unit area after a stated interval from the start of the test and at a constant head and temperature is defined as initial surface absorption. Therefore, the test that measures this property is designated as the ISAT. In this method (Levitt 1971), a circular cap with a minimum surface area of 7.75 $in.^2$ (5000 mm^2) is sealed to the concrete surface. A reservoir attached to the cap is filled with water so that the water level is 8 in. (200 mm) above the concrete surface. The cap is also connected to a horizontal capillary positioned at the same height as the water in the reservoir (Fig. 3.6.4.1.1). At specified intervals (10 minutes, 30 minutes, 1 hour, and 2 hours) from the start of

Table 3.6.4.1.1—Typical ISAT results on well cured and oven-dried concrete (The Concrete Society 1988)

Relative absorption	ISAT results: mL/m²/s			
	Time after starting test			
	10 minutes	30 minutes	1 hour	2 hour
High	> 0.50	> 0.35	> 0.20	> 0.15
Average	0.25 to 0.50	0.17 to 0.35	0.10 to 0.20	0.07 to 0.15
Low	< 0.25	< 0.17	< 0.10	< 0.07

Table 3.6.4.1.2—Relationship between concrete protective quality and Figg water absorption index (Basheer 1993)

Concrete category	Protective quality	Measured time, s
0	Poor	Less than 20
1	Not very good	20 to 50
2	Fair	50 to 100
3	Good	100 to 500
4	Excellent	More than 500

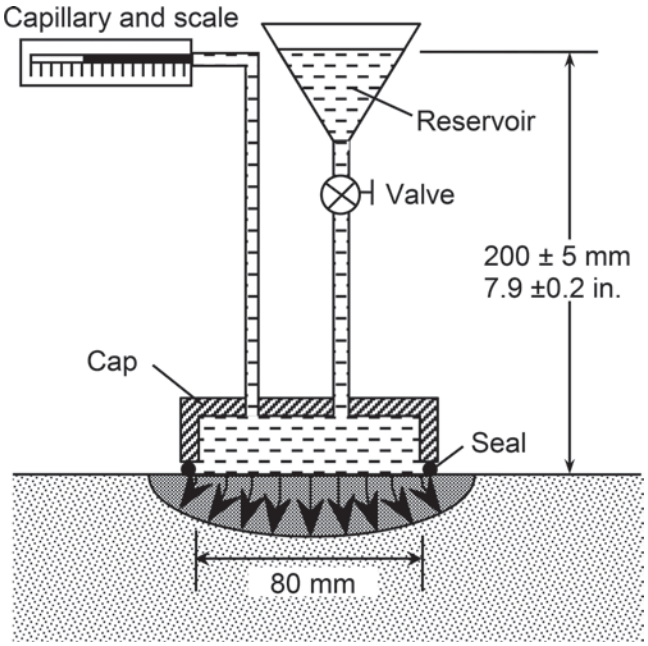

Fig. 3.6.4.1.1—Schematic of ISAT.

the test, the valve below the reservoir is closed and the rate at which water is absorbed into the concrete is measured by the movement of water in the capillary attached to the cap and reported in units of mL/m²/s. This test is standardized in the UK (BS 1881-208). Specimens have to be oven-dried at 221°F (105°C) for the laboratory test and for in-place testing, a drying period of at least 48 hours at ambient temperature and humidity is stipulated. Typical ISAT values for well-cured concrete reported by The Concrete Society (1988) are reproduced in Table 3.6.4.1.1. Equipment for this test is commercially available.

3.6.4.1.2 *Figg water-absorption test*—Figg's original test procedure required a 0.2 in. (5.5 mm) diameter hole to be drilled into the concrete to a depth of 1.2 in. (30 mm). The hole was cleaned, a disk of rigid polymeric foam was pushed into the hole to a depth of 0.8 in. (20 mm) from the surface, and the hole was sealed with silicone rubber (Figg 1973). A hypodermic needle was inserted through the silicone rubber seal and connected to a syringe and capillary via a series of connectors (Fig. 3.6.4.1.2). A water head of 4 in. (100 mm) was applied and the time for the meniscus to travel 2 in. (50 mm) in the horizontal capillary (similar to that used in the ISAT) was recorded. The value obtained was called the absorption index and was measured in seconds. A higher absorption index corresponds to better-quality concrete. Since Figg's initial work, a number of modifications were made to the equipment and procedure to improve the accuracy and repeatability of the results (Cather et al. 1984; Figg 1989). These modifications include a larger hole (1.6 in. [40 mm] deep and 0.8 in. [20 mm] diameter, with a 0.8 in. [20 mm] deep test zone instead of the 0.40 in. [10 mm] deep test zone in Fig. 3.6.4.1.2), an automated measurement of the meniscus travel, and the use of a premolded plug, alleviating the need to wait for the silicone rubber to cure before performing a test. Equipment for this test is commercially available. Table 3.6.4.1.2 gives a tentative classification of the protection afforded by concrete based on the Figg water absorption test (The Concrete Society 1988).

3.6.4.1.3 *Covercrete-absorption test (CAT)*—A deficiency of the ISAT is that the absorption is influenced predominantly by the surface zone. In the Figg test, the absorption is controlled by the concrete deeper than 0.8 in. (20 mm). The CAT tries to overcome these two deficiencies (Dhir et al. 1987) by making an absorption measurement that includes the surface as well as the interior concrete or covercrete. A 0.5 in. (13 mm) diameter hole is drilled to a depth of 2 in. (50 mm), and a gasketted cap is placed over the hole (Fig. 3.6.4.1.3). A tube connected to a reservoir passes through the cap and empties into the hole. The cap contains a second tube connected to a horizontal capillary as in the ISAT and Figg test. The reservoir and capillary are positioned so that a water head of 8 in. (200 mm) is maintained above the center of the hole. The tube to the reservoir is shut off and the movement of the meniscus in the capillary is measured between 10 and 11 minutes after initial contact of the hole with water.

3.6.4.1.4 *Surface sorptivity test*—This test (Basheer et al. 1994, 1995), in which the cumulative inflow of water is measured during the first 15 minutes using a water source that is 2 in. (50 mm) in diameter and at a pressure of 0.28 psi (2 kPa) (approximately 8 in. [200 mm] of water head) (Fig. 3.6.4.1.4). This test pressure is the same as that used in the ISAT. To determine the sorptivity of concrete, the cumulative inflow of water is plotted versus the square root of elapsed time and the slope of the best-fitting line is reported as a sorptivity index in $ft^3/min^{0.5}$ ($m^3/min^{0.5}$). When the rate of water absorption is small, a larger contact area can be used to obtain measurable absorption rates (Basheer et al. 1993); however, the data should be normalized to the 2 in. (50 mm) diameter area. A guard ring arrangement can be used to achieve a one-dimensional (1-D) penetration of water in

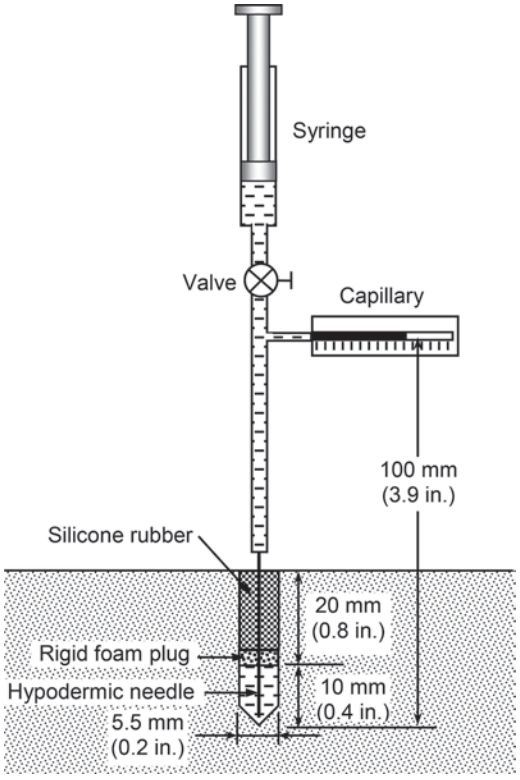

Fig. 3.6.4.1.2—Schematic of original Figg water-absorption test.

the surface sorptivity test and to determine a 1-D sorptivity of concrete (Nolan et al. 1997). The test is sensitive to the internal moisture content of concrete and ambient temperature (Basheer et al. 2001). A modified procedure to measure the sorptivity of surface treated concretes, such as those treated with silanes, is also available (Basheer et al. 1993). For this condition, a bilinear relationship between inflow and square root of time is obtained and it has been demonstrated by Basheer et al. (1993) that the slope of the second part of the graph relates to the protective quality of the surface-treated concretes. The surface sorptivity test apparatus can be attached to the surface by adhesive bonding or clamping to the surface using a rubber seal; the test has great potential for different in-place applications. Table 3.6.4.1.4 provides a tentative classification of concrete quality on the basis of the autoclam sorptivity index (Basheer 1993).

3.6.4.1.5 *Water-permeability tests*—The aforementioned absorption tests involve a low water head. Typically, 8 in. (200 mm) of water is approximately 0.28 psi (2 kPa) above atmospheric pressure and the flow is governed primarily by the sorptivity of the concrete. As a point of reference, atmospheric pressure at sea level is approximately 15 psi (100 kPa).

In-place water-permeability tests have been developed that use higher pressures to obtain indications of the coefficient of permeability of the concrete.

3.6.4.1.6 *Water permeability test*—This method involves measuring the flow of water into the concrete surface under a fixed pressure (Montgomery and Adams 1985). A specially designed cap is either glued to the concrete surface (Fig. 3.6.4.1.4) or clamped to the surface using a rubber ring, providing a watertight seal, and pressurized water is provided by a micro-pump system. A transducer in the chamber measures the water pressure. Before performing the test, the area is saturated by mounting a reservoir of water for at least 24 hours. To carry out the test, the chamber is filled with water and pressurized to 25 psi (172 kPa) above atmospheric pressure. The volume of water entering the concrete at this water pressure is recorded every minute for 15 minutes. The volume of water is plotted versus time, and the slope of the best-fitting line is multiplied by a correction factor to obtain a water permeability coefficient, in ft/s (m/s). This correction factor accounts for the axisymmetric flow in the water permeability test instead of the unidirectional flow required for determining the steady-state water permeability coefficient.

3.6.4.1.7 *Steinert method*—This test method, reported by Steinert (1979), uses the guard ring principle to attain a better approximation of unidirectional flow under pressure (Fig. 3.6.4.1.7). The cap, which is composed of two concentric chambers separated by a circular rubber seal, is glued to the concrete surface. The concentric chambers are filled with water and pressurized to 87 psi (600 kPa) with compressed air. Flow under the inner chamber is approximately unidirectional, so that the record of flow as a function of time is easier to interpret than in the surface water permeability test.

3.6.4.1.8 *Air-permeability tests*—Several tests have been proposed that are based on measurement of the flow of air, or other gases, through concrete. There are relationships between air permeability and other durability indicators, such as water-cementitious materials ratio (*w*/*cm*), strength, and curing efficiency (Whiting 1987). Similar to the water-based tests, air-permeability tests involve either drilling a hole into the concrete surface or the application of a chamber to the surface. In most cases, a vacuum is applied and the decrease of the vacuum with time is taken as an indicator of the air permeability. In general, air-permeability tests are simpler to perform than the water-based tests.

3.6.4.1.9 *Figg air-permeability test*—The original Figg air-permeability test involves the same hole preparation procedure as the water-absorption test described previously (Figg 1973). The tube, however, is connected to a vacuum pump instead of the syringe and a manometer apparatus is used for the water test. The vacuum pump is activated until the pressure inside the hole is decreased to a prescribed value below atmospheric pressure. The valve is closed, and flow of air into the hole reduces the vacuum. The time to obtain a prescribed pressure increase in the hole is measured, and the time in seconds is called the air-permeability index. A higher air-permeability index indicates a less-permeable concrete. In the original Figg test, the prescribed vacuum pressure was –12 psi (–85 kPa) and the prescribed pressure increase was 0.7 psi (5 kPa). In a subsequent modification (Fig. 3.6.4.1.9) intended to improve repeatability, the hole size was increased to 0.4 in. (10 mm) in diameter and 1.6 in. (40 mm) in depth and the prescribed initial vacuum pressure was changed from –12 to –8 psi (–85 to –55 kPa) (Cather et al. 1984). The reduced vacuum was selected to permit the use of hand-operated vacuum pumps. In another modified

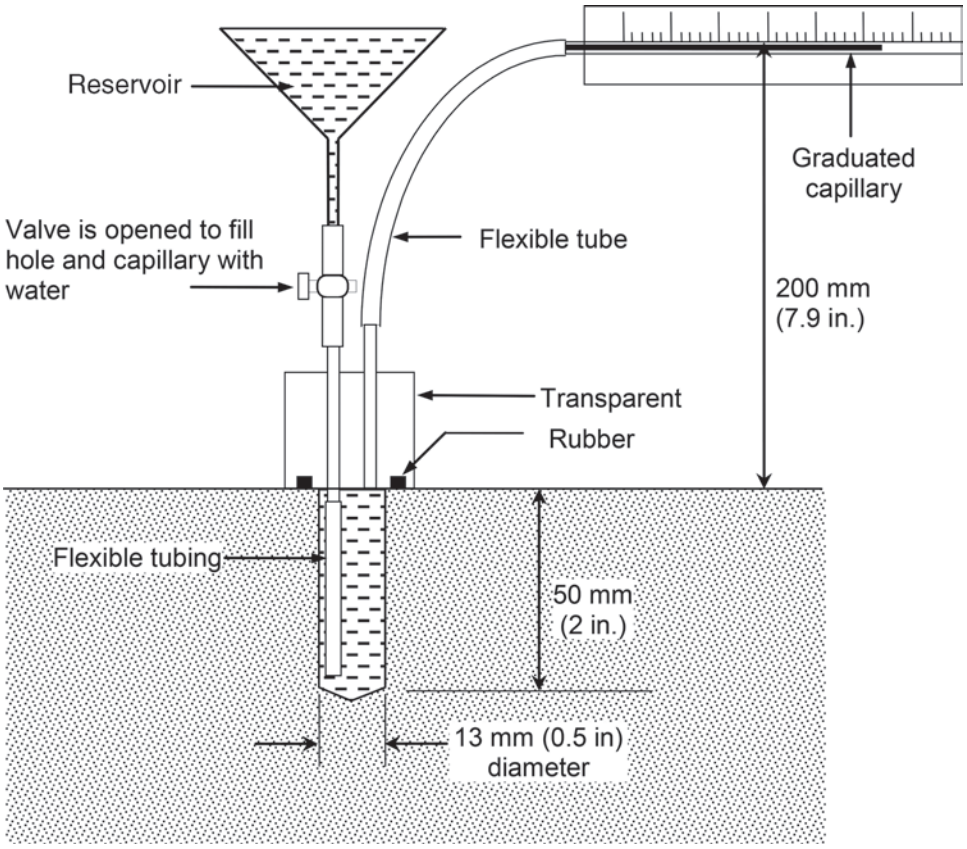

Fig. 3.6.4.1.3—Schematic of covercrete-absorption test (CAT).

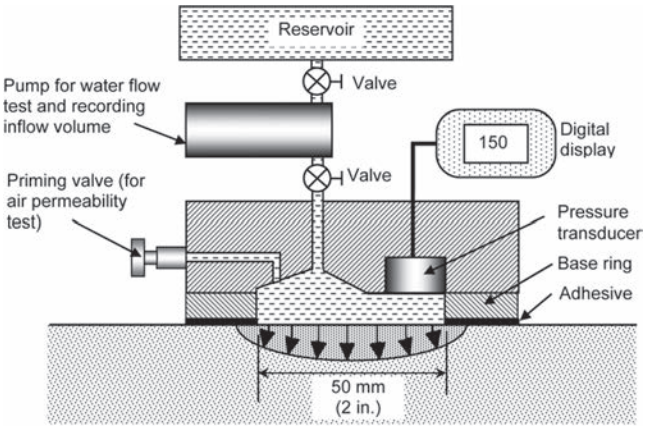

Fig. 3.6.4.1.4—Schematic of surface sorptivity test apparatus.

form of the Figg test (Dhir et al. 1987) intended to improve the repeatability further, the hole diameter was increased to 0.5 in. (13 mm), the depth increased to 2 in. (50 mm), and the prescribed pressure change was taken from –8 to –6.5 psi (–55 to –45 kPa). Table 3.6.4.1.9 presents tentative classification criteria based on Figg air permeability indexes (The Concrete Society 1988).

3.6.4.1.10 *Schönlin test*—The Figg air permeability test gives a measure of the air permeability of the cover zone traversed by the open portion of the hole and requires drilling a hole into the concrete. To avoid having to drill a hole, surface test methods have been proposed. In Schönlin's method (Fig. 3.6.4.1.10), a 2 in. (50 mm) diameter chamber of known volume is placed on the surface, and a vacuum pump is used to evacuate the chamber to a pressure less than –14 psi (–99 kPa) (Schönlin and Hilsdorf 1987). The valve is closed, and the time when the vacuum pressure reaches –14 psi (–95 kPa) is taken as the start of the test. The time required for the vacuum pressure to increase to –10 psi (–70 kPa) is measured. For dense concrete, the vacuum pressure change during 120 seconds is measured instead. Based on these measurements and the known volume of the chamber, a permeability index in units of ft^2/s (m^2/s) is calculated. In an effort to attain a standard moisture condition before testing, the surface is dried with hot air for 5 minutes before testing. A modified form of this test method is available as the Torrent test (Torrent 1992), in which the concept of guard ring is used to achieve a unidirectional inflow of air into the test chamber.

3.6.4.1.11 *Surface airflow test*—The surface airflow (SAF) test is based on a method used within the petroleum

Table 3.6.4.1.4—Protective quality of concrete based on sorptivity index (Basheer 1993)

Protective quality	Sorptivity index, $m^3 \times 10^{-7}/\sqrt{min}$
Very poor	> 3.40
Poor	> 2.60 ≤ 3.40
Good	> 1.30 ≤ 2.60
Very good	≤ 1.30

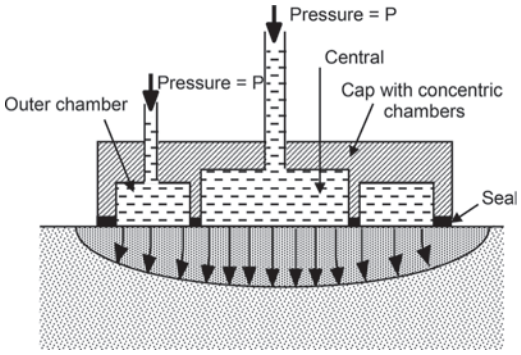

Fig. 3.6.4.1.7—Schematic of Steinert's guard ring method to approximate unidirectional flow.

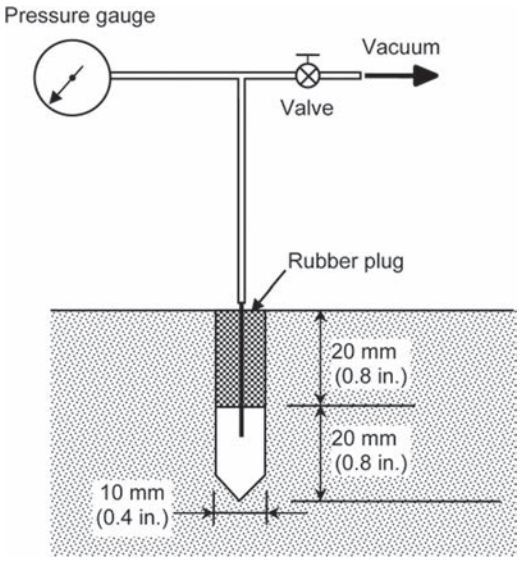

Fig. 3.6.4.1.9—Schematic of modified Figg air-permeability test.

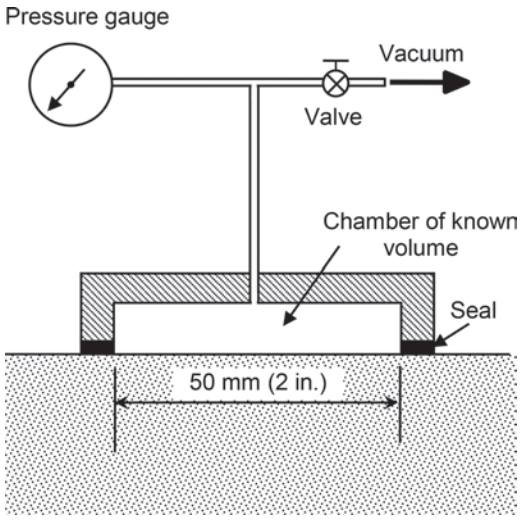

Fig. 3.6.4.1.10—Schematic of Schönlin's surface air-permeability test.

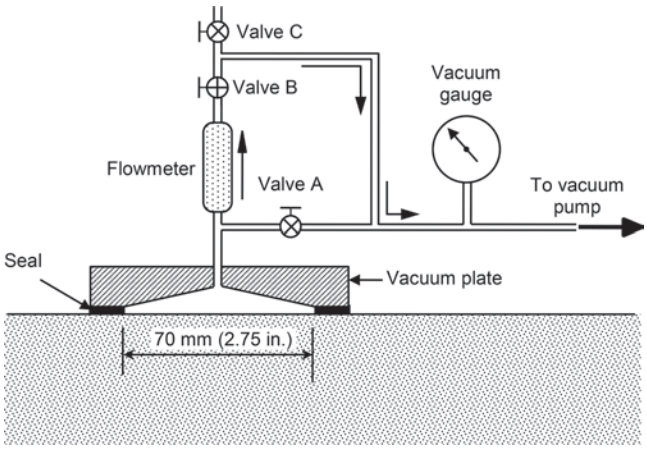

Fig. 3.6.4.1.11—Schematic of SAF test.

Table 3.6.4.1.9—Relationship between concrete protective quality and Figg air permeability index (Basheer 1993)

Concrete category	Protective quality	Measured time, s
0	Poor	Less than 30
1	Not very good	30 to 100
2	Fair	100 to 300
3	Good	300 to 1000
4	Excellent	More than 1000

industry for the rapid determination of the permeability of rock cores (Whiting and Cady 1992). A schematic of the apparatus is shown in Fig. 3.6.4.1.11. A vacuum plate, with a soft rubber ring to provide an airtight seal, is placed on the concrete surface. To conduct the test, Valves A, B, and C are closed and the vacuum pump is activated. The pump is of such capacity that the vacuum pressure should stabilize at approximately –12 psi (–83 kPa) within 15 seconds. Valve A is opened and the vacuum pressure should again stabilize at –12 psi (–83 kPa). Valve B is opened and Valve A is closed, directing airflow through the flowmeter. After 15 seconds, the reading of the flowmeter is recorded. The flow rate in $in.^3$/min (mL/min) is used as an indicator of the surface air permeability. Experiments have demonstrated that the effective depth of the measurement is approximately 0.5 in. (13 mm) (Whiting and Cady 1992). As in the Schönlin test, the surface should be dried with hot air if it is suspected that the surface layer may have a high moisture content.

3.6.4.1.12 *Surface air-permeability test*—The surface permeability system (Fig. 3.6.4.1.4) can also be used to determine an air-permeability index (Basheer 1993). In this test, the water pump is isolated and the air pressure in the test chamber is increased to 7 psi (50 kPa) using a syringe attached to the priming value. The pressure decay is monitored every minute for 15 minutes. The natural logarithm of the pressure, in psi (kPa), is plotted against the elapsed time in minutes and the slope of the best-fitting straight line is reported as the autoclam air-permeability index. Although moisture influences the test results, Basheer et al. (2001) has shown that the quality of concrete can be classified in terms

Table 3.6.4.1.12—Protective quality based on surface air permeability index (Basheer 1993)

Protective quality	Surface air permeability index Ln(Pressure)/min
Very poor	> 0.90
Poor	> 0.50 ≤ 0.90
Good	> 0.10 ≤ 0.50
Very good	≤ 0.10

of the autoclam air-permeability index if measurements are taken when the internal relative humidity in a 0.4 in. (10 mm) deep hole in the cover concrete is less than 80 percent. At higher values of relative humidity, the air permeability measurements are reported to be of no benefit to classify the concrete. Table 3.6.4.1.12 shows the tentative classification that can be used to interpret the surface air-permeability index (Basheer 1993).

3.6.4.1.13 *Ion diffusion test*—Based on the principles of chloride ion migration tests, Basheer et al. (2005) report an in-place ion migration test (Fig. 3.6.4.1.13). This test measures the chloride ions (or any type of ion used in the ion source solution) transported through concrete in the surface zone under an applied potential field of 60 V DC. The onset of the steady rate of migration of ions into the anolyte cell (for example, the cell containing the anode) is identified with the help of conductivity measurements in the anolyte cell from the start of the test at an interval of 15 minutes. When the steady rate of flow condition has been established, five samples of the anolyte are collected at an interval of 10 minutes and the chloride content of the samples determined. These chloride values are plotted versus the corresponding time to obtain the steady rate of flow of the chloride ions, from which the in-place migration coefficient is calculated from the Nernst-Planck equation (Nanukuttan et al. 2006). During testing, the current flow between the electrodes and the temperature of the anolyte are also measured. The temperature is used to normalize the conductivity values to 77°F (25°C), and the current values are plotted versus the corresponding time to determine the initial current, the peak current, and the charge passed at different test duration. Laboratory comparisons have indicated the migration coefficient obtained from the test to be comparable with the effective diffusion coefficient (as that obtained in ASTM C1556 test) for concretes containing both normal portland cement and supplementary cementitious materials (Nanukuttan et al. 2006).

3.6.5 *Advantages and limitations*—The advantages and limitations of the various permeability methods that have been discussed are summarized in Table 3.6.5.

3.6.5.1 *Absorption tests*—The ISAT provides a surface measurement and models water absorption, which is the most common ingress mechanism associated with concrete deterioration. The test has been used extensively in the UK and a considerable amount of field data and experience in using the equipment has been gained. The test is totally nondestructive and can be used on both vertical and horizontal surfaces. Limitations of the ISAT are:

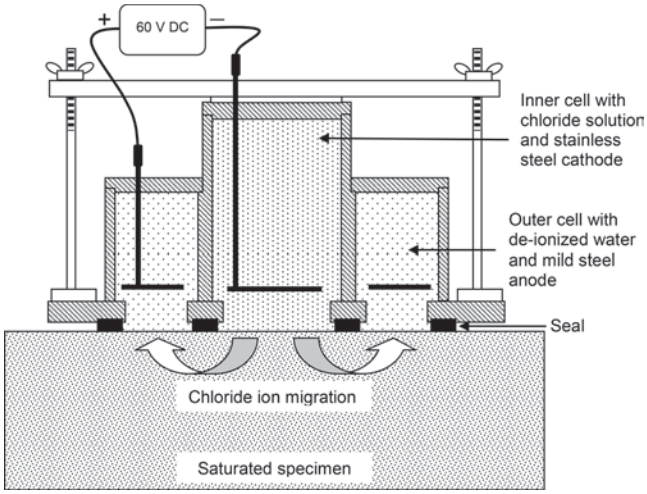

Fig. 3.6.4.1.13—Schematic of ion migration test.

a) For concretes with a low surface sorptivity, the flow path may be considered approximately unidirectional, and the ISAT measurements are related to unidirectional sorptivity measurements (Hall 1989). As the sorptivity of the surface layer increases, however, radial flow becomes significant and there is no reliable relationship between ISAT measurements and sorptivity measurements.

b) Achievement of a watertight seal between the cap and the concrete surface can be difficult in the field. Investigation of modifications to overcome this problem has been performed with some success in the UK.

c) The ISAT is capable of testing only the outer 0.4 to 0.6 in. (10 to 15 mm) of the concrete. When considering reinforcement corrosion, it may be desirable to assess the complete cover zone.

d) Test results are affected by the presence of curing compounds or other surface coatings.

The Figg test requires holes to be drilled into the concrete and the outer 0.8 in. (20 mm) of the concrete has to be sealed off. Surface skin properties are therefore excluded from the measurement. The test is not affected by surface coatings or curing compounds. The CAT also requires drilling a hole, but the measurement includes the effect of all the concrete surrounding the hole, including the surface zone. The main advantage of the CAT, compared with the ISAT and Figg test, is the ability to obtain an integrated absorption measurement of the surface zone to a depth of 2 in. (50 mm), but in the case of both the CAT and Figg tests, microcracking during drilling could influence results.

The surface sorptivity test has all the advantages of the ISAT, but it eliminates the mounting problems of the ISAT. Using the modified ring incorporating a guard ring, it is now possible to obtain the value of sorptivity of concrete. However, the internal humidity of the near-surface concrete up to a depth of 0.4 in. (10 mm) needs to be less than 80 percent to obtain reliable results.

3.6.5.2 *Water-permeability tests*—The Steinert water-permeability test produces an empirical permeability index for a particular concrete. Measurement of an absolute property, rather than an empirical permeability index, is prefer-

Table 3.6.5—Advantages and limitations of the methods

Method	Advantages	Limitations
ISAT	Simple and inexpensive to perform. Portable equipment. Sensitive to changes in concrete quality. Nonintrusive. Considerable experience has been gained in its use.	Unreliable for concrete with a high sorptivity surface layer. Measures absorption of outer surface concrete only and is affected by surface coatings. Difficult to seal circular cap at the concrete surface. Sensitive to concrete moisture condition.
Figg water-absorption test	Not affected by coatings and surface concrete layer. Inexpensive and simple to use.	Intrusive because drilling is necessary. Drilling may affect concrete under test. Sensitive to aggregate characteristics. Sensitive to concrete moisture condition.
Covercrete absorption test	Gives an integrated measure of the entire cover zone.	Intrusive because drilling is necessary. Drilling may affect concrete under test. Sensitive to concrete moisture condition.
Surface sorptivity test	All the advantages of the ISAT. Provides a sorptivity value. Could be used to test surface-treated concretes.	Measures concrete very close to the surface. Sensitive to moisture conte
Surface water permeability test	Measures flow under constant pressure conditions. Provides coefficient of permeability.	Concrete surface is damaged at the place where the ring is bonded. Overall time needed for the test is long.
Steinert method (water permeability)	Measures unidirectional flow. Easier to interpret than CLAM.	Provides a permeability index, not coefficient of permeability. Sensitive to concrete moisture condition. Concrete surface is damaged. Long test time required.
Figg air-permeability test	Inexpensive and simple to use. Not influenced by surface layer or coatings. Less sensitive to moisture condition than water tests.	Sensitive to aggregate characteristics. Intrusive because drilling is required. Drilling may affect concrete under test. Provides a permeability index, not coefficient of permeability.
Schönlin test (air permeability)	Nonintrusive. Less sensitive to moisture condition than water tests. Includes concrete moisture conditioning procedure.	Provides a permeability index, not coefficient of permeability. Measures outer surface concrete only and is affected by surface coatings.
SAF test	Nonintrusive. Less sensitive to moisture condition than water tests. Includes concrete moisture conditioning procedure.	Provides permeability index, not coefficient of permeability. Measures outer surface concrete only and is affected by surface coatings.
Surface air permeability test	Nonintrusive. Sensitivity to quantifying the effect of formwork and curing methods on quality of the cover concrete.	Provides permeability index, not coefficient of permeability. Measures outer surface concrete, not the full concrete cover.
Ion migration test	Nonintrusive. Provides coefficient of diffusion of any ion used in the test.	Requires long test duration (2 to 12 hours, depending on the quality of the concrete). Limited experience on site.

able because there are well-defined relationships between the coefficient of permeability and other durability-related factors (Whiting 1987). This is addressed in the surface water-permeability test by presaturating the test area before performing the test.

Other drawbacks of water-permeability tests are the long testing times (when the time required for saturating the test area is considered) and the need to glue or clamp the equipment to the concrete surface to effectively sustain the applied water pressure.

3.6.5.3 *Air-permeability tests*—In general, most air-permeability techniques are quick and simple to perform. In the case of vacuum-mounted devices, no permanent attachment is needed. Unlike water tests, air-permeability tests do not affect the permeation properties of the concrete. As a result, an air-permeability test can be repeated at the same location.

Surface tests, such as the SAF test, Schönlin's method, and autoclam air-permeability test, are affected primarily by the top 0.6 in. (15 mm) of concrete and do not provide an indication of the permeation properties of the entire cover zone. Tests based on Figg's method require drilling a hole and exclude the near-surface layer in the measurement.

Generally, each test method results in an air-permeability index that can be related to other factors that govern the durability of concrete. In most cases, however, the index obtained by a specific method is not related to the index obtained by another method that uses a different geometry and test pressure.

The in-place migration test to determine the diffusion characteristics of concrete in the cover zone also requires the test area to be saturated before testing. In addition, the test itself requires up to a full day to complete. However, this could be an alternative to coring and performing a laboratory test to determine the diffusion coefficient.

3.6.5.4 *General limitations*—Although the permeability techniques are related to the mechanisms associated with concrete deterioration, certain limitations should be considered when using a particular test method in practice. These limitations include sensitivity to moisture and temperature changes, changes in transport mechanism during the test (for example, sorption to diffusion), variation of air perme-

ability with applied pressure, and the influence of drilling on test values. The empirical nature of most of the tests and the associated complex flow characteristics has prevented the conversion of test results to absolute property measurements.

The most important limitation is, by far, the effect of concrete moisture content at the time of testing. A dry concrete will absorb more water and allow more airflow than the same concrete in a saturated state. A poor-quality concrete tested in a moist condition can result in apparently better indicators of durability than a higher-quality concrete tested in a dry condition. Some methods try to account for this problem by specifying that the test should not be conducted within a certain period after a rainfall. However, because the drying of the concrete is a function of the ambient temperature and relative humidity, specifying a natural drying time does not assure that the moisture content is at a standard level. Other methods specify a period of drying with hot air before testing (Kropp and Hilsdorf 1995). Permeability tests that require presaturation reduce these problems.

For methods based on drilling a test hole, the percussion action of the hammer-drill can have a detrimental and uncontrollable effect on the concrete in the vicinity of the hole. Cracks can be produced in the concrete that allow air and water to flow more readily along them. This condition can produce discrepancies between test results, especially in water absorption.

3.7—Infrared thermography

Infrared thermography has been used for detecting subsurface anomalies within and below concrete elements. The method has been applied to the identification of internal voids, delaminations, and cracks in concrete structures such as bridge decks (Holt and Manning 1978), highway pavements (Weil 2004), parking garages, pipelines (Weil 1989), and buildings. ASTM D4788 describes the use of infrared thermography for detecting delaminations in concrete bridge decks, with and without asphalt overlays. The technique has been used successfully under difficult winter conditions with small temperature variations to identify delaminations close to the underside of bridge decks (Clark et al. 2003). In this latter case, a long wavelength camera was used. This is discussed in 3.7.2.

Infrared thermography has also been used for locating defects within layers of fiber-reinforced polymer sheets and laminates used to strengthen reinforced concrete members. These defects include air voids between sheets or at the concrete interface. Quantitative analysis of recorded thermal data allows determination of the size and approximate depth of the defects (Starnes et al. 2003; Brown and Hamilton 2007). For depth estimation, it is necessary to record the development of the thermal signal under transient heating.

3.7.1 *Principle*—Infrared thermography senses the emission of thermal radiation and produces a visual image from this thermal signal. Thermography, like any system using infrared radiation, measures variation in surface radiance and does not directly measure surface temperature. However, it can be used to detect anomalies in surface radiance that may be related to subsurface conditions of the concrete member.

Infrared thermography for testing concrete is based on two principles. The first principle is that a surface emits energy in the form of electromagnetic radiation. The rate of energy emitted per unit surface area is given by the Stefan-Boltzmann law (Halliday and Resnick 1978)

$$R = e\sigma T^4 \tag{3.7.1}$$

where R is the rate of energy radiation per unit area of surface, W/m^2; e is the emissivity of the surface; σ is the Stefan-Boltzmann constant, 5.67×10^{-8} W/(m^2·K^4); and T is the absolute temperature of the surface, K.

The wavelength of the emitted radiation depends on temperature. As the temperature increases, the wavelength becomes shorter. At a sufficiently high temperature, the radiation is in the visible spectrum. For example, this phenomenon is observed when a nail is heated and emits visible light at high temperatures. However, in the range of room temperature, the wavelength of the emitted radiation is on the order of 10 μm, which is in the infrared region of the spectrum. This radiation can be detected by special sensors that produce electrical signals in proportion to the amount of incident radiant energy. With proper calibration, the output of an infrared sensor can be converted to temperature. Thus, it is possible to measure the surface temperature of concrete without having to make contact with a thermometer or thermocouple.

The second principle is that subsurface anomalies in the concrete affect heat flow through the concrete (Fig. 3.7.1). If the anomalies are not too deep, these changes in heat flow cause localized differences in surface temperature. By measuring surface temperature under conditions of heat flow, the subsurface anomalies can be located.

The required heat-flow condition can be created artificially by using heating lamps, or it can occur naturally by solar heating (heat flow into the structure) and night-time cooling (heat flow out of the structure). The latter methods are often the more economical approach.

In summary, infrared thermography for testing concrete exploits two main heat-transfer mechanisms: conduction and radiation. Sound concrete is more thermally conductive than low-density or cracked concrete. Radiation from the concrete surface depends on the emissivity of the material, which is defined as the ability of the material to radiate energy compared with a perfect black body radiator. Rougher surfaces of the same material have higher emissivity values. Some values of emissivity are (Weil 2004) rough clean concrete (e = 0.95) and shiny steel (e = 0.05). Different surface textures and finishes—for example brush marks, rubber, or oil residues—will affect the surface radiation properties. Thus, care should be exercised to assure that apparent measured temperature differences are not due to differences in emissivity.

The physical parameters determining the emitted infrared radiation measured during a thermographic survey are concrete surface emissivity, surface temperature, concrete thermal conductivity, concrete volumetric-heat capacity, thickness of the heated layer, and intensity of incident solar radiation. The environmental conditions present at the time

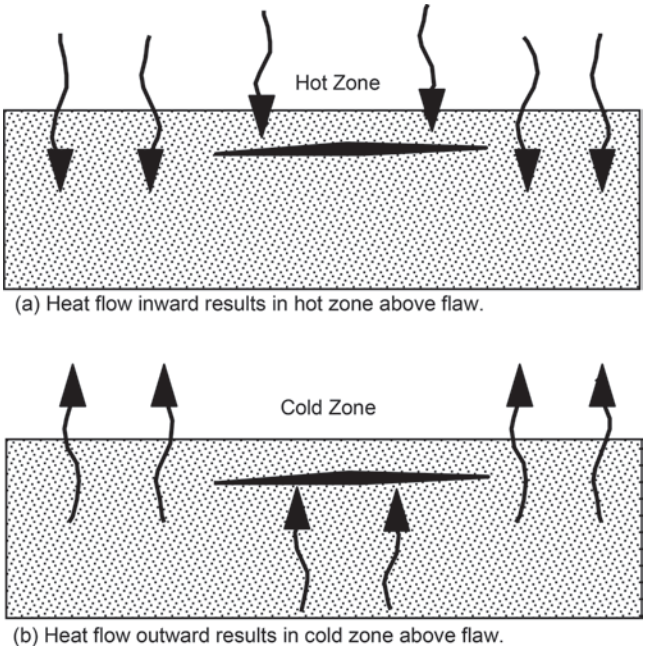

Fig. 3.7.1—Effect of internal anomaly on surface temperature during heat flow.

of testing also affect surface temperature measurements. Clouds reduce solar radiation during the day and reflect infrared radiation at night, slowing heat transfer at the concrete surface. Wind and surface moisture reduce temperature gradients, and water at temperatures below 32°F (0°C) forms ice in voids and cracks. The optimum weather conditions are clear skies, mild wind, dry concrete surface, and intense solar radiation. To overcome environmental influences on testing, guidelines suggested are (ASTM D4788):

a) Remove debris from surface

b) Do not test when standing water, ice, or snow is present; allow surface to dry at least 24 hour before testing

c) Do not test if wind speeds exceed 15 mph (25 km/h)

d) The ground temperature should be above 32°F (0°C)

e) Testing at night should be done under clear skies

Above all else, testing should be performed when the largest heating or cooling gradients are present in the concrete. When cooling conditions are present—for example, testing at night—the concrete above any anomalies will be cooler than the surrounding sound concrete. The reverse is true during heating conditions. The suggested best time for doing infrared surveys is soon after sunrise or 1/2 to 1 hour after sunset. If testing is performed too long after a thermal change, the concrete surface may become thermally saturated such that the thermal anomalies have passed. The amount of time required in direct sunlight to develop detectable anomalies in surface temperature differs for various applications. For example, ASTM D4788 recommends 4 hours of direct sunshine on concrete and 6 hours on asphalt-covered concrete decks for detecting delaminations in bridge decks. For the inspection of fiber-reinforced polymer (FRP) sheets and laminates, pulsed or artificial heating may be required (Brown and Hamilton 2007).

3.7.2 *Equipment*—Thermographic scanning and analysis systems comprise three main components: a scanner/detector unit, a data acquisition/analysis device, and a visual image recorder. The infrared scanner head is an optical camera with lenses that transmit only infrared radiation with wavelengths in the range of 3 to 5.6 μm (shortwave), or 8 to 12 μm (longwave). A system of rotating mirrors is used to enable a two-dimensional (2D) scan of the test object. Older models of infrared detector are normally cooled by liquid nitrogen to a temperature of –321°F (–196°C), and can detect temperature variations as small as 0.2°F (0.1°C). New sensors, however, have been developed that do not require cooling (Kaplan 1994; Matthews et al. 1994). These sensors are composed of a 2D array of materials sensitive to incident infrared radiation. The use of a 2D array eliminates the need for rotating mirrors as in conventional optical-mechanical infrared cameras. The data acquisition and analysis unit includes an analog to digital (A/D) converter, a computer with a high-resolution monitor and a data storage device, and data analysis software. For rapid coverage of large areas, such as highway or airfield pavements, the equipment can be mounted on an automotive vehicle. Figure 3.7.2a illustrates a compact camera that does not require a cooling system. Data obtained by the scanner/detector unit are digitized and displayed as shades of gray or color, depending on the data analysis software. Cooler or hotter regions are identified by a different gray shading or color compared with the surrounding concrete. Normally, a digital video camera is used to provide a record of the region scanned by the infrared camera. Comparison of the visual and infrared images is necessary to ensure that apparent temperature differences in the infrared image are not due to differences in surface emissivity. As an example, Fig. 3.7.2b shows an optical photograph (top) and the corresponding infrared thermogram (bottom) of a bridge. The locations of delamination are identified by the brighter hot spots in the thermographic image. Note that the asphalt patch results in a false indication because of its different emissivity and thermal properties.

For depth estimation, it is necessary to record the development of the thermal signal under transient heating. Software is used to perform time domain analysis of recorded thermal histories to make these estimations (Brown and Hamilton 2007).

3.7.3 *Advantages and limitations*—The advantages and limitations of infrared thermography are summarized in Table 3.7.3. Infrared thermography is a global inspection method that permits large surface areas to be surveyed in a short period of time. The main applications in civil engineering are to detect delaminations in bridge decks and reinforced concrete pavements and the inspection for voids in bonded FRP sheets and laminates used to strengthen deficient structures.

Among its disadvantages is the requirement for the appropriate environmental conditions to achieve the heat-flow conditions needed to detect the presence of subsurface anomalies. Even with the proper heat-flow conditions, however, not all delaminations are detectable. Maser and Roddis (1990) performed analytical studies to gain an understanding of the factors affecting the differences in the

Table 3.7.3—Advantages and limitations of infrared thermography

Advantages	Limitations
A global technique that covers a much greater area than other test methods and is, therefore, cost-effective. Results provide an indication of the percentage of deteriorated area in the survey region.	Expensive equipment. Requires proper environmental conditions for testing. Variations in test response occur with varying environmental conditions (temperature gradient, shaded or direct sunlight, cloud cover, and surface water). As the depth of the anomaly increases, it becomes more difficult to detect. Trained individual needed to assure that acquired data are meaningful and correctly interpreted.

surface temperature of a solid concrete slab and a slab with a delamination. Examples of the results of such analyses are shown in Fig. 3.7.3. Figure 3.7.3(a) shows the analytical model that was used. In the analyses (based on the finite element method), the concrete slab was subjected to a sinusoidal variation of ambient temperature with a 24-hour cycle and a parabolic variation in incident solar radiation. The air temperature varied from 61 to 86°F (16 to 30°C). Figure 3.7.3(b) shows the differences in surface temperature compared with a solid slab for different cover depth and a 0.05 in. (1.27 mm) wide air-filled crack. It is seen that the maximum differential temperature decreases as the depth of the delamination increases. Figure 3.7.3(c) shows the results for different crack widths at a cover depth of 1.5 in. (38 mm). It is seen that the crack width has a strong effect on the maximum temperature differential. It was also found that a water-filled delamination resulted in nearly identical surface temperatures as in a solid slab. Finally, it is noted that whereas infrared thermography can provide information on the areal extent of a subsurface anomaly, it is not able to provide information on its depth.

Fig. 3.7.2a—Infrared camera.

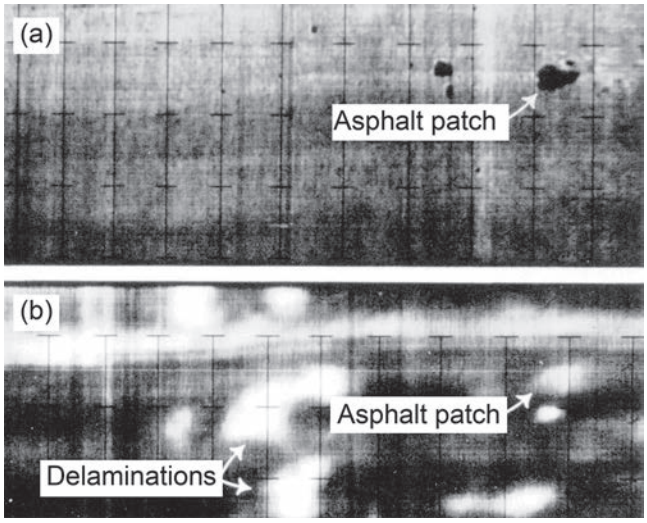

Fig. 3.7.2b—Example of infrared thermography: (a) optical photograph of concrete bridge deck; and (b) infrared thermogram showing hot spots corresponding to locations of concrete delaminations and false indication due to asphalt patch.

3.8—Radar

3.8.1 *Introduction*—Radio detection and ranging (RADAR) is analogous to the pulse-echo technique discussed in 3.2.2, except that electromagnetic waves, which are radio waves or microwaves, are used instead of stress waves. The early uses of this technique were for military applications, but it is now used in a variety of fields. The earliest civil engineering applications were used for the detection of buried pipelines and tanks. This was followed by studies to detect cavities below airfield pavements for determining concrete thickness, locating voids and reinforcing bars, and identifying deterioration in concrete elements (Bungey and Millard 1993; Cantor 1984; Carter et al. 1986; Clemeña 1983; Kunz and Eales 1985; Maser 1986, 1990; Maser and Roddis 1990; Steinway et al. 1981; Ulriksen 1983). Since the 1990s, radar has been used to evaluate the presence of voids in grouted post-tensioning plastic ducts. It has also been used in tandem with other nondestructive testing (NDT) methods to evaluate for voids in metallic post-tensioning ducts by first using radar to evaluate for location of the duct, then using other NDT methods or invasive probing (Williams and Hulse 1995). Following problems with metallic grouted duct tendon inspections, plastic ducts have been used in many new post-tensioned concrete bridge beams as these may be inspected with radar (Bungey et al. 1997; Giannopoulos et al. 2002). Other applications include the detection of voids in grout behind tunnel linings (Davis et al. 2004) and detection of unwanted inclusions, such as clay balls in concrete pavements (Lim 2001). The most attractive features of radar are its ability to penetrate into the subsurface and detect unseen conditions and scan large surface areas in a short period of time, and its high sensitivity to subsurface moisture and embedded metal.

In civil engineering applications, the depths of media being inspected are relatively shallow compared with other uses of radar. As a result, devices for these applications emit short pulses of electromagnetic waves (microwaves). For

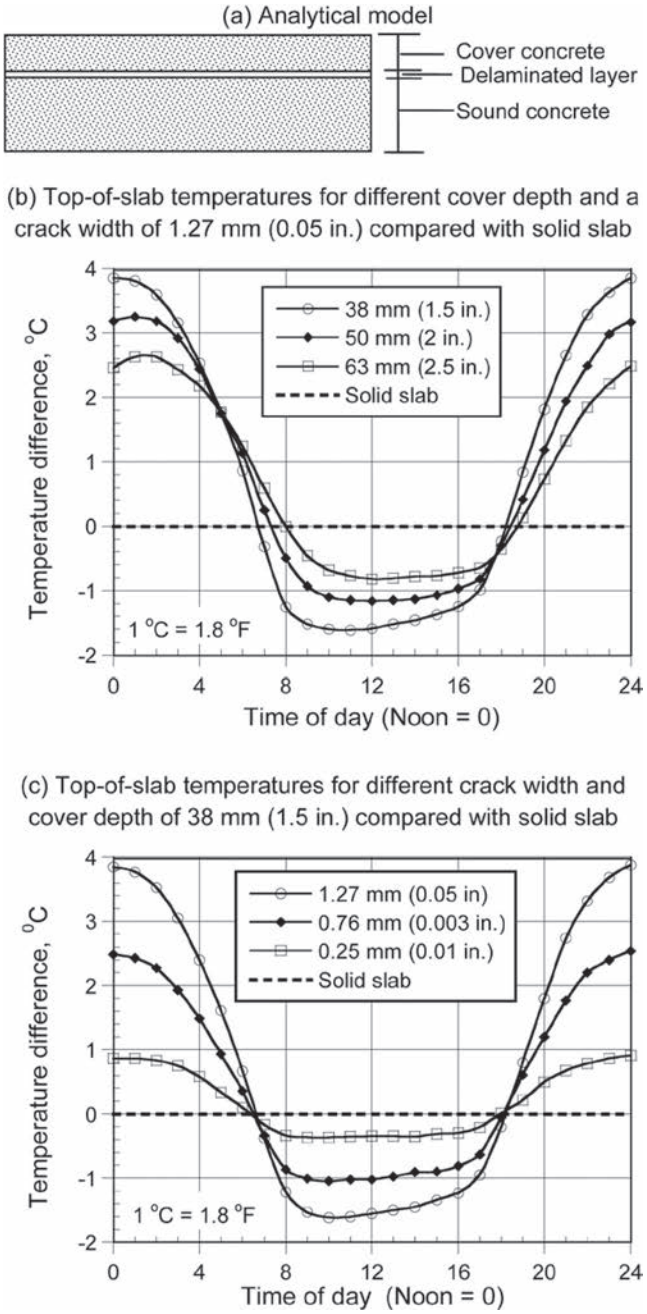

Fig. 3.7.3—Analytical study of infrared thermography: (a) model of concrete bridge deck used in numerical simulation; (b) effect of depth of cover on surface temperature compared with solid slab; and (c) effect of width of air-filled crack on surface temperature compared with solid slab (adapted from Maser and Roddis [1990]).

this reason, the technique is often called short-pulse radar, impulse radar, or ground-penetrating (probing) radar (GPR). Two other approaches considered for structural applications are frequency modulation and synthetic-pulse radar (Bungey and Millard 1993). They are excluded from this section because pulsed systems have gained the greatest practical acceptance and are most readily available commercially.

Sections 3.8.2 through 3.8.5 review the principles of radar, the instrumentation used, data analysis techniques, and some of the inherent limitations. A detailed review of the principles and applications of radar was published by Clemeña (2004).

3.8.2 *Principle*—The operating principle of radar is illustrated in Fig. 3.8.2. An antenna, which is either dragged across the surface or attached to a survey vehicle, transmits short pulses of electromagnetic energy within a specific frequency range that penetrate into the surveyed material. The most commonly used pulses for concrete evaluation range from 1 to 3 nanoseconds (ns) in duration and often contain three or four peaks, as shown in Fig. 3.8.2. These short-duration pulses have nominal center frequency values in air, commonly between 400 MHz and 2.6 GHz for structural surveys. Each pulse travels through the material, and a portion of the energy is reflected back to the antenna when an interface between materials of dissimilar dielectric properties is encountered. The antenna receives the reflected energy and generates an output signal proportional to the amplitude of the reflected electromagnetic field. The received signal, therefore, contains information on the transmitted medium, distance of the reflector, speed of the pulse through the medium, and how much of the pulse was attenuated. These quantities depend on the spatial configuration and electrical properties of the member under investigation.

The following discussion of electromagnetic wave propagation is simplified based on assumptions suitable for civil engineering applications. More detailed treatments are available (Daniels et al. 1988; Halabe et al. 1993, 1995). The primary material properties that affect the transmission and reflection of electromagnetic energy are the dielectric constant and the conductivity. Materials of interest for structural applications of radar, with the exception of metals, are low-loss dielectrics, which mean they absorb little of the propagating electromagnetic field. A material's dielectric constant, also known as dielectric permittivity, is the amount of electrostatic energy stored per unit volume for a unit potential gradient. Electrical conductivity, the reciprocal of electrical resistivity (refer to 3.5), is a measure of the ease with which an electrical current can flow through a material. The ratio of a material's dielectric constant to that of free space (air) is defined as the relative dielectric constant ε_r

$$\varepsilon_r = \frac{\varepsilon}{\varepsilon_o} \tag{3.8.2a}$$

where ε is the dielectric constant (farad/meter), and ε_o is the dielectric constant of free space (air), which is 8.85×10^{-12} farad/meter.

The relative dielectric constant governs the speed of the electromagnetic wave in a particular material. For low-loss materials, which are materials that have a small dissipation of electric or electromagnetic power, the speed of electromagnetic waves C is given by

$$C = \frac{C_o}{\sqrt{\varepsilon_r}} \tag{3.8.2b}$$

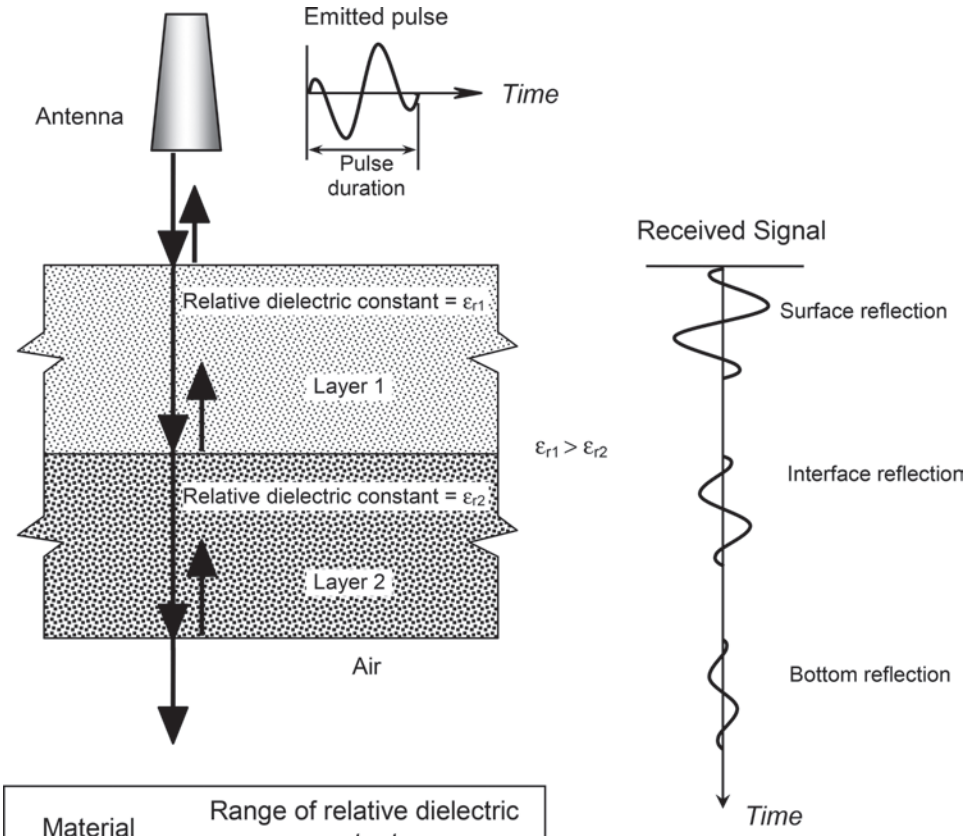

Material	Range of relative dielectric constant, ε_r
Air	1
Portland cement concrete*	6 to 11
Bituminous concrete*	3 to 5
Gravel *	5 to 9
Sand*	2 to 6
Rock*	6 to 12
Water	80

* ASTM D 4748

Fig. 3.8.2—Reflections of electromagnetic radiation pulse at interfaces between materials with different relative dielectric constants (adapted from Carino [1994]).

where C_o is the speed of light in air (3×10^8 m/s); and ε_r is the relative dielectric constant.

Analysis of the recorded time-domain waveforms permits determination of the depth of the reflecting interface, assuming the relative dielectric constant of the material into which the pulse is transmitted is known. The depth of the reflecting interface is obtained from the measured round-trip travel time and the speed of the electromagnetic wave. If the round-trip travel time for the pulse is t, the depth D would be

$$D = \frac{Ct}{2} \tag{3.8.2c}$$

The contrast in dielectric constant determines the amount of reflected energy at the interface between two dissimilar materials. For low-loss dielectrics, the ratio of the reflected to incident amplitudes of the electromagnetic field (reflection coefficient) is given by (Clemeña 2004; Bungey and Millard 1993)

$$\rho_{1,2} = \frac{\sqrt{\varepsilon_{r1}} - \sqrt{\varepsilon_{r2}}}{\sqrt{\varepsilon_{r1}} + \sqrt{\varepsilon_{r2}}} \tag{3.8.2d}$$

where $\rho_{1,2}$ is the reflection coefficient; ε_{r1} is the relative dielectric constant of Material 1 (incident wave); and ε_{r2} is the relative dielectric constant of Material 2.

The dielectric constant of concrete is affected by the nature of the constituent materials and moisture content. By definition, the relative dielectric constant of air equals 1, and typical values for other materials are given in Fig. 3.8.2. Note that the dielectric constant of water is much greater than the other listed materials. This makes water the most significant dielectric contributor to construction materials and explains why radar is highly sensitive to moisture. As the moisture

content increases, the dielectric constant of the material, such as concrete, also increases. Padaratz and Forde (1995) provide an explanation of the effects of moisture on a material's dielectric properties.

An important difference between radar and stress-wave methods, such as the impact-echo method, is the ability of radar to penetrate beyond concrete-air interfaces. For stress waves, the reflection is almost 100 percent because the acoustic impedance of air is negligible compared with concrete. Alternately, the dielectric constants change at a concrete-air interface is not as drastic, and only approximately 50 percent of the incident energy is reflected at a concrete-air interface. This condition results in two significant differences between radar and stress-wave methods. Radar is not as sensitive to the detection of concrete-air interfaces as stress-wave methods. However, because the energy is not totally reflected at the concrete-air interface, radar is able to penetrate beyond such an interface and can be used to assess features below the interface.

Equation (3.8.2d) shows that when the dielectric constant of Material 2 is greater than that of Material 1, the reflection coefficient is negative. This indicates a phase reversal (change in polarity) of the reflected wave, which means that the positive part of the wave is reflected as a negative part (Fig. 3.8.2). At a metal interface, such as between concrete and steel reinforcement, there is complete reflection and the polarity of the reflected wave is reversed. This makes radar effective for locating metallic embedments. Alternately, strong reflections from embedded metals can obscure weaker reflections from other reflecting interfaces that may be present, and multiple reflections from reinforcing bars may mask signals from greater depths.

The conductivity and, to a lesser extent, the dielectric constant, determine the energy loss in a particular material. Signal attenuation may be approximated as follows (Bungey and Millard 1993)

$$\alpha = 1.69 \times 10^3 \frac{\sigma}{\sqrt{\varepsilon_r}} \qquad (3.8.2e)$$

where α is the signal attenuation (dB/m); and σ is the conductivity ($\Omega^{-1}m^{-1}$).

The conductivity of concrete increases with frequency (Halabe et al. 1993). For example, the conductivity at 1 GHz is approximately 1.5 times the direct current (0 Hz) conductivity.

The radar unit measures the arrival time and amplitude of a reflected electromagnetic pulse. Because electromagnetic wave propagation is affected by changes in dielectric properties, variations in the condition and configuration of a structure will cause changes in the received signal. Information is obtained by observing the return time, amplitude, shape, and polarity of the signal. The presence of defects such as voids, honeycombing, and high moisture and chloride content can be inferred from changes in the dielectric constant and conductivity of the concrete. For example, theoretical studies have shown that characteristics of the radar signal are affected by variations in concrete moisture content (Shaw et al. 1993), and by variations in moisture and chloride contents under asphalt overlays (Maser and Roddis 1990). Other studies have considered the effects of shape and size of voids within concrete (Bungey and Millard 1995) and of void size under concrete pavements (Steinway et al. 1981, Halabe et al. 1993). Padaratz and Forde (1995) developed theoretical models for predicting the dielectric properties of concrete as a function of temperature, porosity, moisture and salt contents, and radar frequency. They showed that the electromagnetic wave velocity is frequency-dependent at higher conductivities. In addition, models were developed for radar waveform synthesis and inversion (Halabe et al. 1995; Giannopoulos 1997). The synthesis (forward) model can be used to generate theoretical radar waveforms and conduct parametric studies for layered media, such as overlaid bridge decks and pavements, with features such as reinforcing bars and delaminations. The inversion model has been used, with moderate success, to estimate the physical properties of concrete bridge decks from radar waveforms (Halabe et al. 1995). Others have used the finite element method to simulate the propagation of electromagnetic pulses through concrete (Millard et al. 1993).

Because the radar pulse has a finite duration, the material layers being surveyed have to be sufficiently thick for the reflections from successive layers to be clearly separated. This minimum required thickness can be calculated by using Eq. (3.8.2c) with t equal to 1/3 the pulse duration (based on the resolution being 1/3 of the wavelength, λ) (McCann and Forde 2001). For example, for a pulse duration of 1.5 ns in concrete (approximately equivalent to a 1 GHz central frequency dipole antenna closely coupled to the concrete surface) and a relative dielectric constant of 6 (speed = 5 in./ns [123 mm/ns]), the minimum required thickness would be approximately 1.7 in. (45 mm). Table 3.8.2 summarizes the resolution and minimum depth Z_{min} that can be detected for different center frequencies and concrete conditions. Resolution refers to the smallest target that is detectable. These numbers are based on the assumptions that resolution is based on $\lambda/2$ and the minimum detectable depth is $\lambda/3$. These calculations assume that the center frequency in air of a dipole radar antenna signal reduces by approximately 30 percent when brought into contact with concrete (Padaratz et al. 1997).

3.8.3 *Instrumentation*—Typical instrumentation for radar includes the following main components: an antenna unit, a control unit, a display device, and a storage device. The antenna emits the electromagnetic wave pulse and receives the reflections. For a given material, the depth of penetration and resolution of radar are functions of the frequency content of the pulse. Lower frequencies penetrate deeper but provide less resolution, whereas higher frequencies provide more detail but have less depth of penetration. For an antenna with a 1 GHz nominal center frequency, the penetration depth in concrete is approximately 16 in. (400 mm) (Bungey and Millard 1993). For a given antenna, the actual penetration depends on the moisture content of the concrete (Padaratz and Forde 1995).

Table 3.8.2—Characteristics of radar propagation through concrete

Material	ε_r	Frequency in air, MHz	Frequency in material, MHz	Velocity, in./ns (mm/ns)	Wavelength, in. (mm)	Resolution, in. (mm)	Z_{min}, in. (mm)
Dry concrete	6	1500	1050	4.8 (123)	4.6 (117)	2.3 (59)	1.5 (39)
Damp concrete	10	1500	1050	3.7 (95)	3.5 (90)	1.8 (45)	1.2 (30)
Dry concrete	6	900	630	4.8 (123)	7.7 (195)	3.9 (98)	2.6 (65)
Damp concrete	10	900	630	3.7 (95)	5.9 (151)	3.0 (76)	2.0 (50)
Dry concrete	6	500	350	4.8 (123)	13.8 (351)	3.0 (176)	4.6 (117)
Damp concrete	10	500	350	3.7 (95)	10.7 (271)	6.9 (136)	3.5 (90)
Dry concrete	6	100	70	4.8 (123)	69.2 (1757)	34.6 (879)	23.1 (586)
Damp concrete	9	100	70	3.7 (95)	53.4 (1357)	26.7 (679)	17.8 (452)

Much of the research into the use of radar has centered on the evaluation of reinforced concrete bridge decks and pavements. The equipment used for this purpose is configured to mount on and within a vehicle to allow continuous acquisition of the data as the vehicle travels along the roadway. In this configuration, a noncontact horn antenna is typically mounted to the vehicle approximately 6 to 20 in. (150 to 500 mm) above the pavement surface.

Another configuration is a portable arrangement, in which a small, hand-held dipole antenna is used. The antenna normally is mounted on a calibrated survey cart and placed in contact with the surface to be surveyed. This equipment is used for locating items such as reinforcing bars, embedments, voids, and other anomalies within a concrete mass (Bungey and Millard 1993). It has also been used to locate voids below slabs-on-grade, behind concrete retaining walls, and in grouted masonry block walls.

The control unit is the heart of a radar system. It controls the repetition frequency of the pulse, provides the power to emit the pulse, acquires and amplifies the received signal, and provides output to a display device. Data are stored in a digital storage device or computer for later analysis and interpretation.

The radar signal is displayed on a computer monitor. Computer software is also available to permit various signal processing methods to aid in data interpretation, such as subtraction of a reference signal or color display based on signal amplitude and polarity (Bungey et al. 1991; Chen et al. 1994). More generic software packages can also be used; however, the sophistication of the process is based on the users' familiarity with the generic data-processing software.

3.8.4 *Data analysis*—Radar systems emit pulses continuously at high repetition rates (typically 50 kHz). Whereas this permits scanning of test objects, it also results in a large amount of data. As a result, several techniques employing computer processing, color enhancement, or comparison methods have been developed.

Cluster analysis is a technique for comparing signals (waveforms) with reference signals caused by known conditions. The received signals are normalized to allow direct comparison. Each signal is compared with the previous signals and is assigned to a cluster of similar signals (Cantor 1984). If no other similar signals have been identified, it is assigned to a new cluster. The clusters are then correlated with known conditions as determined through visual inspection, coring, or excavation. The output of the results can be in the form of a strip chart that indicates the nature of the defect at the test position and a measure of the confidence of the prediction. The confidence measure indicates the closeness of fit of an individual signal to the reference signal for that cluster (refer to Cantor [1984] for examples of this type of analysis).

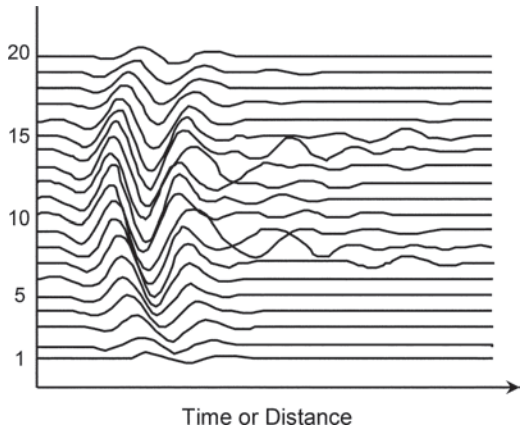

Fig. 3.8.4a—Illustration of topographic plotting technique to reveal differences in radar signals (adapted from Cantor [1984]).

Topographic-plotting (wiggle plot) is a technique that continuously displays or prints each radar trace (amplitude versus time) displaced a fixed distance from the previous trace (Fig. 3.8.4a). When a series of traces are viewed in this way, they take on an appearance similar to a topographic drawing (Cantor 1984). Where the traces are similar to one another, a uniform material is indicated. Where traces overlap or shift from one another, changes are indicated that might signify items such as deterioration, delamination, separation, patches, joints, different materials, and varying thicknesses.

Quantitative peak tracking is a technique that uses signal processing to quantitatively compute the amplitudes and arrival times of significant reflection peaks in the radar waveform (Maser 1990; Ulriksen 1983; Steinway et al. 1981; Carter et al. 1986). These quantitative computations can then be used to calculate and display concrete properties as depth profiles or area contour maps.

A grayscale line scan is presented in Fig. 3.8.4b, which shows a ground-coupled, dipole antenna emitting a radar

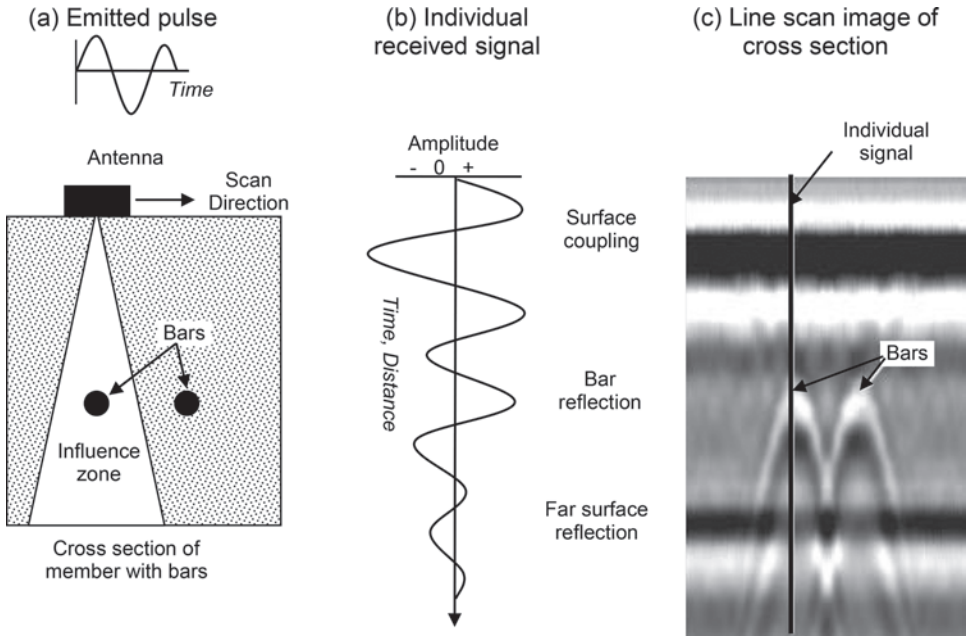

Fig. 3.8.4b—(a) Scanned concrete with two embedded steel bars; (b) received single waveform; and (c) display of output as antenna moves across surface.

pulse into a test object containing two steel bars. The time history of the waveform received by the antenna is presented next to the schematic of the test object. The figure also shows the typical output of the processed signal. The vertical axis represents time, or it can be transformed to depth by knowing ε_r and using Eq. (3.8.2b) and (3.8.2c).

In the line scan mode, the data are plotted in varying shades of gray or color depending on the amplitude of the signal. The output display depends on the number of waveform scans received and the display setting. The user can assign a gray or color scale to represent different levels of signal amplitude. This is an important point to understand for the proper interpretation of results. As the antenna is moved along the concrete surface, changes in the received signal are displayed. The resulting pattern on the screen represents a cross-sectional view of the test object, as illustrated in Fig. 3.8.4b.

As mentioned previously, metals are strong reflectors of electromagnetic waves. This characteristic makes radar very effective in locating buried metal objects, such as reinforcing bars, prestressing and post-tensioning strands, metallic tendon ducts, and conduits. The presence of reinforcing bars results in characteristic patterns in the display output that make them relatively easy to locate. For example, Fig. 3.8.4c(a) and (b) show computer display output obtained in a laboratory specimen in which reinforcing bars were placed 12 in. (300 mm) apart with cover depths of 2, 4, and 6 in. (50, 100, and 150 mm). The bars were embedded in sand contained in a wooden box 8 in. (200 mm) deep. This is a convenient way to study the effects of reinforcement on radar signals because the relative dielectric constant of sand is similar to dry concrete. Figure 3.8.4c(a) shows the results for No. 3 (No. 10) bars, and Fig. 3.8.4c(b) shows the results for No. 11 (No. 36) bars. The vertical dashed lines are identifying markers made by the operator to reference the position of the antenna to the actual locations on the scanned surface. Because bar locations were known in this study, the reference markers were created by the operator as the center of the antenna passed directly over the centerlines of the bars. The symmetrical arch-shaped patterns are typical of reflections from round metallic targets. The centerline of the bars are clearly identified and closer examination of the patterns reveals that the bar depth increases from left to right. The actual shapes of the arches, flat or peaked, depend on the scanning speed of the antenna and the rate at which the radar image is displayed on the computer monitor. It is impossible to infer the bar sizes by simply looking at the patterns on the computer display.

In field scans, the operator lays out a system of grid lines on the surface, and the grid is used to reference the computer output to positions on the structure. Figure 3.8.4d shows the output from a scan across a reinforced concrete slab with bars at unknown locations. The arch-shaped patterns caused by reflection from the bars are clearly evident. Five arches are shown, corresponding to five targets. The four arches at the same depth correspond to reinforcing bars. Note that one of the arches is closer to the top of the display and has a different pattern than the others. The operator identified this reflection as being due to a metal conduit rather than a reinforcing bar. The distance markers, generated as the antenna crossed grid points, can be used to locate the approximate horizontal positions of the bars within the slab. In this display, the settings have been configured so that the positive and negative portions of the waveforms are shown as solid or dashed bands, respectively. A comparison with Fig. 3.8.4c shows that the arches are more peaked in Fig. 3.8.4d. This condition is due to differences in the relative values of antenna scan speed and paper-feed speed. Figure 3.8.4e

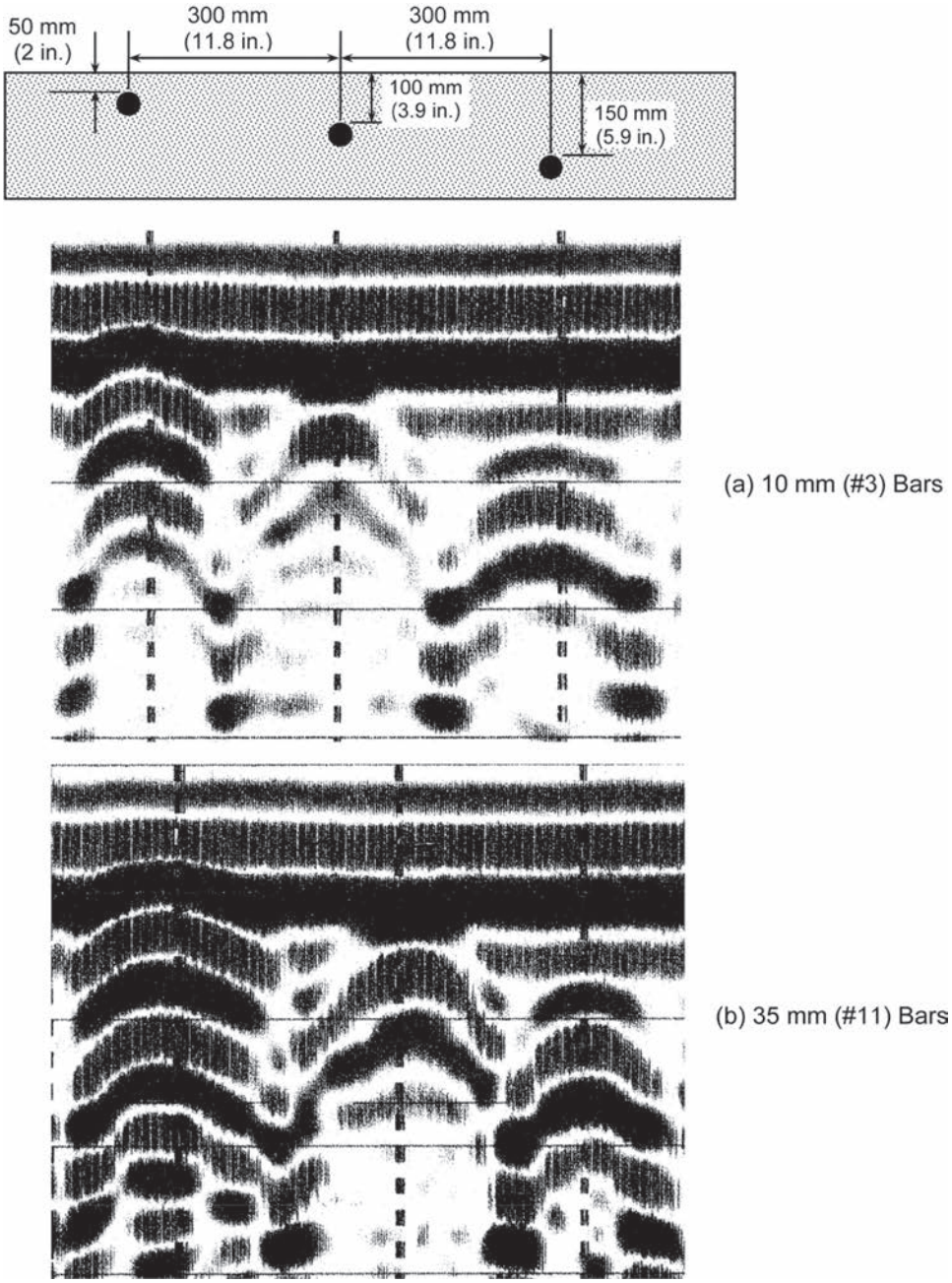

Fig. 3.8.4c—Graphic recorder displays for scans over reinforcing bars embedded at different depths in dry sand: (a) No. 3 (No. 10) bars; and (b) No. 11 (No. 36) bars.

shows a scan across a reinforced concrete slab with three targets at different depths in line scan or wiggle plot mode.

An antenna may be directional and the appropriate antenna orientation will vary according to the target. Often this is done on site by trial and error, as the antenna housing may not indicate the orientation of the individual antenna dipoles and the as built orientation of the target is unknown. To best detect a linear target such as reinforcement or metallic tendon ducts, the antenna motion should be perpendicular to the target. An initial scan should be performed to obtain a general layout of the targets. Once the general layout has been established, a second scan should be made in the same direction. The antenna should be moved more slowly to identify the reflection peak of the target, which identifies

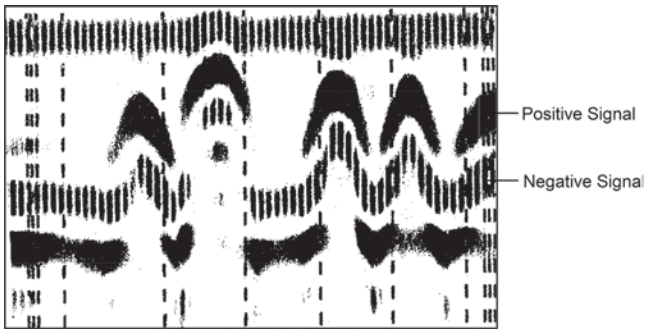

Fig. 3.8.4d—Graphic recorder display for scan across reinforced concrete slab (dashed and solid bands correspond to negative and positive portions of waveforms).

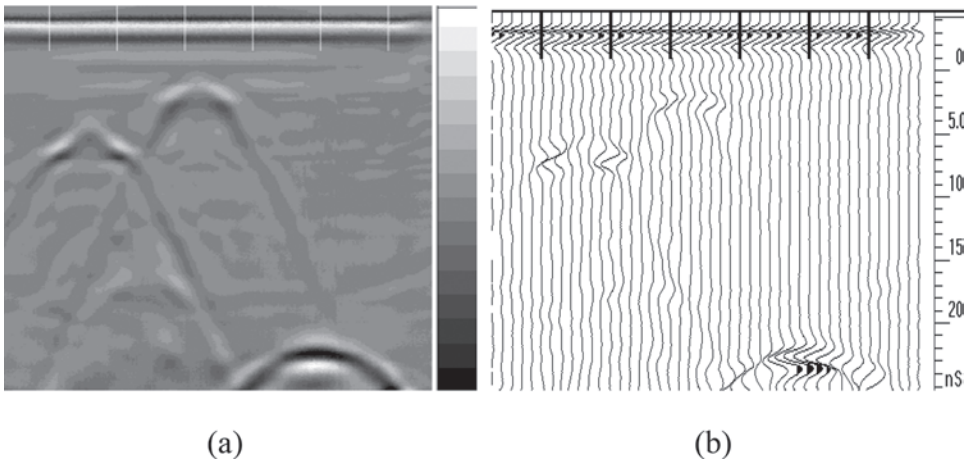

Fig. 3.8.4e—Radar data display from computer: (a) line scan image in gray tones; and (b) wiggle plot (adapted from Colla [1997]). (Note: horizontal axis = distance; vertical axis = two-way travel time in nanoseconds.)

the target location. Once the location has been established, the scan procedure should be performed with the antenna moving in the opposite direction to see if the identified target locations coincide. If the antenna is mounted with a survey wheel, the survey wheel can be drawn backward and the approximate location of the target, with respect to the antenna, is noted by a location marker on the display unit.

Detection of voids in grouted plastic post-tensioned ducts can be performed with the antenna orientation either perpendicular or in-line with the post-tensioned duct. To perform the scan in line with the post-tensioned ducts, the location of the ducts needs to be determined initially. A detailed exposition is given by Giannopoulos et al. (2002).

3.8.5 *Advantages and limitations*—The commonly used antennas irradiate a cone-shaped volume of concrete. At a depth of 8 in. (200 mm), an area of approximately 1 ft^2 (0.1 m^2) is irradiated. At that depth then, multiple passes approximately 1 ft (0.3 m) apart are required to survey a larger section of concrete.

When multiple reinforcing bars are present, there will be multiple arch patterns as shown in Fig. 3.8.4c. As the bar spacing decreases, the arch patterns overlap. Below certain spacing, the individual bars can no longer be discerned and the reflection pattern is similar to the case of a solid-embedded steel plate. The ability to discern individual bars depends on bar size, bar spacing, cover depth, and the configuration of the antenna (Bungey et al. 1994; Padaratz and Forde 1995). Figure 3.8.5 summarizes results obtained using a 1 GHz hand-held antenna. In these experiments, the reinforcing bars were placed in a tank filled with an oil/water emulsion that was formulated to simulate the dielectric properties of concrete. It is seen that for cover depths up to approximately 6 in. (150 mm), the minimum spacing at which individual bars can be discerned increases with increasing cover depth. For cover depths greater than 6 in. (150 mm), the minimum spacing is unaffected by cover depth and depends primarily on bar size (Bungey et al. 1994).

Closely-spaced bars will also prevent detection of features below the layer of reinforcement. This masking effect depends on the wavelength of the electromagnetic waves, the bar size, and cover depth. For the 1 GHz hand-held antenna, No. 10 (32 mm) bars at cover depths of 1 to 2 in. (25 to 50 mm) will prevent detection of underlying features when bar spacings are less than 8 in. (200 mm) (Bungey et al. 1994).

Simple methods do not exist to determine bar size from line scan output. Researchers have attempted to better understand the interactions of radar with cracks, voids, and reinforcing bars (Mast et al. 1990; Utsi 2003). The objective of these studies is to develop procedures to use the recorded data to construct an image of the interior of the concrete. A commercially available radar system that uses multiple antennae to generate three-dimensional (3D) data from a single pass is available. Considerable advances in signal processing have been made. The major radar manufacturers have developed powerful tomographic 3D imaging software, based on multiple passes, to assist in the overall interpretation of the radar survey.

The depth of concrete that can be effectively surveyed depends to some extent on the required resolution (hence, frequency used). Generally, a thickness of 16 to 30 in. (400 to 750 mm) can be surveyed, depending on the nominal antenna frequency and the moisture content of the material. Discontinuities, such as voids, that reflect a large proportion of the energy, will also limit the depth that can be surveyed. Table 3.8.5a lists the likely penetration range of different antennae based on experience. Note that it is unlikely that one would use a frequency below 500 MHz on concrete unless it were a massive structure such as a concrete dam

Due to complexities in using radar to test reinforced concrete, standardized test procedures for detection of flaws generally noted in concrete construction do not exist. However, ASTM standards have been developed (ASTM D4748) to measure the thickness of the upper layer of a multi-layer pavement system and the thickness of asphalt overly. Basically, the technique involves measuring the transit time of the pulse through the pavement layer, and using relationships similar to Eq. (3.8.2b) and (3.8.2c) to calculate the layer thickness. The procedure in ASTM D4748

is based on using a noncontact horn antenna, and some modifications are required for measurements with a contact antenna. The calculated depth depends on the value of the relative dielectric constant. Errors in the assumed value of the relative dielectric constant can lead to substantial inaccuracies in depth estimations (Bungey et al. 1994; Padaratz and Forde 1995). For data obtained with a horn antenna, the relative dielectric constant of the concrete can be computed directly from the amplitude of the surface reflection in the radar signals. For data obtained using a contact antenna, it is necessary to take occasional cores to correlate the actual depth and the corresponding dielectric constant value for the pavement materials. The user is cautioned against using this method on saturated concrete because of the high attenuation and limited penetration of the pulse. In ASTM D4748, it is stated that inter-operator testing of the same materials resulted in thickness measurements within ±1/4 in. (±5 mm)

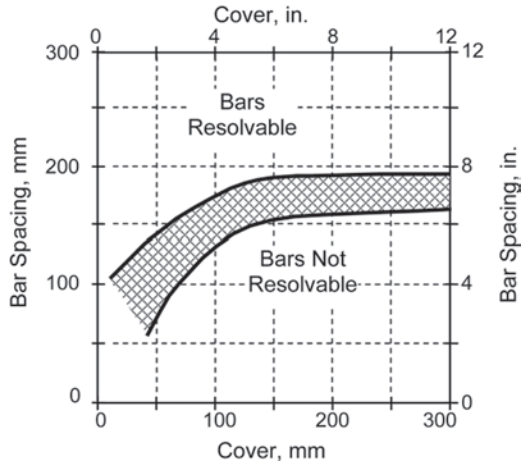

Fig. 3.8.5—Minimum spacing at which individual reinforcing bars can be resolved (adapted from Bungey et al. [1994]).

Table 3.8.5a—Typical penetration depths as a function of the antenna frequency

Depth, ft (m)	Center frequency, MHz
1 to 1.6 (0.3 to 0.5)	1500
1.6 to 3.3 (0.5 to 1)	1000
3.3 to 6.6 (1 to 2)	500
6.6 (2+)	200
23 (7.0)	100

of the actual thickness. Finally, the ASTM standard notes that reliable interpretation of received signals can only be performed by an experienced radar data analyst.

The detection of delaminations in reinforced bridge decks using radar is not straightforward. In studies by Maser and Roddis (1990), it was found that a 1/8 in. (3 mm) air gap in concrete produced little noticeable effect in the received waveform. However, the addition of moisture to the simulated crack resulted in stronger reflections that could be noticed in the waveform. It was also found that the presence of chlorides in moist concrete resulted in high attenuation because of the increased conductivity due to chloride ions (Eq. 3.8.2e). Thus, the ability to detect delaminations will depend on the in-place conditions at the time of testing. In addition, because the reflections from reinforcing bars are much stronger than from a delamination, it is difficult to detect the delamination in the presence of reinforcing bars. ASTM D6087 describes a procedure for evaluating the condition of asphalt-covered concrete bridge decks.

The properties of concrete, as revealed by the radar data, are generally inferences based on the connection between dielectric properties and real conditions of interest. The dimensions of concrete, such as thickness and reinforcing bar depth, can generally be revealed with greater accuracy than properties such as moisture content, chloride content, delamination, and other forms of deterioration, which should be confirmed by exploratory drilling or excavations at key locations. Due to the large number of physical properties affecting the received signal, current application to structural concrete (other than measurements of the spatial configuration of concrete and reinforcement) is restricted mainly to qualitative comparative uses. The advantages and limitations of radar are summarized in Table 3.8.5b.

CHAPTER 4—PLANNING AND PERFORMING NONDESTRUCTIVE TESTING INVESTIGATIONS

4.1—Selection of methods

Chapter 3 reviewed the principles and highlighted the advantages and limitations of well-known nondestructive test (NDT) methods for evaluation of concrete and reinforcement in structures. However, the list of available methods to determine a concrete structural property or to assess structural conditions is rapidly expanding. Based on reliability, simplicity, and economy, some methods or techniques are preferable over others.

Table 3.8.5b—Advantages and limitations of radar

Advantages	Limitations
Noncontact antennas permit high-speed scanning. Very sensitive to presence of embedded metal objects. Ability to penetrate across concrete-air interfaces. Sensitive to the presence of moisture and chlorides.	Region irradiated by the antenna is limited to cone-shaped volume directly below antenna. Congested reinforcement can prevent penetration beyond the reinforcement. Cracks and delaminations are not easy to detect unless moisture is also present in the cracks or region of the delamination. Pulses from high-resolution antennae have limited depth of penetration (12 to 20 in. [300 to 500 mm]). The behavior of electromagnetic pulses propagating through reinforced concrete structures is not completely known. Experienced operator required to operate equipment and interpret results. Large amounts of data obtained during scans.

In 4.1, primary and secondary methods are suggested to determine particular properties or to evaluate particular conditions. A primary method indicates the preferred method. A secondary method indicates an acceptable method that typically would require a greater level of experience to implement, be less reliable, or less rapid. The method chosen should be tailored to the objective of the evaluation. NDT methods can be valuable tools, but a given technique may not be the most practical or yield the most applicable results in all cases. Often, the most sensible and effective approach is to apply a variety of NDT techniques jointly to obtain complementary information.

4.1.1 *Concrete material properties*—Table 4.1.1 summarizes the suggested NDT methods to determine various material properties of hardened concrete. Some of these methods require cores or other types of concrete samples for laboratory testing to establish correlations between the desired concrete property and the NDT results. Others may also be appropriate for testing laboratory-prepared specimens, or for acceptance testing of field concrete. ASTM standard test methods, or other relevant documents, are noted where appropriate.

4.1.2 *Structural properties and conditions*—Table 4.1.2 summarizes selected NDT methods for determining structural properties and conditions. Information derived from conducting these tests is important in evaluating the integrity of a concrete structure, for it can be used to assess remaining service life or to develop strategies for repair and strengthening.

4.1.3 *Evaluation of repairs*—Table 4.1.3 summarizes selected methods that are used to evaluate the effectiveness of repairs. This type of testing is important to ensure consistent quality throughout a repair project. In some circumstances, the results from these tests may be used to determine payment under a contract.

4.1.4 *Personnel qualifications*—With most of the NDT techniques described in this report, the evaluation investigator is attempting to assess a property of concrete or changes in that property caused by the presence of a defect or discontinuity. From that information, the investigator infers the nature of the defect and its severity; reliable results often require a high degree of judgment by the evaluation investigator, supported by a limited amount of corroboration by coring or other forms of direct examination. This judgment should come from those who are knowledgeable about the physics of the NDT method they are using and have sufficient experience in the use of the method and the investigation of structures, which will allow them to accurately interpret NDT results.

In many cases, the investigation requires preliminary interpretation in the field as the testing is in progress. This is necessary to allow the investigator to plan and modify the program on the basis of the results that are recorded to obtain sufficient data at appropriate locations. Therefore, it is usually advisable not to delegate the field investigation and data acquisition to less experienced personnel, unless the lead evaluation investigator is confident that sufficient data of the required quality will be obtained.

4.2—Defining scope of investigation

After the appropriate nondestructive test (NDT) methods are selected, decide the scope of the investigation. This is one of the most difficult aspects of the evaluation process. Ideally, it is important to conduct sufficient testing that guarantees assurance that all important defects or anomalies are detected. In most situations, the amount of testing is limited by the available funds and time constraints, and the evaluation investigator has to design a testing scheme that will yield the most information. The experience of the investigator is critical for designing a successful testing scheme. The investigator should not only understand the inherent capabilities and limitations of the chosen methods, but also understand concrete construction, structural behavior, and deterioration mechanisms. Knowledge of concrete construction is helpful in anticipating the most likely locations of internal anomalies. Knowledge of structural behavior is valuable in selecting portions of the structure most vulnerable to the presence of defects. Knowledge of deterioration mechanisms is important in deciding what should be measured.

4.2.1 *Statistical considerations*—Because of the variety of situations that may be encountered, it is difficult to define a sampling scheme that would be applicable to all NDT methods and all investigations. Global techniques, such as infrared thermography, can be used to inspect the entire exposed surface of a structure. Other scanning techniques, such as ground-penetrating radar, can provide complete inspection along each scan line. Point-by-point tests, such as impact-echo, provide information at the test point. Other methods, such as impulse-response, can provide information about an entire structural element.

ASTM C823/C823M can be adapted to provide some guidance on planning the sampling program. Sampling situations can be assigned to two categories:

1. Where preliminary investigation and other information indicate that conditions are similar throughout the structure
2. Where preliminary investigation and other information indicate that conditions are not similar throughout the structure, the structure is divided into portions within which conditions are similar

For the first category, sampling locations should be distributed randomly or systematically over the region of interest. According to ASTM C823/C823M, any method for determining sampling locations may be employed, provided the locations are established without bias. The intent is to select sampling locations in a manner that allows all locations an equal probability of being selected.

For the second category, each portion that appears to be of similar condition should be sampled independently and treated as a different category, unless and until test results reveal no significant differences.

For point-by-point tests intended to find internal defects, the statistical concepts of quality-control testing may be adapted to select the sample size. For example, a grid of points could be laid out on the surface of the structure. The grid spacing would depend on the smallest defect that the evaluation investigator wishes to detect.

Table 4.1.1—Nondestructive test methods for determining material properties of hardened concrete in existing construction

Property	Method		Comment
	Primary	Secondary	
Compressive strength (ACI 228.1R)	Cores for compression testing (ASTM C42/C42M and C39/C39M); pullout testing (post-installed) (ASTM C900)	Penetration resistance (ASTM C803/C803M)	Strength of in-place concrete; comparison of strength in different locations
Relative compressive strength	Rebound number (ASTM C805/C805M); (UPV) (ASTM C597)	In-place pulloff test (ACI 503.1R: BS 1881-207) with appropriate calibration.	Rebound number influenced by near surface properties; UPV gives average result through the thickness
Tensile strength	Splitting tensile strength of core (ASTM C496/C496M)	In-place pulloff test (ACI 503.1R; ACI 228.1R; BS 1881-207)	Assess tensile strength of concrete
Density	Relative density (specific gravity) of samples (ASTM C642)	Nuclear gauge (ASTM C1040/C1040M)	—
Moisture content	In-place moisture probes (ASTM F2170) Preinstalled fiber optic relative humidity sensors	Nuclear gauge (ASTM C1040/C1040M); moisture content by drying (ASTM C642)	—
Static modulus of elasticity	Compression test of cores (ASTM C469/C469M)	—	—
Dynamic modulus of elasticity	Resonant frequency testing of sawed specimens (ASTM C215)	Ultrasonic pulse velocity (ASTM C597); impact-echo; SASW)	Requires knowledge of density and Poisson's ratio (except ASTM C215); dynamic elastic modulus is typically greater than the static elastic modulus
Shrinkage/expansion	Length change of drilled or sawed specimens (ASTM C341/C341M)	—	Measure of incremental potential length change
Resistance to chloride penetration	90-day ponding test (AASHTO T259; ASTM C1543) permit ion migration test	Electrical indication of concrete's ability to resist chloride ion penetration (ASTM C1202)	Establish relative susceptibility of concrete to chloride ion intrusion; assess effectiveness of chemical sealers, membranes, and overlays
Air content; cement content; and aggregate properties (scaling; alkali-silica reactivity; freezing-and-thawing susceptibility)	Petrographic examination of concrete samples removed from structure (ASTM C856 and ASTM C457/C457M); cement content (ASTM C1084)	Petrographic examination of aggregates (ASTM C294, C295/C295M)	Assist in determination of cause(s) of distress; degree of damage; quality of concrete when originally cast and current
Alkali-silica reactivity (ASR)	Cornell/SHRP rapid test (SHRP-C-315); petrography		Establish in field if observed deterioration is due to ASR
Carbonation, pH	Phenolphthalein (qualitative indication); pH meter Fiber optic pH sensors embedded in concrete	Other pH indicators (for example, litmus paper)	Assess corrosion protection value of concrete with depth and susceptibility of steel reinforcement to corrosion; depth of carbonation.
Fire damage	Petrography; rebound number (ASTM C805/C805M)	SASW; UPV; impact-echo; impulse-response	Rebound number permits demarcation of damaged surface
Freezing-and-thawing damage (in-place)	Petrography	SASW; impulse-response; UPV	—
Chloride ion content	Acid-soluble (ASTM C1152/C1152M) and water-soluble (ASTM C1218/C1218M)	Specific ion probe (SHRP-S-328)	Chloride ingress increases susceptibility of steel reinforcement to corrosion
Air permeability	SHRP surface airflow method (SHRP-S-329) Torrent (1992) and autoclam air-permeability tests	—	Measures in-place permeability index of the near-surface concrete: within 0.6 in. (15 mm)
Electrical resistance of concrete	AC resistance using four-probe resistance meter (FSTM 5-578)	SHRP surface resistance test (SHRP-S-327)	AC resistance useful for evaluating effectiveness of admixtures and cementitious additions; SHRP method useful for evaluating effectiveness of sealers
Water absorption (sorptivity)	ISAT, Figg, covercrete, or autoclam sorptivity tests	—	In-place moisture content considered for interpreting the data

Table 4.1.2—Nondestructive test methods to determine structural properties and assess conditions of concrete

Property/Condition	Method		Comment
	Primary	Secondary	
Reinforcement location	Covermeter; ground- penetrating radar (GPR) (ASTM D4748)	X-ray and γ-ray radiography	Steel location and distribution; concrete cover
Concrete component thickness	Intrusive probing impact-echo (I-E) (ASTM C1383); GPR (ASTM D4748)		Verify thickness of concrete; provide more certainty in structural capacity calculations; I-E requires knowledge of wave speed and GPR of dielectric constant in place of specific calibration to known thickness on site
Steel area reduction	Intrusive probing; ultrasonic thickness gauge (requires direct contact with steel)	Radiography	Observe and measure rust and area reduction in steel; observe corrosion of embedded post-tensioning components; verify location and extent of deterioration; provide more certainty in structural capacity calculations
Local or global strength and behavior	Load test, deflection, or strain measurements	Acceleration, strain, and displacement measurements	Ascertain acceptability without repair or strengthening; determine accurate load rating
Corrosion potentials	Half-cell potential (ASTM C876)	—	Indication of likelihood of corrosion activity
Corrosion rate	Linear polarization (SHRP-S-324 and SHRP-S-330)	—	Corrosion rate of embedded steel; rate influenced by environmental conditions
Location of delaminations, voids, and other hidden defects	Impact-echo; infrared thermography (ASTM D4788); impulse-response; radiography; GPR (ASTM D6087); sounding (ASTM D4580)	Pulse echo, UPV, intrusive drilling, and borescope	Assessment of reduced structural properties; extent and location of internal damage and defects; sounding limited to shallow delaminations

Table 4.1.3—Nondestructive test methods for evaluating repairs

Property/ Condition	Method		Comment
	Primary	Secondary	
Bond strength	Pulloff test (ASTM C1583/ C1583M), CAN/ CSA A23.2; BS 1881-207	—	—
Bond quality (absence of voids at interface)	Pulloff test (as above)	Impact-echo; impulse-response	—
Injection of cracks or voids	Ultrasonic pulse velocity	Impact-echo	Proper geometry required for reliability of UPV

ASTM E122 gives the following relationship for selecting the sample size to estimate the fraction of a lot that is defective

$$n = \left(\frac{k}{E}\right)^2 p_o(1-p_o) \qquad (4.2.1)$$

where n is the sample size; k is the statistical factor based on the risk that the estimated fraction defective does not differ from the true fraction by more than $\pm E$, (k = 1.960 for a risk of 0.05 and 1.645 for a risk level of 0.10); E is the maximum acceptable error between true fraction that is defective and the estimated fraction based on the sample; and p_o is the advance estimate of fraction defective.

Note that to use Eq. (4.2.1), an initial estimate of the fraction defective is necessary because the number of samples depends on this value. Figure 4.2.1 shows plots of Eq. (4.2.1) for values of the acceptable error E equal to 0.05, 0.075, 0.10, and 0.15 and for two risk levels. Figure 4.2.1(a) is for a risk level of 0.10, and Fig. 4.2.1(b) is for a risk level of 0.05. The figures show that the sample size is affected greatly by the maximum acceptable error E. It is also seen that the largest sample size is needed when the true fraction defective equals 0.5. Thus, one possible approach is to select a maximum sample size based on an assumed value of p_o = 0.5, and use a two-stage sampling procedure to perform the testing. In this case, a portion of the required maximum sample size is used to establish an estimate of the fraction defective. With this estimate, a revised sample size is computed using Eq. (4.2.1), and additional tests are performed so that the cumulative number of tests equals the revised sample size. For two-stage sampling, it is suggested that the first sample size be 50 to 70 percent of the maximum size or at least 30 samples (Natrella 1963). Random sampling should be used to select the actual test points on the structure.

The choice of sample size based on statistical principles should be tempered with consideration of price. ASTM E105 states, "No matter how sound a given sampling plan is in a statistical sense, it is not suitable if the cost involved is prohibitive or if the work required is so strenuous that it

leads to short cuts or subterfuge by those responsible for sampling."

ASTM E122 also addresses price considerations and offers recommendations:

> After the required size of sample to meet a prescribed precision is computed..., the next step is to compute the cost of testing this size sample. If the cost is too great, it may be possible to relax the required precision (or the equivalent, which is to accept an increase in the probability that the sampling error may exceed the maximum allowable error *E*) and to reduce the size of the sample to meet the allowable cost.

Williams et al. (2006a,b) discuss the use of random, stratified, and adaptive sampling methods for planning NDT investigations of large concrete structures. Case studies are presented to illustrate the performance of different sampling plans. From limited studies, it appears that random sampling produced the narrowest confidence intervals for proportion of flawed locations; but Williams et al. note that access and price considerations may not always allow random sampling.

4.2.2 *Practical considerations*—For an evaluation program that includes NDT to be justifiable, it should satisfy as many of the following requirements as possible:

a) Approximate the price of an intrusive testing program alone for the same area or volume tested

b) Provide a larger amount of reliable data for the same area or volume examined, thereby yielding more information

c) Include areas that are difficult to examine thoroughly using more traditional or intrusive methods

d) Include reproducible recovered data so that future surveys of the same structure can rely with confidence on the initial NDT data as a base reference

4.2.2.1 *Cost criteria*—It is desirable that a structural condition survey produces a necessary amount of information for a given investment. With limited available funds, the owner or facility manager is faced with a pressing problem that has to be solved thoroughly and quickly with constrained outlay. The evaluation investigator has to recognize conflict or project funding could be jeopardized.

Some practical problems can only be resolved using a combination of intrusive testing and NDT. Condition surveys using visual observation and intrusive sampling and testing alone largely rely on the experience of the investigator to interpret the concrete condition by interpolating between intrusive test points. Usually, a number of core samples at a predetermined sampling density are selected, accompanied by laboratory tests on the cores. This establishes a preliminary cost base for the condition survey.

Nondestructive testing as an alternative to this approach usually proposes a reduction in the number of core samples taken, and fills in the areas between the core samples with NDT at a greater test density. This reduces the uncertainty inherent in the visual and intrusive sampling survey. Reduction in intrusive sampling, together with the speed of most NDT programs, maintains the field survey price at a similar level. Analysis time, however, is usually increased.

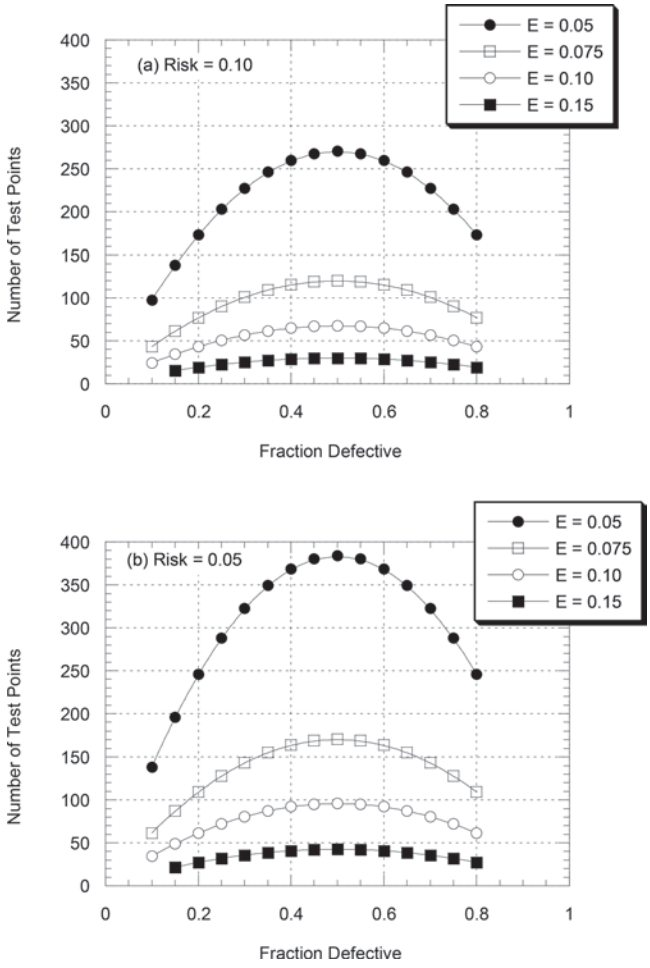

Fig. 4.2.1—Number of test points to estimate fraction defective within an error band of ±E *at risk levels of: (a) 0.10 and (b) 0.05.*

4.2.2.2 *Data density*—The aforementioned price issues imply that nondestructive surveys provide greater test data density than visual and intrusive surveys. It is usually necessary to interpolate the concrete condition between test points in an NDT survey because with most NDT procedures, it is not feasible to test the entire surface of concrete in the structure due to price and time considerations. Table 4.2.2.2 shows examples of test density (spacing between test points) used in typical NDT investigations with different test methods. The ideal test density represents desirable spacings to achieve a statistically valid assessment of the concrete condition; practical density represents spacings used to achieve a balance between statistical rigor and price.

Different testing techniques serve differing purposes, and each test type does not return the same amount of information for the same area or volume of concrete tested. As an example, an impact-echo test on a concrete slab with several layers of steel reinforcement provides information about changes in concrete interface properties immediately below the test point only. The interpretation of the continuity of the detected interfaces between adjacent test points is made subjectively by the evaluation investigator using available knowledge of the slab details and construction history as well

Table 4.2.2.2—Frequency of testing for some representative NDT methods

Test method	Ideal test density	Practical test density	Remarks
Through-transmission pulse velocity	1 to 2 ft (0.3 to 0.6 m) grid	3 to 5 ft (1 to 1.5 m) grid	Typical spacing to check for concrete density and honeycombing
Rebound hammer (one side of wall or slab)	1 to 2 ft (0.3 to 0. 6 m) grid	3 to 5 ft (1 to 1.5 m) grid	Spacing used to assess fire-damaged walls
Impulse-response	1 to 2 ft (0.3 to 0. 6 m) grid	3 to 10 ft (1 to 3 m) grid	Typical spacing used in assessment of chimney stacks, cooling towers, and silos

as personal experience. In contrast, a radar survey across the top of the same slab will give a nearly-continuous image of the uppermost steel layer, but will yield little information about the conditions at the lower reinforcement layers.

4.2.2.3 *Areas with difficult access*—Many concrete structures present access difficulties for programs combining visual inspection and intrusive testing. Examples of such difficult inspection situations include:

a) Retaining walls, grade beams, and slabs-on-grade, where only one side of the element is accessible

b) Deep foundations (piles, drilled shafts, and slurry walls), where nearly all the element is buried

c) Concrete elements located in hazardous areas, such as hazardous material waste tanks and nuclear sites

Nondestructive testing in these cases is often the only economically and practically viable way to obtain sufficient concrete condition information. Several publications refer to the successful application of NDT to these problems and give recommendations for the test types to be used (Davis 1995; Davis and Hertlein 1997).

4.2.2.4 *Data reliability and repeatability*—The data collected should be reliable and repeatable. This implies that:

a) All points tested on the structure can be easily identified at a later date so that tests can be repeated if necessary at the exact test location at any time in the future.

b) The test results in the preliminary survey should be in such a format (for example, graphs and numerical data) that direct comparisons can be made between the original and subsequent test results, which is facilitated by storage of raw test data on computer disks.

c) The investigator should have the statistical confidence in the reproducibility of each test result.

4.3—Numerical and experimental simulations

Many nondestructive test (NDT) methods are based on interactions of certain types of waves (stress or electromagnetic) with the internal structure of the element being tested. For some conditions, the interactions are relatively simple and tests results are easy to interpret. For example, delaminations in slabs or walls can be detected with relative ease using the impact-echo method, or reinforcing bars with shallow cover and wide spacing are located easily with a covermeter or ground-penetrating radar (GPR). However, the evaluation investigator may be faced with complex situations for which the expected responses are not known. In such cases, the investigator should consider performing numerical or experimental simulations before planning the field investigation.

Numerical simulation refers to computing the expected response of the test object to a specific type of test. Experimental simulation refers to constructing mockups with simulated flaws and testing them with the proposed test method. The simulations can have three objectives:

1. To establish whether a given method is capable of detecting the anomaly of interest
2. To establish unflawed responses for use as baseline to compare with flawed responses
3. To determine the critical size at which detection of a flaw becomes uncertain

In addition, numerical simulation can be used in conjunction with measured response to infer the internal conditions of the structure. This is usually called solving the inverse problem. Ideally, the measured response for the internal conditions or material properties of the concrete are electronically documented. Unfortunately, this is impossible except for in the simplest conditions. Thus, the inverse problem is often solved by iteration, which is when the theoretical response is calculated for a given assumed set of conditions and compared with the measured response. The assumed conditions are varied until there is acceptable agreement between the measured and calculated response. With no assurance that a unique set of conditions corresponds to the measured response, the analyst requires an understanding of reasonable values for the assumed conditions.

4.3.1 *Numerical simulation of stress-wave propagation*—Since the 1970s, computer programs based on the finite-element method (FEM), the finite-difference method, and the elastodynamic finite integration method were developed to solve complex dynamic problems involving impact- and wave-defect interaction. Those types of programs have been adapted for simulating stress-wave propagation in impact-based NDT methods, such as application of FEM for the impact-echo method (Sansalone and Carino 1986). A brief description follows of the basics of this simulation method (Sansalone and Streett 1997).

FEM is one numerical technique for obtaining approximate solutions to problems in continuum mechanics. A continuum (in this case, a concrete structure with or without simulated defects) is divided into a finite number of discrete parts (finite elements) that are interconnected at points called nodes. Equations relating the stresses and strains for the individual elements are combined to construct global equations that describe the behavior of the entire continuum. Solutions of these equations give the displacements or stresses for each element for a particular set of boundary conditions and applied loads. In stress-wave propagation analyses, the calculations are carried forward in small-time steps, and time histories of nodal displacements and element stresses are obtained.

The impact is simulated by applying a pressure loading over several elements. The pressure is assumed to vary with time as a half-cycle sine curve, approximating the force-time function associated with the impact of a sphere on the surface of an elastic solid. Impacts of different durations are obtained by changing the period of the half-cycle sine curve. The concrete is modeled as a linear elastic homogeneous material. This assumption is valid because

a) The strains produced by the stress waves in impact-echo testing are very small

b) The frequency components in the propagating waves are typically less than approximately 80 kHz and the smallest wavelengths are approximately 2 in. (50 mm). At these wavelengths, concrete appears homogeneous to the propagating waves

Defects (voids or cracks) can be represented by omitting elements in the finite-element mesh used to model the test object, or elements may be assigned much lower values of density and elastic modulus. Absorbing boundaries can be used to allow the analyst to model portions of larger structural members. Greater accuracy, less computational time, or both, are the result. Without such absorbing elements, finite-element models should be sufficiently large that the responses due to reflections from the boundaries do not interfere with reflections from the simulated defects.

Finite-element simulations require an individual experienced in the FEM and familiarity with the nature of programs that solve wave propagation problems. Validity of the results hinges on using acceptable mesh geometry, choosing the correct time step and other measures to assure stable calculations (if explicit codes are used) and accurate results, specifying the correct loading and boundary conditions, and correct simulation of the defect to be investigated.

Once the correct model has been developed, the calculated displacement of a node close to the impact point is treated as the transducer signal and used to calculate the amplitude spectrum. Parametric studies can be performed by varying factors:

a) Duration of the impact

b) Location of the impact point and receiver relative to the location of the defect

c) Size and location of defect

d) Other parameters

Some examples of results obtained by finite element simulations can be found in Cheng and Sansalone (1993), Lin and Sansalone (1992a,b,c), Lin and Sansalone (1993, 1994a, 1996), Sansalone et al. (1997), and Williams et al. (1997).

The following example is taken from the work summarized in Jaeger et al. (1996) and involves detecting a void in the grouted tendon duct of a post-tensioned concrete structure. A three-dimensional (3D) numerical model was used to represent the geometry. Figure 4.3.1a shows the geometry and an amplitude spectrum obtained from the finite-element simulation. The secondary peak at 26.4 kHz corresponds to reflection from the air void in the ungrouted duct. The peak at 4.4 kHz is less than the thickness frequency of the solid plate. The presence of the air void causes the shift to a lower frequency, and this frequency shift is an additional indicator

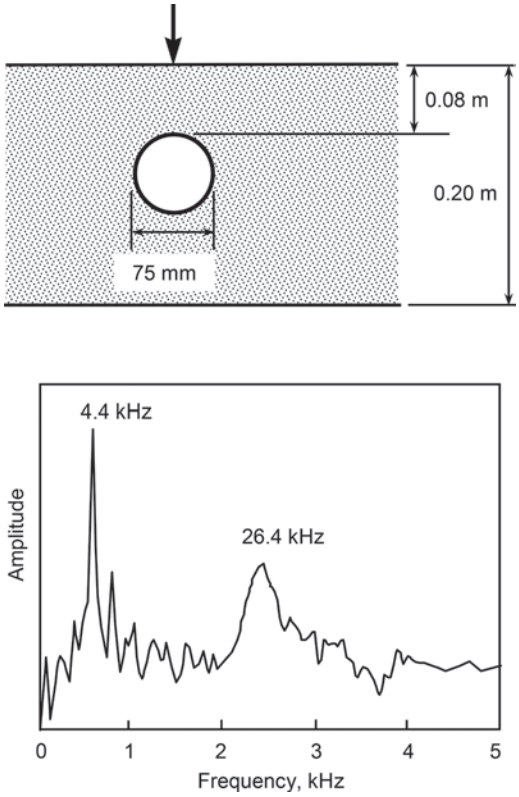

Fig. 4.3.1a—Spectrum obtained from finite element simulation of impact-echo test on concrete section containing ungrouted duct. (Note: 3.3 ft = 1 m; 1 in. = 25.4 mm.)

of an anomaly in the plate (Jaeger et al. 1996). Figure 4.3.1b shows the result from an impact-echo test performed on the web of an I-beam in a post-tensioned bridge. All key features of the responses are similar, and the overall agreement between the numerical simulation and field test is excellent. (Note that the P-wave speed in the numerical model and actual beam were the same.) Such results are typical, and the FEM has served as a powerful tool in developing the current understanding of the impact-echo method and its applications.

4.3.2 *Simulation of wave propagation in deep foundations*—Numerical techniques have been used to study wave propagation in deep foundations to:

a) Match predicted responses with real test responses for either sonic-echo or impulse-response methods

b) Model pile behavior for use in the impedance-logging analytical method

Interpretation of low strain pile testing is based on the theory of one-dimensional (1-D) stress-wave propagation within the pile shaft. After the shaft head is struck with a hand-held hammer, a low strain stress wave travels down the shaft at a velocity that depends on the density and elastic modulus of the concrete. Any change in the shaft's shape, continuity, or material properties results in changes in the shaft impedance at the point of the anomaly, and a portion of the incident wave is reflected back to the pile head. Interpretation of the test response depends on the quality of the recorded signals as well as identification of the parameters controlling the pile response, such as soil conditions, pile

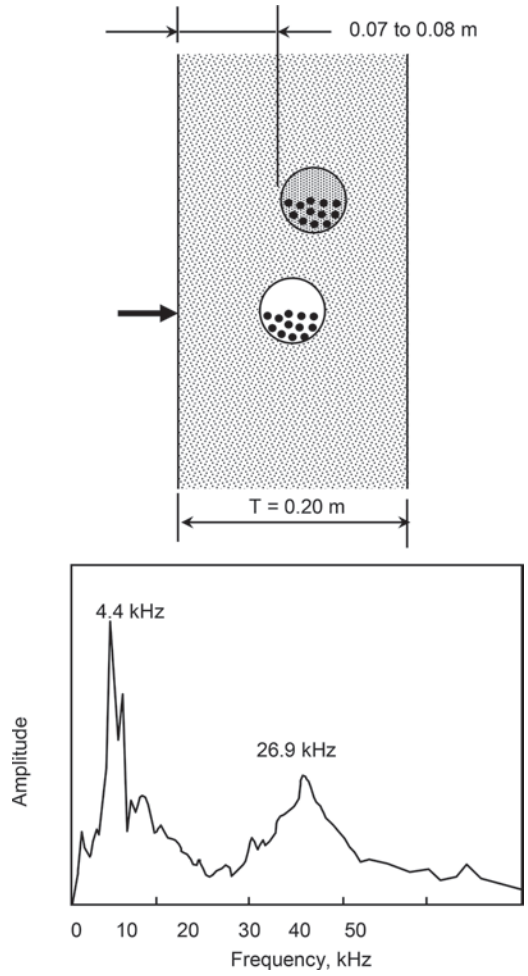

Fig. 4.3.1b—Spectrum obtained from impact-echo test carried out over ungrouted duct in post-tensioned beam. (Note: 3.3 ft = 1 m.)

size, and shape. Therefore, the result of simulation matching is only as good as the quality of the real test signal.

4.3.2.1 *Impulse-response*—The first reference to simulation models using numerical techniques is in Davis and Dunn (1974), where a numerical model was developed for harmonic vibration testing (forerunner of impulse-response) of drilled shafts. Based on the analogy between the equations of motion and those of an electrical circuit, an analog electrical circuit model was used to represent the pile response. The force applied to the pile head was represented by an applied sinusoidal current and the resulting voltage represented the pile head velocity. Other electrical components were used to account for the density of the concrete and of the soil, the wave speed in the concrete and in the soil, and the diameter of the pile. The pile was divided into different segments, with different mechanical characteristics, that were converted to the equivalent analog circuits. The computed response of the circuit was compared with the measured response (velocity/force) and the characteristics of the segments were adjusted until there was good agreement between the two responses. This process is analogous to the inversion procedure used in the spectral analysis of surface wave (SASW) test.

The analyst should prepare as much information as can be obtained about the real pile and soil conditions before attempting the simulation. This helps reduce the number of steps required to obtain a matching fit between the real and simulated mobility-frequency plots. Typical values of material properties that can be used as a first try are:

a) Concrete bar wave (C_b) velocity from 12,500 to 13,500 ft/s (3800 to 4100 m/s)

b) Concrete density from 144 to 150 lb/ft^3 (2300 to 2400 kg/m^3)

c) Soil density from 106 to 119 lb/ft^3 (1700 to 1900 kg/m^3)

d) Shear-wave velocity in soil from 330 to 990 ft/s (100 to 300 m/s)

Errors in estimated depths of anomalies or pile toe arise principally from error in the estimation of the concrete pile stress-wave velocity. An error of ±330 ft/s (±100 m/s) will result in a depth error of approximately ±2.5 percent.

4.3.2.2 *Sonic-echo tests*—Simulation of velocity-time waveforms from sonic-echo pile tests became practical with the advent of digital signal processing techniques in the 1980s (Middendorp and Reiding 1988). Reflections recorded in a sonic-echo signal are caused by impedance changes in the pile shaft (necks, bulges, cracks, pile tip, or changes in concrete quality), and in soil resistance. All changes in shaft impedance are modeled as variations in shaft cross section. Gather as much information as possible about the site soil profile to simulate the response waveform.

The matching of sonic-echo test signals is performed in three steps:

1) A reference pile response for a given pile population at the site is selected by testing the pile population and selecting an average response.

2) The shaft and toe resistances are derived for the reference pile. Because the shaft and toe resistances have a dominant effect on the test response, the derivation of the soil model is a prerequisite. To obtain the soil parameters, it is assumed that the reference pile has a uniform diameter. It is necessary to use as much information as is available about the site soil conditions at the beginning of this step. The shaft and toe resistances are adjusted until there is a good match between the measured and simulated signals.

3) The discontinuities in the pile under simulation are derived. Discontinuities cause reflections that are displayed in the sonic-echo waveform. By measuring the travel time for the arrival of the first reflection, the location of the discontinuity can be determined. In the two most frequently used methods (Rausche et al. 1988; Starke and Janes 1988), the impact force is applied as the input to the pile head in the computer model, and the measured velocity at the pile head is taken as the reference signal for the calculated response. The cross section of the computer model shaft is varied at the signal reflection location until a good match is found between the calculated and the measured signals.

In these simulations, the pile is modeled as a series of springs and dashpots to represent the pile cross section and the effect of the surrounding soil. As when modeling the impulse-response test, the analyst requires as much information as possible about the real pile and soil conditions before

attempting a sonic-echo simulation. The most commonly used simulation methods are proprietary to the equipment manufacturers and are sold with their own testing systems. However, if good-quality sonic-echo test signals can be obtained, it is possible to develop response simulations using the approach outlined previously for the impulse-response method. Again, as in the impulse-response simulation, the selected value of the concrete stress-wave velocity is critical in accurately predicting depths of features.

4.3.2.3 *Impedance-logging analysis*—The impedance-logging technique (refer to 3.3.3) is, in essence, an extension of the matching of measured impulse-response test results described previously. To obtain an impedance log profile, the following steps are necessary:

a) Good-quality test signals should be obtained, including both the force and the velocity responses in the time domain. Minimum sampling rate for most shaft lengths studied should be 10 kHz, with a minimum of 1024 data points for each waveform. A reflected signal from the pile tip should also be present in the velocity waveform.

b) The first analytical step is to remove the following from the velocity waveform: 1) the motion of the top of the shaft caused by the hammer impact; and 2) the effects of the impedance changes resulting from changes in soil profile. This is achieved by calculating a theoretical mobility plot for an infinitely long, defect-free shaft with the nominal shaft diameter and known lateral soil variations. This computed mobility plot is subtracted from the test response. This gives a reflected mobility response containing information about changes in the shaft geometry and in the surrounding soil. Next, the impulse response in the time domain is calculated by taking the inverse fast Fourier transform (FFT) of the reflected mobility plot. This is called a relative reflectogram, which contains the time history of the reflections that return to the top of the shaft.

c) By applying a selected amplification function to this calculated time response, the return signal strength can be approximated to a constant value down the entire length of the pile shaft.

d) The reflectogram so obtained does not quantify the absolute shaft impedance, nor does it distinguish between changes in impedance caused by shaft conditions or those caused by lateral soil variation. The real impulse-response test result, however, does quantify the shaft impedance at the pile head that can be used to calculate the impedance down the shaft as a function of time from

$$Z(t) = Z(0)\exp\left(2\int_0^t R(t)dt\right) \qquad (4.3.2.3)$$

where $Z(t)$ is the the shaft impedance as a function of time; $Z(0)$ is the the nominal impedance at the top of the shaft; and $R(t)$ is the reflection coefficients from the scaled relative reflectogram.

e) Finally, the impedance as a function of depth is obtained from $Z(t)$ by converting time-to-depth using the compression wave velocity of the pile material. As in simulation of both the impulse-response and sonic-echo methods, if the unit weight and compression wave velocity of the pile are known, changes in impedance correspond to changes in the cross-sectional area of the pile. The resulting impedance-depth plot, which can be drawn as a plot of either diameter or cross-sectional area with depth, is the final impedance log (Fig. 3.3.3.1).

As in other simulations of pile response, the analyst should have all available soil data and pile construction records to calculate the relative reflectogram.

4.3.3 *Simulation of ground-penetrating radar*—Numerical techniques can also be used to model the propagation of electromagnetic waves through concrete and to study the reflection and refraction of these waves at buried interfaces. Two modeling techniques used are the FEM and the ray-tracing method. In the finite-element technique, the same approaches are used as stress-wave propagation. The structure is modeled by a mesh of finite elements, with each element having dielectric properties to represent different materials. The electromagnetic field in the test object due to a specified input field is computed as a function of time. This method allows the analyst to visualize (by means of post-processing programs) the propagation of the field through the test object and how the field interacts with buried targets.

In the ray-tracing technique, the analyst chooses two points, where the electromagnetic pulse is introduced and where the response is to be calculated. A series of possible ray paths that can connect these two points is determined. The response associated with each ray is computed, taking into consideration the reflection coefficients at points of reflection and the attenuation due to travel distance. The responses due to the arrival of each ray at the point of interest are added together to obtain the total response that would represent the theoretical waveform recorded by a perfect receiver.

In addition to ray-tracing methods in the time domain, synthesis of the radar waveform may be accomplished by treating the reinforced concrete structures to be tested as a multilayered medium with regular cylindrical subsurface anomalies (reinforcing bars) (Halabe et al. 1995). A frequency-domain synthesis fully accounts for the multiple reflections and the frequency dependence of dielectric properties. Using the FFT, a transmitted electromagnetic pulse can be decomposed in the frequency domain into a number of sine waves with different frequencies. A closed-form solution for the complex reflection coefficient for a multi-layered medium and a single-frequency sine wave can then be used with superposition to synthesize the radar waveform for the multi-layer medium in the frequency domain. The presence of the reinforcing bars greatly affects the recorded radar waveform. The reinforcing bars can be treated as regular cylindrical subsurface anomalies with a uniform depth and spacing. Equations for the time-domain response for the reinforcing bar grid combined with the equations for the frequency-domain responses for the multi-layered medium are combined to obtain a synthetic waveform for a reinforced concrete structure based on geometric layout and physical properties. This waveform synthesis is sensitive to

the exact shape of the pulse emitted by a particular antenna. Using the radar waveform synthesis model, the effects on the radar waveform of various parameters such as porosity, water and chloride content, cracks and delaminations, and reinforcing bar layout can be assessed.

4.3.4 *Simulation of thermal anomalies*—Thermography directly senses emitted infrared radiation. Because there is no calibration to an absolute radiation level, the relative strength and location of the thermal anomalies are detected. Thermal response of concrete structural members may be numerically simulated using a finite element program with capabilities for transient heat-flow analysis. The concrete structure is modeled by a mesh of elements, with each element having thermal properties characteristic of the appropriate parts of the concrete structure. For example, a thermal model composed of a damaged zone with altered thermal properties layered between sound concrete zones can be used to model a delaminated concrete deck (Maser and Roddis 1990). The deck properties that should be specified are the thickness of the cover, delamination, and lower deck layers; the thermal conductivity and volumetric-heat capacity of the sound and damaged concrete; and the heat-transfer coefficients for the top and bottom of the deck. The environmental conditions of ambient temperature and incident solar radiation, both varying on a diurnal cycle, drive the thermal response of the model. Because the driving forces are a function of time, the system is not static. The system could be treated as if it were static if the deck response time to variations in the driving forces were short compared with the length of time the driving forces fluctuated. This condition for quasi-static behavior is not satisfied for the deck model because the thickness and volumetric heat capacity of the concrete give the deck significant thermal inertia, slowing the system's response time. The thermal model should therefore account for transient heat-flow behavior.

4.3.5 *Laboratory and field mockups*—A possible alternative to numerical modeling, when the evaluation investigator is faced with a new or unusual testing condition, is to fabricate and test specimens (mockups) that simulate the expected field conditions. It is possible to use portions of the actual structure as a mockup if it is certain that the tested area is sound or contains a flaw. Such experimental mockups can also be used to verify new numerical models. Like numerical simulation, mockups can be used to establish:

a) Whether a certain anomaly can be detected
b) The best testing configuration to detect a specific defect
c) The baseline response of an unflawed object

When NDT methods based on wave propagation are used, the specimens should be designed carefully to ensure that the boundary reflections do not interfere with reflections from the anomaly of interest. The material for the mockups should be selected so that it has properties similar to that expected in the field. Depending on the test method, similar properties may mean similar density, elastic constants, conductivity, or dielectric properties. For example, if the evaluation investigator is interested in evaluating the ability of different covermeters to detect individual reinforcing bars when there is a complex or congested layout, it is unnecessary to make concrete specimens. Because the response of covermeters is not influenced by the concrete (except when field concrete contains a significant amount of iron-bearing aggregate), the mockup can be made using a wooden frame to support the bars, or the bars can be embedded in sand. This allows the investigator to consider different situations with little additional effort. Likewise, for a mockup to be tested with GPR, it is unnecessary to use concrete. Depending on specific objectives of the tests, it is possible to create mockups using moist sand to represent the concrete. The moisture content of the sand will affect the attenuation of the electromagnetic pulses. Investigators have also used water/oil emulsions for accurate modeling of the dielectric and conductivity properties of concrete (Bungey et al. 1994). The use of the emulsion instead of concrete permits changes to the testing configuration without having to cast new concrete specimens.

For test methods based on stress-wave propagation, concrete specimens should be used to model correct mismatches in acoustic impedance (wave speed times density) between concrete and the anomaly. Several approaches can be used to simulate defects. For example, rigid foam insulation board can be used to simulate air voids (Sansalone and Carino 1986), thin sheets of flexible plastic foam have been used to simulate cracks (Cheng and Sansalone 1993), and thin metal sheets that are withdrawn after final setting have been used to simulate surface opening cracks (Sansalone et al. 1997). Honeycombing has been simulated by casting a mass composed of cement paste and coarse aggregate (Sansalone and Carino 1986). The absence of fine aggregate leads to voids between the coarse aggregate, which simulate the structure of honeycombed concrete. After the mass has hardened, it is cast into the mockup specimen.

4.3.5.1 *Field mockups of deep foundations*—Stress-wave methods evaluate the integrity and continuity of concrete piles and drilled shafts, either by direct transmission testing or sonic logging (3.3.4) or by reflection of stress waves propagated down the shaft by impacting the head of the pile, which is sonic-echo (3.3.1) or impulse-response testing (3.3.2).

Sonic logging of piles can be modeled in the laboratory, as described in the previous section. Pile head impact tests, however, rely on the channeling of dispersive stress waves down cylindrical or prismatic structural members with length/diameter ratios typically between 10:1 and 40:1. Paquet (1968) points out that the frequencies used for both harmonic (vibration and impulse-response) and echo tests are relatively low, and the corresponding wave lengths are great compared with typical pile diameters.

Both the impulse-response and sonic-echo tests are affected by soil damping. If it is required to study the effect of soil damping on the pile response, then the wavelengths in the soil are much greater than the pile diameter. For example, a soil with a shear wave velocity of 2620 ft/s (800 m/s) at a frequency of 500 Hz has a wavelength is 5.2 ft (1.6 m), close to the pile diameter. At higher frequencies, the calculated damping would be a poor approximation of the true value.

For these reasons, tests on scaled-down laboratory pile models do not produce satisfactory results. Recognizing this early on in the development of methods, several full-

scale test sites have been constructed worldwide to test the validity and accuracy of various NDT methods. Usually, various defects or shape changes have been included in the test shafts. Full-scale experimental sites include:

a) London, England, 1969 (Levy 1970)
b) Ghent, Belgium, 1987 (Holeyman et al. 1988)
c) Northumberland, England 1987 (Kilkenny et al. 1988)
d) California, 1989, FHWA trials (Baker et al. 1993)
e) Texas, 1990, FHWA trials (Baker et al. 1993)
f) Delft, Netherlands, 1992 (Anon 1992)
g) University of Houston, 1996 (Samman and O'Neill 1997)
h) Northwestern University (Finno et al. 1997)
i) BAM, Berlin, Germany (Niederleithinger et al. 2009)

In several of these cases, initial tests were performed blind, without prior knowledge of the shaft lengths, the location and type of built-in defects, or shape changes. Accuracy and reliability of the test methods were then assessed by test-site sponsors. At least two of the sites (Northumberland and FHWA Texas) have been preserved for future testing as methods are refined and developed.

Descriptions of test shafts, the installed defects, and results of initial test programs are described in the references provided. Note in particular the reference to Baker et al. (1993) for evaluation of the most recent state of development of stress-wave methods, as well as the nuclear-based, gamma-gamma logging method.

4.4—Correlation with intrusive testing

Because nondestructive test (NDT) methods provide indirect information about the conditions of the test object, it is not good practice to rely only on NDT for most condition surveys. Supplemental intrusive sampling or probing is often necessary to make a sound evaluation. A professional standard of care, relevant to the consequences, is necessary to determine the amount of supplemental intrusive sampling or probing to make a sound evaluation. Intrusive techniques serve several functions because they:

a) Provide verification of the NDT results
b) Assess the conditions at selected points when the NDT results are inconclusive
c) Provide samples for additional testing to supplement the NDT investigation
d) Refine the correlation between NDT results and actual conditions

Because the NDT methods that have been discussed are not generally well understood by those requesting the investigation, providing the results of intrusive sampling or probing to compare with the NDT results is an effective means to instill confidence in the NDT results. If intrusive probing does not confirm NDT results, then the probing information should also be provided to help explain the inherent limitations of a given method. Although probing will increase investigation price, it is a necessity for difficult investigations.

Confirmation of NDT test results on a routine basis is necessary to ensure consistency and veracity of the testing. Ideally, the selection of the confirmation probing should be based on a sample size that is sufficient to provide some predetermined measure of statistical confidence. As a minimum, it is recommended that confirmation be conducted on a routine basis, such as daily on small-scale testing projects or weekly on large-scale projects.

Samples needed for other tests can be obtained by coring or sawing. The NDT tests should be performed first with the sampling locations selected after preliminary analysis of the results. If possible, samples should be recovered at test points where an anomaly has been clearly detected, there is no indication of an anomaly, and the NDT results are inconclusive.

When samples are not required for additional tests, different intrusive probing methods may be used. These may include chipping away the concrete with a hammer and chisel, using power-driven jackhammers, or drilling holes. A very effective approach is to drill a hole and inspect inside using a rigid boresope or flexible fiberscope. Another example is to pour water into a drilled hole to provide information about the relative size of interconnected void space.

4.5—Reporting results

Vast amounts of data can be acquired during the nondestructive test (NDT) investigation. One challenge for the evaluation investigator is selecting a data-presentation format that is easily interpreted by those who make decisions based on the investigation results. This is especially important when investigating conditions that change with time. In such cases, it is critical that the test locations be documented accurately. Photographs to supplement written records are recommended. Before beginning the investigation, the evaluation investigator should reach an agreement with the client on the method of presenting the results. The final report format may have to be adjusted due to changes in the nature of the investigation that could arise from unexpected conditions.

The use of drawings to summarize the reduced data is an effective supplement to tabular data. For example, contour plots can be used to summarize the results of ultrasonic pulse velocity or half-cell potential surveys. Background data can be documented in an appendix. On large-scale testing programs, electronic storage can be a beneficial way to manage the data. Moreover, the permanent record of the test results is convenient for follow-up testing at a later date to assess changes in conditions of the structure.

CHAPTER 5—REFERENCES

Committee documents are listed first by document number and year of publication followed by authored documents listed alphabetically.

American Concrete Institute

ACI 201.1R-08—Guide for Conducting a Visual Inspection of Concrete in Service

ACI 207.3R-94—Practices for Evaluation of Concrete in Existing Massive Structures for Service Conditions (Reapproved 2008)

ACI 222R-01—Protection of Metals in Concrete against Corrosion (Reapproved 2010)

ACI 224.1R-07—Causes, Evaluation, and Repair of Cracks in Concrete Structures

ACI 228.1R-03—In-Place Methods to Estimate Concrete Strength

ACI 349.3R-02—Evaluation of Existing Nuclear Safety-Related Concrete Structures (Reapproved 2012)

ACI 362.2R-00—Guide for Structural Maintenance of Parking Structures

ACI 437R-03—Strength Evaluation of Existing Concrete Buildings

ACI 503.1R-92—Standard Specification for Bonding Hardened Concrete, Steel, Wood, Brick, and Other Materials to Hardened Concrete with a Multi-Component Epoxy Adhesive (Reapproved 2003)

ASTM International

ASTM C39/C39M-12—Standard Test Method for Compressive Strength of Cylindrical Concrete Specimens

ASTM C42/C42M-12—Standard Test Method for Obtaining and Testing Drilled Cores and Sawed Beams of Concrete

ASTM C192/C192M-07—Standard Practice for Making and Curing Concrete Test Specimens in the Laboratory

ASTM C215-08—Standard Test Method for Fundamental Transverse, Longitudinal, and Torsional Frequencies of Concrete Specimens

ASTM C294-05—Standard Descriptive Nomenclature for Constituents of Concrete Aggregates

ASTM C295/C295M-12—Standard Guide for Petrographic Examination of Aggregates for Concrete

ASTM C341/C341M-06—Standard Practice for Length Change of Cast, Drilled, or Sawed Specimens of Hydraulic Cement Mortar and Concrete

ASTM C457/C457M-11—Standard Test Method for Microscopical Determination of Parameters of the Air-Void System in Hardened Concrete

ASTM C469/469M-10—Standard Test Method for Static Modulus of Elasticity and Poisson's Ratio of Concrete in Compression

ASTM C496/C496-11—Standard Test Method for Splitting Tensile Strength of Cylindrical Concrete Specimens

ASTM C597-09—Standard Test Method for Pulse Velocity Through Concrete

ASTM C642-06—Standard Test Method for Density, Absorption, and Voids in Hardened Concrete

ASTM C803/C803M-03(2010)—Standard Test Method for Penetration Resistance of Hardened Concrete

ASTM C805/C805M-08—Standard Test Method for Rebound Number of Hardened Concrete

ASTM C823/C823M-12—Standard Practice for Examination and Sampling of Hardened Concrete in Constructions

ASTM C856-11—Standard Practice for Petrographic Examination of Hardened Concrete

ASTM C876-09—Standard Test Method for Corrosion Potentials of Uncoated Reinforcing Steel in Concrete

ASTM C900-06—Standard Test Method for Pullout Strength of Hardened Concrete

ASTM C1040/C1040M-08—Standard Test Methods for In Place Density of Unhardened and Hardened Concrete, Including Roller Compacted Concrete, by Nuclear Methods

ASTM C1084-10—Standard Test Method for Portland Cement Content of Hardened Hydraulic Cement Concrete

ASTM C1152/C1152M-04—Standard Test Method for Acid-Soluble Chloride in Mortar and Concrete

ASTM C1202-12—Test Method for Electrical Indication of Concrete's Ability to Resist Chloride Ion Penetration

ASTM C1218/C1218M-99(2008)—Standard Test Method for Water-Soluble Chloride in Mortar and Concrete

ASTM C1383-04(2012)—Standard Test Method for Measuring the P-Wave Speed and the Thickness of Concrete Plates Using the Impact-Echo Method

ASTM C1543-10—Standard Test Method for Determining the Penetration of Chloride Ion into Concrete by Ponding

ASTM C1556-11—Standard Test Method for Determining the Apparent Chloride Diffusion Coefficient of Cementitious Mixtures by Bulk Diffusion

ASTM C1583/C1583M-04—Standard Test Method for Tensile Strength of Concrete Surfaces and the Bond Strength or Tensile Strength of Concrete Repair and Overlay Materials by Direct Tension (Pull-off Method)

ASTM C1740-10 Standard Practice for Evaluating the Condition of Concrete Plates Using the Impulse-Response Method

ASTM D4580-03(2007)—Standard Practice for Measuring Delaminations in Concrete Bridge Decks by Sounding

ASTM D4748-10—Standard Test Method for Determining the Thickness of Bound Pavement Layers Using Short Pulse Radar

ASTM D4788-03(2007)—Standard Test Method for Detecting Delaminations in Bridge Decks Using Infrared Thermography

ASTM D5882-07—Standard Test Method for Low Strain Impact Integrity Testing of Deep Foundations

ASTM D6087-08—Standard Test Method for Evaluating Asphalt Covered Concrete Bridge Decks Using Ground Penetrating Radar

ASTM D6760-08—Standard Test Method for Integrity Testing of Concrete Deep Foundations by Ultrasonic Cross-hole Testing

ASTM E105-1—Standard Practice for Probability Sampling of Materials

ASTM E122-09 Standard Practice for Calculating Sample Size to Estimate, With Specified Precision, the Average for a Characteristic of a Lot or Process

ASTM F2170-11—Standard Test Method for Determining Relative Humidity in Concrete Floor Slabs Using In-Situ Probes

ASTM G15-03—Standard Terminology Relating to Corrosion and Corrosion Testing

ASTM G57-06(2012)—Standard Test Method for Field Measurement of Soil Resistivity Using the Wenner Four-Electrode Method

American Association of State Highway and Transportation Officials

AASHTO T259-02—Standard Method of Test for Resistance of Concrete to Chloride Ion Penetration

AASHTO T277-07—Standard Method of Test for Electrical Indication of Concrete's Ability to Resist Chloride Ion Penetration

British Standards Institute

BS 1881-204:1998—Recommendations on the Use of Electromagnetic Covermeters

BS 1881-205:1986—Recommendations for Radiography of Concrete

BS 1881-207:1992—Recommendations for the Assessment of Concrete Strength by Near-to-Surface Tests.

BS 1881-208:1996—Recommendations for the determination of the initial surface absorption of concrete

Canadian Standards Association

CSA A23.2-09—Test Methods and Standard Practices for Concrete

Strategic Highway Research Program (SHRP)

SHRP-C-315—Handbook for the Identification of Alkali-Silica Reactivity in Highway Structures

SHRP-S-324—Condition Evaluation of Concrete Bridges Relative to Reinforcement Corrosion Volume 2: Method for Measuring the Corrosion Rate of Reinforcing Steel

SHRP-S-327—Condition Evaluation of Concrete Bridges Relative to Reinforcement Corrosion Volume 5: Method for Evaluating the Effectiveness of Penetrating Sealers

SHRP-S-328—Condition Evaluation of Concrete Bridges Relative to Reinforcement Corrosion Volume 6: Method for Field Determination of Total Chloride Content

SHRP-S-329—Condition Evaluation of Concrete Bridges Relative to Reinforcement Corrosion Volume 7: Method for Field Measurement of Concrete Permeability

SHRP-S-330—Condition Evaluation of Concrete Bridges Relative to Reinforcement Corrosion Volume 8: Procedure Manual

Abraham, O.; Le, T.-P.; Cote, P.; and Argoul, P., 2002, "Two Enhanced Complementary Impact Echo Approaches for the Detection of Voids in Tendon Ducts," IABMAS '02, UPC, Barcelona, Spain, pp. 151-152.

Alexander, A. M., and Thornton Jr., H. T., 1989, "Ultrasonic Pitch-Catch and Pulse-Echo Measurements in Concrete," *Nondestructive Testing of Concrete*, ACI SP-112, H. S. Lew, ed., American Concrete Institute, Farmington Hills, MI, pp. 21-40.

Andrade, C., and Alonso, C., 2004, "Test Methods for On-Site Corrosion Rate Measurement of Steel Reinforcement in Concrete by Means of the Polarization Resistance Method," *Materials and Structures*, V. 37, Nov., pp. 623-643.

Anon, 1992, "Results of Delft University Pile Integrity Testing Competition," *Ground Engineering*., V. 25, Oct./Nov., also discussions, *Ground Engineering*, Apr. and July-Aug. 1993).

Baker Jr., C. N.; Drumwright, E. E.; Briaud, J.-L.; Mensah-Dumwah, F.; and Parikh, G., 1993, "Drilled Shafts for Bridge Foundations," FHWA-RD-92-004, Federal Highway Administration, Washington, DC

Baker Jr., C. N., and Khan, F., 1971, "Caisson Construction Problems and Correction in Chicago," *Journal of the Soil Mechanics and Foundations Division*, ASCE, V. 97, No. 2, pp. 417-440.

Basheer, L.; Cleland, D. J.; Basheer, P. A. M.; and Long, A. E., 1993, "An In-Situ Method for Assessing Surface Treated Concrete," *Concrete 2000, Economic and Durable Construction Through Excellence*, International Conference, E&F Spon, pp. 805-814.

Basheer, P. A. M., 1993, "A Brief Review of Methods for Measuring the Permeation Properties of Concrete In-Situ," *Proceedings, Buildings, and Structures*, Institution of Civil Engineers, V. 99, No. 1, Feb., pp. 74-83.

Basheer, P. A. M.; Andrews, R. J.; Robinson, D. J.; and Long, A. E., 2005, "'PERMIT' Ion Migration Test for Measuring the Chloride Ion Transport of Concrete on Site," *Non-destructive Testing and Evaluation International*, V. 38, pp. 219-229.

Basheer, P. A. M.; Long, A. E.; and Montgomery, F. R., 1994, "The Autoclam—A New Test for Permeability, *Concrete*, Journal of the Concrete Society, July-Aug., pp. 27-29.

Basheer, P. A. M.; Long, A. E.; and Montgomery, F. R., 1995, "'Clam' Tests for Measuring In-Situ Permeation Properties of Concrete," *NDT & E International*, V. 12, pp. 53-73.

Basheer, P. A. M.; Nolan, E.; and Long, A. E., 2001, "Near-Surface Moisture Gradients and In-Situ Permeation Tests," *Construction & Building Materials*, V. 15, No. 2-3, pp. 105-114.

Bay, J. A., and Stokoe, K. H., 1990, "Field Determination of Stiffness and Integrity of PCC Members Using SASW Method," *Proceedings of Conference on Nondestructive Evaluation of Civil Structures and Materials*, National Science Foundation, Boulder, CO, pp. 71-85.

Berg, F.; Olgaard, P. L.; and Jorgensen, J. L., 1989, "Method of Determining the Density of Substrata," U.S. Patent 4,820,919.

Berke, N. S., and Hicks, M. C., 1992, "Estimating the Life Cycle of Reinforced Concrete Decks and Marine Piles Using Laboratory Diffusion and Corrosion Data," *Corrosion Forms and Control for Infrastructure*, ASTM STP-1137, ASTM International, West Conshohocken, PA, pp. 207-231.

Bradfield, G., and Gatfield, E., 1964, "Determining the Thickness of Concrete Pavements by Mechanical Waves: Directed Beam Method," *Magazine of Concrete Research*, V. 16, No. 46, Mar., pp. 49-53.

Briard, M., 1970, "Controle de Pieux par la Methode de Vibrations (Pile Construction Control Using the Vibration Method)," Annales de l'Institut Technique du Batiment, No. 270, June, pp. 105-107.

Broomfield, J., 1996, "Field Measurement of the Corrosion Rate of Steel in Concrete Using a Microprocessor Controlled Unit with a Monitored Guard Ring for Signal Confinement," *Techniques to Assess the Corrosion Activity of Steel Reinforced Concrete Structures*, ASTM STP 1276, N. S. Berke, E. Escalante, C. Nmai, and D. Whiting, eds., pp. 91-106.

Brown, J. R., and Hamilton, H. R., 2007, "Heating Methods and Detection Limits for Infrared Thermography

Inspection of Fiber-Reinforced Polymer Composites," *ACI Materials Journal*, V. 104, No. 5, Sept.-Oct., pp. 481-490.

Bungey, J. H., and Millard, S. G., 1993, "Radar Inspection of Structures," *Structures and Buildings Journal*, V. 99, May, pp. 173-186. (London)

Bungey, J. H., and Millard, S. G., 1995, "Detecting Subsurface Features in Concrete by Impulse Radar," *Nondestructive Testing and Evaluation*, V. 12, pp. 33-51.

Bungey, J. H.; Millard, S. G.; and Grantham, M. G., 2006, *Testing of Concrete in Structures*, fourth edition, Spon Press, London, 352 pp.

Bungey, J. H.; Millard, S. G.; and Shaw, M. R., 1994, "The Influence of Reinforcing Steel on Radar Surveys of Structural Concrete," *Construction & Building Materials*, V. 8, No. 2, pp. 119-126.

Bungey, J. H.; Millard, S. G.; and Shaw, M. R., 1997, "Radar Assessment of Post-Tensioned Concrete," *Structural Faults + Repair-97*, Engineering Technics Press, V. 1, pp. 331-339.

Bungey, J. H.; Millard, S. G.; Shaw, M. R.; and Thomas, C., 1991, "Operational Aspects of Radar Investigations," *British Journal of NDT*, V. 33, No. 12, Dec., pp. 599-605.

Cady, P. D., and Gannon, E. J., 1992, "Condition Evaluation of Concrete Bridges Relative to Reinforcement Corrosion, Volume 8: Procedure Manual," *SHRP-S/FR-92-110*, Strategic Highway Research Program, National Research Council, Washington, DC, 124 pp.

Cantor, T. R., 1984, "Review of Penetrating Radar as Applied to Nondestructive Evaluation of Concrete," *In-Situ/Nondestructive Testing of Concrete*, SP-82, V. M. Malhotra, ed., American Concrete Institute, Farmington Hills, MI, pp. 581-601.

Carino, N. J., 1992, "Performance of Electromagnetic Covermeters for Nondestructive Assessment of Steel Reinforcement," *NISTIR 4988*, National Institute of Standards and Technology, Gaithersburg, MD, Sept., 130 pp.

Carino, N. J., 1994, "Recent Developments in Nondestructive Testing of Concrete," *Advances in Concrete Technology*, second edition, MSL 94-1(R), V. M. Malhotra, ed., CANMET, Natural Resources Canada, Ottawa, ON, Canada, pp. 281-337.

Carino, N. J., 2004a, "Stress Wave Propagation Methods," *Handbook on Nondestructive Testing of Concrete*, second edition, V. M. Malhotra and N. J. Carino, eds., CRC Press, Boca Raton, FL, and ASTM International, West Conshohocken, PA.

Carino, N. J., 2004b, "Methods to Evaluate Corrosion of Reinforcement," *Handbook on Nondestructive Testing of Concrete*, second edition, V. M. Malhotra and N. J. Carino, eds., CRC Press, Boca Raton, FL, pp. 11-1 to 11-24.

Carino, N. J.; Sansalone, M.; and Hsu, N. N., 1986, "Flaw Detection in Concrete by Frequency Spectrum Analysis of Impact-Echo Waveforms," *International Advances in Nondestructive Testing*, V. 12, W. J. McGonnagle, ed., Gordon & Breach Science Publishers, New York, pp. 117-146.

Carter, C. R.; Chung, T.; Holt, F. B.; and Manning, D., 1986, "An Automated Signal Processing System for the Signature Analysis of Radar Waveforms from Bridge Decks," *Canadian Electrical Engineering Journal*, V. 11, No. 3, pp. 128-137.

Cather, R.; Figg, J. W.; Marsden, A. F.; and O'Brien, T. P., 1984, "Improvements to the Figg Method of Determining the Air Permeability of Concrete," *Magazine of Concrete Research*, V. 36, No. 129, Dec., pp. 241-245.

Chen, H. L. R.; Halabe, U. B.; Sami, Z.; and Bhandarkar, V., 1994, "Impulse Radar Reflection Waveforms of Simulated Reinforced Concrete Bridge Decks," *Materials Evaluation*, V. 52, No. 12, pp. 1382-1388.

Cheng, C., and Sansalone, M., 1993, "The Impact-Echo Response of Concrete Plates Containing Delaminations: Numerical, Experimental, and Field Studies," *Materials and Structures*, V. 26, No. 159, June, pp. 274-285.

Chung, H. W., and Law, K. S., 1985, "Assessing Fire Damage of Concrete by the Ultrasonic Pulse Technique," *Cement, Concrete and Aggregates*, V. 7, No. 2, Winter, pp. 84-88.

Clark, M. R.; McCann, D. M.; and Forde, M. C., 2003, "Application of Infrared Thermography to the Non-Destructive Testing of Concrete and Masonry Nridges," *NDT&E International*, Elsevier Science, V. 36, pp. 265-275.

Clear, K. C., 1989, "Measuring Rate of Corrosion of Steel in Field Concrete Structures," *Transportation Research Record*, V. 1211, pp. 28-37.

Clemeña, G., 1983, "Nondestructive Inspection of Overlaid Bridge Decks with Ground Probing Radar," *Transportation Research Record* No. 899, Transportation Research Board, Washington, DC, pp. 21-32.

Clemeña, G. G., 2004, "Short-Pulse Radar Methods," *Handbook on Nondestructive Testing of Concrete*, Chapter 3, V. M. Malhotra and N. J. Carino, eds., CRC Press, Boca Raton, FL, pp. 253-274.

Clemeña, G. G.; Jackson, D. R.; and Crawford, G. C., 1992a, "Benefits of Using Half-Cell Potential Measurements in Condition Surveys of Concrete Bridge Decks," *Transportation Research Record*, V. 1347, pp. 46-55.

Clemeña, G. G.; Jackson, D. R.; and Crawford, G. C., 1992b, "Inclusion of Rebar Corrosion Rate Measurements in Condition Surveys of Concrete Bridge Decks," *Transportation Research Record*, V. 1347, pp. 37-45.

Colla, C., 1997, "NDT of Masonry Arch Bridges," PhD thesis, The University of Edinburgh, Department of Civil and Environmental Engineering, Edinburgh, UK, 242 pp.

Colla, C., 2002, "Advanced Impact Echo Technique for NDE of Post-Tensioned Concrete," *IABMAS'02*, UPC, Barcelona, July, pp. 177-178.

Collico Savio, D.; Mariscotti, M. A. J.; and Ribeiro Guevara, S., 1995, "Elemental Analysis of a Concrete Sample by Capture Gamma-Rays with a Radioisotope Source," *Nuclear Instruments and Methods in Physics*, V. B95, pp. 379-388.

Daniels, D. J.; Gunton, D. J.; and Scott, H. F., 1988, "Introduction to Subsurface Radar," *Proceedings Institution of Electrical Engineers*, V. 135, Part F, No. 4, Aug., pp. 278-320.

Das Gupta, N. C., and Tam, C. T., 1983, "Non-destructive Technique for Simultaneous Detection of Size and Cover

of Embedded Reinforcement," *The British Journal of Non-Destructive Testing*, V. 25, No. 6, Nov., pp. 301-304.

Davis, A. G., 1995, "Nondestructive Evaluation of Existing Deep Foundations," *Journal of Performance of Constructed Facilities*, V. 9, No. 1, Feb., pp. 57-74.

Davis, A. G., 2002, "The Nondestructive Impulse Response test in North America: 1985-2001," *NDT&E International*, V. 36, pp. 185-193.

Davis, A. G., and Dunn, C. S., 1974, "From Theory to Field Experience with the Nondestructive Vibration Testing of Piles," *Proceedings of the Institute of Civil Engineers*, V. 57, Part 2, Dec., pp. 571-593.

Davis, A. G.; Evans, J. G.; and Hertlein, B. H., 1997, "Nondestructive Evaluation of Concrete Radioactive Waste Tanks," *Journal of Performance of Constructed Facilities*, ASCE, V. 11, No. 4, pp. 161-167.

Davis, A. G., and Hertlein, B. H., 1987, "Nondestructive Testing of Concrete Pavement Slabs and Floors with the Transient Dynamic Response Method," *Proceedings of the International Conference on Structural Faults and Repair*, London, V. 2, July, pp. 429-433.

Davis, A. G., and Hertlein, B. H., 1990, "Assessment of Bridge Deck Repairs by a Nondestructive Technique," *Proceeding of the NATO Advanced Research Workshop on Bridge Evaluation, Repair, and Rehabilitation*, A. J. Nowak, ed., Kluwer Academic Publishers, Boston, MA, Apr., pp. 229-233.

Davis, A. G., and Hertlein, B. H., 1994, "A Comparison of the Efficiency of Drilled Shaft Down-hole Integrity Tests," *Proceedings of the International Conference on Design and Construction of Deep Foundations*, FHWA, Orlando, FL, Dec., V. III, pp. 1272-1286.

Davis, A. G., and Hertlein, B. H., 1995, "Nondestructive Testing of Concrete Chimneys and Other Structures," *Conference on the Nondestructive Evaluation of Aging Structures and Dams, Proc. SPIE 2457*, Oakland CA, June, pp. 129-136.

Davis, A. G., and Hertlein, B. H., 1997, "Evaluation of the Integrity of Some Large Concrete Foundations Using NDT," *Innovations in Nondestructive Testing of Concrete*, SP-168, S. Pessiki and L. Olson, eds., American Concrete Institute, Farmington Hills, MI, pp. 333-356.

Davis, A. G.; Hertlein, B. H.; Lim, M. K.; and Michols, K. A., 1996, "Impact-Echo and Impulse Response Stress Wave Methods: Advantages and Limitations for the Evaluation of Highway Pavement Concrete Overlays," *Conference on the Nondestructive Evaluation of Bridges and Highways, Proc. SPIE 2946*, Scottsdale AZ, Dec., pp. 88-96.

Davis, A. G., and Kennedy, J., 1998, "Impulse Response Testing to Evaluate the Degree of Alkali-Aggregate Reaction in Concrete Drilled-Shaft Foundations for Electricity Transmission Towers," *Conference on the Nondestructive Evaluation of Utilities and Pipelines II, Proc. SPIE 3398*, San Antonio, TX, Apr., pp. 178-185.

Davis, A. G.; Lim, M. K.; and Petersen, C. G., 2004, "Rapid and Economical Evaluation of Concrete Tunnel Linings with Impulse Response and Impulse Radar Nondestructive Methods," *NDT&E International*, V. 38, No. 3, pp. 181-186

Davis, A. G., and Robertson, S. A., 1975, "Economic Pile Testing," *Ground Engineering*, V. 8, No. 3, pp. 40-43.

De La Haza, A. O.; Peteresen, C.; and Samokrutov, A., 2008, "3D Imaging of Concrete Structures Using Ultrasonic Shear Waves," *Proceedings of the 12th International Conference Structural Faults & Repair-2008*, Edinburgh, Engineering Technics Press.

DFI, 2006, *Manual for Nondestructive Testing and Evaluation of Drilled Shafts*, Deep Foundations Institute, Hawthorn, NJ, 79 pp.

Dhir, R. K.; Hewlett, P. C.; and Chan, Y. N., 1987, "Near Surface Characteristics of Concrete: Assessment and Development of In-Situ Test Methods," *Magazine of Concrete Research*, V. 39, No. 141, Dec., pp. 183-195.

Escalante, E., 1989, "Elimination of IR Error in Measurements of Corrosion in Concrete," *The Measurement and Correction of Electrolyte Resistance in Electrochemical Tests*, ASTM STP-1056, L. L. Scribner and S. R. Taylor, eds., ASTM International, West Conshohocken, PA, pp. 180-190.

FDOT, 2004, "Concrete Resistivity as an Electrical Indicator of its Permeability," *Florida Sampling and Testing Methods*, STM 5-578, Florida Department of Transportation, Tallahassee, FL, Jan.

Feliú, S.; González, J. A.; and Andrade, C., 1996, "Electrochemical Methods for On-Site Determinations of Corrosion Rates of Rebars," *Techniques to Assess the Corrosion Activity of Steel Reinforced Concrete Structures*, ASTM STP-1276, N. S. Berke, E. Escalante, C. Nmai, and D. Whiting, eds., ASTM International, West Conshohocken, PA, pp. 107-118.

Feliú, S.; González, J. A.; Andrade, C.; and Feliu, V., 1989, "Polarization Resistance Measurements in Large Concrete Specimens: Mathematical Solution for Unidirectional Current Distribution," *Materials and Structures: Research and Testing*," V. 22, No. 129, May, pp. 199-205.

Feliú, S.; González, J. A.; Feliu Jr., S.; and Andrade, M. C., 1990a, "Confinement of the Electrical Signal for In-Situ Measurement of Polarization Resistance in Reinforced Concrete," *ACI Materials Journal*, V. 87, No. 5, Sept.-Oct., pp. 457-460.

Feliú, S.; González, J. A.; Escudero, M. L.; Feliu Jr., S.; and Andrade, M. C., 1990b, "Possibilities of the Guard Ring for Electrical Signal Confinement in the Polarization Measurements of Reinforcements," *The Journal of Science and Engineering Corrosion*, V. 46, No. 12, pp. 1015-1020.

FHWA, 2005, "Use of Magnetic Tomography Technology to Evaluate Dowel Bar Placement," *TechBrief*, Concrete Pavement Technology Program, FHWA, U.S. Department of Transportation, Oct., wwwcf.fhwa.dot.gov/pavement/pccp/pubs/06002/06002.pdf (accessed Jan. 2012.)

Figg, J. W., 1973, "Methods of Measuring the Air and Water Permeability of Concrete," *Magazine of Concrete Research*, V. 25, No. 85, Dec., pp. 213-219.

Figg, J. W., 1989, "Concrete Surface Permeability: Measurement and Meaning," *Chemistry & Industry*, Nov., pp. 714-719.

Finno, R. J.; Gassman, S. L.; and Osborn, P. W., 1997, "Non-Destructive Evaluation of a Deep Foundation Test Section at the Northwestern University National Geotechnical Experimentation Site," *Federal Highway Administration Report*.

Fitzgerald, A. E.; Higginbotham, D. E.; and Grabel, A., 1967, *Basic Electrical Engineering*, McGraw-Hill, New York.

Flis, J.; Sehgal, A.; Li, D.; Kho, Y. T.; Sabol, S.; Pickering, H.; Osseao-Asare, K.; and Cady, P. D., 1992, "Condition Evaluation of Concrete Bridges Relative to Reinforcement Corrosion, Volume 2: Method for Measuring the Corrosion Rate of Reinforcing Steel," SHRP-S/FR-92-104, Strategic Highway Research Program, National Research Council, Washington, DC, 105 pp.

Frølund, T.; Jensen, F. M.; and Bassler, R., 2002, "Determination of Reinforcement Corrosion Rate by Means of the Galvanostatic Pulse Technique," *First International Conference on Bridge Maintenance, Safety and Management*, IABMAS, 8 pp.

Garboczi, E. J., 1990, "Permeability, Diffusivity, and Microstructural Parameters: A Critical Review," *Cement and Concrete Research*, V. 20, pp. 591-601.

Ghorbanpoor, A.; Borchelt, R.; Edwards, M.; and Abdel Salam, E., 2000, "Magnetic-Based NDE of Prestressed and Post-tensioned Concrete Members—The MFL System," FHWA-RD-00-026, Federal Highway Administration, McLean, VA, 107 pp.

Giannopoulos, A., 1997, "The Investigation of Transmission-line Matrix and Finite-Difference Time-Domain Methods for the Forward Problem of Ground Probing Radar," DPhil thesis, University of York, Department of Electronics, York, UK.

Giannopoulos, A.; MacIntyre, P.; Rodgers, S.; and Forde, M. C., 2002, "GPR Detection of Voids in Post-Tensioned Concrete Bridge Beams," Ninth International Conference, GPR-2002, Santa Barbara, CA, pp. 376-381.

Gibson, A., and Popovics, J. S., 2005, "Lamb Wave Basis for Impact-Echo Method Analysis," *Journal of Engineering Mechanics*, No. 131, pp. 438-443.

Hagemaier, D. J., 1990 *Fundamentals of Eddy Current Testing*, American Society for Nondestructive Testing, Inc., Columbus, OH.

Halabe, U. B.; Maser, K. R.; and Kausel, E. A., 1995, "Condition Assessment of Reinforced Concrete Structures Using Electromagnetic Waves," *ACI Materials Journal*, V. 92, No. 5, Sept.-Oct., pp. 511-523.

Halabe, U. B.; Sotoodehnia, A.; Maser, K. R.; and Kausel, E. A., 1993, "Modeling the Electromagnetic Properties of Concrete," *ACI Materials Journal*, V. 90, No. 6, Nov.-Dec., pp. 552-563.

Hall, C., 1989, "Water Sorptivity of Mortars and Concretes: A Review," *Magazine of Concrete Research*, V. 41, No. 147, June, pp. 51-61.

Halliday, D., and Resnick, R., 1978, *Physics*, third edition, John Wiley & Sons, New York.

Heisey, J. S.; Stokoe II, K. H.; and Meyer, A. H., 1982, "Moduli of Pavement Systems from Spectral Analysis of Surface Waves," *Transportation Research Record* No. 853, Transportation Research Board, Washington, DC, pp. 22-31.

Hertlein, B. H., and Davis, A. G., 2006, *Nondestructive Testing of Deep Foundations*, first edition, John Wiley & Sons, New York, and Chichester, UK, 290 pp.

Hillger, W., 1993, "Imaging of Defects in Concrete by Ultrasonic Pulse-Echo Technique," *Proceedings of the Fifth International Conference on Structural Faults & Repair-93*, V. 3, University of Edinburgh, Engineering Technics Press, pp. 59-65.

Holeyman, A.; Legrand, C.; Lousberg, E.; and D'Haenens, A., 1988, "Comparative Dynamic Pile Testing in Belgium," *Proceedings of the 3rd International Conference on the Application of Stres—Wave Theory to Piles*, B. H. Fellenius, ed., Ottawa, ON, Canada, pp. 542-554.

Holt, F. B., and Manning, D. G., 1978, "Infrared Thermography for the Detection of Delaminations in Concrete Bridge Decks," *Proceedings of the 4th Biennial Infrared Information Exchange*, pp. A61-A71.

Hönig, A., 1984, "Radiometric Determination of the Density of Fresh Shielding Concrete In Situ," *In-Situ/Nondestructive Testing of Concrete*, SP-82, V. M. Malhotra, ed., American Concrete Institute, Farmington Hills, MI, pp. 603-618.

Howkins, S. D., 1968, "Measurement of Pavement Thickness by Rapid and Nondestructive Methods," *NCHRP Report 52*, Highway Research Board, National Research Council, Washington, DC, 82 pp.

Iddings, F. A., and Melancon, J. L., 1986, "Detection of Voids in Plastic Concrete Roadways," *Review of Progress in Quantitative Nondestructive Evaluation*, D. O. Thompson and D. E. Chimenti, eds., V. 5B, Plenum Press, New York, pp. 1655-1663.

Im, S. B.; Hurlebaus, S.; and Trejo, D., 2010, "Inspection of Voids in External Post-Tensioned Tendons," *Transportation Research Record* No. 2172, Transportation Research Board, Washington, DC, pp. 115-122.

Jaeger, B. J.; Sansalone, M. J.; and Poston, R. W., 1996, "Detecting Voids in Grouted Tendon Ducts of Post-Tensioned Concrete Structures Using the Impact-Echo Method," *ACI Structural Journal*, V. 93, No. 4, July-Aug., pp. 462-472.

Jones, R., 1949, "The Non-Destructive Testing of Concrete," *Magazine of Concrete Research*, No. 2, June, pp. 67-78.

Jones, R., 1955, "A Vibration Method for Measuring the Thickness of Concrete Road Slabs in Situ," *Magazine of Concrete Research*, V. 7, No. 20, July, pp. 97-102.

Jones, R., 1962, "Surface Wave Technique for Measuring the Elastic Properties and Thickness of Roads: Theoretical Development," *British Journal of Applied Physics*, V. 13, pp. 21-29.

Kalinski, M. E., 1997, "Nondestructive Characterization of Damaged and Repaired Areas of a Concrete Beam Using the SASW Method," *Innovations in Non-Destructive Testing of Concrete*, SP-168, S. Pessiki and L. Olson, ed., American Concrete Institute, Farmington Hills, MI, 360 pp.

Kaplan, H., 1994, "Commercial Applications for Thermal Imaging Instruments, An Update," *Proceedings of Infrared*

Technology XX, SPIE—The International Society for Optical Engineering, V. 2269, pp. 8-17.

Kessler, R. J.; Powers, R. G.; and Paredes, M. A., 2005, "Resistivity Measurements of Water Saturated Concrete as an Indicator of Permeability," *Corrosion 2005*, NACE, 10 pp.

Kessler, R. J.; Powers, R. G.; Vivas, E.; Paredes, M. A.; and Virmani, Y. P., 2008, "Surface Resistivity as an Indicator of Concrete Chloride Penetration Resistance," *Concrete Bridge Conference HPC—Safe, Affordable, and Efficient*, St. Louis, MO.

Kilkenny, W. M.; Lilley, D. M.; and Akroyd, R. F., 1988, "Steady State Vibration Testing of Piles with Known Defects," *Proceedings of the 3rd International Conference on the Application of Stress-Wave Theory to Piles*, B. H. Fellenius, ed., Ottawa, ON, Canada, pp. 91-98.

Kozlov, V. N.; Samokutov, A. A.; and Shevaldykin, V., 1997, "Thickness Measurement and Flaw Detection in Concrete Using Ultrasonic Echo Method," *Nondestructive Testing and Evaluation*, V. 13, pp. 73-84.

Krautkrämer, J., and Krautkrämer, H., 1990, *Ultrasonic Testing of Materials*, fourth edition, Springer-Verlag, New York, 677 pp.

Kropp, J., and Hilsdorf, H. K., eds., 1995, *Performance Criteria for Concrete Durability*, E&FN Spon, London, 327 pp.

Kunz, J. T., and Eales, J. W., 1985, "Remote Sensing Techniques Applied to Bridge Deck Evaluation," *Strength Evaluation of Existing Concrete Bridges*, SP-88, T. C. Liu, ed., American Concrete Institute, Farmington Hills, MI, pp. 237-258.

Lauer, K. R., 2004, "Magnetic/Electrical Methods," Chapter 10, *Handbook on Nondestructive Testing of Concrete*, second edition, V. M. Malhotra and N. J. Carino, eds., CRC Press, Boca Raton, FL, pp. 10-1 to 10-21.

Leslie, J. R., and Cheesman, W. J., 1949, "An Ultrasonic Method of Studying Deterioration and Cracking in Concrete Structures," *ACI Journal*, V. 46, No. 1, Jan., pp. 17-36.

Levitt, M., 1971, "The ISAT—A Non-Destructive Test for the Durability of Concrete," *British Journal of Non-Destructive Testing*, V. 13, No. 4, July, pp. 106-112.

Levy, J. F., 1970, "Sonic Pulse Method of Testing Cast In Situ Piles," *Ground Engineering*, V. 3, No. 3, pp. 17-19.

Lim, M. K., 2001, "NDE Using Impulse Radar to Evaluate Material Properties in Concrete Structures," *Proceedings of the 9th International Conference Structural Faults & Repair-2001*, Commonwealth Institute, Engineering Technics Press. (CD-ROM)

Lin, J. M., and Sansalone, M., 1993, "The Transverse Elastic Impact Response of Thick Hollow Cylinders," *Journal of Nondestructive Evaluation*, V. 12, No. 2, pp. 139-149.

Lin, J. M., and Sansalone, M., 1994a, "The Impact-Echo Response of Hollow Cylindrical Concrete Structures Surrounded by Soil or Rock, Part 1—Numerical Studies," *ASTM Geotechnical Testing Journal*, V. 17, No. 2, June, pp. 207-219.

Lin, J. M., and Sansalone, M., 1994b, "The Impact-Echo Response of Hollow Cylindrical Concrete Structures Surrounded by Soil or Rock, Part 2—Field Studies," *ASTM Geotechnical Testing Journal*, V. 17, No. 2, June, pp. 220-226.

Lin, J. M., and Sansalone, M., 1996, "Impact-Echo Studies of Interfacial Bond Quality in Concrete: Part I—Effects of Unbonded Fraction of Area," *ACI Materials Journal*, V. 93, No. 3, May-June, pp. 223-232.

Lin, Y., and Sansalone, M., 1992a, "Transient Response of Thick Circular and Square Bars Subjected to Transverse Elastic Impact," *The Journal of the Acoustical Society of America*, V. 91, No. 2, Feb., pp. 885-893.

Lin, Y., and Sansalone, M., 1992b, "Transient Response of Thick Rectangular Bars Subjected to Transverse Elastic Impact," *The Journal of the Acoustical Society of America*, V. 91, No. 5, May, pp. 2674-2685.

Lin, Y., and Sansalone, M., 1992c, "Detecting Flaws in Concrete Beams and Columns Using the Impact-Echo Method," *ACI Materials Journal*, V. 89, No. 4, July-Aug., pp. 394-405.

Lin, Y., and Su, W. C., 1996, "Use of Stress Waves for Determining the Depth of Surface-Opening Cracks in Concrete Structures," *ACI Materials Journal*, V. 93, No. 5, Sept.-Oct., pp. 494-505.

Liu, Z., and Beaudoin, J. J., 2000, "The Permeability of Cement Systems to Chloride Ingress and Related Test Methods," *Cement, Concrete, and Aggregates*, V. 22, No. 1, June, pp. 16-23.

Mailer, H., 1972, "Pavement Thickness Measurement Using Ultrasonic Techniques," *Highway Research Record*, No. 378, pp. 20-28.

Malhotra, V. M., 1976, *Testing Hardened Concrete: Nondestructive Methods*, American Concrete Institute Monograph No. 9, Iowa State University Press, Ames, IA, 204 pp.

Mariscotti, M. A. J.; Jalinoos, F.; Frigerio, T.; Ruffolo, M.; and Thieberger, P., 2009, "Gamma-Ray Imaging for Void and Corrosion Assessment," *Concrete International*, V. 31, No. 11, Nov., pp. 48-53.

Martin, J.; Broughton, K. J.; Giannopoulos, A.; Hardy, M. S. A.; and Forde, M. C., 2001, "Ultrasonic Tomographic Impact-Echo NDT of Grouted Duct P-T R. C. Beams," *NDT&E International*, V. 34, pp. 107-113.

Martin, J., and Forde, M. C., 1995, "Influence of Concrete Properties on Impulse Hammer Spectrum and Compression Wave Velocity," *Journal of Construction & Building Materials*, Sept., No. 4, pp. 245-255.

Martin, J.; Hardy, M. S. A.; Usmani, A. S.; and Forde, M. C., 1998, "Accuracy of NDE in Bridge Assessment," *Engineering Structures*, V. 20, No. 11, pp. 979-984.

Maser, K. R., 1986, "Detection of Progressive Deterioration in Bridge Decks Using Ground Penetrating Radar," *Experimental Assessment of the Performance of Bridges*, Proceedings of ASCE/EM Division Specialty Conference, Boston, MA, Oct., pp. 42-57.

Maser, K. R., 1990, "New Technology for Bridge Deck Assessment," New England Transportation Consortium Final Reports (Phase I Report FHWA-NETC-89-01, Phase II Report FHWA-NETC-90-1), Center for Transportation Studies, MIT, 1990.

Maser, K. R., and Roddis, W. M., 1990, "Principles of Thermography and Radar for Bridge Deck Assessment,"

Journal of Transportation Engineering, V. 116, No. 5, Sept.-Oct., pp. 583-601.

Mast, J. E.; Lee, H.; Chew, C.; and Murtha, J., 1990, "Pulse-Echo Holographic Techniques for Microwave Subsurface NDE," *Proceedings of Conference on Nondestructive Evaluation of Civil Structures and Materials*, National Science Foundation, Boulder, CO, pp. 177-191.

Matthews, J. H.; Porter, S. G.; Dennis, P. N. J.; and Watton, R., 1994, "Infrared Detectors in the UK-A 10 Year Update Benefits of Uncooled IR Sensors," *Proceedings of Infrared Technology XX*, SPIE—The International Society for Optical Engineering, V. 2269, pp. 678-686.

McCann, D. M., and Forde, M. C., 2001, "Review of NDT Methods in the Assessment of Concrete and Masonry Structures," *NDT&E International*, V. 34, pp. 71-84.

Middendorp, P., and Reiding, F. J., 1988, "Determination of Discontinuities in Piles by TNO Integrity Testing and Signal Matching Techniques," *Proceedings of the 3rd International Conference on Application of Stress-Wave Theory to Piles*, International Society of Soil Mechanics and Foundation Engineering, B. H. Fellenius, ed., Ottawa, ON, Canada, pp. 33-43.

Millard, S. G.; Bungey, J. H.; and Shaw, M., 1993, "The Assessment of Concrete Quality Using Pulsed Radar Reflection and Transmission Techniques," *Proceedings of the International Conference on NDT in Civil Engineering*, The British Institute of NDT, Southampton, UK, pp. 161-185.

Millard, S. G.; Ghassemi, M. H.; and Bungey, J. H., 1990, "Assessing the Electrical Resistivity of Concrete Structures for Corrosion Durability Studies," *Corrosion of Reinforcement in Concrete*, C. L. Page, K. W. J. Treadway, and P. B. Bamforth, eds., Elsevier Applied Science, New York, pp. 303-313.

Millard, S. G.; Harrison, J. A.; and Edwards, A. J., 1989, "Measurement of the Electrical Resistivity of Reinforced Concrete Structures for the Assessment of Corrosion Risk," *The British Journal of Non-Destructive Testing*, V. 31, No. 11, Nov., pp. 617-621.

Mitchell, T. M.; Lee, P. L.; and Eggert, G. J., 1979, "The CMD: A Device for the Continuous Monitoring of the Consolidation of Plastic Concrete," *Public Roads*, V. 42, No. 148.

Mitchell, T. W., 2004, "Radioactive/Nuclear Methods," Chapter 12, *Handbook on Nondestructive Testing of Concrete*, V. M. Malhotra and N. J. Carino, eds., CRC Press, Boca Raton, FL.

Montgomery, F. R., and Adams, A., 1985, "Early Experience with a New Concrete Permeability Apparatus," *Proceedings of the Second International Conference on Structural Faults & Repair-85*, Engineering Technics Press, Edinburgh, Scotland, pp. 359-363.

Moore, M.; Phares, B.; Graybeal, B.; Rolander, D.; and Washer, G., 2001, "Reliability of Visual Inspection for Highway Bridges—Volume I, Final Report," FHWA-RD-01-020, Federal Highway Administration, McLean, VA, June, 516 pp.

Morris, W.; Moreno, E. I.; and Sagues, A. A., 1996, "Practical Evaluation of Resistivity of Concrete in Test Cylinders Using Wenner Array Probe," *Cement and Concrete Research*, V. 26, No. 12, pp. 1779-1787.

Muldoon, R.; Chalker, A.; Forde, M. C.; Ohtsu, M.; and Kunisue, F., 2007, "Identifying Voids in Plastic Ducts in Post-Tensioning Prestressed Concrete Members by Resonant Frequency of Impact Echo, SIBIE and Tomography," *Construction & Building Materials*, V. 21, No. 3, pp. 527-537.

Naik, T. R.; Malhotra, V. M.; and Popovics, J. S., 2004, "The Ultrasonic Pulse Velocity Method," *Handbook on Nondestructive Testing of Concrete*, V. M. Malhotra and N. J. Carino, eds., CRC Press, Boca Raton, FL.

Nanukuttan, S. V.; Basheer, P. A. M.; and Robinson, D. J., 2006, "Further Developments of the PERMIT Ion Migration Test for Determining the Chloride Diffusivity of Concrete," *Structural Faults & Repair-2006*, M. C. Forde, ed., Engineering Technic Press, June, 14 pp.

Natrella, M., 1963, *Experimental Statistics*, NBS Handbook 91, U.S. Government Printing Office.

Nazarian, S., and Desai, M. R., 1993, "Automated Surface Wave Method: Field Testing," *Journal of Geotechnical Engineering*, V. 119, No. 7, July, pp. 1094-1111.

Nazarian, S., and Stokoe II, K. H., 1986a, "In-Situ Determination of Elastic Moduli of Pavement Systems by Spectral-Analysis-of-Surface-Waves Method (Practical Aspects)," *Research Report 368-1F*, Center for Transportation Research, The University of Texas at Austin, May.

Nazarian, S., and Stokoe II, K. H., 1986b, "In-Situ Determination of Elastic Moduli of Pavement Systems by Spectral-Analysis-of-Surface-Waves Method (Theoretical Aspects)," *Research Report 437-2*, Center for Transportation Research, University of Texas at Austin, Austin, TX, Aug.

Nazarian, S.; Stokoe II, K. H.; and Hudson, W. R., 1983, "Use of Spectral Analysis of Surface Waves Method for Determination of Moduli and Thickness of Pavement Systems," *Transportation Research Record* No. 930, Transportation Research Board, Washington, DC, pp. 38-45.

Niederleithinger, E.; Wiggenhauser, H.; and Taffe, A., 2009, "The NDT-CE Test and Validation Center in Horstwalde," *Proceedings of NDTCE'09, Non-Destructive Testing in Civil Engineering*, Nantes, France.

NORDTEST NT Build 443, 1995, "Concrete, Hardened: Accelerated Chloride Penetration," NORDTEST, Espoo, Finland, 5 pp.

Nokken, M. R., and Hooton, R. D., 2006, "Electrical Conductivity Testing," *Concrete International*, V. 28, No. 10, Oct., pp. 58-63.

Nolan, E.; Ali, M. A.; Basheer, P. A. M.; and Marsh, B. K., 1997, "Testing the Effectiveness of Commonly Used Site Curing Regimes," *Materials and Structures*, V. 30, Jan, Feb., pp. 53-60.

Ohtsu, M., and Watanabe, T., 2002, "Stack Imaging of Spectral Amplitudes Based on Impact Echo for Flaw Detection," *NDT&E International*, V. 35, pp. 189-196.

Olson, L. D., and Wright, C. C., 1990, "Nondestructive Testing for Repair and Rehabilitation," *Concrete International*, V. 12, No. 3, Mar., pp. 58-64.

Olson, L. D.; Wright, C. C.; and Stokoe, K. H., 1990, "Strides in Nondestructive Testing," *Civil Engineering*, ASCE, V. 60, No. 5, May, pp. 52-55.

Padaratz, I. J., and Forde, M. C., 1995, "A Theoretical Evaluation of Impulse Radar Wave Propagation through Concrete," *Journal of Non-Destructive Testing & Evaluation*, V. 12, pp. 9-32.

Padaratz, I. J.; Hardy, M. S. A.; and Forde, M. C., 1997, "Coupling Effects of Radar Antennae on Concrete," *Proceedings of the 4th International Conference on NDT-CE*, University of Liverpool, V. 1, pp. 237-245.

Paquet, J., 1968, "Etude Vibratoire des Pieux en Beton: Reponse Harmonique (Vibration Study of Concrete Piles: Harmonic Response)," Annales de l'Institut Technique du Batiment, France, 21st year, V. 245, pp. 789-803, (English translation by X. Yee in Master of Eng. Report, 1991, University of Utah, pp. 33-77).

Paquet, J., 1991, "A New Method for Testing Integrity of Piles by Dynamic Impulse: The Impedance Log," *International Colloquium on Deep Foundations*, École des Ponts et Chaussées, Paris, France, Mar., pp. 1-10. (in French)

Pederson, C. M., and Senkowski, L. J., 1986, "Slab Stabilization of PCC Pavements," Report to TRB Annual Conference, Washington, DC, *Transportation Research Record* No. 1083, National Research Council, Washington, DC, Jan., pp. 1-7.

Perenchio, W. F., 1989, "The Condition Survey," *Concrete International*, V. 11, No. 1, Jan., pp. 59-62.

Pratt, D., and Sansalone, M., 1992, "Impact-Echo Signal Interpretation Using Artificial Intelligence," *ACI Materials Journal*, V. 89, No. 2, Mar.-Apr., pp. 178-187.

Preiss, K., 1971, "Checking of Cast-in-Place Concrete Piles by Nuclear Radiation Methods," *British Journal of Non-Destructive Testing*, V. 13, No. 3, pp. 70-76.

Preiss, K., and Caiserman, A., 1975, "Nondestructive Integrity Testing of Bored Piles by Gamma Ray Scattering," *Ground Engineering*, V. 8, No. 3, pp. 44-46.

Proctor Jr., T. M., 1982, "Some Details on the NBS Conical Transducer," *Journal of Acoustic Emission*, V. 1, No. 3, pp. 173-178.

Rausche, F.; Likins, G. E.; and Hussein, M., 1988, "Pile Integrity by Low and High Strain Impacts," *Proceedings of the 3rd International Conference on Application of Stress-Wave Theory to Piles*, International Society of Soil Mechanics and Foundation Engineers, B. H. Fellenius, ed., Ottawa, ON, Canada, May 25-27, pp. 44-55.

Rausche, F., and Seitz, J., 1983, "Integrity Testing of Shafts and Caisson," Specialty Session on Shafts and Caissons, ASCE Annual Convention, Philadelphia, PA, 17 pp.

Richart Jr., F. E.; Woods, R. D.; and Hall, J. R., 1970, *Vibrations of Soils and Foundations*, Prentice-Hall, Inc., Englewood Cliffs, NJ.

Rix, G. J., and Stokoe, K. H., 1989, "Stiffness Profiling of Pavement Subgrades," *Transportation Research Record* No. 1235, Transportation Research Board, Washington, DC, pp. 1-9.

Roberge, P., 2008, *Corrosion Engineering: Principles and Practice*, McGraw-Hill, 754 pp.

Rodríguez, P.; Ramírez, E.; and González, J. A., 1994, "Methods for Studying Corrosion in Reinforced Concrete," *Magazine of Concrete Research*, V. 46, No. 167, June, pp. 81-90.

Saleh, H. H., and Livingston, R. A., 2000, "Experimental Evaluation of a Portable Neutron-Based Gamma-Spectroscopy System for Chloride Measurements in Reinforced Concrete," *Journal of Radioanalytical and Nuclear Chemistry*, V. 244, No. 2, pp. 367-371.

Samman, M. M., and O'Neill, M. W., 1997, "The Reliability of Sonic Testing of Drilled Shafts," *Concrete International*, V. 19, No. 1, Jan., pp. 49-54.

Sansalone, M., 1997, "Impact Echo: The Complete Story," *ACI Structural Journal*, V. 94, No. 6, Nov.-Dec., pp. 777-786.

Sansalone, M., and Carino, N. J., 1986, "Impact-Echo: A Method for Flaw Detection in Concrete Using Transient Stress Waves," *NBSIR 86-3452*, National Bureau of Standards, Sept., 222 pp.

Sansalone, M., and Carino, N. J., 1988, "Impact-Echo Method: Detecting Honeycombing, the Depth of Surface-Opening Cracks, and Ungrouted Ducts," *Concrete International*, V. 10, No. 4, Apr., pp. 38-46.

Sansalone, M., and Carino, N. J., 1989a, "Detecting Delaminations in Concrete Slabs With and Without Overlays Using the Impact-Echo Method," *ACI Materials Journal*, V. 86, No. 2, Mar.-Apr., pp. 175-184.

Sansalone, M., and Carino, N. J., 1989b, "Laboratory and Field Study of the Impact-Echo Method for Flaw Detection in Concrete," *Nondestructive Testing of Concrete*, SP-112, H. S. Lew, ed., American Concrete Institute, Farmington Hills, MI, Mar., pp. 1-20.

Sansalone, M.; Lin, J. M.; and Streett, W. B., 1997, "A Procedure for Determining P-Wave Speed in Concrete for Use in Impact-Echo Testing Using a P-Wave Speed Measurement Technique," *ACI Materials Journal*, V. 94, No. 6, Nov.-Dec., pp. 531-539.

Sansalone, M. J., and Streett, W. B., 1997, *Impact-Echo: Nondestructive Evaluation of Concrete and Masonry*, Bullbrier Press, Ithaca, NY, 339 pp.

Scheel, H., and Hillemeier, B., 2003, "Location of Prestressing Steel Fractures in Concrete," *Journal of Materials in Civil Engineering*, V. 15, No. 3, June, pp. 228-234.

Schickert, M.; Krause, M.; and Müller, W., 2003, "Ultrasonic Imaging of Concrete Elements Using Reconstruction by Synthetic Aperture Focusing Technique," *Journal of Materials in Civil Engineering*, V. 15, No. 3, June, pp. 235-246.

Schönlin, K., and Hilsdorf, H., 1987, "Evaluation of the Effectiveness of Curing of Concrete Structures," *Concrete Durability: Katharine and Bryant Mather International Conference*, SP-100, J. M. Scanlon, ed., American Concrete Institute, Farmington Hills, MI, pp. 207-226.

Serway, R. A., 1983, *Physics for Scientists & Engineers with Modern Physics*, Saunders College Publishing, Philadelphia, PA.

Shaw, M. R.; Millard, S. G.; Houlden, M. A.; Austin, B. A.; and Bungey, J. H., 1993, "A Large Diameter Transmission Line for the Measurement of Relative Permittivity of

Construction Materials," *British Journal of Non-destructive Testing*, V. 35, No. 12, pp. 696-704.

Shevaldykin, V. G.; Samokrutov, A. A.; and Kozlov, V. N., 2003, "Ultrasonic Low-Frequency Short-Pulse Transducers with Dry Point Contact—Development and Application," *International Symposium on Non-Destructive Testing in Civil Engineering*.

Snyder, K. A.; Ferraris, C.; Martys, N. S.; and Garboczi, E. J., 2000, "Using Impedance Spectroscopy to Assess the Viability of the Rapid Chloride Test for Determining Concrete Conductivity," *Journal of Research of the National Institute of Standards and Technology*, V. 105, pp. 497-509.

Stain, R. T., 1982, "Integrity Testing," *Civil Engineering*, UK, Apr., pp. 55-59, and May, pp. 77-87.

Starke, W. F., and Janes, M. C., 1988, "Accuracy and Reliability of Low Strain Integrity Testing," *Proceedings of the 3rd International Conference on Application of Stress-Wave Theory to Piles*, International Society of Soil Mechanics and Foundation Engineering, B. H. Fellenius, ed., Ottawa, ON, Canada, pp. 19-32.

Starnes, M. A.; Carino, N. J.; and Kausel, E. A., 2003, "Preliminary Thermography Studies for Quality Control of Concrete Structures Strengthened with Fiber-Reinforced Polymer Composites," *Journal of Materials in Civil Engineering*, ASCE, V. 15, No. 3, June, pp. 266-273.

Steinbach, J., and Vey, E., 1975, "Caisson Evaluation by Stress Wave Propagation Method," *Journal of Geotechnical Engineering*, V. 101, Apr., pp. 361-378.

Steinert, J., 1979, "Nondestructive Determination of the Depth of Penetration of Water in Gravel Concrete at the Structure," *Forschungsbeiträge für die Baupraxis*, pp. 151-162.

Steinway, W. J.; Echard, J. D.; and Luke, C. M., 1981, "Locating Voids Beneath Pavements Using Pulsed Electromagnetic Waves," *NCHRP Report 237*, Transportation Research Board, National Research Council, Washington, DC, Nov.

Stern, M., and Geary, A. L., 1957, "Electrochemical Polarization: I—A Theoretical Analysis of the Shape of Polarization Curves," *Journal of the Electrochemical Society*, V. 104, No. 1, Jan., pp. 56-63.

Stern, M., and Roth, R. M., 1957, "Anodic Behavior of Iron in Acid Solutions," *Journal of the Electrochemical Society*, V. 104, No. 6, June, pp. 390-392.

Tam, C. T.; Lai, L. H.; and Lam, P. W., 1977, "Orthogonal Detection Technique for Determination of Size and Cover of Embedded Reinforcement," *Journal of Institution of Engineers*, V. 22, June, pp. 6-16.

Tang, L., 2002, "Calibration of the Electrochemical Methods for the Corrosion Rate Measurement of Steel in Concrete: NORDTEST Project No. 1531-01," *SP Report 2002:25*, Swedish National Testing and Research Institute, 54 pp.

Teodoru, G. V. M., 1994, "Nondestructive Testing of Concrete from Research to the Use in the Practice," *International Advances in Nondestructive Testing*, V. 17, W. J. McGonnagle, ed., Gordon & Breach Science Publishers, New York, pp. 117-137.

Teodoru, G. V. M., 1996, "NDT-Methods for Concrete on the Move Into the 21st Century," *Proceedings of the Fourteenth World Conference on NDT*, New Delhi, India, C.G. Krishnadas, R. Baldev, C. R. L. Murthy, and T. Javakumar, eds., Oxford & IBH Publishing Co., V. 1, pp. 123-129.

Teodoru, G. V. M., and Herf, J., 1996, "Engineering Society Cologne Presents Itself (NDT Methods)," *Proceedings of the Fourteenth World Conference on NDT*, New Delhi, India, C.G. Krishnadas, R. Baldev, C. R. L. Murthy, and T. Javakumar, eds., Oxford & IBH Publishing Co., V. 2, pp. 939-943.

The Concrete Society, 1988, "Permeability Testing of Site Concrete," *Technical Report* No. 31, Surrey, UK, Aug., 95 pp.

Thieberger, P.; Mariscotti, M. A. J.; Ruffolo, M. D.; and Frigerio, T., 2009, "Method and Arrangement for Improving Tomographic Determinations, Particularly Suitable for Inspection of Steel Reinforcement Bars in Concrete Structures," Patent No. WO/2008/060398.

Tipler, P. A., 1991, *Physics for Scientists and Engineers*, third edition, V. 2, Worth Publishers, New York.

Tomsett, H. N., 1980, "The Practical Use of Ultrasonic Pulse Velocity Measurements in the Assessment of Concrete Quality," *Magazine of Concrete Research*, V. 32, No. 110, Mar., pp. 7-16.

Torrent, R. J., 1992, "A Two-Chamber Vacuum Cell for Measuring the Coefficient of Permeability to Air of the Concrete Cover on Site," *Materials and Structures*, V. 25, pp. 358-365.

Ulriksen, C. P. F., 1983, *Application of Impulse Radar to Civil Engineering*, doctoral thesis, Lund University, Department of Engineering Geology, Sweden.

Utsi, V., 2003, "Minimum Delamination Width for GPR," *Proceedings of the Tenth International Conference: Structural Faults + Repair-2003*, Engineering Technics Press, Edinburgh, Scotland.

Van Koten, H., and Middendorp, P., 1981, "Interpretation of Results from Integrity Tests and Dynamic Load Tests," *Application of Stress Wave Theory in Piles*, Balkema, Rotterdam.

Weil, G. J., 1989, "Nondestructive Remote Sensing of Subsurface Utility Distribution Pipe Problems Using Infrared Thermography." *Proceedings of the 2nd International Conference on Pipeline Construction*, Centrum Hamburg, Oct.

Weil, G. J., 2004, "Infrared Thermographic Techniques," *Handbook on Nondestructive Testing of Concrete*, V. M. Malhotra and N. J. Carino, eds., CRC Press, Boca Raton, FL.

Wenner, F., 1916, "A Method of Measuring Earth Resistivity," *Science Paper* No. 258, U.S. Bureau of Standards Bulletin.

Whitehurst, E. A., 1967, *Evaluation of Concrete Properties from Sonic Tests*, American Concrete Institute Monograph No. 2, Iowa State University Press, Ames, IA, 94 pp.

Whiting, D., 1987, "Permeability of Selected Concrete," *Permeability of Concrete*, SP-108, D. Whiting and A. Walit, eds., American Concrete Institute, Farmington Hills, MI, pp. 195-222.

Whiting, D., and Cady, P. D., 1992, "Condition Evaluation of Concrete Bridges Relative to Reinforcement Corrosion, Volume 7: Method for Field Measurement of Concrete Permeability," SHRP-S/FR-92-109, National Research Council, Washington, DC, 87 pp.

Williams, H. T., and Hulse, M. E., 1995, "From Theory to Field Experience with Inspection of Post-Tensioned Bridges," *Proceedings of the 6th International Conference on Structural Faults + Repair-95*, V. 1, Engineering Technics Press, Edinburgh, Scotland, pp. 199-202.

Williams, T. J.; Nozick, L. K.; Sansalone, M. J.; and Poston, R. W., 2006a, "Sampling Techniques for Evaluating Large Concrete Structures: Part I," *ACI Structural Journal*, V. 103, No. 3, May-June, pp. 399-408.

Williams, T. J.; Nozick, L. K.; Sansalone, M. J.; Poston, R. W.; and Kesner, K., 2006b, "Sampling Techniques for Evaluating Large Concrete Structures: Part II," *ACI Structural Journal*, V. 103, No. 4, July-Aug., pp. 505-512.

Williams, T. J.; Sansalone, M.; Streett, W. B.; Poston, R.; and Whitlock, R., 1997, "Nondestructive Evaluation of Masonry Structures Using the Impact-Echo Method," *The Masonry Society Journal*, V. 15, No. 1, June, pp. 47-57.

Yuan, D., and Nazarian, S., 1993, "Automated Surface Wave Method: Inversion Technique," *Journal of Geotechnical Engineering*, V. 119, No. 7, July, pp. 1112-1126.

APPENDIX A: THEORETICAL ASPECTS OF MOBILITY PLOT OF PILE

Dynamic pile mobility is defined as the pile mechanical admittance (which is the inverse of the pile impedance) when the pile is subjected to a vertical dynamic force. Mobility is measured as velocity/force (*V*/*F*) and is expressed in metric units as m/s/N.

The theory of the mobility response of a pile in soil has been fully developed in Davis and Dunn (1974). The principles of mobility-frequency response curve interpretation are based on the following premises.

When a perfect, laterally unrestrained (free) pile of length *L* resting on the surface of an elastic foundation is excited by a continuous sinusoidal axial force with peak value F_o, the pile head achieves a maximum velocity V_0. As the frequency of the applied force is varied, the amplitude of the pile head velocity has peak values at equally spaced frequencies (resonant frequencies). The frequency interval, Δf, between the peaks is given by

$$\Delta f = \frac{C_b}{2L} \tag{A.1a}$$

where C_b is the speed of stress-wave propagation along the pile axis.

In the case of an infinitely rigid elastic base, the lowest resonant frequency is equal to $C_b/4L$. In contrast, when the pile rests on an infinitely compressible base, the lowest resonant frequency approaches zero. In real conditions, the lowest resonant frequency lies between zero and $C_b/4L$.

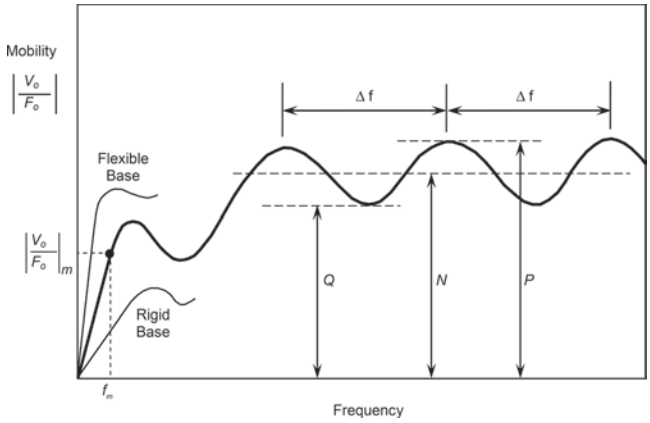

Fig. A.1—Theoretical mobility plot for impulse-response test of perfect pile in homogeneous soil.

When the pile is embedded in soil, the pile movement is damped by that lateral soil. The mobility curve is attenuated to give the typical response shown in Fig. 3.3.2.1a. The denser the soil and the longer the pile, the greater is the attenuation, with increasing reduction in the difference between the maximum and minimum amplitudes. Figure A.1 summarizes the mobility response from a perfect pile. A soil damping factor σ (Briard 1970) can be given by

$$\sigma = \frac{\rho_s \beta_s}{\rho_c C_b r} \tag{A.1b}$$

where ρ_s is the soil density; ρ_c is the concrete density; β_s is the lateral soil shear wave velocity at the pile/soil interface; and *r* is the pile radius.

The geometric mean value of mobility in the resonant portion of the plot is known as the average mobility *N* and is given by

$$N = \frac{1}{\rho_c C_b A_c} \tag{A.1c}$$

where A_c is the pile cross-sectional area. This is the inverse of the pile impedance.

The maximum and the minimum amplitudes *P* and *Q* provide a measure of the soil damping effect from the relationships

$$\begin{aligned} P &= N \coth(\sigma L) \\ Q &= N \tanh(\sigma L) \end{aligned} \tag{A.1d}$$

This can also be expressed as

$$N = \sqrt{PQ} \tag{A.1e}$$

and σL can be calculated from

$$\coth(\sigma L) = \sqrt{PQ} \tag{A.1f}$$

The mass of the pile M_p is calculated as

$$M_p = L\rho_c A_c = \frac{1}{2\Delta f N} \quad \text{(A.1g)}$$

The pile dynamic stiffness k_d is calculated from the mobility response curve at very low frequencies (usually in the range 0 to 60 Hz). At these low frequencies, inertial effects are insignificant and the pile-soil unit behaves as a spring, giving a linear response at the start of the mobility curve. The slope of this line is the pile compliance and the inverse of the compliance is the pile dynamic stiffness k_d

$$k_d = \frac{2\pi f_m}{\left(\frac{V_o}{F_o}\right)_m} \text{ in units of N/m} \quad \text{(A.1h)}$$

where f_m is the frequency corresponding to the end of the initial linear portion of the mobility plot.

The mobility response curves obtained from real piles are seldom as simple as the theoretical curve for a perfect pile in homogeneous soil shown in Fig. A.1. Several factors affect the shape of the mobility curve. The most common are

a) Variations in pile diameter

b) Variations in the pile concrete quality with pile depth

c) Variations in the lateral soil stiffness

d) The top section of pile being exposed above ground level, sometimes known as the reveal

The general effect of these factors is to produce superimposed variations in the geometric mean mobility on the general mobility plot. Figure 3.3.2.1a shows such a variation in the mean between 460 and 1360 Hz, which is a result of a free pile head 6.9 ft (2.1 m) in length ($2\Delta f$ = 1800 Hz). The interpretation of mobility plots with superimposed features requires experience. Help can be provided by computer simulation models, as described in Davis and Dunn (1974).

American Concrete Institute®
Advancing concrete knowledge

As ACI begins its second century of advancing concrete knowledge, its original chartered purpose remains "to provide a comradeship in finding the best ways to do concrete work of all kinds and in spreading knowledge." In keeping with this purpose, ACI supports the following activities:

- Technical committees that produce consensus reports, guides, specifications, and codes.
- Spring and fall conventions to facilitate the work of its committees.
- Educational seminars that disseminate reliable information on concrete.
- Certification programs for personnel employed within the concrete industry.
- Student programs such as scholarships, internships, and competitions.
- Sponsoring and co-sponsoring international conferences and symposia.
- Formal coordination with several international concrete related societies.
- Periodicals: the ACI Structural Journal and the ACI Materials Journal, and Concrete International.

Benefits of membership include a subscription to Concrete International and to an ACI Journal. ACI members receive discounts of up to 40% on all ACI products and services, including documents, seminars and convention registration fees.

As a member of ACI, you join thousands of practitioners and professionals worldwide who share a commitment to maintain the highest industry standards for concrete technology, construction, and practices. In addition, ACI chapters provide opportunities for interaction of professionals and practitioners at a local level.

American Concrete Institute
38800 Country Club Drive
Farmington Hills, MI 48331
U.S.A.
Phone: **248-848-3700**
Fax: **248-848-3701**

www.concrete.org

Report on Nondestructive Test Methods for Evaluation of Concrete in Structures

The AMERICAN CONCRETE INSTITUTE

was founded in 1904 as a nonprofit membership organization dedicated to public service and representing the user interest in the field of concrete. ACI gathers and distributes information on the improvement of design, construction and maintenance of concrete products and structures. The work of ACI is conducted by individual ACI members and through volunteer committees composed of both members and non-members.

The committees, as well as ACI as a whole, operate under a consensus format, which assures all participants the right to have their views considered. Committee activities include the development of building codes and specifications; analysis of research and development results; presentation of construction and repair techniques; and education.

Individuals interested in the activities of ACI are encouraged to become a member. There are no educational or employment requirements. ACI's membership is composed of engineers, architects, scientists, contractors, educators, and representatives from a variety of companies and organizations.

Members are encouraged to participate in committee activities that relate to their specific areas of interest. For more information, contact ACI.

www.concrete.org

American Concrete Institute®
Advancing concrete knowledge